C1QL1 & c-KIT molecular complexes : cell surface signaling pathways acting at neuronal synapses and beyond

Shayan Moghimyfiroozabad

Sorbonne Université

Ecole doctorale Cerveau, Cognition, Comportement (Ed158)
Center for Interdisciplinary Research in Biology (CIRB), Collège de France, CNRS, INSERM, Université PSL

C1QL1 & c-KIT molecular complexes: cell surface signaling pathways acting at neuronal synapses and beyond

Par Shayan Moghimyfiroozabad

Thèse de doctorat de Neurosciences

Dirigée par Fekrije Selimi

Présentée et soutenue publiquement le 16 juin 2023.

Devant un jury composé de :

Pr. Sophie Chauvet, présidente

Pr. Annalisa Buffo, rapportrice

Dr. Fabrice Ango, rapporteur

Dr. Mathieu Letelllier, Examinateur

Dr. Tim Czopka, Examinateur

Acknowledgements:

The list is very long. I should thank my beloved supervisor and teammates who became my second family here (FS, SS, BUC, MV, MP, CBL, LM, FUQ, and MC). During all these years, I learnt from you not only scientific thinking and methodology, but also so many other things related to a normal human life. Without the great supervision of Fekrije with her high-level standards, feedback and support of the other members of the lab, Severine, Beetsi, Celia, Maxime, Maela, Francisco and Lea, this work could not be accomplished.

I should also thank the members of the jury for evaluating and correcting my work. In addition, I would like to take this opportunity and thank all members of Terret-Verlhac team (FC, NZ, LB, RB, MET, MHV, MA, CDS, EN, AAJ) for being such a nice neighbor and bringing positive and supportive atmosphere to our corridor, as well as all the people from other teams (NG, MF, TB, CH, NE, MK, PB, CP, RB).

I would like to thank my friends for their pure heart and everlasting support (FA, NR, RM, MB, SV, SA, EE, AE, SS). I would like to add to this list my previous supervisors and teachers from Baha'i institute for higher education (KNA, KS, NK, BK).

At last but not least, I would like to acknowledge the importance of my dearest extended family in Iran, my parents and brothers, my cousins (specially Sepehr), my aunts (specially Farah) and uncles (specially Fariborz), my dearest grandma, and Ghazal, and the rest of the family outside of Iran (specially NA and her family). I should also thank specially Roohallah, the closest support from the family for being always present in sorrow and happiness.

Table of contents:

List of figures:

Introduction

Results

Part 1: The transmembrane receptor tyrosine kinase c-KIT is involved in the development of olivocerebellar circuit in a lobule-specific manner.

Part 2: Mapping and targeting of *C1ql1*-expressing cells in the mouse.

Part 3: A molecularly-defined non-redundant subpopulation of OPCs controls the generation of myelinating oligodendrocytes during postnatal development.

Abbreviations:

AEP: Anterior entopeduncular area

aGPCR: adhesion GPCR

AIS: Axon initial segment

AldC: Aldolase C

AMPA: α-amino-3-hydroxy-5-methyl-4-isoxazolepropionic acid

bacTRAP: bacterial artificial chromosome translating ribosome affinity purification

BAI: Brain-specific angiogenesis inhibitor

CaBP: Calbindin 1 protein

CF: Climbing fiber

CGE: Caudal ganglionic eminences

cKO: Conditional knockout

Cit-k: Citron-kinase

Cntn6: Contactin-6

CNS: Central nervous system

COP: Committed OPC

CUB: Complement C1r/C1s, Uegf, Bmp1

C1QL: Complement component 1, q subcomponent-like protein

CSP: Cell surface protein

CSPG4: Chondroitin sulfate proteoglycan 4

CTF: C-terminal fragment

Cys: cysteine residue

DTA: Diphtheria toxin

Embryonic day: E

EGL: External granular layer

FGF2: Fibroblast growth factor 2

FLRT3: Fibronectin leucine-rich transmembrane protein 3

GABA: γ-Aminobutyric acid

GAD65: Glutamic acid decarboxylase 65

GAIN: GPCR autoproteolysis–inducing domain

gC1q: globular C1q domain

GEF: Guanine nucleotide exchange factor

GPR17: G protein-coupled receptor 17

GO: Gene ontology

GPCR: G-protein coupled receptor

GPI: Glycosylphosphatidylinositol

GPS: GPCR proteolysis site

HEK: Human embryonic kidney

HIF: Hypoxia-inducible factors

HUVECs: Human umbilical vein endothelial cells

HRM: Hormone receptor motif

IFNγ: Interferon-gamma

IGL: Internal granular layer

IL: interleukin

IO: Inferior olive

ION: Inferior olivary neuron

IRES: Internal ribosome entry site

ISH: *In situ* hybridization

JM: Juxtamembrane domain

KA: Kainic acid

KI: Kinase insert domain

KNN: K-nearest neighbor

KO: Knockout

LC: Lugaro cell

LGE: Lateral ganglionic eminences

LPHN: Latrophilin

LTP: Long-term potentiation

MAP: Mitogen-activated protein

MBP: Myelin binding protein

MF: Mossy fiber

MGE: Medial ganglionic eminence

ML: Molecular layer

MLI: Molecular layer interneuron

MMRRC: Mutant Mouse Resource and Research Center

NF: Neurofilament protein

NG2: Neural/glial antigen 2

NMDAR: *N*-methyl-D-aspartate receptor

Nptx2/Narp: Neuronal Pentraxin 2

NRX1α/1β: Neurexin1α and 1β

NTF: N-terminal fragment

NSPC: Neural stem/progenitor cell

OL: Oligodendrocyte

Olf: Olfactomedin domain

OPC: Oligodendrocyte precursor cells

P: Postnatal day

PBM: PDZ-binding motif

PC: Purkinje cell

PCL: Purkinje cell layer

PDGF: Platelet-derived growth factor

PDGFRa: Platelet-derived growth factor receptor A

PF: Parallel fiber

PI3'-kinases: Phosphatidylinositol 3'-kinases

PRR: Proline-rich region

PTGDS: Prostaglandin D2 synthase

Pvalb: Parvalbumin

RBL: Rhamnose-binding lectin domain

RL: Rhombic lip

RTKs: Receptor tyrosine kinases

RTN4Rs: RTN4/NoGo-Receptors

RT-PCR: Reverse transcription polymerase chain reaction

SCF: Stem cell factor

SEM: Standard error of the mean

SFKs: Src family kinases

SHH: Sonic Hedgehog

smFISH: Single molecule fluorescence *in situ* hybridization

SPR: surface plasmon resonance

SSA: Splicing site

STRR: Serine/threonine-rich region

TEN2: Teneurin 2

TG2: Transglutaminase-2

TK1/2: Tyrosine kinase subdomain 1/2

TM: Transmembrane domain

TSRs: Thrombospondin type 1 repeats

UBS: Unipolar brush cells

UMAP: Uniform manifold approximation and projection

VC: Ventral cochlear nucleus

VGLUT2: Vesicular glutamate transporter 2

VZ: Ventricular zone

WM: White matter

WT: Wildtype

Summary:

Proper brain development relies on cellular proliferation, migration and differentiation of various cell populations, recognition and adhesion between different cell types. Cell surface molecular complexes are essential for many of these processes. A given receptor complex can be used at several stages and might play different roles in various cell populations. During my PhD, I worked on two cell surface molecular complexes and their role during postnatal development of the mouse brain. First, I studied the role of the c-KIT/SCF complex in neuronal connectivity. c-KIT is a well-known proto-oncogene and a transmembrane receptor tyrosine kinase that controls cell survival, proliferation and maintenance of various tissues (e.g. hematopoietic tissue) as well as cell-cell adhesion. I identified the presence of c-KIT at different types of synapses of cerebellar Purkinje cells (PC) during postnatal development: synapses made by the climbing fibers (CFs), the axons of inferior olivary neurons located in the brainstem, and synapses made by molecular layer interneurons (MLIs). Data from the Allen Brain Atlas show that the gene coding the c-KIT ligand, *Scf*, is expressed in the target neuron (PC), suggesting a potential role for the c-KIT/SCF complex in the formation and maintenance of cell-cell contacts in the olivocerebellar circuit. Using postnatal conditional knockout of *c-Kit* in MLIs, I showed that loss of function of c-KIT during the fourth postnatal week decreases the size of the presynaptic boutons of MLIs on PCs in a lobule-specific manner, while their density remains unchanged. The removal of c-KIT from MLIs also decreases the volume of presynaptic boutons from the CFs. Since this loss of c-KIT happens after synapse formation in this model, these data suggest a role for the c-KIT/SCF pathway in maintaining proper connectivity and function of the olivocerebellar circuit, and identify a potential new role for this class of receptor tyrosine kinases in brain function. In parallel, I characterized a new Cre-driver mouse line that was generated to enable inferior olivary neuron-specific knockout of *c-Kit* during postnatal development. In this line, Cre is knocked in the gene coding for C1QL1, a secreted molecule involved in CF-PC synapse formation and highly expressed in inferior olivary neurons. During this characterization, I discovered that *C1ql1* is expressed in a subtype of glial cells, oligodendrocyte precursor cells (OPCs). OPCs tile the whole central nervous system during development and adulthood. They play several key functions across the brain including the generation of oligodendrocytes. Whether the functional diversity of OPCs is the result of genetically defined subpopulations or of their regulation by external factors has not been established. We discovered that a subpopulation of OPCs found across the brain starts to express *C1ql1* during the first postnatal week in the mouse brain. Ablation of *C1ql1*-expressing OPCs, which constitute about 30-50% of total OPCs, in the mouse is not compensated by the remaining OPCs, and results in a large decrease in oligodendrocyte numbers and lack of myelination in many brain regions. Therefore, *C1ql1* is a molecular

marker of a functionally non-redundant subpopulation of OPCs, which controls the generation of myelinating oligodendrocytes. Overall my thesis work shows that a given cell surface molecular complex can control various aspects of synapse formation and function between neurons while playing roles in other aspects of brain development, such as defining the functional diversity of non-neuronal cells. Whether these complexes trigger their canonical pathways or they function through other non-canonical mechanisms in different contexts of development should be further investigated. It remains to be demonstrated whether this signaling redundancy underlies a common orchestration of various aspects of brain development and function.

Resumé :

Le bon développement du cerveau repose sur la prolifération cellulaire, la migration et la différenciation de diverses populations cellulaires, la reconnaissance et l'adhésion entre différents types de cellules. Les complexes moléculaires de la surface cellulaire sont essentiels pour bon nombre de ces processus. Un complexe récepteur donné peut être utilisé à plusieurs stades et peut jouer différents rôles dans diverses populations cellulaires. Au cours de mon doctorat, j'ai travaillé sur deux complexes moléculaires de surface cellulaire et sur leur rôle au cours du développement postnatal du cerveau de la souris. Tout d'abord, j'ai étudié le rôle du complexe c-KIT/SCF dans la connectivité neuronale. c-KIT est un proto-oncogène bien connu et un récepteur tyrosine kinase transmembranaire qui contrôle la survie cellulaire, la prolifération et le maintien de divers tissus (par exemple, le tissu hématopoïétique) ainsi que l'adhésion cellule-cellule. J'ai identifié la présence de c-KIT dans différents types de synapses des cellules de Purkinje (PC) du cervelet au cours du développement postnatal : les synapses produites par les fibres grimpantes (CF), les axones des neurones de l'olivaire inférieur situés dans le tronc cérébral, et les synapses produites par les interneurones de la couche moléculaire (MLI). Les données de l'Atlas du cerveau Allen (Allen Brain Atlas) montrent que le gène codant le ligand de c-KIT, *Scf*, est exprimé dans le neurone cible (PC), ce qui suggère un rôle potentiel pour le complexe c-KIT/SCF dans la formation et le maintien des contacts cellule-cellule dans le circuit olivo-cérébelleux. En utilisant l'élimination (le knockout) conditionnel postnatal de *c-Kit* dans les MLI, j'ai montré que la perte de fonction de c-KIT pendant la quatrième semaine postnatale diminue la taille des boutons présynaptiques des MLI sur les PC d'une manière spécifique au lobule, alors que leur densité reste inchangée. L'élimination de c-KIT des MLI diminue également le volume des boutons présynaptiques des PC. Comme cette perte de c-KIT survient après la formation des synapses dans ce modèle, ces données suggèrent un rôle pour la voie c-KIT/SCF dans le maintien d'une connectivité et d'un fonctionnement corrects du circuit olivo-cérébelleux, et identifient un nouveau rôle potentiel pour cette classe de récepteurs tyrosine kinase dans les fonctions cérébrales. Parallèlement, j'ai caractérisé une nouvelle lignée de souris Cre-driver qui a été générée pour permettre l'élimination (le knockout) spécifique de *c-Kit* dans les neurones de l'olivaire inférieur pendant le développement postnatal. Dans cette lignée, Cre est inséré dans le gène codant pour C1QL1, une molécule sécrétée impliquée dans la formation des synapses CF-PC et fortement exprimée dans les neurones de l'olivaire inférieur. Au cours de cette caractérisation, j'ai découvert que *C1ql1* est exprimé dans un sous-type de cellules gliales, les cellules précurseurs d'oligodendrocytes (OPC). Les OPC couvrent l'ensemble du système nerveux central au cours du développement et à l'âge adulte. Elles jouent plusieurs rôles clés dans le cerveau, notamment la génération d'oligodendrocytes. Il n'a pas été établi si la diversité

fonctionnelle des OPC est le résultat de sous-populations génétiquement définies ou de leur régulation par des facteurs externes. Nous avons découvert qu'une sous-population d'OPC présente dans tout le cerveau commence à exprimer *C1ql1* au cours de la première semaine postnatale dans le cerveau de la souris. L'ablation des OPC exprimant *C1ql1*, qui constituent environ 30 à 50 % du total des OPC, chez la souris n'est pas compensée par les OPC restants et entraîne une forte diminution du nombre d'oligodendrocytes et une absence de myélinisation dans de nombreuses régions du cerveau. Par conséquent, *C1ql1* est un marqueur moléculaire d'une sous-population d'OPC fonctionnellement non redondante, qui contrôle la génération d'oligodendrocytes myélinisants. Dans l'ensemble, mes travaux de thèse montrent qu'un complexe moléculaire de surface cellulaire donné peut contrôler divers aspects de la formation et de la fonction des synapses entre les neurones, tout en jouant un rôle dans d'autres aspects du développement du cerveau, tels que la définition de la diversité fonctionnelle des cellules non neuronales. Il convient d'étudier plus avant si ces complexes déclenchent leurs voies canoniques ou s'ils fonctionnent par le biais d'autres mécanismes non canoniques dans différents contextes de développement. Il reste à démontrer que cette redondance de signalisation sous-tend une orchestration commune de divers aspects du développement et du fonctionnement du cerveau.

Introduction

1. PART1: Cell surface proteins:

The surfaceome is constituted by the biomolecules found on the cell surface and includes cell surface proteins (CSPs) which play crucial functions in different aspects of the biology of the cell. They are at the interface between intra- and extracellular pathways, conveying messages from one side to the other. They can work as the receptors for biomolecules (e.g. hormones, neurotransmitters), drugs or pathogens, interact with the extracellular matrix, form channels to selectively permit the passage of ions and small molecules, and interact with proteins expressed by or released from other cells or the same one (Figure 1) (Bausch-Fluck et al., 2019; Pauwels et al., 2022; Vilen et al., 2022). Several characteristics of the surfaceome, such as their type, modifications, amount and spatiotemporal organization, are essential factors in defining cellular identity and its capacity in interacting with the external microenvironment during development and in malignancies (Bausch-Fluck et al., 2019). Due to their importance and accessibility, CSPs are the most common therapeutic targets (Bausch-Fluck et al., 2019; Vilen et al., 2022).

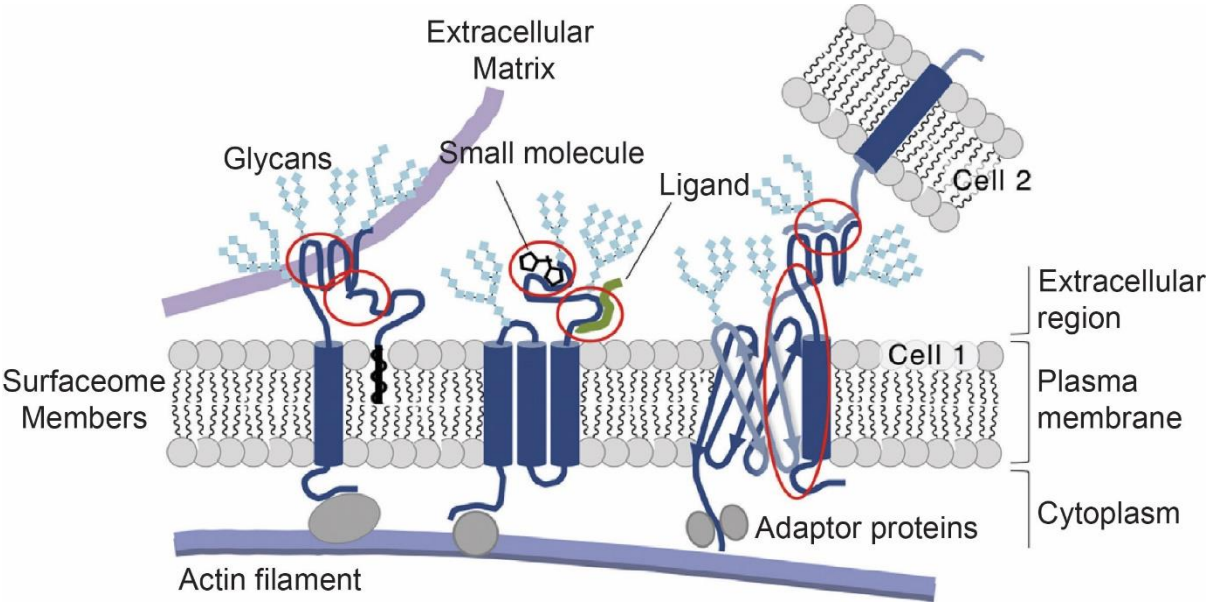

Figure 1. A schematic network of surfaceome signaling. The regions of interaction are encircled in red. α-helical and β-barrel transmembrane domains are represented by cylinders and lines, respectively. CSPs are depicted in dark blue. *Taken from* (Bausch-Fluck et al., 2019).

CSPs play fundamental roles in the function and development of various tissues and systems (Bausch-Fluck et al., 2019; Pauwels et al., 2022). Using a machine-learning method, it has been estimated that ~2,900 entries of ~20,000 human proteins of all tissues and

developmental stages are CSPs (Bausch-Fluck et al., 2019), which shows the abundance and importance of these proteins in normal development and physiology of the human body. Some CSPs are restricted to one particular physiological system, and some have ubiquitous roles. For example, the receptors that are involved in antigen recognition and presenting are critical for the function of the immune system (Bausch-Fluck et al., 2019; Pauwels et al., 2022), while receptor tyrosine kinases (RTKs), such as c-KIT or Eph receptor, play key role in cell proliferation, survival and migration, and are important in several systems (Lennartsson and Rönnstrand, 2012; Pasquale, 2008).

CSPs are categorized into two groups: 1) Integral/intrinsic CSPs that have one or several transmembrane domains. Single transmembrane CSPs are subdivided into several types: Type 1 have their C-terminus inside the cell and their signal peptide is removed. Type 2 have their C-terminus extracellular with a short intracellular domain and their N-terminus close to the transmembrane domain. Type 3 are similar to Type 1 with no signal sequence. Type 4 have their C-terminus outside of the cell with a short extracellular domain. The multiple transmembrane CSPs can be classified into more groups based on the number of transmembrane domains and the position of their C/N-termini (Pauwels et al., 2022). For example, G-protein coupled receptors (GPCRs) have 7 transmembrane domains binding to different types of G-proteins intracellularly (Pierce et al., 2002). 2) Peripheral/extrinsic CSPs that lack a transmembrane domain, but can bind to the external bilipid layer through several mechanisms such as insertion of a hydrophobic domain, or electrostatic association of their positively charged motifs with the negatively charged phospholipids (Pauwels et al., 2022).

In the following sections, I focus on two cell surface signaling pathways that were analyzed during my thesis and their contribution to nervous system development: a subfamily of GPCRs called adhesion GPCRs and receptor tyrosine kinases (RTKs).

1.1. BAIs and their C1QL ligands:

1.1.1. General principles of adhesion GPCRs signaling:

GPCRs are the biggest and most ubiquitous family of cell surface receptors in mammals (Pierce et al., 2002). The second biggest subfamily of GPCRs (after Rhodopsin family with > 600 members) is the adhesion GPCRs (aGPCRs) with 33 members in human, and 31 in rodents. They are known for their long extracellular N-terminus with multiple domains involved in cell-ECM and cell-cell adhesion, giving them the title adhesion GPCR (Hamann et al., 2015; Schiöth et al., 2010).

aGPCRs are divided into 9 groups mainly based on the homology between their extracellular N-terminal motifs which have mainly adhesive roles. Except ADGRA1 (GPR123) from Group III, all the other aGPCRs have a GPCR proteolysis site (GPS) within the GPCR autoproteolysis–inducing (GAIN) domain. Most of these aGPCRs are auto-cleaved at the GPS site close to their 7 transmembrane domains, but their extracellular N-terminal fragment (NTF) remains attached to the rest of the receptor via non-covalent bonds (Hamann et al., 2015; Schiöth et al., 2010).

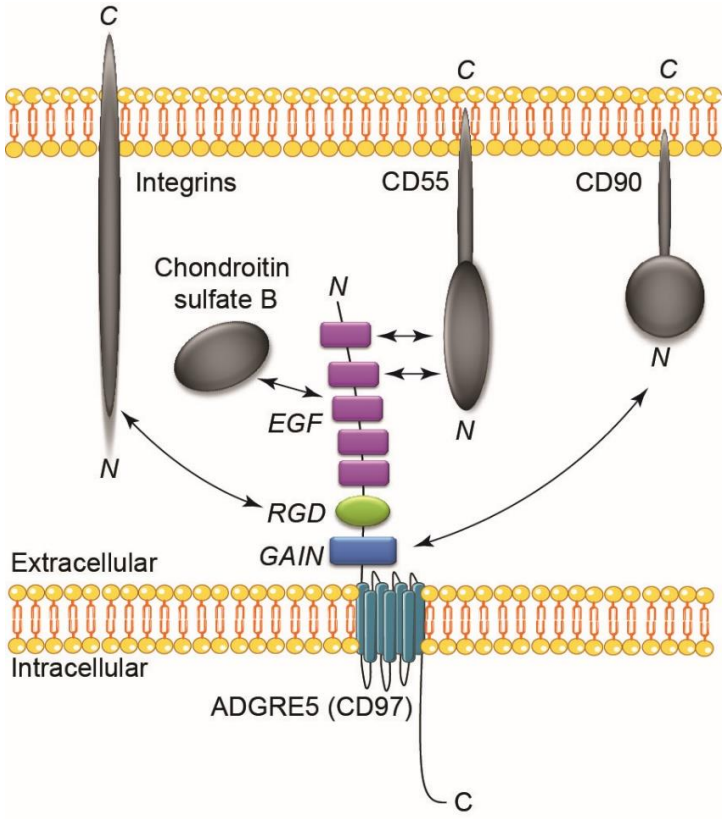

Figure 2. The schematic structure of ADGRE5 (CD97) and its interactome. Each interactor binds to a specific domain on the N-terminal fragment of CD97. Arrows show the domains that interact with each other. GAIN: GPCR autoproteolysis–inducing domain. RGD: Arg-Gly-Asp integrin-binding motif. EGF: epidermal growth factor like domain. *Adapted from* (Hamann et al., 2015).

The interactomes and ligands for most of aGPCRs are still unknown, but some of the so far deorphanized aGPCRs show interactions with several partners on either other cells (trans), the same ones (cis) or with the ECM (Hamann et al., 2015). This can be illustrated by *Adgre5* (CD97), the first and most known deorphanized aGPCRs (Figure 2) (Hamann et al., 2015, 1996). The first ligand for *Adgre5* (CD97) is CD55 discovered on all blood cells.

Adhesion assays show that COS cells expressing *Adgre5* (CD97) bind to CD55-expressing erythrocytes. Addition of antibodies against *Adgre5* (CD97) to the medium or using CD55-deficient erythrocytes prevents their binding to *Adgre5* (CD97)-expressing COS cells (Hamann et al., 1996). This interaction is limited in each species. It means that human CD97 binds only to human, but not mouse, CD55 and vice versa (Stacey et al., 2003). Using ligand-binding assays, the second interactor of *Adgre5* (CD97) was discovered to be chondroitin sulfate B, which binds to CD97 in a sulfation- and Ca^{2+}-dependent manner. In contrast with CD97-CD55 interaction, CD97-chondroitin sulfate B binding is conserved across species (Stacey et al., 2003). $\alpha_5\beta_1$ and $\alpha_v\beta_3$ integrins are the other ligands binding to Arg-Gly-Asp (RGD) sequence of CD97 extracellular N-terminal domain (Wang et al., 2005). *Adgre5* (CD97) can also interact with CD90 expressed on activated endothelial cells. This interaction happens via the GAIN-containing region of CD97 independent of calcium (Wandel et al., 2012). As we see, all these ligands bind to different motifs on the extracellular N-terminal domain of *Adgre5* (CD97) with their distinct domains (Hamann et al., 2015, 1996; Wandel et al., 2012; Wang et al., 2005).

aGPCRs are present on almost all the cells in mammals (Hamann et al., 2015). For example, *Adgre5* (CD97) is expressed in several cell types such as myocytes, epithelial, myeloid, lymphoid, placental and hematopoietic stem cells, but not in neurons or glial cells, in mouse and human (Hamann et al., 2015, 1996; Stacey et al., 2003). In the hematopoietic system, the level of CD97 in leukocytes can be regulated by one of its ligands expressed on leukocytes and stromal cells, CD55. In CD55-deficient mice, *Adgre5* (CD97) is overexpressed on the membrane of leukocytes. Exposure of CD55-deficient leukocytes to CD55 (for example by their transfer into WT mice) rapidly decreases CD97 expression on the cell surface but increases the level of CD97 NTF (soluble form of CD97) in the blood. The physical forces in the blood, due to blood stream, result in shedding of CD97 NTF from the rest of the receptor. In the absence of these physical forces, for example in the case of microglia, no shedding of CD97 NTF is observed (Karpus et al., 2013). These results show that in the tissue, where the physical forces such as shear stress is low, CD97-CD55 interaction helps CD97-expressing leukocytes stay in contact with the CD55-stromal cells. On the other hand, in blood circulation and in the presence of shear stress, CD97-CD55 interaction leads to downregulation of CD97 from cell surface of leukocytes, avoiding their aggregation in the blood vessels (Hamann et al., 2015; Karpus et al., 2013). The other role of CD97 is in the cardiovascular system. The NTF of CD97, either attached to or separate from the rest of the CD97, works as a chemoattractant and proangiogenic factor for endothelial cells such as human umbilical vein endothelial cells (HUVECs), via its interaction with integrins, to promote adhesion, migration and invasion of these cells (Wang et al., 2005). During inflammation, the activated endothelial cells express CD90, another ligand of CD97, on their membrane to recruit leukocytes to the

inflammatory site by directly binding to their CD97 (Wandel et al., 2012). Therefore, CD97 plays several roles in different tissues based on the interactor available in the environment.

On the other hand, there are some aGPCRs that are specific to one or few cell types (Hamann et al., 2015). For example, *Adgre1* (EMR1) which belongs to the same subfamily as *Adgre5* (CD97) (Subfamily II / E (EGF-TM7)) is considered as a marker for murine monocytes, macrophages and phagocytic cells in several tissues due to its restricted expression in these cells (Gordon et al., 2011). Surprisingly, the human ortholog of EMR1, ADGRE1, is specifically expressed in eosinophils, while no trace of its expression is found in macrophages and monocytes (Hamann et al., 2007). No function is suggested for the role of ADGRE1 (EMR1) in human, but in vitro experiment on the mouse ortholog, *Adgre1* suggests its binding to a potential receptor on natural killer cells leading to the interaction between monocytes and these cells in response to a bacterial infection. However, in vivo studies have shown that the migration and development of tissue macrophages are normal in *Adgre1* knockout mice. Both in vivo and in vitro experiments have shown the importance of *Adgre1* (EMR1) in the generation of antigen-specific efferent CD8+ regulatory T cells, which are involved in the inhibition of antigen-specific immunity, upon inoculation of antigen into the anterior chamber of the eye as a model for peripheral immune tolerance. These results show the importance of *Adgre1* (EMR1) in peripheral tolerance (Gordon et al., 2011; Hamann et al., 2016; Lin et al., 2005).

1.1.2. BAIs function in and outside the central nervous system:

Different types of cells in the nervous system express more than half of aGPCRs, showing their importance in the function, development, and integrity of this system. These aGPCRs play important roles in the control of neurulation, synapse formation, myelination, cortical development and other functions of the nervous system (Hamann et al., 2015; Sigoillot et al., 2016; Strokes and Piao, 2010). For example, latrophilin-1 (LPHN1) is member of the latrophilin subfamily of aGPCRs that is highly expressed in the nervous system (Hamann et al., 2015; Sigoillot et al., 2016). LPHN1 interacts with several ligands such as Teneurin 2 (TEN2), neurexin1α and 1β (NRX1α/1β), fibronectin leucine-rich transmembrane protein 3 (FLRT3), and Contactin-6 (Cntn6) in cis or trans to modulate neuronal survival/apoptosis, axon growth and synapse formation/stability (Boucard et al., 2014; Hamann et al., 2015; Sigoillot et al., 2016; Silva et al., 2011; Zuko et al., 2016). In this section, I will talk about the function and signaling pathways of brain-specific angiogenesis inhibitors (BAIs) and their ligands, Complement C1q-Like (C1QLs) subfamily.

1.1.2.1 *Adgrbs* (BAIs):

Brain-specific angiogenesis inhibitors (BAIs/*Adgrb*s) constitute a subfamily of aGPCRs found in vertebrates. Their NTF contains a GAIN domain adjacent to an HRM (similar to LPHNs), several (4 - 5) thrombospondin type 1 repeats (TSRs) and either a RGD sequence (only in BAI1) or a CUB (complement C1r/C1s, Uegf, Bmp1) domain (only in BAI3). In their intracellular domain, an α-helical RKR (Arg-Lys-Arg) motif and a terminal PDZ-binding motif (PBM) are observed in all the 3 members. A proline-rich region (PRR) is present in the BAI1 C-terminal domain (Figure 3) (Hamann et al., 2015; Moon et al., 2018; Sigoillot et al., 2016; Südhof, 2018).

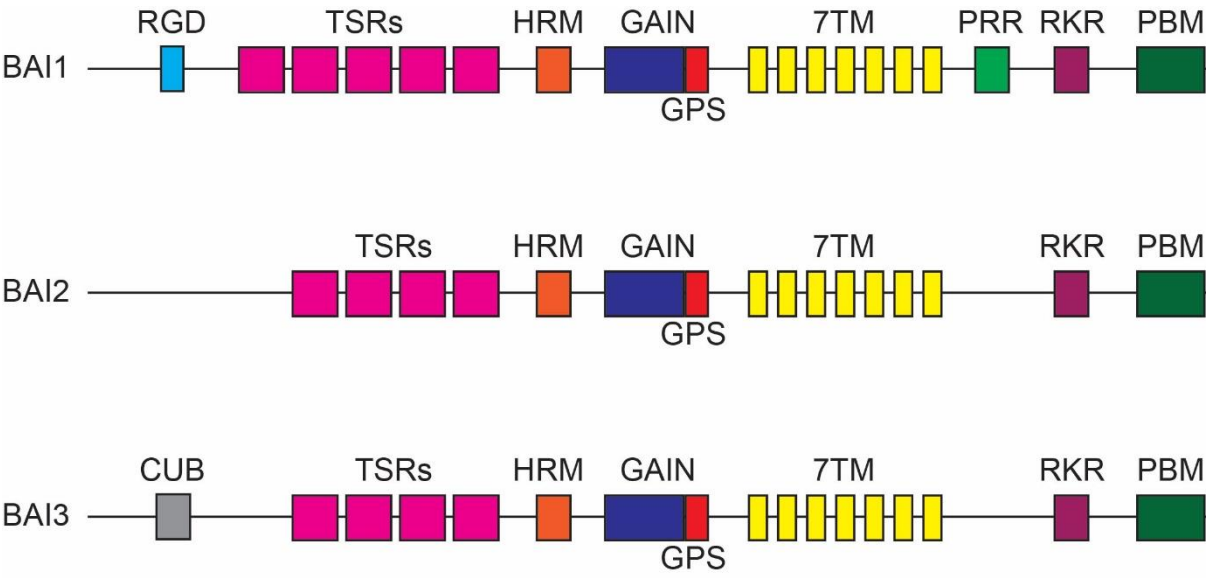

Figure 3. A schematic primary structure of BAIs in mammals. N-terminus (on the left) to C-terminal (on the right). RGD: Arg-Gly-Asp integrin-binding motif. TSR: thrombospondin type 1 repeat. HRM: hormone receptor motif. GAIN: GPCR autoproteolysis–inducing domain. GPS: GPCR proteolysis site. 7TM: 7-transmembrane domain. PPR: proline rich region. RKR: Arg-Lys-Arg motif. PBM: PDZ-binding motif. CUB: Complement C1r/C1s, Uegf, Bmp1) domain. *Adapted from* (Moon et al., 2018; Sigoillot et al., 2016).

BAIs play a role in both neural and non-neural processes. Non-neuronal functions of BAIs are very diverse and include other tissues than the nervous system (Figure 4). For example, BAI1 is involved in the recognition and phagocytosis of dead cells by macrophages shown by both in vitro (using macrophage cells lines) and in vivo engulfment assays. Apoptotic cells express phosphatidylserine on their surface, which binds directly to BAI1 TSRs region, leading to BAI1 intracellular interaction with ELMO and Dock180 to form a complex. This

complex works as a guanine nucleotide exchange factor (GEF) for the small GTPase Rac to trigger phagocytosis via modulation of the actin cytoskeleton (Park et al., 2007). BAIs are also involved in the recognition and phagocytosis of bacterial cells (via interaction of bacterial lipopolysaccharide (LPS) with BAI1 TSRs), inhibition of angiogenesis (via the 2-step cleavage of BAI1 NTF to release anti-angiogenic vasculostatin 40), and fusion of myoblast cells (via interaction of BAI1 and BAI3 with ELMO and Dock180) (Moon et al., 2018; Nair et al., 2021). The detailed mechanism of contribution of BAI3 in myoblast fusion has been shown in mice. Studies in cultured model of myoblast differentiation have shown the inhibitory effect of the interaction of BAI3 with its ligands, secreted C1QL1-4, on myoblast fusion. In vivo experiments on chicken embryos confirm these results. The association of C1q domain of C1QL4 with CUB domain in NTF of BAI3 is responsible for this inhibitory effect on myoblast fusion (Hamoud et al., 2018).

In the nervous system, BAIs are expressed by both neurons and glial cells, with different functions on the development and integrity of the tissue (J. Wang et al., 2021). The function of BAIs (except BAI2 which is a negative regulator of hippocampal neurogenesis (Okajima et al., 2011)) in the neurons is mainly known to be related to the formation of dendrites, spines and synapses, particularly during the early postnatal brain development (Sigoillot et al., 2016). This period corresponds with the maximal expression of the 3 members of BAIs in rodent brains (Koh et al., 2001, 2001; Sigoillot et al., 2016). BAI1 & 3 are enriched in the postsynaptic densities in the excitatory synapses. BAI3's interaction with ELMO and Dock180 regulates the actin cytoskeleton in the dendrites and control dendrite morphogenesis in the Purkinje cells (PCs) of the cerebellum (Lanoue et al., 2013). The excitatory synapses formed by climbing fibers from inferior olivary neurons on PCs are partially formed via the interaction of secreted C1QL1 from climbing fibers with BAI3 on PCs (Kakegawa et al., 2015; Sigoillot et al., 2015). Studies in cultured neurons as well as in vivo experiments have shown that projecting neurons from amygdala to medial prefrontal cortex release C1QL3 to interact with postsynaptic BAI3 to form or maintain excitatory synapses involved in fear and emotional memory (Martinelli et al., 2016). Studies on synaptosome preparations from adult mouse brains using western blot show the interaction of BAI1 with PSD95 and synaptophysin in postsynaptic densities via its PDZ-binding domain in its C-terminal (Stephenson et al., 2013). With its other cytosolic domains, BAI1 binds to $G\alpha_{12/13}$, PAR3/TIAM1, and BAIAP2 to activate several signaling molecules such as Rho GTPase, Rac1, and ERK, to regulate the formation and maintenance of dendritic spines, synapses and synaptic plasticity (Sigoillot et al., 2016; Stephenson et al., 2013).

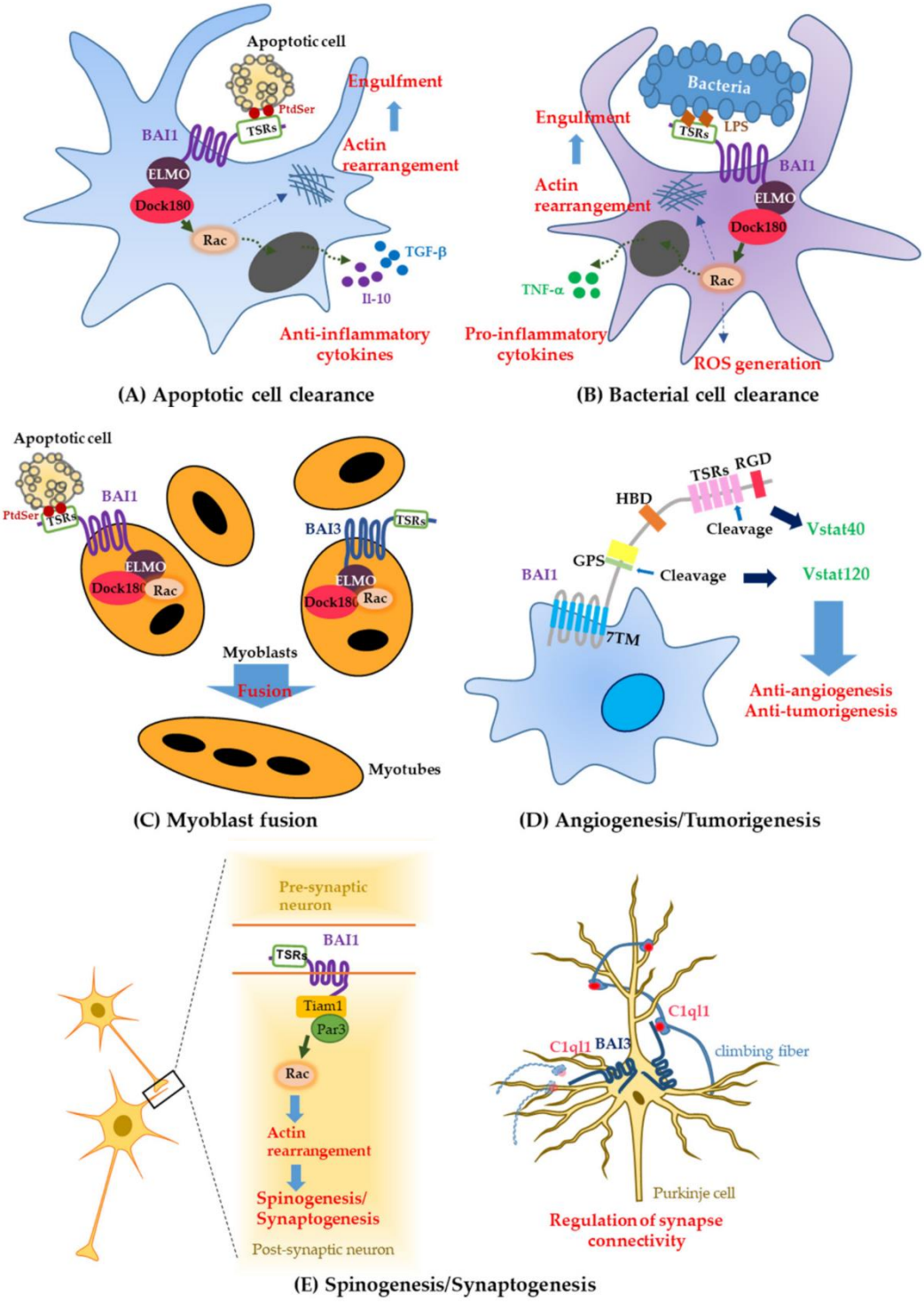

Figure 4. Different functions of the BAIs. BAI1 as a recognition and phagocytosis receptor to engulf dead cells and bacteria (A&B). BAI1 & 3 as the intermediates for fusion of myoblast (C). BAI1 as an inhibitor of tumor and blood vessel formation (D). BAI1 & 3 as synaptic organizers (E). *Taken from* (Moon et al., 2018).

C1QLs are not the only ligands of BAIs. RTN4/NoGo-Receptors (RTN4Rs) are CSPs found in neurons and recently discovered as new ligands for BAI1 & 3 using several approaches such as pull-down assay and crystallography (J. Wang et al., 2021). The interaction of RTN4Rs with BAIs expressed by postsynaptic neurons is involved in synaptogenesis and dendritic arborization, while their interaction with BAIs expressed by glial cells plays role in axon growth. In both cases, the leucine-rich repeat domain of RTN4Rs interact with one TSR domain of BAIs (J. Wang et al., 2021). Loss of function of RTN4Rs in human neurons co-cultured with mouse glial cells (from WT or BAIs-KO mice) shows a decrease in density and volume of excitatory synaptic boutons, several pre- and postsynaptic proteins, synaptic transmission, as well as an increase in dendritic arborization independent of BAIs in glial cells and an increase in axonal growth dependent of BAIs in glial cells. These observations suggest that the interaction of neuronal RTN4Rs with neuronal BAIs promotes synaptogenesis while inhibits dendritic arborization. On the other hand, their interaction with glial BAIs prevents axonal arborization and growth, confirming the “NoGo” title of these receptors (J. Wang et al., 2021). Even though the expression of BAIs had been reported in glial cells before, such as BAI1 in microglia and its role in regulation of phagocytosis of apoptotic neurons in the brain (Mazaheri et al., 2014), the interaction of RTN4Rs-BAIs is an example of cell surface mechanisms that is shared between neurons and glial cells with different developmental consequences.

1.1.2.2 The BAIs ligands C1QLs:

The secreted complement component 1, q subcomponent-like proteins (C1QLs) are a 4-member subfamily (C1QL1-4) belonging to the family of C1q complement proteins. C1q proteins are involved in the complement cascade of the innate immune system. The C1q family is divided to several other subfamilies which are found in different tissues. Two of them (C1QLs and CBLNs) are highly enriched in the nervous system and considered as synaptic organizers, molecules controlling different aspects of synapse formation, maintenance and function: CBLNs and C1QLs subfamilies (Yuzaki, 2017). The hallmark of all the C1q proteins is their C-terminal globular C1q domain (gC1q), involved in the trimer formation of C1QLs discovered via their crystal structures. They can form both homo and heteromers in vitro. C1QLs trimers can form higher-order oligomers via their two cysteine residues located after the signal peptide in the N-terminus. They also have a collagen-like sequence, which is found in some other C1q family proteins. C1QLs have several Ca^{2+} binding sites that control their stability (Figure 5) (Iijima et al., 2010; Ressl et al., 2015).

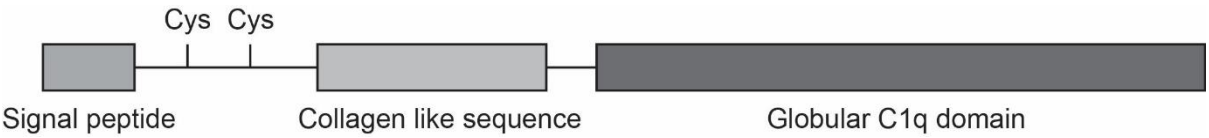

Figure 5. A schematic primary structure of C1QLs in mammal from N-terminus (on the left) to C-terminal (on the right). The length of each domain is set to the scale. The globular C1q domain (gC1q) is the largest domain with ~140 residues. Cys: cysteine residue. *Adapted from* (Ressl et al., 2015).

C1QLs are highly expressed in the CNS and adipose tissue. Some other tissues also express C1QLs in lower amounts in adult mice as shown by reverse transcriptase (RT)-PCR analysis: testis (*C1ql1* & *4*), liver, ovary and small intestine (*C1ql1*), kidney (*C1ql1*, *2* & *4*), and stomach (*C1ql4*) (Iijima et al., 2010; Yuzaki, 2017). Using *in situ* hybridization (ISH), the expression patterns of *C1qls* have been studied during mouse development and adulthood in the brain: the expression of *C1ql1* and *3* is observed at embryonic day 13 (E13) in the rhombencephalon, while *C1ql2* mRNA is detected few days later (E17) in the diencephalon. The expression of *C1ql4* is generally weak during development and adulthood. At P0 and P7, several regions of the brain, such as cerebral cortex, hippocampus and some nuclei in the brainstem (e.g. inferior olive (IO)) and midbrain, as well as the external granular layer (EGL) of the cerebellum express *C1ql1*. Some of these regions such as IO and ventral cochlear nucleus (VC) maintain the expression of *C1ql1* during adulthood, while regions such as EGL lose its expression during the 2nd postnatal week. From P14 until adulthood, *C1ql2* is expressed in the hippocampus, corpus callosum and anterior fissure. The expression of *C1ql3* increases from P7 and is found in the cerebral cortex, dentate gyrus of hippocampus, and deep cerebellar nuclei (Iijima et al., 2010; Sigoillot et al., 2015). Using Nissl-staining to label neurons and ISH, the expression of *C1qls* is confirmed in neurons. Since their expression is also found in some white matter, such as corpus callosum, it is suggested that glial cells also express *C1qls* (Iijima et al., 2010). In this study, no specific marker for different groups of glial cells was used to identify them for further analysis.

Since C1QLs are present both during development and adulthood in different types of cells and regions in the brain, it is possible that they may have several functions. The function that is very well characterized for C1QLs in the brain is their contribution in formation and maintenance of excitatory synapses (Bolliger et al., 2011; Kakegawa et al., 2015; Sigoillot et al., 2015; Yuzaki, 2017). BAI3 is the only receptor found so far for all the C1QLs in the brain using affinity chromatography and cell surface labeling assay. Using pull-down experiment on

HEK293 cells extract, it has been shown that the gC1q of C1QL3 interacts with a TSR domain of BAI3 in the brain (Bolliger et al., 2011). In myoblast cells, the gC1q of C1QL4 binds to the CUB domain of BAI3 to induce its inhibitory effect on their fusion (Hamoud et al., 2018). In another study, surface plasmon resonance (SPR) assays show that removal of CUB domain from BAI3 inhibits its binding to C1QL1 completely, while CUB domain alone has a lower affinity for C1QL1 in comparison with a full-length BAI3 (Ka = 0.3μM vs 2μM) (Kakegawa et al., 2015), suggesting the importance of other extracellular regions of BAI3 in increasing the affinity of CUB to this ligand. Since the localization of both C1QLs and BAI3 is enriched in neurons, the effect of their interaction has been investigated. Significant reduction in excitatory synaptic density is observed after administration of the recombinant C1QLs gC1q domains to neuronal culture from hippocampus without any change in other morphological characteristics. In the case of C1QL3, this effect is rescued by addition of recombinant thrombospondin repeats of BAI3 to the medium (Bolliger et al., 2011). As we mentioned in the previous section, binding of C1QL1 from presynaptic CFs to BAI3 of postsynaptic PCs is involved their excitatory synapse formation in vivo. Using an RNAi approach to knockdown *C1ql1* in inferior olivary neurons, the origin of CFs, in vivo or using a full *C1ql1* knockout mice show a reduction in the synaptic territory of CFs on PC dendrites, a decrease in the density of their synaptic puncta, and a weaker synaptic transmission as well as impaired synaptic plasticity and motor learning. All these results demonstrate the importance of C1QL1-BAI3 interaction in the formation, stability and integrity of CF-PC synapses (Kakegawa et al., 2015; Sigoillot et al., 2015). C1QL3 is another member of C1QL family which, similar to C1QL1, binds to BAI3 in vivo and promotes synapse formation and stability, as mentioned in the previous section. Using constitutive knockout of *C1ql3*, it has been shown that lack of C1QL3 in the basolateral amygdala projecting neurons to medial prefrontal cortex results in a decrease in excitatory synapse numbers, while no effect on inhibitory synapses is observed (Martinelli et al., 2016). All these results show the importance of C1QLs-BAI3 interaction in synapse organization, but no other function has been attributed so far to this interaction in the brain.

1.2. Receptor Tyrosine kinases:

Receptor tyrosine kinases (RTKs) are a family of cell surface receptors evolutionary conserved from nematodes to humans, necessary for several cell functions such as survival, migration, division, differentiation, and metabolism. They are divided into 20 classes with similar structure (Figure 6): an extracellular region containing different domains interacting with ligands, a single transmembrane domain, and an intracellular region which includes the protein tyrosine kinase domain and juxtamembrane regulatory sequences. Generally, RTKs

are monomers in their inactive state. Binding of the ligand results in their dimerization/oligomerization and activates their intracellular tyrosine kinase domain which phosphorylates tyrosine residues on each other cytosolic domains. Then, the dimerized phosphorylated RTK trigger several signaling pathways by recruiting and phosphorylating other signaling molecules (Lemmon and Schlessinger, 2010).

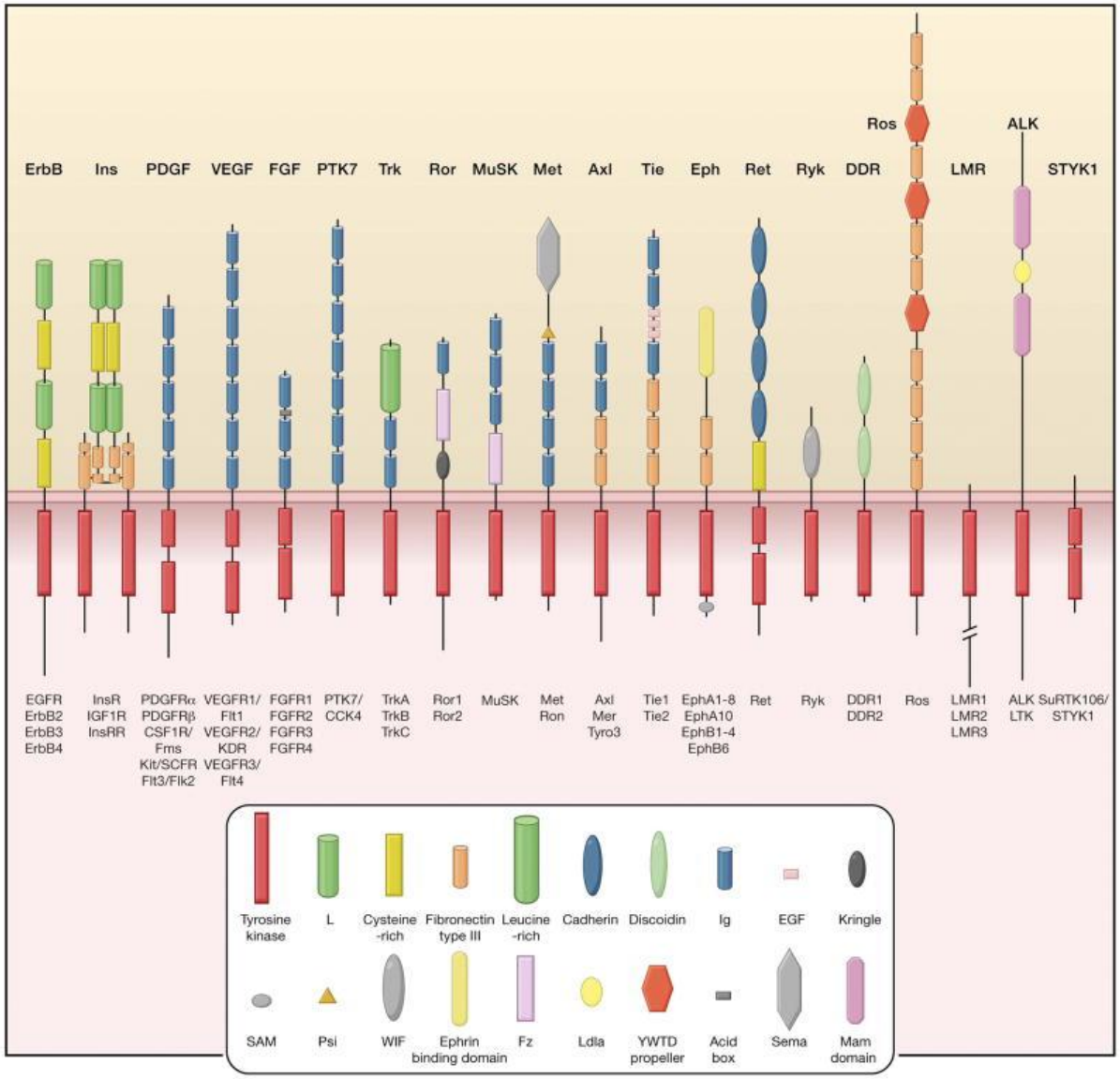

Figure 6. The 20 classes of receptor tyrosine kinases in human. The members of each subfamily are listed below each receptor. Class I to XX from left to right. c-KIT is in the class III (PDGF). *Taken from* (Lemmon and Schlessinger, 2010).

RTKs can play different roles in various tissues. For example, Eph receptors and their membrane-bound ligands, ephrins, are highly expressed in the brain, immune system, pancreas and bones. In the nervous system, Eph receptors and ephrins are involved in synapse formation, establishment of topographic interactions between two neuronal populations and neuronal-glial communication, while in immune system they play a role in the survival and maturation of T cells. In pancreas, they contribute to glucose homeostasis (Pasquale, 2008; Triplett and Feldheim, 2012). In the next section, I will focus on another RTK whose function is not very well known in the nervous system: c-KIT.

1.2.1. **c-KIT & SCF:**

c-KIT is a member of the platelet-derived growth factor (PDGF) receptor subfamily of RTKs, encoded by the murine white spotting (*w*) locus. c-KIT plays critical roles in gametogenesis (both oogenesis and spermatogenesis), melanogenesis and hematopoiesis. It has five immunoglobulin-like sequences in its external region, followed by a transmembrane sequence, a ~30-amino acid juxtamembrane domain, and two tyrosine kinase subdomains separated by a ~80-amino acid kinase insert domain in the cytosolic region (Figure 7). The ligand of c-KIT is called stem cell factor (SCF), encoded by the steel (*Sl*) locus on mouse chromosome 10. SCF has two isoforms: soluble or transmembrane, regulated at both the mRNA and the protein levels. The two isoforms are only different in Exon 6. The longer isoform with 248 residues containing Exon 6 is cleaved by some proteases at the membrane to produce a 165-residue soluble SCF. The shorter isoform with 220 residues stays as a transmembrane CSP. Both soluble and membrane SCF generate homodimers via noncovalent bonds (Figure 8). The homodimer of SCF interacts with the first 3 Ig-like domains of two c-KIT monomers, bringing them close to each other, so the last two Ig-like domains (4 & 5) bind together to form a c-KIT homodimer. Subsequently, each kinase domain phosphorylates several tyrosine residues on different intracellular regions of the adjacent c-KIT to activate the homodimer. The activated c-KIT homodimer triggers several signaling pathways such as mitogen-activated protein (MAP) kinases, phosphatidylinositol 3'-kinases (PI3'-kinases), Src family kinases, and phospholipases, to regulate the various processes within the cell (Huang et al., 1990; Lemmon and Schlessinger, 2010; Lennartsson and Rönnstrand, 2012).

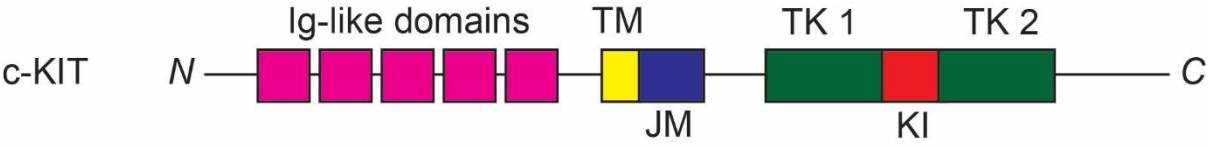

Figure 7. A schematic primary structure of c-KIT in mouse/human. The N-terminal region is located extracellularly and the C-terminal region intracellularly. TM: transmembrane domain. JM: juxtamembrane domain. TK1/2: tyrosine kinase subdomain 1/2. KI: kinase insert domain. *Adapted from* (Lennartsson and Rönnstrand, 2012).

1.2.2. **c-KIT & SCF in the brain:**

The expression of *c-Kit* and *Scf* is observed from embryonic development to adulthood in rodent's brains. Using ISH in the adult rat brain, the expression of *c-Kit* is found in the forebrain (e.g. olfactory bulb, striatum, cerebral cortex, and several other regions), the brainstem (e.g. inferior colliculus and the spinal vestibular nucleus), and the cerebellum (e.g. deep cerebellar nuclei and molecular layer of the cerebellar cortex). Using the same technique, the mRNA of *Scf* is detected in the forebrain (e.g. olfactory bulb and thalamus) and the cerebellum (in PCs). Since several of these regions expressing either *c-Kit* or *Scf* connect to each other, it is suggested that the interaction between these two molecules contributes to the establishment of the connectivity between the neuronal populations (Guijarro et al., 2013; Hirota et al., 1992).

Although the expression of *c-Kit* and *Scf* has been described more than 2 decades ago in the brain, their role in the development and function of nervous system is not very well known. In one study, the role of tyrosine kinase activity of c-KIT was investigated in hippocampal synaptic potentiation, spatial learning and memory using *c-Kit* mutant rats with a very low tyrosine kinase activity (Katafuchi et al., 2000). c-KIT and SCF immunostainings is observed in one of the pathways of hippocampus that is involved in spatial learning and memory. In these mutant rats, the spatial learning is impaired as shown by the Morris water maze test, and synaptic potentiation measured by patch clamp is decreased, suggesting a role for tyrosine kinase activity of c-KIT in synaptic function (Katafuchi et al., 2000). In another study, the proliferative effect of SCF in neurogenesis is shown both in vitro and in vivo. Via this effect of SCF, hypoxia induces cell division in mouse cortical cultures. The secretion of SCF is directly correlated with the period of hypoxia. Using immunostaining, the localization of c-KIT is observed in neuroproliferative zones in the rat brain. Intraventricular injection of SCF in the rat brain increased the number of proliferative neurons in these zones labeled by BrdU and NeuN (the marker for proliferation and neurons, respectively), suggesting the contribution of c-KIT/SCF signaling in neurogenesis (Jin et al., 2002). SCF not only has stimulatory effect on

proliferation, but also induces migration of neural stem/progenitor cell (NSPC) toward the injured location in the brain. Both in vitro and in vivo approaches have shown that neurons in the injury zone overexpress SCF which interacts with c-KIT localized on the surface of NSPCs, triggers its tyrosine kinase activity, in order to induce their migration toward the site of damage (Sun et al., 2004). Embryonic knockdown of *c-Kit* in rat brain using in utero electroporation, or specific knockout of *c-Kit* in mouse brain cortical neurons using Cre lox system, slows down the radial migration of neurons in the cortex in a SCF-dependent manner, while overexpression of *c-Kit* in these cortical neurons speeds up this process during development. On the other hand, c-KIT is critically involved in the connectivity of callosal fibers to their targets within the contralateral cortex independent of SCF (Guijarro et al., 2013).

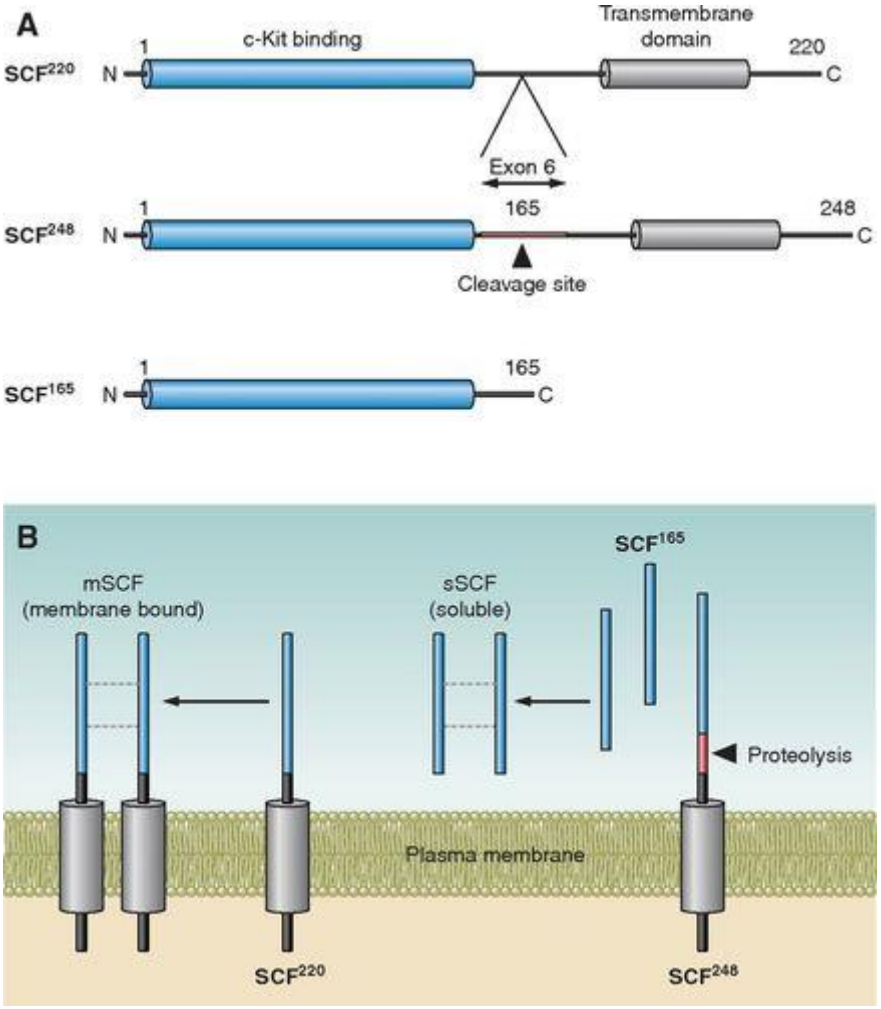

Figure 8. A schematic primary structure of SCF isoforms and its cleavage. A) Two membrane-bound isoforms of SCF are generated via alternative splicing of Exon 6. B) Cleavage of the larger isoform at the cell surface generates soluble SCF, while the shorter isoform stays as membrane bound. The dashed lines represent the noncovalent bonds. *Taken from* (Lennartsson and Rönnstrand, 2012).

In the cerebellum of adult rats, protein expression of c-KIT is detected in the axons of basket cells using 3,3′-Diaminobenzidine (DAB) immunostaining. Basket cells are one type of inhibitory interneurons in the molecular layer of cerebellar cortex, that wrap around the axon initial segments of PCs in the cerebellar cortex to make inhibitory synapses in a structure called pinceau. Using the same staining technique, the protein expression of SCF is observed in the postsynaptic partner of basket cells, PCs, suggesting a role for c-KIT/SCF signaling in connectivity between these two neuronal populations. Acute systemic injection of kainic acid (KA) to stimulate neuronal activity in adult rats has shown transient upregulation of c-KIT and SCF in the cerebellar extracts 24-48 hours after injection, as well as a change in the localization of SCF in the PCs. In control condition, SCF is mainly localized in the dendritic tree and soma of PCs, while it mainly moves to the axon of PCs 24-48 hour after KA-induced neuronal activity (Kim et al., 2003). All these results suggest a potential role for c-KIT/SCF in connectivity between basket cells and PCs, which could be modulated by neuronal activity. No data is available regarding the role of this interaction in synapse formation during development.

2. PART 2: The cerebellar cortex as a model to study neuronal connectivity:

2.1. Cytoarchitecture of the cerebellar cortex:

The cerebellum is at the center of motor learning and movement coordination and its stereotyped architecture is very well known (Figure 9). The cerebellar cortex receives several afferents from different regions of the brain. Two of the main afferents are called mossy fibers (MFs) and climbing fibers (CFs). MFs are coming from several nuclei in the brainstem and spinal cord, transferring cortical and peripheral information to the granule cells in the cerebellar cortex via glutamatergic connections. CFs are the axons of inferior olivary neurons (IONs) located in the inferior olive in the brainstem who make excitatory synapses on the Purkinje cells (PCs) in the cortex of cerebellum. The inhibitory PCs at the heart of function of the cerebellum, are the only output of the cerebellar cortex, targeting deep cerebellar nuclei located in the white matter of the cerebellum. PCs receive several excitatory and inhibitory inputs. In addition to CFs, PCs receive excitatory inputs from parallel fibers (PFs) coming from granule cells in the cortex of cerebellum, which convey the information from MFs (Grangeray et al., 2016; Reeber et al., 2013; Yamada and Hoshino, 2016).

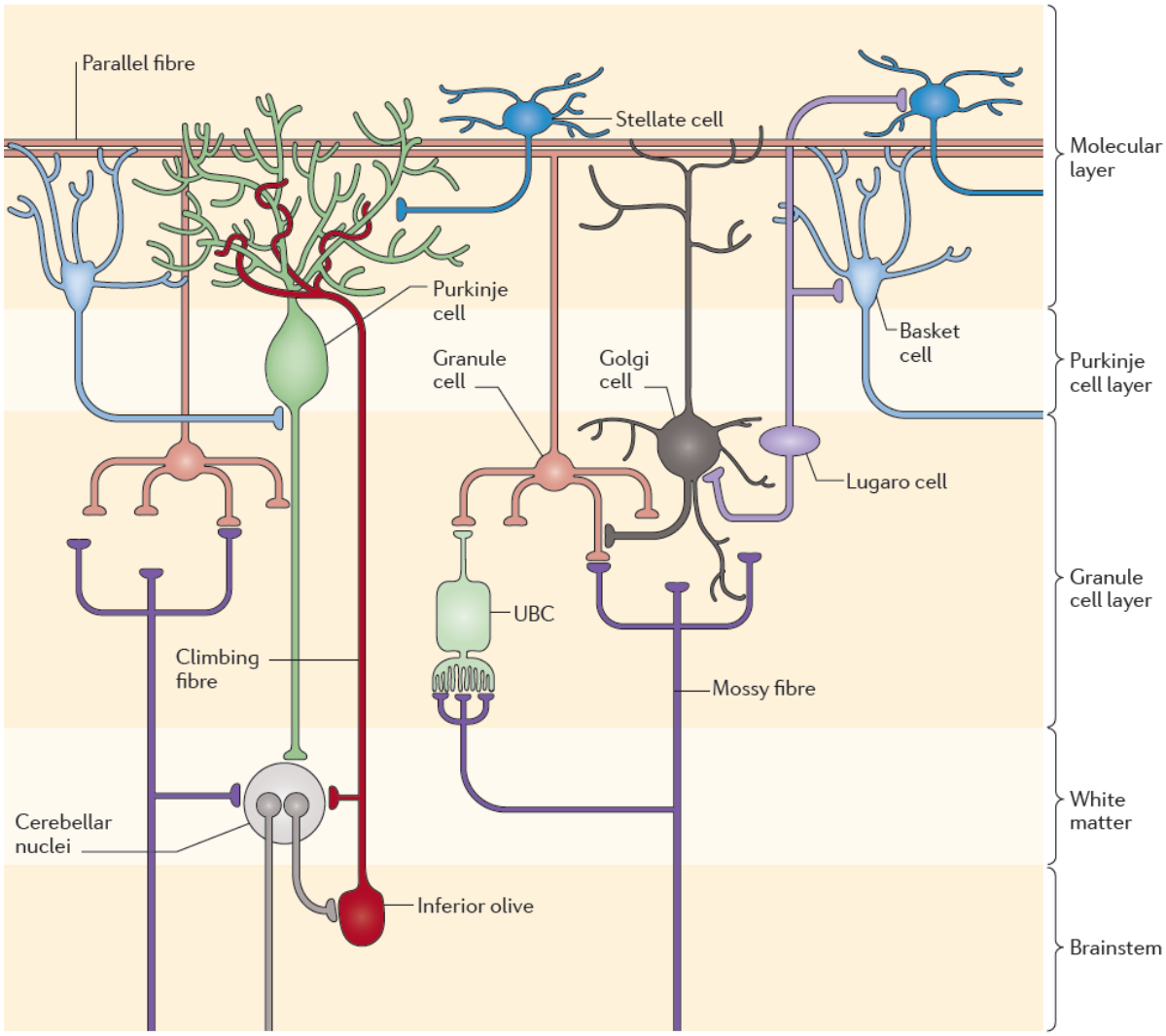

Figure 9. A schematic cytoarchitecture of the cerebellum and olivocerebellar circuit. All different types of excitatory and inhibitory neurons in the cerebellum are represented. UBS: unipolar brush cells. *Taken from* (Cerminara et al., 2015).

PCs also receive inhibitory inputs from the two GABAergic interneurons located in the molecular layer of the cerebellar cortex, the area where the dendritic trees of PCs reside: stellate and basket cells. Stellate cells are found in the top two-thirds of the molecular layer and project to PC dendrites. They receive excitatory input from CFs and PFs and inhibitory inputs from other molecular layer interneurons (MLIs) to control the activity of PCs. They also connect to each other via gap junctions to temporally synchronize their neuronal activity (Cerminara et al., 2015; Liu and Dubois, 2016). Basket cells are found in the deep one-third of the molecular layer, connect to the cell body of PCs and form an upside-down cone-shaped structure around their axon initial segment (AIS) called pinceau. Via inhibitory synapses, passive electrical inhibition or both in the pinceau, basket cells control the output of PCs. Similar to stellate cells, basket cells receive inhibitory input from both stellate and basket cells, as well as recurrent PC axons. PFs also make glutamatergic synapses on basket cells. Basket cells can be activated by the spillover of glutamate from CF excitatory synapses (Cerminara et al., 2015; Watanabe, 2016).

There are other interneurons in the cortex of cerebellum, but they do not project to PCs. One of them is Golgi cells, located in the granule cell layer of the cerebellar cortex, and the only inhibitory input into granule cells. Golgi cells are known for their long dendrites passing through the molecular layer until the pial surface, where they receive excitatory inputs from PFs. They also receive excitatory afferents directly on their soma and dendrites in the granule cell layer from axons of granule cells as well as MFs. Via their dendrites in their molecular layer, Golgi cells receive inhibitory input only from Lugaro cells (Dieudonné, 2016). Lugaro cells are glycinergic/GABAergic interneurons located in the granule cell and PC layers, extending their dendrites in the granule cell layer, while sending their axons to connect with the stellate, basket and Golgi cells. They receive GABAergic input from PCs via their recurrent axons, and it is suggested that Lugaro cells received excitatory input from MFs (Hirono, 2016). The last group of interneurons are unipolar brush cells (UBCs). UBCs are excitatory interneurons found in granule cell layer, receiving afferents from MFs that convey vestibular information. They contact granule cells (Martina and Sekerková, 2016).

2.2. Development of the cerebellar cortex:

Similar to its cytoarchitecture, the development of the cerebellum is well described in the literature, and provides a popular model for investigating development of neuronal circuits and connectivity. In mouse, it starts at E8.5 from a region at the boundary between midbrain and hindbrain by protruding two symmetrical bulges which fuse together within a few days to form the vermis and two hemispheres. Meanwhile, two germinative zones are formed which disappear at birth. One in the rhombic lip (RL), is characterized by the expression of transcription factor ATOH1, and gives rise to all the glutamatergic neurons in the cerebellum such as granule cell and UBCs. The other one in the ventricular zone (VZ), is expressing the pancreas transcription factor 1-a (PTF1A), and gives rise to all the GABAergic neurons in the cerebellum (e.g. PCs and MLIs). The granule cell progenitors from RL migrate at E13.5 along the pial surface of the cerebellum, where they generate the external granular layer (EGL) at E16, while the dividing precursor cells from VZ move into the prospective white matter of the cerebellum to generate GABAergic neurons in a two-step process. In the first step, PCs and deep cerebellar nuclei neurons projecting to inferior olive are generated locally. In the second step, some precursor cells migrate to the cortex of the cerebellum while getting the identities of interneurons. PCs are generated between E11-13, move radially towards the future cerebellar cortex within a few days to make the PC layer. At this stage, PC layer is composed of several layer of PCs (multi-cell thickness). Subsequently, they all align with each other and form a single-cell layer during the first postnatal week. The progenitors of inhibitory interneurons are formed at E12 and later in the VZ. They start to express the transcription factor *Pax2*, move into the cortex of the cerebellum and proliferate into the inhibitory interneurons during the late embryonic period until the second postnatal week with the peak of generation at P5. The interneurons in the deep cerebellar nuclei are the first to be generated, then granule cell layer interneurons (Lugaro and Golgi cells), and finally MLIs (basket and stellate cells) (Hoshino, 2016; Leto et al., 2016).

The cortical circuits in the cerebellum and their synapses are formed postnatally (Figures 10 & 11), but not homogeneously in all the lobules. Different lobules organize the circuits at different speed, but all of them mature before the end of the fourth postnatal week. CFs are the first afferents and start to form their synapses on perisomatic protrusions coming out of PC cell bodies at birth. At this stage, several CFs target one PC with the same synaptic strength, but within one week, one of them wins the competition for synaptic territory, is strenghtened, and translocates its synapses to the growing proximal dendrites of the target PC, while the other CFs lose their contacts within a two-step process: early and late steps of CF synapse elimination. The early step starts from P7, independent of granule cells formation and PF-PC synaptogenesis. It is suggested that neuronal activity plays an important role in this step. The late step starts at around P12. The excitatory and inhibitory synapses from PF

and basket cells on PCs are critical for this step. PFs are the second excitatory synapses formed on distal dendrites of PCs from P6 to the fourth postnatal week in an inside-out manner. In another word, the PFs closer to PC somata are formed earlier than the others. The PF-PC synaptogenesis peaks during the second postnatal week. Basket cells start to innervate PC soma around P7 and form the pinceau around AIS of PCs around P9 which matures until the end of the 3rd postnatal week. The axons of the basket cells are actively involved in the second step of CF synapse elimination from the PC soma during the pinceau maturation. The inhibitory synapses from stellate cells are formed later than basket cells synapses, arrived to their peak during the end of the second postnatal week (K. Hashimoto et al., 2016; Sassoè-Pognetto, 2016). Even though great works have been done so far to describe the details of the connectivity between different types of neurons in the cerebellar cortex, there are still several aspects of this complex system that remained unknown. One of these aspects is the molecular mechanisms involved in topographical organization of olivocerebellar circuit.

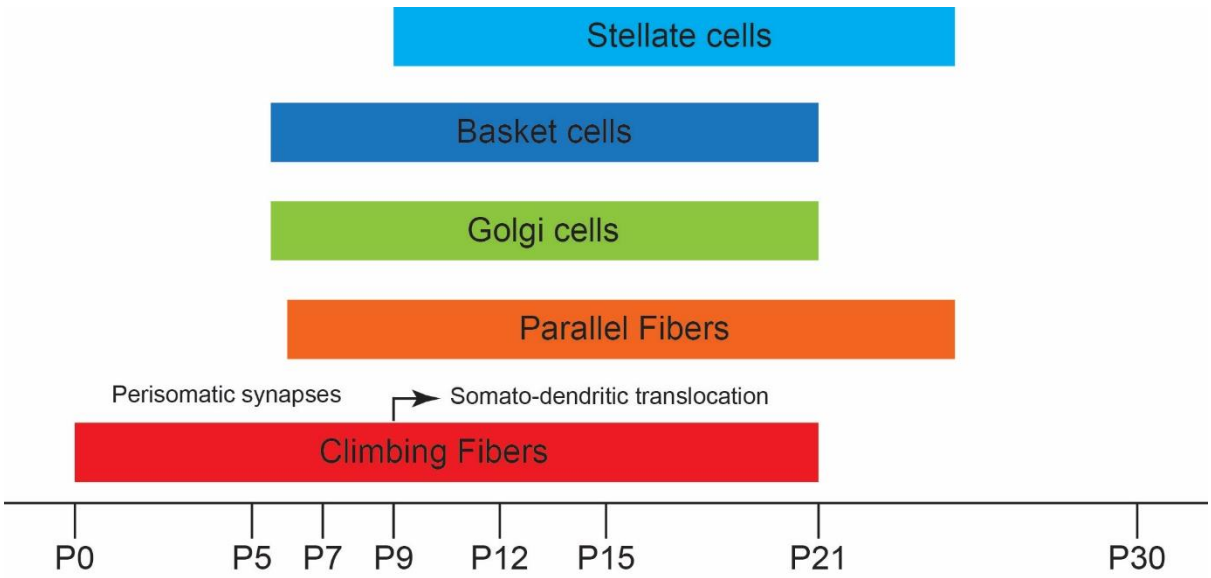

Figure 10. Timetable of development of synapse formation in the cerebellar cortex during the first four postnatal weeks. *Adapted and modified from* (Sassoè-Pognetto, 2016).

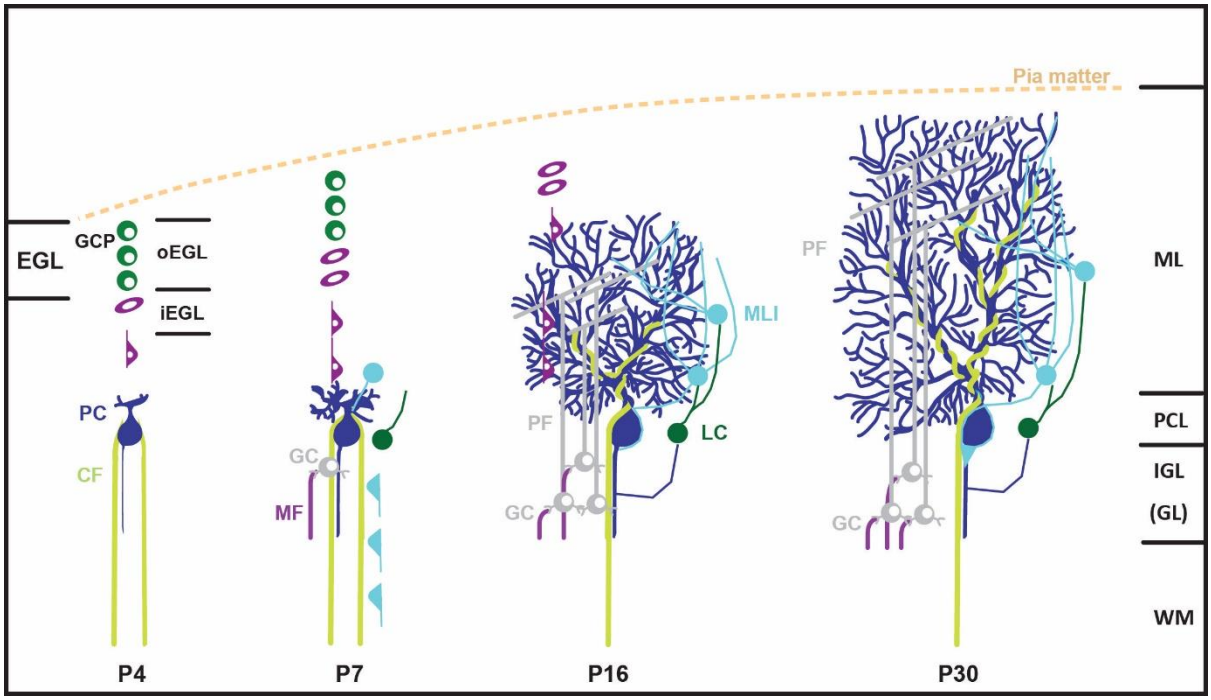

Figure 11. The schematic representation of postnatal development of the cerebellar cortex. CF: climbing fiber. PC: Purkinje cell. GCP: granule cell progenitor. MF: mossy fiber. PF: parallel fiber. GC: granule cell. GL: Granular layer. LC: Lugaro cell. ML: molecular layer. MLI: ML interneuron. PCL: PC layer. EGL: external granular layer. IGL: internal granular layer. WM: white matter.

2.3. Olivocerebellar topographical organization:

Topographical organization, the relative ordered arrangements of cellular connections between two areas, is one of the main characteristics of vertebrate brains (Thivierge and Marcus, 2007), and is observed in sensory projections to the brain (McLaughlin and O'Leary, 2005; O'Leary et al., 1999), in motor cortex (Aflalo and Graziano, 2006), in non-sensory/motor regions such as entorhinal-hippocampal circuit (Tamamaki and Nojyo, 1995), and in the cerebellum (Sugihara and Shinoda, 2007, 2004).

The circuitry of the cerebellum is made of parallel anatomical-functional modules organized parasagittally, controlling for example different motor groups. In each module, IONs in the brainstem project to PCs in the cerebellar cortex through topographically organized sets of CFs (Chaumont et al., 2013; Reeber et al., 2013; Sugihara and Shinoda, 2007, 2004; Voogd and Glickstein, 1998). The development of the cerebellar modules is a complex process dependent on activity and genetic mechanisms (Reeber et al., 2013; Sillitoe and Joyner, 2007). A broad topography is established by mainly genetic factors at birth (Chédotal et al., 1997; Reeber et al., 2013; Sotelo et al., 1984), and transformed to the refined adult map during postnatal development (Sillitoe and Hawkes, 2013). In parallel to the establishment of this

topographical map, PCs become organized in molecular stripes/zones characterized by the differential expression of molecular markers such as Zebrin II (Aldolase C / AldC) or phospholipase C β4 (PLCβ4) (Sillitoe and Hawkes, 2013). Since a PC is labelled with either AldC or PLCβ4, not both at the same time, they are used as markers of topographical patterning in the cerebellar cortex (Reeber et al., 2013). Similar to these two markers, some other molecules such as several members of Eph family, Cadherins and Protocadherins, have been discovered to be differentially expressed in IONs and suggested as markers for olivocerebellar topography (Reeber et al., 2013). For example, cell adhesion molecule protocadherin 10 (PCDH10) is found in some parts of IO as well as some $AldC^{+}$ PCs. Olivocerebellar axonal labelling shows that the $Pcdh10^{+}$ IONs project to $Pcdh10^{+}$ PCs, suggesting *Pcdh10* as a molecular marker for the topography of a subset of olivocerebellar tracts. However, no functional role has been shown for PCDH10 in this organization yet (Sarpong et al., 2018). Thus, the molecular mechanisms responsible for the establishment of olivocerebellar topography remain to be deciphered.

3. PART 3: Oligodendrocyte precursor cells (OPCs) and their general characteristics:

Named “Cell of all trades” in a review article by Akay et al. (Akay et al., 2021) or as I would like to call them “a cell for all seasons of the brain”, Oligodendrocyte (OL) precursor cells (OPCs) are one of the glial cell types (e.g. astrocytes, OLs, microglia, etc) in the brain and spinal cord tiling the tissue from late embryonic time to the end of adult age (Dawson et al., 2003). Also called NG2 cells or polydendrocytes (Hill and Nishiyama, 2014), OPCs constitute ~5% of all cells in the central nervous system during development and adulthood (~3% in the gray matter and ~9% in the white matter). In the adult brain, they are the main proliferative cells. OPCs all express neural/glial antigen 2 (NG2, chondroitin sulfate proteoglycan 4 (*Cspg4*)) and platelet-derived growth factor receptor A (PDGFRa), and lose this expression when they differentiate into OLs (Dawson et al., 2003; Rivers et al., 2008). However, several aspects of OPCs show their heterogeneity.

The diversity in morphology is the first aspect of OPCs where their heterogeneity is apparent (Figure 12). In general, OPCs have an irregular soma, with several branched extensions. Numerous bouton-shaped structures are observed at the end or along the extensions of OPCs, which may show the site of connections with neurons. In the gray matter of rodents (Figure 12A-E), OPCs usually have a star-shape soma with the extended processes radiating toward all the directions, while in their white matter (Figure 12G-I), they have elongated cell bodies squeezed between the myelinated fibers with more organized extensions that are parallel to the axons (Dawson et al., 2003). In zebrafish spinal cord, OPCs can be divided into two groups, based on the position of their soma in the medial (neuron rich) or lateral (axo-dendritic) part of the tissue. The first group has an elaborate network of extensions, while the second group has less complex arborization. Even though the extensions of both groups are found in the lateral part of spinal cord, these OPCs have distinct shapes/sizes and the motility of their extensions are different. The OPCs located in the axo-dendritic part of the spinal cord move their processes entirely within one hour, while the other group only remodels the tips of their extensions (Marisca et al., 2020). In general, OPCs have different morphologies, sizes and dynamics based on the region they are located in.

As we can guess from the title given by Akay et al. to OPCs (cell of all trades), these cells have various roles in the brain, such as OL generation and contribution to myelination, immunomodulatory, synaptic and vascular functions (Akay et al., 2021). The diversity of OPCs is not restricted to their functions or morphologies, but also extends to their origin and development (Bergles and Richardson, 2016), their transcriptomes (Marques et al., 2016), the diversity of ion channels and receptors they express (Spitzer et al., 2019), and their sensitivity

to external signals (van Tilborg et al., 2018). Overall, OPCs are a heterogeneous population in different biological aspects (van Tilborg et al., 2018).

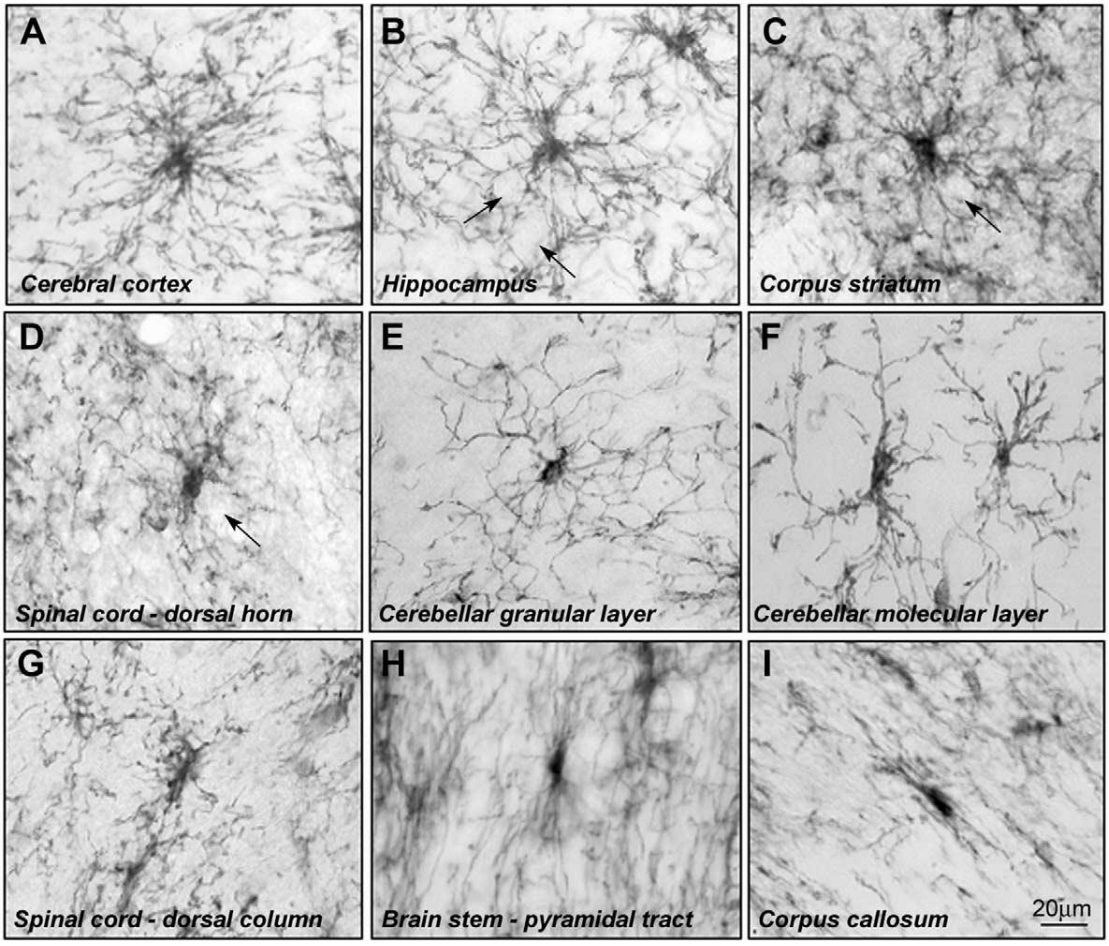

Figure 12. Diverse morphologies of OPCs according to their brain location. OPCs were immunolabelled with NG2 in several regions of the adult rat brain and spinal cord. Arrows point to the location of neuronal somata in B, C, and D. *Taken from* (Dawson et al., 2003).

3.1. Diversity in the developmental origin:

In rodents, the generation of OPCs starts from embryonic day 11.5–12.5 (E11.5 – E12.5), depending on the brain region, via several sequential waves of different origins which are all generated by P0 (van Tilborg et al., 2018) (Figure 13). At the end of the first postnatal week, the number of OPCs peaks, and then gradually decreases and stabilizes before P90. Their differentiation rate into OLs also changes during this period: the maximum level is at P14-21, and then the rate gradually declines within one year (Figure 14) (Nishiyama et al., 2021). To better understand the developmental origin of OPCs and their dynamics, I will focus

on three regions of the central nervous system, where the development of OPCs have been well studied (van Tilborg et al., 2018).

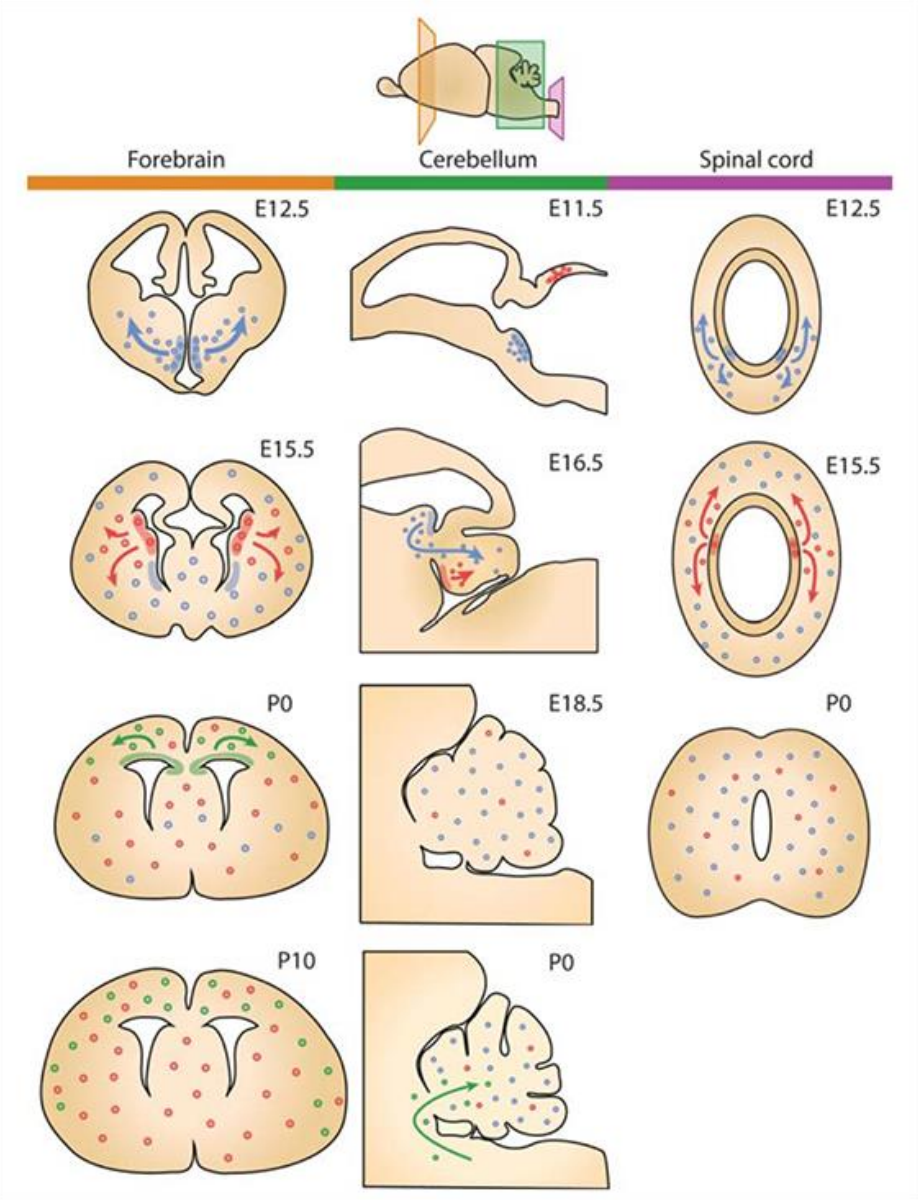

Figure 13. Scheme showing the different waves of OPCs generation and their time points in the forebrain, cerebellum and spinal cord. The arrows show the migratory path of each wave. *Taken from* (van Tilborg et al., 2018).

3.1.1. **Development of OPCs in the forebrain:**

The development of OPCs in the forebrain happens via three sequential waves of generation. The first wave appears at around E12.5 from *Nkx2.1*-expressing precursors in the ventricular zone of the ventral forebrain (medial ganglionic eminence (MGE) and anterior entopeduncular area (AEP)). The first OPCs occupy all regions of the forebrain within a few

days. The second wave of OPCs coming from *Gsh2*-positive precursors in the lateral and caudal ganglionic eminences (LGE and CGE) appears at ~E15.5 and migrates to all regions of the forebrain. The last wave of OPCs originates from *Emx1*-expressing cortical precursors at birth. During postnatal development, the OPCs from the first wave disappear gradually from the forebrain, leaving their territory to other OPCs from forebrain or diencephalon (Kessaris et al., 2006). Thus, the OPCs are not only different in their sites of origin, but also in their genetic lineage with progenitors identified by different molecular markers (e.g. *Nkx2.1*, *Gsh2*, and *Emx1*).

3.1.2. **Development of OPCs in the cerebellum:**

Similar to what is observed in the forebrain, the development of oligodendroglia in the cerebellum happens via three sequential waves (van Tilborg et al., 2018). The majority of cerebellar OPCs arise from the first wave. The first OPCs arise from *Olig2*-expressing neuroepithelial cells in the metencephalic ventral rhombomere 1 region in the extracerebellar ventricular zones at ~E11.5 and arrive to the cerebellum at E16.5. The second wave of OPCs, making up only 6% of cerebellar OPCs, comes from the cerebellar ventricular zone at E16.5. These two waves populate the whole cerebellum at E18.5 (Grimaldi et al., 2009; R. Hashimoto et al., 2016; van Tilborg et al., 2018). The last wave of OPCs originate from subependymal layers of the 4th ventricle postnatally and enter in the cerebellum through the superior medullary velum and peduncles (Reynolds and Wilkin, 1988).

3.1.3. **Development of OPCs in the spinal cord:**

There are two embryonic streams of OPCs emerging sequentially from the ventral to the dorsal axis and that make the oligodendroglia population in the spinal cord. The first OPCs are generated at ~E12.5 from the ventral ventricular zone of the spinal cord in a Sonic Hedgehog (SHH)-dependent manner. They are distributed uniformly in the whole spinal cord and constitute 80 % of the total OPCs at P0. The second wave of OPCs is generated at ~E15.5 from the dorsal ventricular zone in a SHH-insensitive mode and populates mainly the dorsal regions of the spinal cord, constituting the remaining 20% of OPCs by birth (Tripathi et al., 2011; van Tilborg et al., 2018).

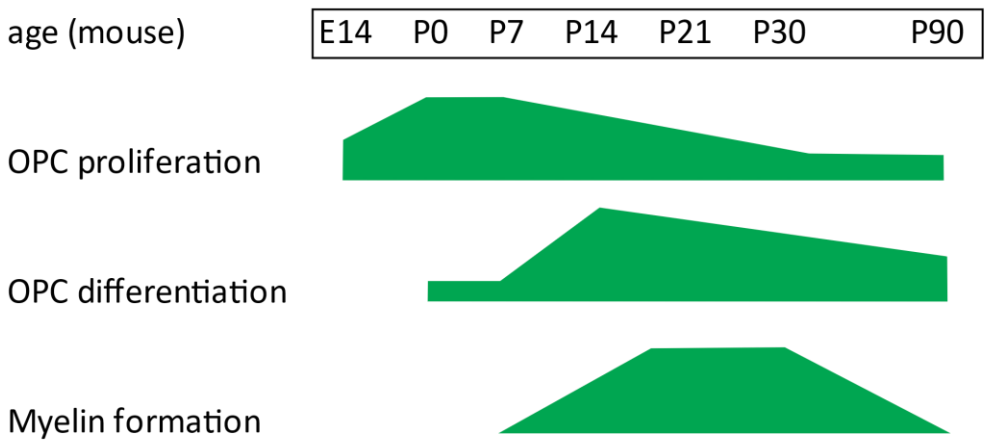

Figure 14. Diagram showing the period of OPC proliferation, differentiation and myelin formation in the mouse central nervous system. *Adapted from* (Nishiyama et al., 2021).

3.2. Diversity in OPC proliferation and differentiation rate:

Proper myelination of the brain relies on the generation of the correct number of OLs and OPCs in the developing brain. This is the results of an equilibrium between cell division, differentiation and apoptosis (Barres and Raff, 1994; Dawson et al., 2003). The OPC division rate can vary. For example, OPCs in the white matter proliferate faster than the ones in the gray matter, and this proliferation rate decreases with age (Dawson et al., 2003; Hill and Nishiyama, 2014). The duration of the cell cycle also changes significantly with age, from ~6h at E13.5 to ~1-5 weeks at P60 or ~6 month at P540, and with the brain region, from ~3 days in corpus callosum to ~19 days in the cortex (Calver et al., 1998; Hill and Nishiyama, 2014; Psachoulia et al., 2009; Young et al., 2013). External stimuli, such as the redox state or presence of PDGF, as well as cell intrinsic mechanisms can affect the proliferation of OPCs in a heterogeneous manner (Hill and Nishiyama, 2014). OPCs are also diverse in terms of their differentiation rate based on the region and developmental stages. In the white matter, where the need for myelination is much higher, OL generation is higher and faster. This rate changes significantly during the first two postnatal weeks, peaks at P14 and decreases gradually with age (Figure 14). Consequently, the balance between OPC proliferation and differentiation changes in favor of proliferation after the period of intense myelination. External signals can also change the speed of OPC differentiation (Baxi et al., 2017; Hill and Nishiyama, 2014; Nishiyama et al., 2021; Rivers et al., 2008). In zebrafish, the two groups of OPCs whose somata are found in the neuron-rich (medial) and axo-dendritic (lateral) parts of spinal cord show differences in quiescence and differentiation rate. Single-cell transcriptomics on these two groups show enrichment of differentiation and proliferation markers in the OPCs of the

axo-dendritic part, while the genes for quiescence are mostly found in OPCs of the neuron-rich part. Short- and long-term time-lapse imaging show that the axo-dendritic OPCs have a much higher rate of differentiation than the other group, even though the processes of both groups are found in the axodendritic area (Marisca et al., 2020).

3.3. Molecular diversity of OPCs:

Two cell surface molecules, NG2 and PDGFRa, are characteristic markers of OPCs and are co-expressed by almost all OPCs (> 99%). They are immediately downregulated upon differentiation of OPCs into OLs (Rivers et al., 2008). The expression of NG2 and PDGFRa is regulated by SOX10, a transcription factor which is considered as one of the markers of the oligolineage cells. Activation of PDGF signaling via interaction of PDGFRa with its ligand, PDGF-A (PDGF-AA), is a critical step in the control of cell division, survival, and differentiation of OPCs during CNS development and adulthood. After the establishment of all the different waves of OPCs at the end of the first postnatal week, a region-specific diversity appears in the response of OPCs to PDGF signaling. For example, OPCs in the gray matter show less activation of PDGFRa in the presence of PDGF than the OPCs in the white matter, due to the difference in intracellular mechanisms regulating the activity of the receptor. This shows that OPCs sense their environment in a region-specific manner (Hill and Nishiyama, 2014; Nishiyama et al., 2021).

Another level of molecular diversity in OPCs arises from their differences in expression of receptors and ion channels on their cell surface, which gives them their electrophysiological properties or sensitivity to the environment. Recently, it has been shown that OPCs in mice start as a homogeneous population during development based on their electrophysiological properties (Spitzer et al., 2019). During postnatal development, they become heterogeneous between regions and ages, by expressing functional voltage-gated potassium and sodium channels, AMPA/kainate receptors, and NMDA receptors differentially (Spitzer et al., 2019). For example, using patch clamp recordings, it has been shown that the expression of NMDARs appears postnatally, increases during P6-P35, during the peak of myelination, then decreases with age. The OPCs in the unmyelinated regions such as the molecular layer of the cerebellum lose NMDARs much faster than the OPCs in the actively myelinated regions such as the corpus callosum (Spitzer et al., 2019). Activation of the receptors and ion channels have regulatory impacts on the dynamics OPCs. For example, G protein-coupled receptor 17 (GPR17) is expressed in a subpopulation of OPCs all over the CNS (Akay et al., 2021; Li et al., 2020; van Tilborg et al., 2018), and seems to inhibit their differentiation into OLs. Activation

of GABA or AMPA receptors prevents OPC proliferation, while NMDA receptor activation promotes their differentiation (Li et al., 2020).

Another aspect of OPC molecular heterogeneity is the diversity in their transcriptomes. Several studies used single cell transcriptomics to analyze this level of diversity in OPCs. For example, one study analyzed OPCs obtained from zebrafish at 5 days post fertilization and identified four clusters of OPCs. These four clusters differ in the expression of some of the OPC molecular signatures such as *Cspg4* (encoding NG2), *gpr17*, and *myrf* (Marisca et al., 2020). In another example, single-cell transcriptomics performed on E13.5, P7 and P21 shows that OPCs arising from different regions of the mouse forebrain and spinal cord with different transcriptomes during embryonic period converge transcriptionally into three clusters, OPC1a, OPC1b and OPC cycling, at P7 (Marques et al., 2018). The first two main clusters of OPCs (OPC1a and b) generate several groups of mature OLs after their differentiation during P21-60 (Marques et al., 2018). Despite the transcriptional convergence of mouse OPCs at P7, another study shows that knockout of the cytoskeleton regulator Citron-kinase (*Cit-k*), involved in DNA repair, has differential effects on OPCs based on their location in the ventral or dorsal forebrain of mouse during postnatal development. Knockout of *Cit-k* in mice results in cell senescence in ventral OPCs, while promotes cell death in dorsal ones. The vulnerability of these two groups of OPCs to Cit-k loss is related to their developmental origin (which wave of OPCs they belong), and their molecular mechanisms, making the ventral OPCs less sensitive to DNA damage and oxidative stress (Boda et al., 2022). Altogether, these studies show OPCs are molecularly a diverse population, and their diversity can change with age.

3.4. Diversity in Neuron-OPC synapses:

OPCs are the only glial cell type receiving synaptic inputs from neurons. They are postsynaptic partners of excitatory and inhibitory neurons in different regions of the brain, such as cortex, cerebellum, hippocampus and pons (Figure 15). Mostly, they receive only one type of input. For example, OPCs in the medial nucleus of the trapezoid body of pons receive excitatory (glutamatergic) inputs from globular bushy cells in the anterior ventral cochlear nucleus, or OPCs in the dentate gyrus of hippocampus are contacted by local glutamatergic granule cells as well as glutamatergic pyramidal neurons of the hippocampal CA3 region. In some rarer cases, OPCs are innervated by different types of synapses. For example, OPCs in the somatosensory cortex receive inhibitory inputs from local GABAergic fast-spiking and non-fast-spiking interneurons as well as glutamatergic synapses from thalamocortical neurons. In another example, OPCs in CA1 region of hippocampus are innervated by local

GABAergic interneurons and glutamatergic pyramidal neurons in CA3 region (Bergles et al., 2000; Li et al., 2020; Orduz et al., 2019; Trotter et al., 2010).

Neuron-OPC synapses are one of the tools that help OPCs sense their environment, especially neuronal activity. Neuronal activity contributes to the regulation of the dynamics of the oligolineage cells. The frequency of the activity of the neuron (e.g. the stimulation pattern) as well as the type of the neurotransmitter (e.g. glutamate) and the receptor (e.g. AMPA) can modulate migration, proliferation and differentiation of OPCs. During the differentiation of OPCs into pre-myelinating OLs and subsequently myelinating OLs, these direct synapses formed by neurons on OPCs change to extrasynaptic communications by modifying the type and number of some of their receptors and ion channels (Figure 16) (Li et al., 2020).

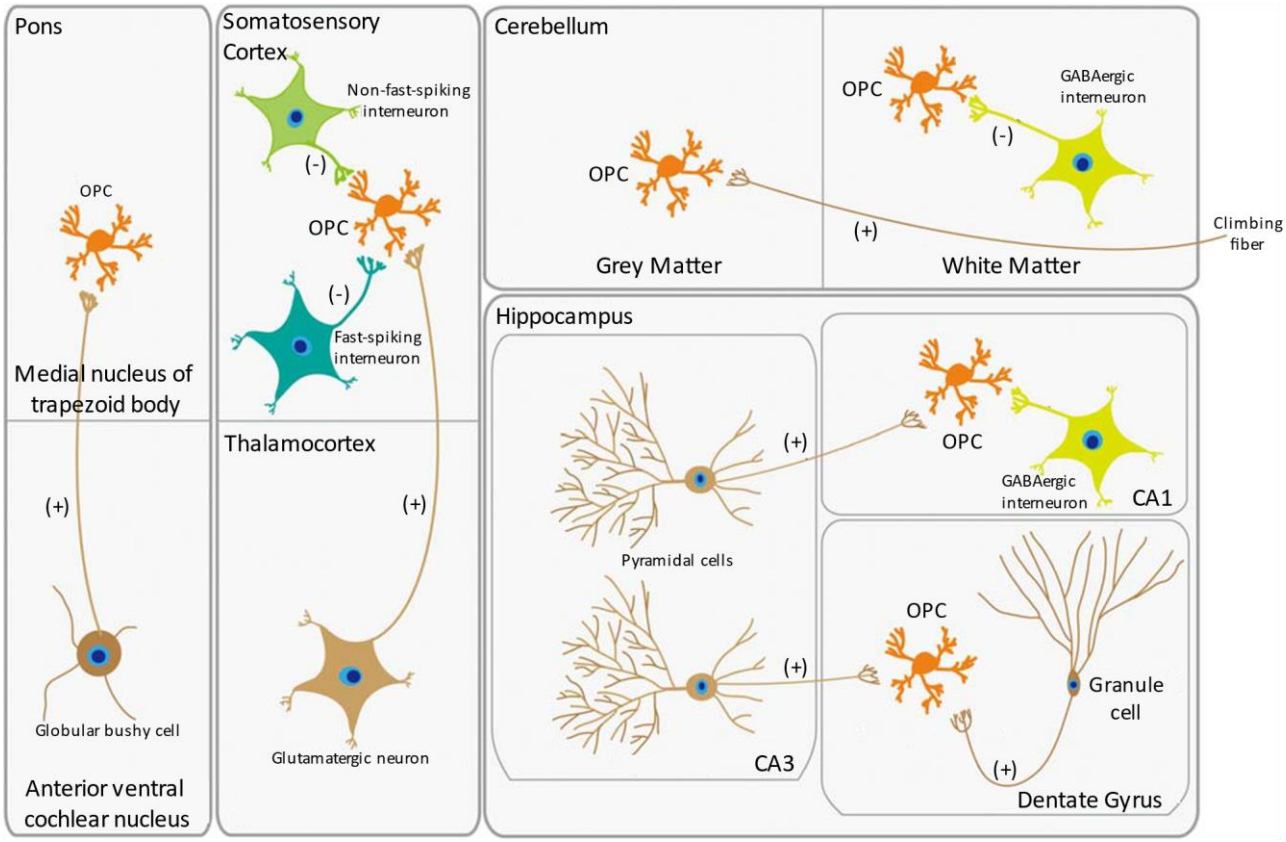

Figure 15. Diagram representing the innervation of OPCs in different regions of the brain. *Taken from* (Li et al., 2020).

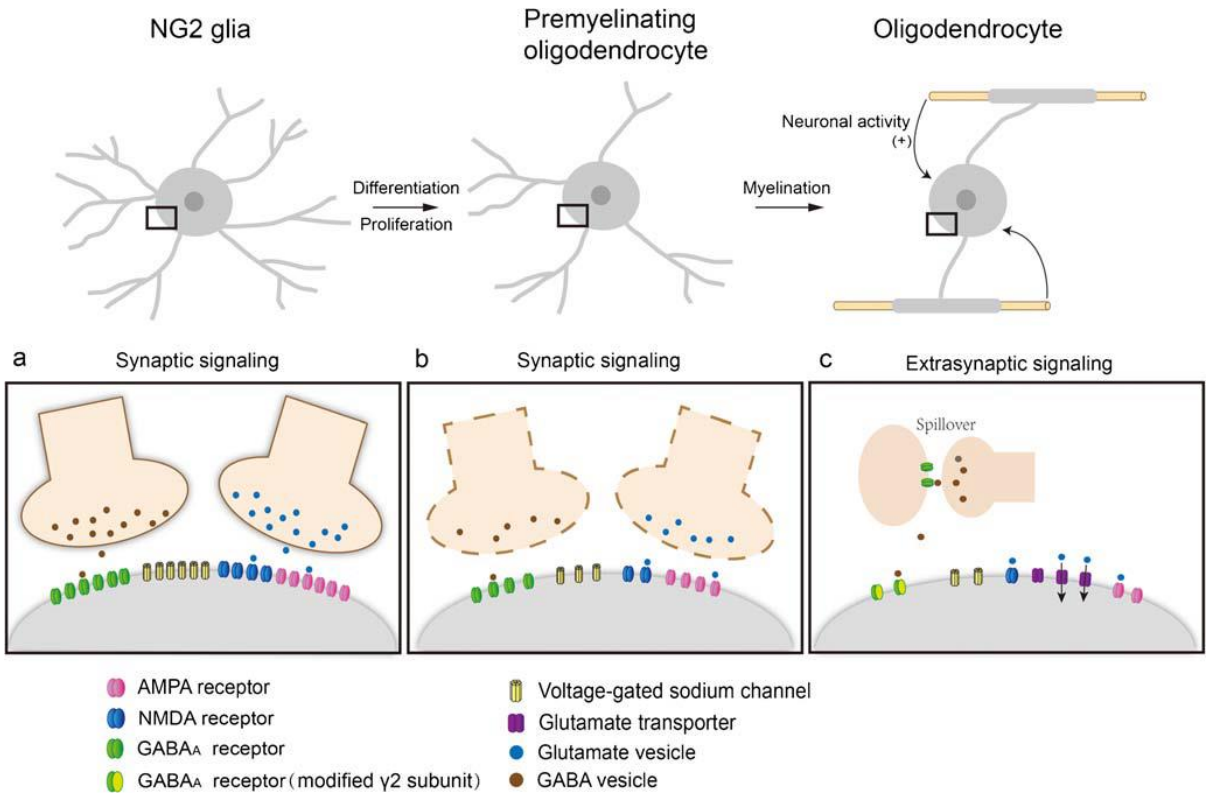

Figure 16. Direct synapses formed on postsynaptic OPCs from neurons will change to extrasynaptic signaling during OPC differentiation to OLs. In general, the number of different receptors and ion channels is decreased, and glutamate transporters are expressed on the contacts by OPCs during this process. $GABA_A$ receptors are replaced by another type of $GABA_A$ receptors where their γ2 subunits are modified. *Taken from* (Li et al., 2020).

3.5. Diversity in OPC functions:

A major function of OPCs is to generate myelinating OLs (Baxi et al., 2017; Bergles and Richardson, 2016; Rivers et al., 2008), but they have a variety of other functions in the brain (Figure 18) (Akay et al., 2021). In the following sections, the different progenies as well as the non-canonical roles of OPCs are briefly introduced.

3.5.1. Diversity in the progeny of OPCs:

OLs are the main, but not the only, product of OPCs. OPCs can generate other types of glia or neurons as well in some conditions (Figure 17). In vitro experiments show the differentiation of OPCs into astrocytes by adding fetal calf serum in rat cultures (Raff et al., 1985, 1983). In vivo studies show that OPCs differentiate into a subpopulation of protoplasmic astrocytes (type 2) only in the gray matter of the ventral forebrain (>30% to total astrocytes)

or spinal cord, but not fibrous astrocytes in the white matter (Small et al., 1987; Trotter et al., 2010; Zhu et al., 2008a, 2008b). These results suggest that the ability of OPCs to generate protoplasmic astrocytes is not only region-dependent, but also an age-specific process, since OPCs generated prenatally can generate astrocytes (Hill and Nishiyama, 2014). It is suggested that differentiation into OLs is the default mode of OPCs, while external signals can change the fate of OPCs to protoplasmic astrocyte (Akay et al., 2021).

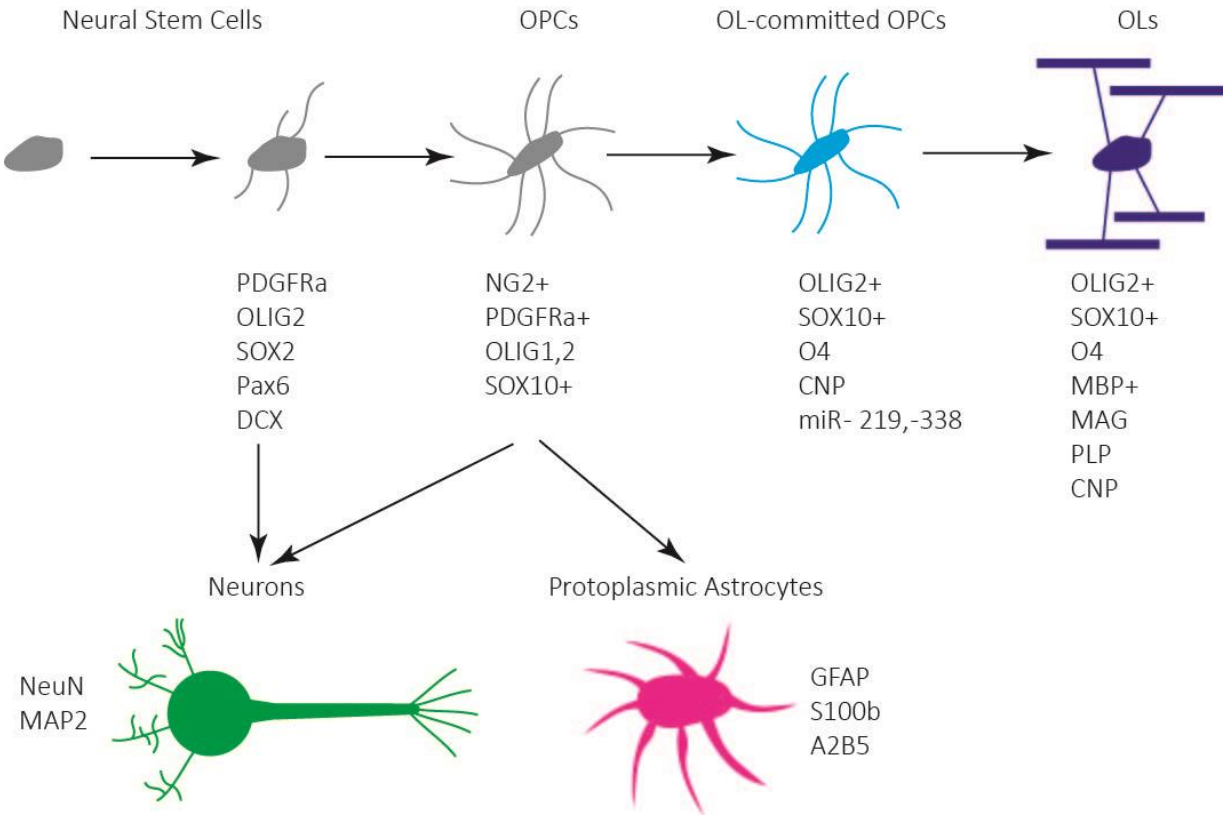

Figure 17. Diagram illustrating the progenies of OPCs and their markers. *Adapted from* (Akay et al., 2021; Trotter et al., 2010).

OPCs express some of the markers of neural stem/progenitor cells such as DCX, Pax6 and Sox2 at low levels, raising the question if they can differentiate into neurons (Guo et al., 2010; Robins et al., 2013). OPCs in culture can dedifferentiate into multipotential neural stem cells by adding some external factors, and subsequently generate neurons (Kondo and Raff, 2000). In vivo studies have shown that OPCs can give rise to neurons in the piriform cortex and hypothalamus of the adult mouse. These neurons which have electrical activity and are functional, are integrated into the neuronal circuits (Guo et al., 2010; Rivers et al., 2008; Robins et al., 2013; Trotter et al., 2010).

3.5.2. **Modulation of neuronal signaling and neural circuits:**

OPCs can modulate neuronal connections in two ways: release of neuromodulatory factors or engulfment of neuronal extensions such as axons or synapses. OPCs can regulate the neuron-neuron synapses via NG2 ectodomain shedding in an activity-dependent manner. In this process, *α*- and γ-secretases, such as ADAM10 or 17, constitutively cleave NG2 into three domains. The extracellular domain is subsequently released into the extracellular matrix. The cleavage and release of NG2 is regulated by activity. Removal of NG2 or blockade of its shedding in pyramidal neurons of the cortex decreases NMDAR-dependent long-term potentiation (LTP) and changes the composition of AMPA receptors (Sakry et al., 2014). In addition to NG2, OPCs release other neuromodulatory proteins such as neuronal Pentraxin 2 (Nptx2/Narp), Prostaglandin D2 synthase (PTGDS) and fibroblast growth factor 2 (FGF2). Studies on primary OPC cultures showed the cleavage of NG2 can affect the expression level of PTGDS via the NG2 intracellular domain. Ablation of OPCs during one week in adult mice impaired glutamatergic neurotransmission in pyramidal neurons and glutamate uptake by the astrocytes in the prefrontal cortex (Birey et al., 2015). FGF2 is suggested to be the neuromodulatory factor responsible for this phenotype (Akay et al., 2021; Birey et al., 2015; Sakry et al., 2015).

OPCs can engulf and phagocytose axons in the mouse cortex and regulate the arborization of axons in the zebrafish visual cortex. They have more phagolysosomes than the microglia (Buchanan et al., 2021). In addition to axons, OPCs can prune synapses in an activity- and microglia-dependent manner (Auguste et al., 2022). The ablation of microglia decreases the synaptic pruning activity of the OPCs, while exposure to sensory inputs increases this activity. In general, this function of OPCs is important in the refinement of neural circuits as well as neuronal signaling and subsequently affects the behavior of the animal (such as visual processing) (Auguste et al., 2022; Buchanan et al., 2021; Xiao et al., 2022).

3.5.3. **Brain vascularization and angiogenesis:**

OPCs are essential for vascularization and angiogenesis during embryonic development. The first wave OPCs (*Nkx2.1*-derived OPCs) are found in proximity of developing blood vessels in the forebrain. Embryonic ablation of this subpopulation of OPCs disturbs the branching and refinement of the vascular network (Minocha et al., 2015). OPCs also use blood vessels as scaffolds to migrate throughout the CNS during development. During migration, OPCs interact directly with endothelial cells expressing the CXCR4 ligand SDF1 (CXCL12) via Wnt signaling. It is suggested that this signaling pathway is important for the differentiation of OPCs during their migration (Tsai et al., 2016). One reason for the

interaction between OPCs and blood vessels is the importance of oxygen levels for the differentiation of OPCs. Hypoxia significantly decreases the number of OLs in the corpus callosum via hypoxia-inducible factors (HIF) 1/2α. Activation of HIF triggers Wnt signaling in the OPCs by secretion of Wnt7a/b which stops differentiation and myelination in an autocrine manner. Release of Wnt7a/b has a proliferative effect on endothelial cells in a paracrine manner, stimulating angiogenesis in the CNS (Yuen et al., 2014). Thus, the interaction between OPCs and blood vessels is essential for OPC dynamics and myelination as well as brain vascularization.

3.5.4. **Interaction with the immune system in the brain:**

OPCs interact with the immune cells in the brain. This interaction plays an important role in immune homeostasis as well as OPC development (Akay et al., 2021; Pepper et al., 2018). Microglia can modulate the proliferation and differentiation of OPCs in the adult brain. Depletion of a subpopulation of microglia decreases OPC numbers and their differentiation into OLs in the corpus callosum and cerebellum (Hagemeyer et al., 2017). The underlying mechanism for this interaction is partially known. The transglutaminase-2 (TG2) from microglia interacts with laminin in the extracellular matrix and the adhesion G protein-coupled receptor ADGRG1 on OPCs to stimulate the proliferation of OPCs and myelin formation (Giera et al., 2018).

OPCs can reciprocally modulate the activity of microglia in inflammation. Ablation of OPCs in the adult rat hippocampus induces microglia activation and excessive inflammation which results in neuronal apoptosis via microglia-dependent IL-1β pro-inflammatory cascade (Nakano et al., 2017). OPCs, as well as OLs, can produce several immunomodulatory factors, such cytokines (e.g. Il-1β, CASP4, NLRP1, NLRP3 and NLRC4) to affect the immune responses (Zeis et al., 2016). During neuroinflammatory conditions such as multiple sclerosis, OPCs express myelin peptides as well as MHC class I molecules induced by the interferon-gamma (IFNγ) in the CNS. Consequently, cytotoxic T cells are activated by these molecules to attack OPCs as their target. These results show that OPCs can function as antigen presenting cells (Kirby et al., 2019).

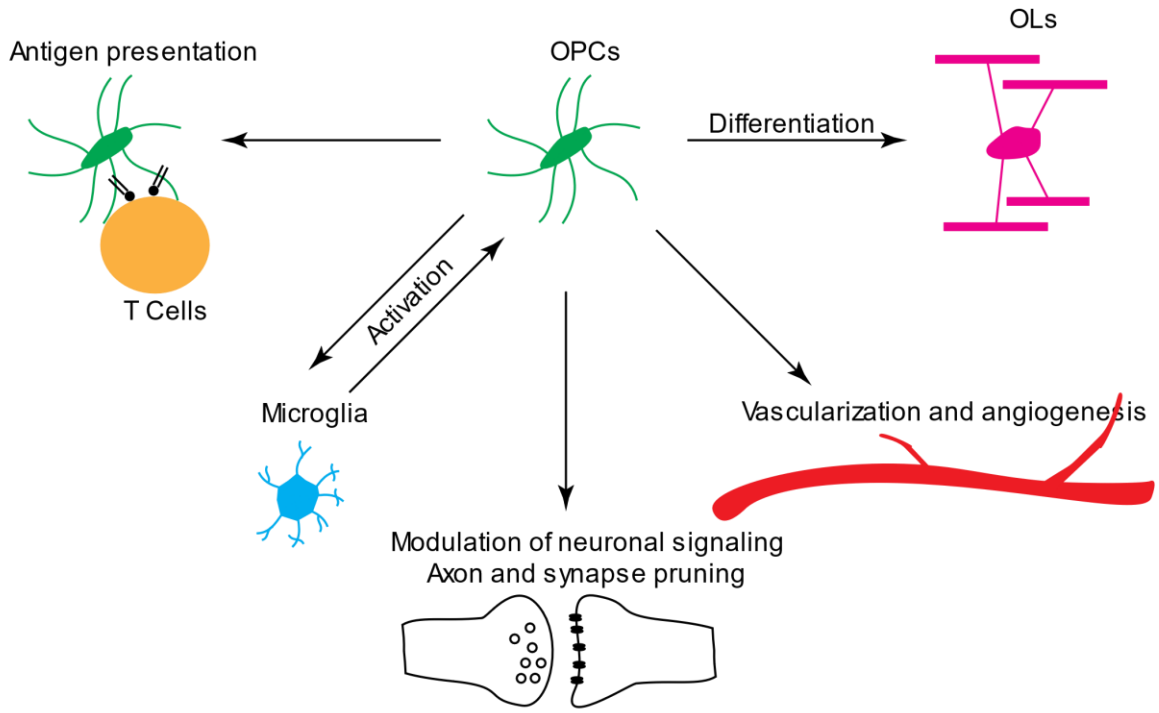

Figure 18. OPCs and their different functions.

Results

One of the most intriguing features of the brain is its complexity. It is apparent at various levels, ranging from the diversity of cell types to the complex connectivity underlying its function. Its precise circuitries are topographically organized to represent several sensory inputs and motor outputs in different structures and separate the functions of various regions in the brain. Brain circuits are made of two types of neurons: excitatory and inhibitory neurons that connect to each other at a precise subcellular level. The cerebellum, with its well-known stereotyped structure at the subcellular level, is a strong model to study the development of circuit formation (Reeber et al., 2013; Sillitoe and Hawkes, 2013). This story started from the cerebellar cortex, particularly one of the most beautiful neurons among all the other cells in the brain: Purkinje cell. I was interested in the development of the topographical connectivity of different excitatory and inhibitory inputs with the two subsets of PCs: AldC+ and AldC-. Invention of new techniques such as single-cell transcriptomics has helped us to identify more levels of heterogeneity among cell populations that look identical. IONs, one of the excitatory afferents to PCs, are a heterogeneous population with several molecular markers (Reeber et al., 2013). I wanted to use the heterogeneity in transcriptomes of IONs to identify genes that contribute to the topographical organization of their connectivity with PCs. The first part of the results describes an ongoing study showing the potential implication of the c-KIT signalling pathway in the connectivity of two afferents, excitatory IONs and inhibitory molecular layer interneurons, on PCs.

To perform functional analysis of selected candidate genes and test their potential contribution in the development of the olivocerebellar connectivity, a genetic tool was required to enable specific targeting of IONs. C1QL1, a synaptic organiser specific for ION-PC connections (Kakegawa et al., 2015; Sigoillot et al., 2015), is strongly expressed in IONs during all their life (Iijima et al., 2010). The regulatory sequence of the *C1ql1* gene was hypothesized to be a good driver to express the CRE recombinase in these cells, thus enabling their targeting with the use of the CRE/lox system. The second part of the results presents the development of the *C1ql1*^{Cre} mouse line and its characterization. This article is ready for submission.

During the characterization of *C1ql1*^{Cre} mouse model using different Cre-dependent reporter mice, we observed that a non-neuronal up to then unidentified cell population expresses *C1ql1*. We identified that a subpopulation of oligodendrocyte precursor cells (OPCs) all over the brain expresses *C1ql1*. Using several molecular techniques such as single-cell transcriptomics or smFISH, we showed that OPCs can be divided into two almost equal subpopulations based on the expression of *C1ql1*, illustrating again brain complexity this time at the level of glial cell heterogeneity, not neurons. Since OPCs have multiple functions, the main questions were: Do *C1ql1*-expressing OPCs have a particular function?

And what is the role of C1QL1 in this function? The last part of the results is an article answering these questions and ready to be submitted for publication.

The story started from neurons in the cerebellum and ended with OPCs in the forebrain. In the first one, I was interested in the link between heterogeneity and topography and connectivity, while in the second one, the link between heterogeneity and function intrigued me. In all the stories, I was interested in the non-canonical roles of the genes. In the first one, the role of a proto-oncogene in connectivity formation between neurons and in the second one, a synaptic organizer as a functional marker in OPCs. All these results together show the dual or multiple functions of the investigated genes in the body.

At the end, I should mention the contribution of several people in these three collective works: The high throughput qPCR in the first part of the results was performed by Marine Delagrange from Plateforme qPCR-HD-GPC (Institut de Biologie de l'Ecole Normale Supérieure, Paris, France). The home-made plugins to quantify immunofluorescence data in the first and third parts of the results were developed by Philippe Mailly and Heloise Monet from CIRB Imaging facility (ORION). The stereotaxic injection of viral particles as well as the related immunofluorescence experiments in the second part was performed by Séverine M. Sigoillot from Selimi's team. The immunofluorescence experiments on the *C1ql1*$^{Cre/WT}$/R26$^{hM4Di,-mCitrine/WT}$ heterozygous mice in the second part and all the smFISH experiments in the third part of the results were performed by Maela A. Paul from Selimi's team. The electrophysiology experiment in the second part was performed by Fekrije Selimi. The single cell transcriptomics data analysis in the third part was performed by Fekrije Selimi and Lea Bellenger (from Sorbonne Université, Paris, France).

Part 1: The transmembrane receptor tyrosine kinase c-KIT is potentially involved in the development of the olivocerebellar circuit in a lobule-specific manner.

Article in preparation.

Title:

The transmembrane receptor tyrosine kinase c-KIT is potentially involved in the development of the olivocerebellar circuit in a lobule-specific manner.

Shayan Moghimyfiroozabad[1], Fekrije Selimi[1]

[1]Center for Interdisciplinary Research in Biology (CIRB), College de France, CNRS, INSERM, Université PSL, Paris, France

Abstract:

Proper brain development relies on the proliferation, migration, differentiation, recognition and adhesion between different cell populations. Some molecular pathways regulate normal development of various tissues including the brain. One of these pathways is c-KIT/SCF signaling. c-KIT is a well-known proto-oncogene and a transmembrane receptor tyrosine kinase that controls cell survival, proliferation and maintenance of various tissues (e.g. hematopoietic tissue) as well as cell-cell adhesion. c-KIT is expressed in the brain during development and regulates migration. While it is found at certain synapses, its function in synapse development and/or function has not been described. We show that c-KIT is present at different types of synapses of cerebellar Purkinje cells (PCs) during postnatal development: synapses made by the climbing fibers (CFs), the axons of inferior olivary neurons located in the brainstem, and synapses made by molecular layer interneurons (MLIs). Data from the Allen Brain Atlas show that the gene coding the *c-Kit* ligand, *Scf*, is expressed in the target neuron (PC), suggesting a potential role for the c-KIT/SCF complex in the formation and maintenance of cell-cell contacts in the olivocerebellar circuit. Postnatal conditional knockout of *c-Kit* in MLIs during the fourth postnatal week leads to morphological defects in the presynaptic boutons of MLIs on PCs, but also the ones from CFs. Since this loss of c-KIT happens after synapse formation in this model, these data suggest a role for the c-KIT/SCF pathway in maintaining proper connectivity and function of the olivocerebellar circuit, and identify a potential new role for this class of receptor tyrosine kinases in brain function.

Introduction:

During brain development, a vast variety of neuronal populations need to be precisely connected through specialized structures called synapses to build neural circuits. Neural circuits are at the heart of all functions of the nervous system. The development of neural circuits is based on finding the path to target the right area, selecting the right partner to connect and making the functional synaptic connections on the appropriate subcellular territory of the partner (Sanes and Yamagata, 2009; Sanes and Zipursky, 2020). Several classes of trans-synaptic and adhesion molecules are involved in these steps such as brain angiogenesis inhibitors (BAIs), cadherins or ephrins and their receptors. Most of these molecules are multifunctional during development and adulthood. They are expressed in non-neuronal tissues and have non-synaptic roles in addition to their contributions to axon guidance or synapse formation (Südhof, 2018). For example, Eph receptors are a family of receptor tyrosine kinases (RTKs) that bind to their membrane-bound ligands, ephrins. They are not only involved in various cell functions such as growth, migration and survival in several tissues (e.g. lymphoid organs or bones), but also in axon guidance and topographic organization in the brain (such as retinocollicular circuit) (Pasquale, 2008; Triplett and Feldheim, 2012).

The proto-oncogene c-KIT is a RTK involved in cell division, migration and survival in several tissues. c-KIT signaling is activated upon binding to its ligand, stem cell factor (SCF) (Lennartsson and Rönnstrand, 2012). SCF has two variants: membrane bound and soluble, giving a dual function to its interaction with c-KIT: activation of intracellular signaling pathway and cell adhesion/junction (Tabone-Eglinger et al., 2014). The c-KIT/SCF interaction is important in the maintenance and regeneration of hematopoietic stem cells, melanocytes and germ cells (Kimura et al., 2011; Tabone-Eglinger et al., 2014). In the developing and adult brain, *c-Kit* is expressed in several regions such as cerebral cortex (Guijarro et al., 2013), hippocampus (Katafuchi et al., 2000) and cerebellum (Kim et al., 2003). In the cerebral cortex, c-KIT is involved in radial migration of neurons during development via an SCF-dependent mechanism, while it contributes to the establishment of callosal projections independent of soluble SCF (Guijarro et al., 2013). Knockdown or knockout of *c-Kit* in the cortex during an early developmental period (embryonic day 15.5 (E15.5) – postnatal day 5 (P5)), delayed radial migration of neurons and perturbed their projections to the other hemisphere, while overexpression of c-Kit speeded up their radial migration (Guijarro et al., 2013). Homozygous rats for a *c-Kit* mutation leading to strongly disturbed tyrosine kinase activity, showed reduced spatial memory and decreased long-term potentiation in the mossy fiber-CA3 pathway (Katafuchi et al., 2000), suggesting a synaptic function.

The cerebellum, with its very well-described stereotyped circuitry which develops postnatally, is a good model to study the development and function of neuronal circuits. The GABAergic Purkinje cells (PCs), the only output of the cerebellar cortex, receive excitatory inputs from inferior olivary neurons (IONs) located in the brainstem through topographically organized sets of axons called climbing fibers (CFs). Parallel fibers coming from granule cells in the cortex of the cerebellum are the second source of excitatory afferents to PCs (Reeber et al., 2013; Voogd and Glickstein, 1998). PCs also receive inhibitory afferents from local interneurons residing in the molecular layer of the cerebellum (Sotelo, 2011). All these different inputs are connected on specific subcellular localizations on PCs (Sotelo, 2008), making this neuron a powerful model to study neuronal connectivity.

The development of a topographical connectivity between CFs and PCs, as well as precise targeting of various afferents on defined subcellular localizations on PCs is a complex process dependent on activity and genetic mechanisms (Reeber et al., 2013; Sillitoe and Joyner, 2007; White et al., 2014a; Zhou et al., 2020a). In particular, the molecular recognition pathways that control this organization and their regulation by neuronal activity are not well understood. In the cortex of the cerebellum, *c-Kit* and *Scf* are expressed by molecular layer interneurons and their targets, Purkinje cells, respectively (Kim et al., 2003). Neuronal activity induced by systemic administration of kainic acid transiently increased the expression level of both c-KIT and SCF, particularly at the inhibitory synapses on the axon initial segment of PCs (Kim et al., 2003). Despite these results, the function of c-KIT/SCF signaling at synapses remains unknown. In this study, we show that c-KIT is expressed differentially from early postnatal development until adulthood in two different types of afferents (CFs and MLIs) to PCs, and is localized in both their axons and synapses. *c-Kit* mRNA expression in IONs is modulated by physiological sensory deprivation. Using conditional knockout of *c-Kit* in MLIs during postnatal development, we show that loss of c-KIT from MLIs during the fourth postnatal week diminishes the volume of not only their presynaptic boutons, but also the presynaptic boutons of CFs on PCs in a lobule specific manner. Since the removal of c-KIT occurs after synaptogenesis of MLIs and CFs on PCs, these results suggest a function for the c-KIT/SCF interaction in maintaining proper connectivity of this circuit.

Results:

The differential expression of *Cdh9*, *Pcdh20*, and *c-Kit* in the inferior olivary neurons is modulated by neuronal activity during postnatal development.

In the olivocerebellar circuit, topographically organized sets of CFs from IONs project to PCs in the cortex of the cerebellum (Reeber et al., 2013; Voogd and Glickstein, 1998). This topographical organization develops during the first 3 postnatal weeks (Reeber et al., 2013). To identify molecules involved in the establishment of this topographical organization, we searched for genes that are differentially expressed by IONs during development. We used the comparative analysis of the gene expression profiles of two subpopulations of IONs obtained via the bacterial artificial chromosome (bac) translating ribosome affinity purification (bacTRAP) method (Figure 1a). In this method, ribosomal protein L10a tagged to EGFP is expressed in a specific cell group using a given promoter, and affinity purification of polysomal mRNAs gives access to the ready-to-translate transcriptome of this cell group (Heiman et al., 2008). Using *s100a10* and *Cdk6* drivers, we had access to the bacTRAP profiles of all IONs as well as some other cells in the brainstem, and a subpopulation of IONs, respectively, in the adult mouse (Veleanu et al., 2022a). Comparative analysis of these two profiles revealed 3 lists of genes: 1532, 1408, and 972 genes. Two of these lists contain genes that are differentially expressed in ION: genes enriched in *s100a10*- or *Cdk6*-IONs. In these lists, we searched for those involved in cell-cell interactions, and thus potentially in the topographic organization of ION to PC connectivity, based on their associated biological process and cellular component GO terms. Using DAVID and ToppGene gene ontologies (GO) on these two lists, we selected total of 368 genes involved in cell/membrane adhesion, junction and guidance, or genes with homo/heterophilic binding affinity for further data curation in the Allen developing mouse brain atlas (https://developingmouse.brain-map.org/). 17 genes were selected at this step. Since the bacTRAP experiment was performed on adult mice, the expression pattern of the shortlisted genes from GO analysis were also analyzed at P4 (Allen brain atlas), a stage when the precise topographical organization of olivocerebellar circuit is not established yet (Reeber et al., 2013; White and Sillitoe, 2013). Several candidate gene families with differential or partial expression in the inferior olive at P4 were found (Figure 1b, *top panel*): *Cdh9*, *Pcdh20*, and *c-Kit*. At P56, the expression of *Cdh9* diminishes greatly in the inferior olivary neurons, while the expression of *Pcdh20* and *c-Kit* becomes more homogeneously (Figure 1b, *bottom panel*).

Many recognition molecules in the nervous system are regulated by neuronal activity. Neuronal activity and synaptic transmission are also known to participate in the refinement of the connectivity between IONs and PCs (Reeber et al., 2013; Sillitoe and Joyner, 2007; White et al., 2014a). To check the effect of neuronal activity on the expression of the selected candidates, *Cdh9*, *Pcdh20* and *c-Kit*, two different, pharmacological and physiological, models were used (Figure 1c). The pharmacological approach was designed to increase neuronal activity. For this, harmaline is injected intraperitoneally to activate the olivocerebellar circuit

broadly (LeDoux and Lorden, 2002). High-throughput RT-qPCR analysis of the brainstem and cerebellum of P14 mice injected with physiological serum (NaCl 0.9% solution) or harmaline from P10 to P14 (Figure 1c, *top panel*) shows a 23.9 and 17.6% decrease in the expression levels of *Cdh9* in the brainstem (mean ± SEM = 2.968 ±0.195 vs 2.260 ± 0.142 in the control and harmaline-treated animals, respectively) and *Pcdh20* in the brainstem (mean ± SEM = 8.600 ± 0.490 vs 7.089 ± 0.159), respectively (Figure 1c). No change was observed in their expression levels in the cerebellum (data not shown), as well as the expression level of *c-Kit* in the brainstem (Figure 1c). High-throughput RT-qPCR quantification of samples from mice treated with one injection of physiological serum or harmaline at P14 (Figure S1b) shows no change in the expression of any of the candidate genes. These results indicate that the effect on gene expression of harmaline are detected only after chronic treatment and might be correlated to changes in connectivity. In order to decrease neuronal activity in the network during development, we used sensory deprivation. All the whiskers of the mouse pups were trimmed every other day from P3 to P21 (Arakawa and Erzurumlu, 2015). RT-qPCR analysis of the brainstem of P21 control or whisker-trimmed mice (Figure 1c, *bottom panel*) shows a 45.1% increase in the expression level of *c-Kit* in the brainstem (mean ± SEM = 30.05 ± 5.719 vs 43.59 ± 4.399 in the control and whisker-trimmed animals, respectively), while no significant change was observed for *Cdh9* and *Pcdh20* in the brainstem (Figure 1c, *bottom panel*) or in the cerebellum (data not shown). To conclude, chronic, but not acute, increase or decrease of neuronal activity can differentially change the expression levels of the three candidate genes.

Among the three selected candidates, two of them (PCDH20 and CDH9) belong to the cadherin and protocadherin families that are known to have homo/heterophilic affinity and are involved in molecular recognition between neurons (Duan et al., 2014; Kim et al., 2010; Williams et al., 2011). The role of c-KIT is quite unknown in neural circuit formation. In situ hybridization (ISH) taken from Allen brain atlas shows the expression of *Scf,* the ligand of c-KIT, in PCs at P4 and P56 (Figure S1a), suggesting a role for this cell surface signaling pathway in olivocerebellar circuit formation and maintenance. Similar to *c-Kit*, *Scf* shows differential expression amongst PCs, even more pronounced at P56 than at P4 when patches of PCs clearly lacked *Scf* expression (Figure S1a). For the differential expression to have functional relevance, it needs to also be detected at the protein level. We performed co-immunostaining for c-KIT and FOXP4, a marker for IONs, on brainstem coronal slices at different ages during postnatal development (Figure S2). At all the analyzed ages, a differential localization of c-KIT is observed. In another word, c-KIT intensity is heterogeneous between different subregions of IO. For example, in the slices shown from all the three ages, the intensity of c-KIT is lower in the dorsal part in comparison with the ventral part (Figure S2). Overall, these results show the differential expression of c-KIT during postnatal development

in IONs both at the mRNA and protein level. The heterogeneous expression of *Scf* mRNA during the same period in the target of IONs, PCs, suggests a potential role for the interaction of c-KIT with its receptor in the topography of connectivity in the olivocerebellar circuit.

c-KIT is localized at a subpopulation of the synaptic contact sites made by molecular layer interneurons and climbing fibers on Purkinje cells.

The protein expression of c-KIT has been reported in the presynaptic areas of MLIs on PCs in adult rats (Kim et al., 2003). MLIs form their first synapses on the dendritic tree of PCs around P7 and arrive to the axon initial segment (AIS) of PCs around P9 to form a tightly packed mesh-like structure full of synaptic vesicles called the pinceau (Sotelo, 2008). Using immunofluorescence detection of c-KIT in parasagittal sections of the cerebellar cortex at P2, P4, and P10, localization of c-KIT is observed throughout the different layers of the cerebellar cortex, except in the external granular layer (EGL). At P2, before the peak of MLIs generation at P5 (Yamanaka et al., 2004), c-KIT is found almost homogeneously in the cerebellar cortex, while at P10, it is concentrated in the PC layer (Figure 2a). At P14, at the time when the maturation of pinceaux has started (Sotelo, 2008), localization of c-KIT is observed all over the molecular layer, strongly around the soma of MLIs and their extensions on the dendritic tree, cell body and AIS of PCs (Figure 2b). Using immunolabeling for glutamic acid decarboxylase 65 (GAD65) as a marker of inhibitory synapses on PC, localization of c-KIT is observed in some, but not all, inhibitory boutons at P14 (Figure 2b). c-KIT immunostaining was detected at the AIS of PCs at P14. At P34, c-KIT immunostaining is still present all over the molecular layer, showing its maintained expression by both basket cells and stellate cells (Figure 2b). At AIS, a strong accumulation of c-KIT was observed in a cup-like structure where it colocalized with GAD65 boutons, in line with the mature state of the pinceau. Except in pinceaux, where all the GAD65 boutons colocalized with c-KIT, presence of c-KIT was observed in some, but not all, inhibitory synapses on PCs (Figure 2b). Altogether, c-KIT is present at the molecular layer interneurons as well as in a subpopulation of their synapses on their target PCs from the second postnatal week onward.

Our results show the expression of c-KIT in inferior olivary neurons in the brainstem (Figure 1 and S2). Is c-KIT transported in their axons and localized at the CF/PC synapses? To investigate the localization of c-KIT at CFs, we used the *Igsf9*-GFP mouse model in which soluble GFP is expressed by some IONs and allows CF visualization (https://www.gensat.org/). At P4, c-KIT is localized in the PC layer, around PC soma and dendritic tree, as well as some fibers (Figure S3). Partial, but not full, colocalization of c-KIT with some *Igsf9*-GFP^{+} CFs is observed around or close to the PC soma (Figure S3). Co-

immunostaining for c-KIT and vesicular glutamate transporter 2 (VGLUT2) as a marker of presynaptic boutons of CF synapses on PC shows the localization of c-KIT in some, but not all, CF boutons on PCs at P2 and P4 (Figure 2c), a period when synapse formation by CFs on PCs has started (Sotelo, 2008). Overall, our results show the presence of c-KIT in restricted segments of some CFs as well as some CF-PC synapses.

Various cerebellar inhibitory interneurons express c-KIT differentially in a lobule-dependent manner.

Basket cells and stellate cells, the two subtypes of MLIs, originate from identical progenitor cells, but follow two distinct migration trajectories and postnatal developmental processes to arrive to their final laminar position in the molecular layer of the cerebellum and differentiate (Cadilhac et al., 2021). The interaction of stellate cells with immature granule cells in the external granular layer and its importance in laminar localization and differentiation of stellate cells have been shown recently using two-photon imaging (Cadilhac et al., 2021). On the other hand, studies using electron microscopy and immunohistochemical analysis show the replacement of CFs territories on PC soma by basket cells in an earlier phase than the laminar positioning of stellate cells (Sotelo, 2008). Recently, *c-Kit* has been used as a specific genetic driver to target both subtypes of MLIs in adult mice (Amat et al., 2017). Even though the role of c-KIT/SCF interaction has been shown in the radial migration of neurons in the cerebral cortex and the projection of callosal fibers (Guijarro et al., 2013), their specific role in target recognition and synapse formation and maintenance in PCs has never been tested. To investigate this question, the Cre/Lox system was used to conditionally knockout *c-Kit* in molecular layer interneurons (Figure 3a). We used a floxed *c-Kit* (*c-Kit*^{fl}) mouse line that is designed to delete *c-Kit* in the cells expressing CRE-recombinase (Kimura et al., 2011). In this mouse line, a cassette with a splice acceptor site (SA) and an *IRES-GFP-polyAs* gene flanked by two loxP sequences is inserted into the intron between exon 8 and 9 in anti-sense orientation. An intact *c-Kit* transcript is transcribed in the control condition, while in the presence of Cre, the inserted cassette is flipped resulting in the activation of the inserted cassette and silencing of the downstream elements in the *c-Kit* gene encoding the transmembrane domain and kinase activity. In the absence of the transmembrane and kinase domains, c-KIT loses its cell membrane localization (Kimura et al., 2011). The *c-Kit*^{fl} mice were crossed with the *Pvalb*$^{ires\text{-}Cre}$ mouse that expresses Cre in all Parvalbumin-expressing cells including MLIs (Hippenmeyer et al., 2005) (Figure 3a). In the adult cerebellum, *Pvalb* is found only in MLIs and PCs (Stichel et al., 1986). Its transient expression is observed in the

precursors of GCs in the EGL (Wang et al., 2022), but since c-KIT is not expressed by these cells, it won't affect our interpretation of the results.

c-KIT immunostaining was used to assess the loss of *c-Kit* expression induced by Cre recombinase activity in *Pvalb*$^{+}$ cells (Figure 3b). Interestingly, we observed a heterogeneity in the expression of c-KIT in the control conditions (*Pvalb*$^{wt/wt}$*; c-Kit*$^{wt/wt}$ or *Pvalb*$^{wt/wt}$*; c-Kit*$^{fl/fl}$ or *Pvalb*$^{ires\text{-}Cre/wt}$*; c-Kit*$^{wt/wt}$) at P28 and later (> P28). In the vermis, c-KIT immunostaining has the lowest intensity in the anterior lobules (lobules I - V), while it increases dramatically in the central and posterior lobules (lobules VI - X) (Figure 3b, *top panel*). c-KIT is completely lost in most of the lobules, except lobule X, in cerebellar sections taken from *Pvalb*$^{ires\text{-}Cre/wt}$*; c-Kit*$^{fl/fl}$ mice older than P28. Higher magnification of c-KIT immunostaining shows that c-KIT completely disappears from the pinceaux of PCs in all the four analyzed lobules (III, VI, IX, X) as well as the molecular layer in lobules III and IX of cerebellar slices of > P28 mice (Figure 3b, *bottom panel*). Since this conditional knockout should not affect *c-Kit* expression in the inferior olivary neurons and no trace of c-KIT is observed in the molecular layer of these two lobules, we conclude that the CFs in these two lobules do not contain c-KIT at this age. In lobules VI and X of the conditional knockout animals, some c-KIT^{+} fibers were observed. In lobule VI, some of these fibers seem to cross the whole molecular layer, a characteristic that excludes CFs (since CFs occupy only the 70% inner territory of the molecular layer (Sigoillot et al., 2015)), but can be attributed to Lugaro and Golgi/candelabrum cells, two groups of inhibitory interneurons residing in Purkinje cell and granular layer of the cerebellum, respectively (Sotelo, 2011). Single cell transcriptomic data from the cerebellum shows that in addition to MLIs, Lugaro cells and a subpopulation of Golgi cells express *c-Kit* (Kozareva et al., 2021). Since Golgi and some Lugaro cells do not express *Pvalb* (Kozareva et al., 2021), their *c-Kit* expression is not affected, supporting the idea that the c-KIT^{+} fibers in lobule VI are mostly Golgi and Lugaro cells. Among all the four analyzed lobules in the vermis, c-KIT^{+} Golgi and Lugaro cells are found in lobule VI, but not in other lobules. In addition to lobule VI, some c-KIT immunostaining was observed in the outer part of the molecular layer in lobule X (Figure 3b, *bottom panel*). The morphology of these cells and the pattern of their extensions suggest that they are stellate cells. No diversity in the expression of *Pvalb* in MLIs has been reported so far (Wang et al., 2022) but cannot be excluded. Another explanation would be that the amount of Cre expressed in these lobule X stellate cells is insufficient to induce the recombination. Overall, c-KIT is localized differentially in interneurons of the molecular layer of the cerebellum, with an anterior to posterior gradient in the vermis. Conditional knockout of *c-Kit* in *Pvalb*-expressing cells leads to its full loss in almost all the lobules, and reveals its expression by various types of interneurons depending on the lobules.

Loss of *c-Kit* in *Pvalb*-expressing interneurons affects both climbing fiber and molecular layer interneuron connectivity on Purkinje cells in a lobule-specific manner.

The formation of the first contacts between MLIs and PCs occurs at P7 (Sotelo, 2008). Data from Allen brain atlas shows no expression of *Pvalb* in the cerebellum at P4, but strong expression by MLIs and PCs at P14, suggesting the expression of *Pvalb* starts during the second postnatal week. Using the same $Pvalb^{ires\text{-}Cre}$ mice as ours to cross with a reporter mouse line, no/low signal of interest was observed in the MLIs and PCs at P14, suggesting a delay in CRE recombination (Wang et al., 2022). Thus, our strategy will allow us to study the role of c-KIT/SCF signaling only on synapse function and maintenance in inhibitory contacts on PCs and not their formation. Effects of removal, knockdown or overexpression of genes involved in connectivity of CF or MLI to PCs can be measured via different parameters such as density of the presynaptic boutons and their volume using specific markers (Sigoillot et al., 2015). To investigate the effect of removal of c-KIT in *Pvalb*-expressing cerebellar interneurons on the connectivity of PCs with their two afferents, CF and MLI, we performed co-immunolabeling of VGLUT2, GAD65, and Aldolase C (AldC, a marker of Zebrin II$^+$ PCs) on sagittal cerebellar slices at vermis (Figure 4, *top panel*). AldC / Zebrin II is a marker for parasagittal zones in the cerebellar cortex, called modules (Reeber et al., 2013). Since AldC$^+$ and AldC$^-$ PCs have differences in their electrophysiological activities (such as spiking frequency) (Zhou et al., 2014) and the size of basket cell's pinceau (Zhou et al., 2020a), we used this marker instead of a general marker for all PCs (such as CaBP) in the immunostaining experiments to ensure that we compare the same class of PCs in our analysis (AldC$^+$, except in lobule III). Preliminary data have been obtained on the effect of c-KIT loss-of-function on the density and volume of VGLUT2$^+$ (CF) and GAD65+ (inhibitory) presynaptic clusters in the molecular layer of *c-Kit* conditional knockout ($Pvalb^{ires\text{-}Cre/wt}$; $c\text{-}Kit^{fl/fl}$: CRE/FF) and the three controls ($Pvalb^{wt/wt}$; $c\text{-}Kit^{wt/wt}$: WT/WT, $Pvalb^{wt/wt}$; $c\text{-}Kit^{fl/fl}$: WT/FF, $Pvalb^{ires\text{-}Cre/wt}$; $c\text{-}Kit^{wt/wt}$: CRE/WT). Quantifications for GAD65$^+$ clusters show no difference in the cluster density among the different genotypes in the four analyzed lobules, while the GAD65$^+$ cluster volume seems to be diminished in certain lobules of CRE/FF mice (Figure 4, *bottom panel*). A similar phenotype might be observed for VGLUT2 boutons (Figure 4, *middle panel*). If reproduced, these data on lobule-specific effect on the volume of both VGLUT2 and GAD65 clusters in *c-Kit* conditional knockout in cerebellar inhibitory interneurons suggest an interaction between the connectivity of CF and MLI to PCs: weakening the connectivity of the inhibitory afferent to PC negatively regulates the excitatory connectivity from CFs on the same target.

Discussion:

Expression of c-KIT and SCF by MLIs and PCs respectively, and its modulation by acute kainic acid injection had been described previously in adult rats suggesting a role in synaptic function and plasticity (Kim et al., 2003). In this study, we describe for the first time the heterogeneous expression of c-KIT in both IONs and MLIs during development and adulthood, and its localization in a subset of synapses made by these afferents on their target PCs. At the mRNA level, the expression of *c-Kit* is modulated by sensory deprivation. In addition to MLIs, we showed the expression of c-KIT in some other inhibitory interneurons residing specifically in lobule VI in the vermis of the cerebellum. Our preliminary functional analysis using conditional knockout of *c-Kit* in MLIs after the 2nd postnatal week suggests an effect on the maturation or function of both VGLUT2^{+} and GAD65^{+} presynaptic boutons only in PCs of lobule VI in the cerebellar vermis.

During the second postnatal week, the CFs translocate from PC soma to its dendrites, while basket cells (one of the two MLIs) make their synapses on PC soma and AIS (Sotelo, 2008). Since both of these synapses were seen on the PC soma at the same time, it is suggested that the translocation of CFs from soma and the replacement of their territory by basket cells axon is not via a direct competition between these two afferents (Sotelo, 2008). Expression of c-KIT by those two afferents and of its ligand by the target PCs suggests that this molecular pathway could control the establishment of their territories between the CFs and MLIs on PCs. Our results show the localization of c-KIT on the CFs and a subpopulation of their synaptic contacts on PCs at P2 and P4, as well as its presence on the axons of MLIs and a subpopulation of their inhibitory synapses on PCs both at P14 and P34. These observations support the suggested role for c-KIT signaling in the organization of subcellular localization of CF and MLI territories on PCs.

The use of *Pvalb*$^{ires\text{-}Cre}$ allowed us to conditionally knockout *c-Kit* in MLIs only after the 2nd postnatal week. To investigate the role of c-KIT in the establishment of the CF and MLI connectivity on PCs, we are planning to remove *c-Kit* earlier during postnatal development (e.g. 1st postnatal week) by injecting ION- or MLI-specific serotypes of CRE-expressing adeno associated viruses (AAVs) into the cerebellar cortex of *c-Kit*$^{fl/fl}$. To study the role of the interaction of c-KIT with SCF in PC connectivity with its afferents, conditional removal of *Scf* from PCs via crossing *Scf*$^{fl/fl}$ mice with *L7(Pcp2)*$^{ires\text{-}Cre}$ (a PC-specific CRE mouse line) is a powerful tool and ongoing. Our preliminary data validates the absence of *Scf* mRNA from the cerebellar extracts of P28 mice using RT-qPCR. We need to monitor the time of removal of *Scf* from PCs in these mice to further perform functional analysis on the density and volume of VGLUT2 and GAD65 boutons.

Our preliminary results show a decrease in the volume of both CF and MLI synapses on PCs in the molecular layer of lobule VI after *c-Kit* loss of function. This observation suggests an equilibrium between CF and inhibitory inputs on PCs. The decrease in the volume of GAD65 (inhibitory) boutons is the direct effect of the absence of c-KIT in these synapses, suggesting changes in their transmission. Electrophysiological analysis is ongoing to test this hypothesis. We hypothesize that this weakening is sensed by PCs via homeostatic synaptic plasticity (Pozo and Goda, 2010), inducing an unknown mechanism to decrease the synaptic transmission of CFs to PCs, leading to the volume reduction of VGLUT2 boutons, to make a balance between the two excitatory and inhibitory inputs arriving onto PCs. The regulatory impact of GABAergic synaptic transmission on the development of CF connectivity on PCs has been already shown in mice during postnatal development (Nakayama et al., 2012). Conditional loss of function of GABA synthesizing enzyme GAD67 from PCs and MLIs, as well as pharmacological inhibition of GAD activity, leads to decreased GABAergic neurotransmission, deficient CF synapse elimination and maintenance of their multi-innervation on PCs from P10 to P16 in a Ca^{2+}-dependent manner (Nakayama et al., 2012). Local administration of diazepam, a sensitizer of $GABA_A$ receptor, from P10 to P14 promotes CF synapse elimination and rescues the multi-innervation phenotype (Nakayama et al., 2012). The molecular mechanisms underlying this regulatory effect are not yet known. Does c-KIT/SCF signaling contributes to the role of inhibitory inputs in the refinement of CF connectivity on PCs?

The molecular mechanisms involved in subcellular targeting of PCs by various excitatory and inhibitory afferents are partially known (Ango et al., 2021; Reeber et al., 2013; Yuzaki, 2017). The C1Q complement protein C1QL1 is a secreted protein released by CFs to form and maintain their excitatory synapses on proximal dendrites of PCs (Kakegawa et al., 2015; Sigoillot et al., 2015). Removal of C1QL1 from CFs reduces their territory on PCs dendrites (Kakegawa et al., 2015; Sigoillot et al., 2015). The axon guidance molecule semaphorin-3A (SEMA3A), secreted from PCs around their soma and AIS, and its receptor Neuropilin-1 (NRP1), expressed by BCs on their axons from P8 to P21, are involved in BC axon guidance, branching and targeting on AIS of PCs to form the pinceau (Cioni et al., 2013; Telley et al., 2016). Interaction of SEMA3A with NRP1 triggers the Src kinase FYN signaling in BCs to recruit soluble guanylyl cyclase to the axon cone and promote axon growth via regulation of actin dynamics (Cioni et al., 2013). Knockdown of SEMA3A or FYN or inhibition of soluble guanylyl cyclase decreases the branching of BCs specifically at PC layer (Cioni et al., 2013), while expression of SEMA3A guides the growth of BC axons (Telley et al., 2016). In addition to the axon guidance role in BCs toward SEMA3A-releasing PC soma, NRP1 functions as a recognition molecule by binding to the cell adhesion molecule neurofascin-186

(NF186) localized in the PC AIS during pinceau formation (Telley et al., 2016). This interaction requires the presence of SEMA3A, which stabilizes the NRP1 at the pinceau and promotes its interaction with NF186 (Ango et al., 2021; Telley et al., 2016). This is one of the mechanisms of target recognition at the pinceau level. Probably c-KIT/SCF signaling is another mechanism that is not only restricted to pinceaux, but covers wider territory of MLIs on PCs, and is involved in balance between CF- and MLI-PC connectivity.

Methods and Materials:

Animals:

All mice were kept in the authorized animal facilities of the CIRB, College de France, under a 12 hour light: 12 hour dark cycle with water and food supplied ad libitum. All animal protocols and animal facilities were approved by the Comité Régional d'Ethique en Expérimentation Animale (#2001) and the veterinary services (D-75-05-12). *Igsf9*-GFP mice (STOCK Tg(Igsf9-EGFP)JR10Gsat/Mmucd, RRID:MMRRC_030804-UCD) were obtained from the Mutant Mouse Resource and Research Center (MMRRC) at University of California at Davis, an NIH-funded strain repository, and was donated to the MMRRC by Nathaniel Heintz, Ph.D., The Rockefeller University, GENSAT. This line is maintained on FVBN background. *Pvalb*$^{ires\text{-}Cre}$ mice (B6.129P2-Pvalbtm1(cre)Arbr/J, RRID:IMSR_JAX:017320) were and *c-Kit*^{fl} mice (B6.Cg-Kittm1.1Sraf/Mmjax, RRID:MMRRC_042035-JAX) were received from The Jackson Laboratory. Both lines are maintained on the C57BL/6J background. OF1 mice (Charles River Laboratories, Wilmington, USA) were used for the immunolabeling, whisker trimming and acute and chronic harmaline injection. In all experiments, littermate mice from both sexes were used as controls for the analysis.

Whisker Trimming:

The whisker trimming protocol was obtained from (Arakawa and Erzurumlu, 2015) with some modifications (Figure 2a). The whiskers of P3 pups were trimmed using an animal hair super trimmer (Wahl manufacturing company, Ilinois, US) every other day until P21. For the control condition, the hair trimmer was turned on in the proximity of the ears of the animals for 30 seconds. The animals were sacrificed at P21, and their cerebella and brainstems (containing inferior olive) were extracted and frozen immediately in liquid nitrogen and stored at -80C°.

Harmaline Injection:

In the chronic injection model, harmaline hydrochloride dihydrate (Sigma, Cat# H1392, 50mg/kg weight of the animal diluted in physiological serum) or physiological serum (NaCl 0.9% solution) was injected intraperitoneally every day from P10 to P14 in OF1 mice (Figure 2a). The animals were sacrificed a few hours after the last injection. In the acute injection model, harmaline hydrochloride dihydrate (Sigma, Cat# H1392, 50mg/kg weight of the animal diluted in physiological serum) or physiological serum was injected intraperitoneally at P14 in OF1 mice (Figure 2a). The animals were sacrificed 3 hours after the injection. In both models, the cerebella and brainstems (containing inferior olive) were extracted and frozen immediately in liquid nitrogen and stored at -80C°.

Gene expression analysis

RNA extraction and cDNA synthesis:

Total RNA from the frozen cerebella and brainstems was purified using the Qiagen RNeasy mini kit (Qiagen, Venlo, Netherlands, #74104), according to manufacturer's instruction. cDNA was synthetized using 100 ng of total RNA and SuperScript™ VILO™ cDNA Synthesis Kit (Life Technologies, California, USA, #11754050) according to manufacturer's instruction.

qPCR:

Quantitative PCR on cDNA samples was performed using FAM-labeled *c-Kit* probe (Taqman Gene Expression Assay, ThermoFisher, Assay ID: Mm00445212_m1), *Scf* (Taqman Gene Expression Assay, ThermoFisher, Assay ID: Mm00442972_m1), *Cdh9* (Taqman Gene Expression Assay, ThermoFisher, Assay ID: Mm03412730_m1), *Pcdh20* probes (Taqman Gene Expression Assay, ThermoFisher, Assay ID: Mm00724499_m1), and VIC-labeled *Rpl13a* probe as a reference (Taqman Gene Expression Assay, ThermoFisher, Assay ID: Mm01612986-gH) and the TaqMan Universal Master Mix II, with UNG (Applied Biosystems, #4440038) according to manufacturer's instructions. Bio-Rad CFX Manager was used for data analysis. The threshold for both FAM & VIC channels was set at 500. The relative expression of each candidate gene to *Rpl13a* was calculated based on the following formula: Relative expression = $(2^{-(\text{Cq of } \textit{Candidate} \text{ gene} - \text{Cq of } \textit{Rpl13a})}) \times 100$

High throughput RTqPCR:

High-throughput quantitative RT-PCR was performed as previously described in (Paul et al., 2023; Veleanu et al., 2022a). Briefly, cDNAs were synthesized using 100 ng of total RNAs with high quality and integrity (mean RNA Quality Number of 9.6) using Reverse Transcription Master Mix from Fluidigm™ (California, USA) on a Nexus Thermocycler (Eppendorf®, Hambourg, Germany; protocol: 5min at 25°C, 30min at 42°C, heat-inactivation of the reverse transcriptase 5min at 85°C and then 4°C). cDNA samples were diluted 5 times in low TE buffer (10mM Tris; 0.1mM EDTA; pH = 8.0; TEKNOVA®, Fisher Scientific, Massachusetts, USA) and used for specific target multiplex pre-amplification using Fluidigm® PreAmp Master Mix and pooled TaqMan® Gene Expression assays (Life Technologies, California, USA) with a final concentration of 180nM for each assay (protocol: 95°C for 2min, followed by 18 cycles at 95°C for 15s and 60°C for 4min). The same Taqman Gene expression assays listed in the qPCR were used.

Quantitative PCR was performed using the high-throughput platform BioMark™ HD System and the 96.96 GE Dynamic Arrays (Fluidigm®). The expression of target genes was quantified in the 5 times diluted pre-amplified cDNAs by quantitative PCR on 96.96 microfluidic chips. The loaded Dynamic Array was transferred to the Biomark™ real-time PCR instrument and amplified by PCR (25°C for 30min and 70°C for 60min for thermal mix; 50°C for 2min and 95°C for 10min for hot start; 40 cycles at 95°C for 15s and 60°C for 1min). ROX was used as a passive reference and single probe FAM-MGB as a fluorescent detector. To determine the quantification cycle Ct, data were processed by automatic threshold for each assay, with linear derivative baseline correction using BioMark Real-Time PCR Analysis Software 4.0.1 (Fluidigm®). The quality threshold was set at the default setting of 0.65.

The raw data from gene expression analysis were extracted and analyzed using MATLAB. The data were normalized to *Rpl13a*, which showed the most stable expression among all the samples, based on the aforementioned formula in “qPCR” section.

Immunofluorescence:

Brains from mice at P4, P10, P14, P28 – 35, and P40 were fixed using intracardiac perfusion of 4% PFA in PBS solution. Brains were extracted, post-fixed with the same solution at 4°C for 2 - 4 hours, and transferred to 30% sucrose/PBS at 4°C for cryoprotection. 30 µm-thick sections were prepared using a freezing microtome and kept in 0.02% NaN_3 in PBS solution at 4°C until use.

For immunostaining, brainstem or cerebellar sections were incubated in blocking buffer (4% donkey serum and 1% Triton X-100 in PBS solution) for 1 hour at room temperature, followed by incubation with primary antibodies in 1% donkey serum and 1% Triton X-100 in PBS overnight at 4°C with agitation. Primary antibodies were: GFP (1:1000, chicken, ab13970, Abcam, Cambridge, UK), c-KIT (1:1000, goat, AF1356, R&D Systems, Minnesota, US), CaBP (1:2000, rabbit, CB38, Swant, Marly, Switzerland), GAD65 (1:500, mouse, ab26113, Abcam, Cambridge, UK), VGLUT2 (1:7000, guinea pig, AB2251, Millipore, Molsheim, France), FOXP4 (1:1000, rabbit, ABE74, Sigma Aldrich, Missouri, USA), Aldolase C (1:2000, rabbit, received kindly from Izumi Sugihara). The floating sections were washed 3 times in 1% Triton X-100 in PBS for 10 minutes, followed by incubation with secondary antibodies (Alexa Fluor 488-, and 568- and 647-labeled donkey/goat anti-mouse, guinea pig, goat, rabbit, or chicken IgGs (H+L); 1:1000, Invitrogen or Life Technologies) in 1% Triton X-100 in PBS for 2 hours at room temperature. Then, sections were washed 3 times in 1% Triton X-100 in PBS for 10 minutes, and incubated for 10 min at room temperature with Hoechst 33342 (0,2 mg/mL, Sigma, Gothenburg, Sweden, cat#H6024) and 0.4% Triton X-100 in PBS. Sections were mounted using ProLong Gold Antifade Reagent (Invitrogen, #P36930).

Image acquisition and analysis:

Images of the whole cerebellum (Figure 3b) were obtained using a Zeiss Axiozoom V16 macroscope, equipped with a digital camera (AxioCam HRm) using a 25x oil objective (pixel size: 2.602 µm). The mosaic images of the brainstem (Figure S1) were taken using a spinning-disk confocal CSU-W1 microscope with a 25X objective (Z-plane step size: 1) and reconstructed using the Metamorph software. All the other images were taken using a spinning-disk confocal CSU-W1 microscope with a 63X oil objective (Z-plane step size: 0.19 µm). One z-plane is shown in the figures.

VGLUT2 and GAD65 quantifications were performed as described previously (Paul et al., 2023). All the images were normalized using the quantile-based normalization plugin on Fiji. A home-made plugin was developed based on the 3D Weka Segmentation plugin to count the number and measure the volume of VGLUT2 or GAD65 clusters (https://github.com/orion-cirb/Vglut2_GFP_Weka_Shayan). The 3D Weka Segmentation training was performed manually. All the steps were performed blind to the genotypes.

Statistical analysis:

All the data were analyzed and represented using GraphPad Prism. They are represented as mean ± SEM. The student's t-test was used to measure the differences between two groups when they had normal distribution. The non-parametric Mann-Whitney test was used when the two groups didn't have normal distribution.

Acknowledgements:

We would like to thank Philippe Mailly and Heloise Monet from CIRB Imaging facility (ORION) for their contribution in developing the home-made plugins to quantify immunofluorescence data, Marine Delagrange from the Plateforme qPCR-HD-GPC (Institut de Biologie de l'Ecole Normale Supérieure, Paris, France) to perform high throughput qPCR, and CIRB administration, imaging and animal facilities personnels. This work was supported by funding from: European Research Council ERC consolidator grant SynID 724601 (to FS), INCA PEDIAHR21-014 (to FS). SM received a PhD thesis funding from la Ligue Nationale Contre le Cancer and Ecole des neurosciences de Paris il-de-France (ENP). Since 2019, ENP has changed to la Fondation des Neurosciences Paris (FNP).

References:

Amat, S.B., Rowan, M.J.M., Gaffield, M.A., Bonnan, A., Kikuchi, C., Taniguchi, H., Christie, J.M., 2017. Using c-kit to genetically target cerebellar molecular layer interneurons in adult mice. PLoS ONE 12, e0179347. https://doi.org/10.1371/journal.pone.0179347

Ango, F., Gallo, N.B., Van Aelst, L., 2021. Molecular mechanisms of axo-axonic innervation. Curr. Opin. Neurobiol. 69, 105–112. https://doi.org/10.1016/j.conb.2021.03.002

Arakawa, H., Erzurumlu, R.S., 2015. Role of whiskers in sensorimotor development of C57BL/6 mice. Behav. Brain Res. 287, 146–155. https://doi.org/10.1016/j.bbr.2015.03.040

Cadilhac, C., Bachy, I., Forget, A., Hodson, D.J., Jahannault-Talignani, C., Furley, A.J., Ayrault, O., Mollard, P., Sotelo, C., Ango, F., 2021. Excitatory granule neuron precursors orchestrate laminar localization and differentiation of cerebellar inhibitory interneuron subtypes. Cell Rep. 34. https://doi.org/10.1016/j.celrep.2021.108904

Cioni, J.-M., Telley, L., Saywell, V., Cadilhac, C., Jourdan, C., Huber, A.B., Huang, J.Z., Jahannault-Talignani, C., Ango, F., 2013. SEMA3A Signaling Controls Layer-Specific Interneuron Branching in the Cerebellum. Curr. Biol. 23, 850–861. https://doi.org/10.1016/j.cub.2013.04.007

Duan, X., Krishnaswamy, A., De la Huerta, I., Sanes, J.R., 2014. Type II Cadherins Guide Assembly of a Direction-Selective Retinal Circuit. Cell 158, 793–807. https://doi.org/10.1016/j.cell.2014.06.047

Guijarro, P., Wang, Y., Ying, Y., Yao, Y., Jieyi, X., Yuan, X., 2013. In vivo knockdown of ckit impairs neuronal migration and axonal extension in the cerebral cortex. Dev. Neurobiol. 73, 871–887. https://doi.org/10.1002/dneu.22107

Heiman, M., Schaefer, A., Gong, S., Peterson, J.D., Day, M., Ramsey, K.E., Suárez-Fariñas, M., Schwarz, C., Stephan, D.A., Surmeier, D.J., Greengard, P., Heintz, N., 2008. A Translational Profiling Approach for the Molecular Characterization of CNS Cell Types. Cell 135, 738–748. https://doi.org/10.1016/j.cell.2008.10.028

Hippenmeyer, S., Vrieseling, E., Sigrist, M., Portmann, T., Laengle, C., Ladle, D.R., Arber, S., 2005. A Developmental Switch in the Response of DRG Neurons to ETS Transcription Factor Signaling. PLoS Biol. 3, e159. https://doi.org/10.1371/journal.pbio.0030159

Kakegawa, W., Mitakidis, N., Miura, E., Abe, M., Matsuda, K., Takeo, Y.H., Kohda, K., Motohashi, J., Takahashi, A., Nagao, S., Muramatsu, S., Watanabe, M., Sakimura, K., Aricescu, A.R., Yuzaki, M., 2015. Anterograde C1ql1 Signaling Is Required in Order to Determine and Maintain a Single-Winner Climbing Fiber in the Mouse Cerebellum. Neuron 85, 316–329. https://doi.org/10.1016/j.neuron.2014.12.020

Katafuchi, T., Li, A.-J., Hirota, S., Kitamura, Y., Hori, T., 2000. Impairment of Spatial Learning and Hippocampal Synaptic Potentiation in c-kit Mutant Rats. Learn. Mem. 7, 383–392.

Kim, D., Im, J. o., Won, Y. j., Yoon, S. y., Lee, E. j., Lee, J. h., Hong, H. n., 2003. Upregulation of c-Kit receptor and stem cell factor in cerebellar inhibitory synapses in response to kainic acid. J. Neurosci. Res. 71, 72–78. https://doi.org/10.1002/jnr.10466

Kim, S.Y., Mo, J.W., Han, S., Choi, S.Y., Han, S.B., Moon, B.H., Rhyu, I.J., Sun, W., Kim, H., 2010. The expression of non-clustered protocadherins in adult rat hippocampal formation and the connecting brain regions. Neuroscience 170, 189–199. https://doi.org/10.1016/j.neuroscience.2010.05.027

Kimura, Y., Ding, B., Imai, N., Nolan, D.J., Butler, J.M., Rafii, S., 2011. c-Kit-Mediated Functional Positioning of Stem Cells to Their Niches Is Essential for Maintenance and Regeneration of Adult Hematopoiesis. PLOS ONE 6, e26918. https://doi.org/10.1371/journal.pone.0026918

Kozareva, V., Martin, C., Osorno, T., Rudolph, S., Guo, C., Vanderburg, C., Nadaf, N., Regev, A., Regehr, W.G., Macosko, E., 2021. A transcriptomic atlas of mouse cerebellar cortex comprehensively defines cell types. Nature 598, 214–219. https://doi.org/10.1038/s41586-021-03220-z

LeDoux, M.S., Lorden, J.F., 2002. Abnormal spontaneous and harmaline-stimulated Purkinje cell activity in the awake genetically dystonic rat. Exp. Brain Res. 145, 457–467. https://doi.org/10.1007/s00221-002-1127-4

Lennartsson, J., Rönnstrand, L., 2012. Stem Cell Factor Receptor/c-Kit: From Basic Science to Clinical Implications. Physiol. Rev. 92, 1619–1649. https://doi.org/10.1152/physrev.00046.2011

Nakayama, H., Miyazaki, T., Kitamura, K., Hashimoto, K., Yanagawa, Y., Obata, K., Sakimura, K., Watanabe, M., Kano, M., 2012. GABAergic Inhibition Regulates Developmental Synapse Elimination in the Cerebellum. Neuron 74, 384–396. https://doi.org/10.1016/j.neuron.2012.02.032

Pasquale, E.B., 2008. Eph-Ephrin Bidirectional Signaling in Physiology and Disease. Cell 133, 38–52. https://doi.org/10.1016/j.cell.2008.03.011

Paul, M.A., Sigoillot, S.M., Marti, L., Delagrange, M., Mailly, P., Selimi, F., 2023. Stepwise molecular specification of excitatory synapse diversity on a target neuron. https://doi.org/10.1101/2023.01.03.521946

Pozo, K., Goda, Y., 2010. Unraveling mechanisms of homeostatic synaptic plasticity. Neuron 66, 337–351. https://doi.org/10.1016/j.neuron.2010.04.028

Reeber, S., White, J., George-Jones, N., Sillitoe, R., 2013. Architecture and development of olivocerebellar circuit topography. Front. Neural Circuits 6.

Sanes, J.R., Yamagata, M., 2009. Many Paths to Synaptic Specificity. Annu. Rev. Cell Dev. Biol. 25, 161–195. https://doi.org/10.1146/annurev.cellbio.24.110707.175402

Sanes, J.R., Zipursky, S.L., 2020. Synaptic Specificity, Recognition Molecules, and Assembly of Neural Circuits. Cell 181, 536–556. https://doi.org/10.1016/j.cell.2020.04.008

Sigoillot, S.M., Iyer, K., Binda, F., González-Calvo, I., Talleur, M., Vodjdani, G., Isope, P., Selimi, F., 2015. The Secreted Protein C1QL1 and Its Receptor BAI3 Control the Synaptic Connectivity of Excitatory Inputs Converging on Cerebellar Purkinje Cells. Cell Rep. 10, 820–832. https://doi.org/10.1016/j.celrep.2015.01.034

Sillitoe, R.V., Joyner, A.L., 2007. Morphology, Molecular Codes, and Circuitry Produce the Three-Dimensional Complexity of the Cerebellum. Annu. Rev. Cell Dev. Biol. 23, 549–577. https://doi.org/10.1146/annurev.cellbio.23.090506.123237

Sotelo, C., 2011. Camillo Golgi and Santiago Ramon y Cajal: the anatomical organization of the cortex of the cerebellum. Can the neuron doctrine still support our actual knowledge on the cerebellar structural arrangement? https://doi.org/10.1016/j.brainresrev.2010.05.004

Sotelo, C., 2008. Development of “pinceaux” formations and dendritic translocation of climbing fibers during the acquisition of the balance between glutamatergic and γ-aminobutyric acidergic inputs in developing purkinje cells. https://doi.org/10.1002/cne.21501

Stichel, C.C., Kägi, U., Heizmann, C.W., 1986. Parvalbumin in cat brain: isolation, characterization, and localization. J. Neurochem. 47, 46–53. https://doi.org/10.1111/j.1471-4159.1986.tb02829.x

Südhof, T.C., 2018. Towards an Understanding of Synapse Formation. Neuron 100, 276–293. https://doi.org/10.1016/j.neuron.2018.09.040

Tabone-Eglinger, S., Calderin-Sollet, Z., Pinon, P., Aebischer, N., Wehrle-Haller, M., Jacquier, M.-C., Boettiger, D., Wehrle-Haller, B., 2014. Niche anchorage and signaling through membrane-bound Kit-ligand/c-kit receptor are kinase independent and imatinib insensitive. FASEB J. Off. Publ. Fed. Am. Soc. Exp. Biol. 28, 4441–4456. https://doi.org/10.1096/fj.14-249425

Telley, L., Cadilhac, C., Cioni, J.-M., Saywell, V., Jahannault-Talignani, C., Huettl, R.E., Sarrailh-Faivre, C., Dayer, A., Huber, A.B., Ango, F., 2016. Dual Function of NRP1 in Axon Guidance and Subcellular Target Recognition in Cerebellum. Neuron 91, 1276–1291. https://doi.org/10.1016/j.neuron.2016.08.015

Triplett, J.W., Feldheim, D.A., 2012. Eph and ephrin signaling in the formation of topographic maps. Semin. Cell Dev. Biol. 23, 7–15. https://doi.org/10.1016/j.semcdb.2011.10.026

Veleanu, M., Urrieta-Chávez, B., Sigoillot, S.M., Paul, M.A., Usardi, A., Iyer, K., Delagrange, M., Doyle, J.P., Heintz, N., Bécamel, C., Selimi, F., 2022. Modified climbing fiber/Purkinje cell synaptic connectivity in the cerebellum of the neonatal phencyclidine model of schizophrenia. Proc. Natl. Acad. Sci. 119, e2122544119–e2122544119. https://doi.org/10.1073/pnas.2122544119

Voogd, J., Glickstein, M., 1998. The anatomy of the cerebellum. Trends Neurosci. 21, 370–375. https://doi.org/10.1016/S0166-2236(98)01318-6

Wang, W.X., Qiao, J., Lefebvre, J.L., 2022. PV-IRES-Cre mouse line targets excitatory granule neurons in the cerebellum. Mol. Brain 15, 85. https://doi.org/10.1186/s13041-022-00972-1

White, J.J., Arancillo, M., Stay, T.L., George-Jones, N.A., Levy, S.L., Heck, D.H., Sillitoe, R.V., 2014. Cerebellar Zonal Patterning Relies on Purkinje Cell Neurotransmission. J. Neurosci. 34, 8231–8245. https://doi.org/10.1523/JNEUROSCI.0122-14.2014

White, J.J., Sillitoe, R.V., 2013. Development of the cerebellum: from gene expression patterns to circuit maps. WIREs Dev. Biol. 2, 149–164. https://doi.org/10.1002/wdev.65

Williams, M.E., Wilke, S.A., Daggett, A., Davis, E., Otto, S., Ravi, D., Ripley, B., Bushong, E.A., Ellisman, M.H., Klein, G., Ghosh, A., 2011. Cadherin-9 Regulates Synapse-Specific Differentiation in the Developing Hippocampus. Neuron 71, 640–655. https://doi.org/10.1016/j.neuron.2011.06.019

Yamanaka, H., Yanagawa, Y., Obata, K., 2004. Development of stellate and basket cells and their apoptosis in mouse cerebellar cortex. Neurosci. Res. 50, 13–22. https://doi.org/10.1016/j.neures.2004.06.008

Yuzaki, M., 2017. The C1q complement family of synaptic organizers: not just complementary. Curr. Opin. Neurobiol., Molecular Neuroscience 45, 9–15. https://doi.org/10.1016/j.conb.2017.02.002

Zhou, H., Lin, Z., Voges, K., Ju, C., Gao, Z., Bosman, L.W., Ruigrok, T.J., Hoebeek, F.E., De Zeeuw, C.I., Schonewille, M., 2014. Cerebellar modules operate at different frequencies. eLife 3, e02536. https://doi.org/10.7554/eLife.02536

Zhou, J., Brown, A.M., Lackey, E.P., Arancillo, M., Lin, T., Sillitoe, R.V., 2020. Purkinje cell neurotransmission patterns cerebellar basket cells into zonal modules defined by distinct pinceau sizes. eLife 9, e55569. https://doi.org/10.7554/eLife.55569

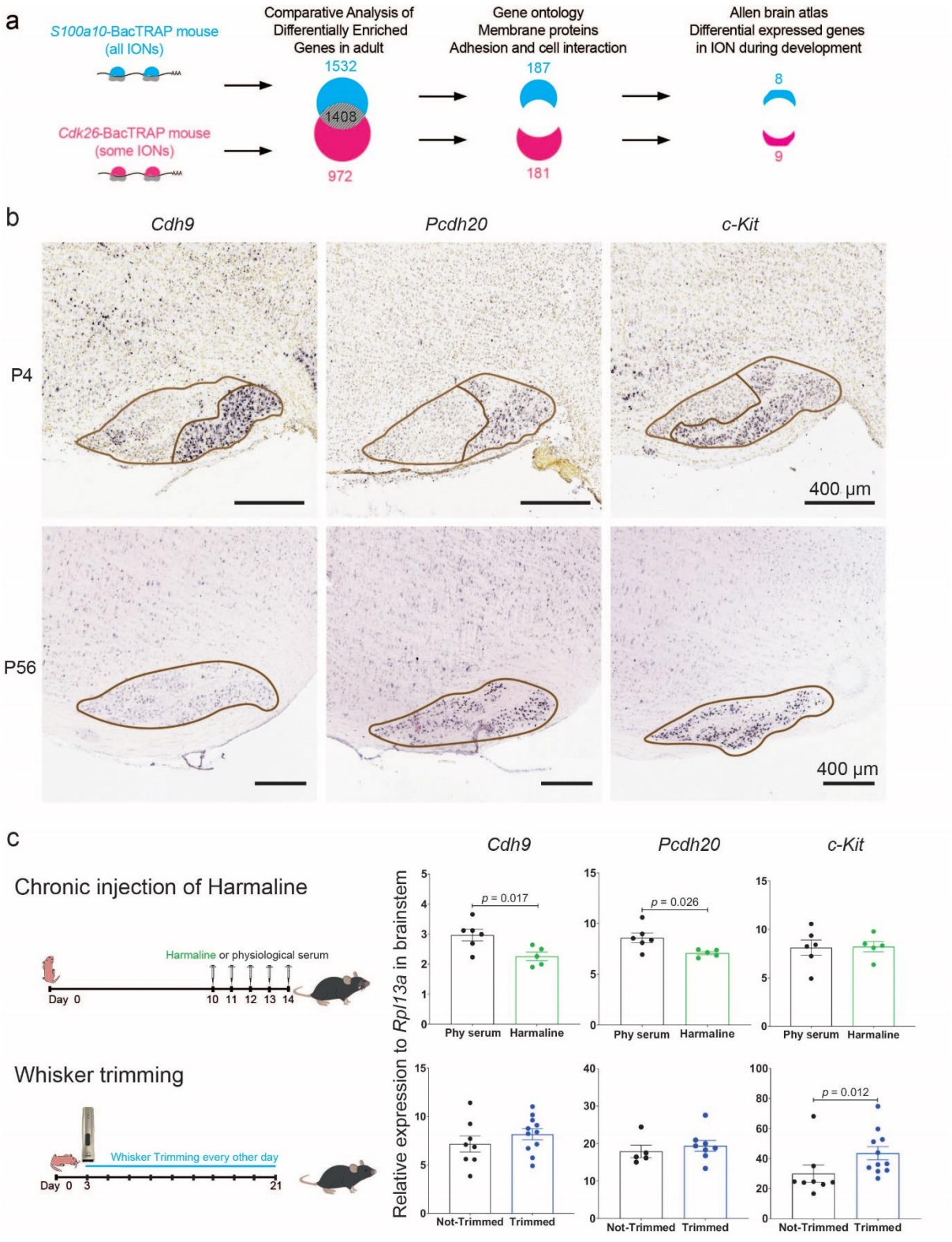

Figure 1. *Cdh9*, *Pcdh20*, and *c-Kit* expression is heterogeneous and neuronal activity-dependent in the inferior olivary neurons during development and adulthood. a) Workflow of comparative analysis of the gene expression profiles obtained using two bacTRAP lines, driven by s100a10 and Cdk6 drivers, to target all and a subpopulation of inferior olivary neurons, respectively. The two lists (S100a10: light blue, Cdk6: pink) were

compared together to exclude common genes (black). Gene ontology analysis was performed using DAVID & ToppeGene to identify genes coding membrane proteins involved in adhesion and cell surface interaction. The shortlisted genes were checked in Allen Brain Atlas for partial/heterogeneous expression in the inferior olive during development. b) In situ hybridization for *Cdh9*, *Pcdh20*, and *c-Kit* mRNAs in parasagittal sections of the mouse brainstem at P4 (*upper panel*) show their partial/heterogeneous expression in IONs, while at P56 (*lower panel*) show more homogeneous expression for *Pcdh20* and *c-Kit*, and much lower expression for *Cdh9* in the brainstem. In the upper panel, the sections of inferior olive with high and low expression are delineated by lines. In the lower panel, the boundary of inferior olive is delineated with lines. Scale bars = 400 µm. *The images were taken from Allen brain mouse development atlas (https://developingmouse.brain-map.org/).* c) Diagram of two experimental designs to modulate neuronal activity (*left panel*). In the chronic experiment, harmaline or vehicle was injected every day from P10 to P14. In the second experiment, whiskers were trimmed from P3 to P21 every other day. Expression of *Cdh9*, *Pcdh20*, and *c-Kit* were measured in the brainstem. Data are represented as mean ± SEM. n = 5 – 10 animals. Mann Whitney test. p indicated only when significant. Phy serum: Physiological serum.

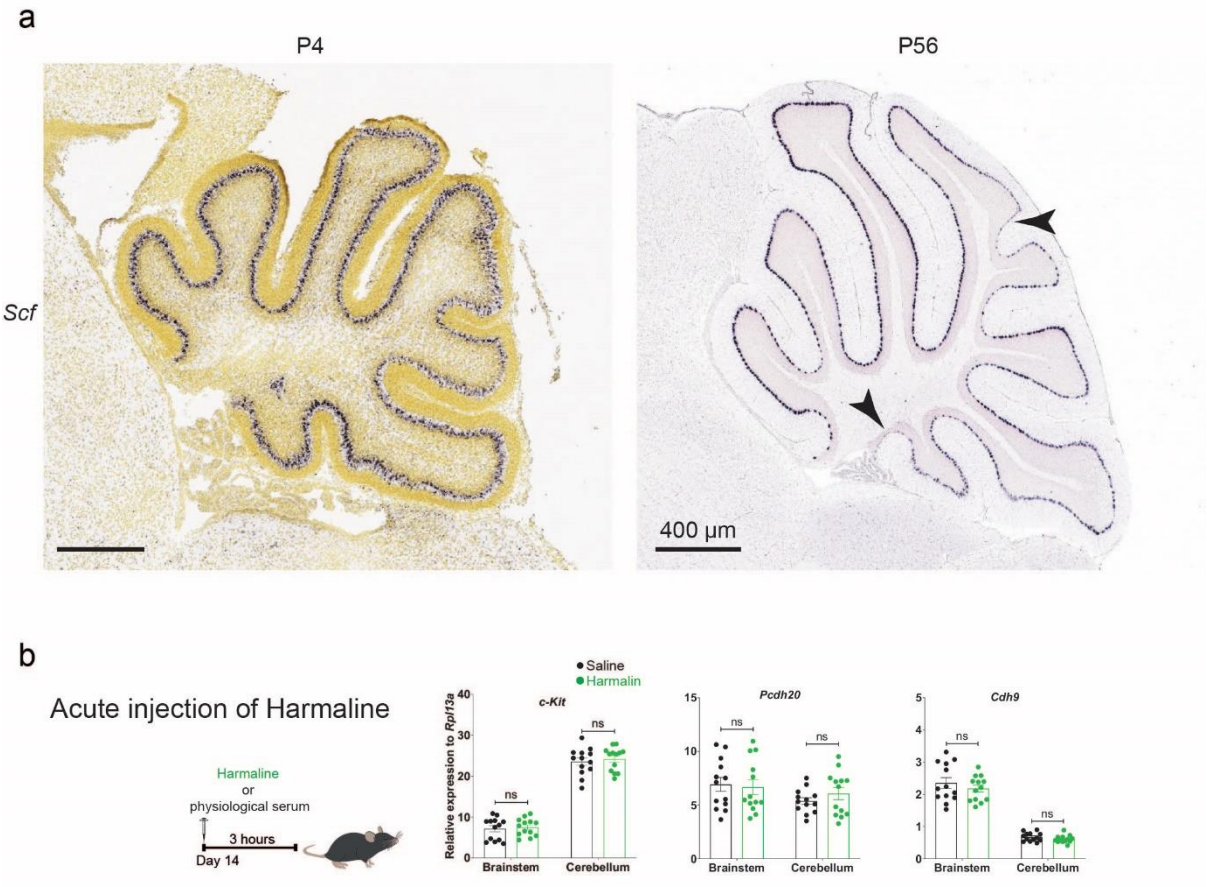

Figure S1. *Scf*, coding the ligand of c-KIT, is expressed heterogeneously in the Purkinje cells of the cerebellum. In situ hybridization labeling of c-KIT ligand, *Scf*, in parasagittal sections of P4 and P56 cerebellum shows its heterogeneous expression in Purkinje cells. The parts of cerebellar cortex with lower expression of *Scf* are shown with a black arrowhead. Scale bars = 400 µm. T*he images were taken from Allen brain mouse development atlas*. b) Diagram of the experimental design of acute harmaline injection to modulate neuronal activity (*left panel*). The P14 animals were sacrificed 3 hours after the injection of harmaline or vehicle. Expression of *Cdh9*, *Pcdh20*, and *c-Kit* were measured in the brainstem and cerebellum. Data are represented as mean ± SEM. n = 13 animals. Mann Whitney test. ns = not significant.

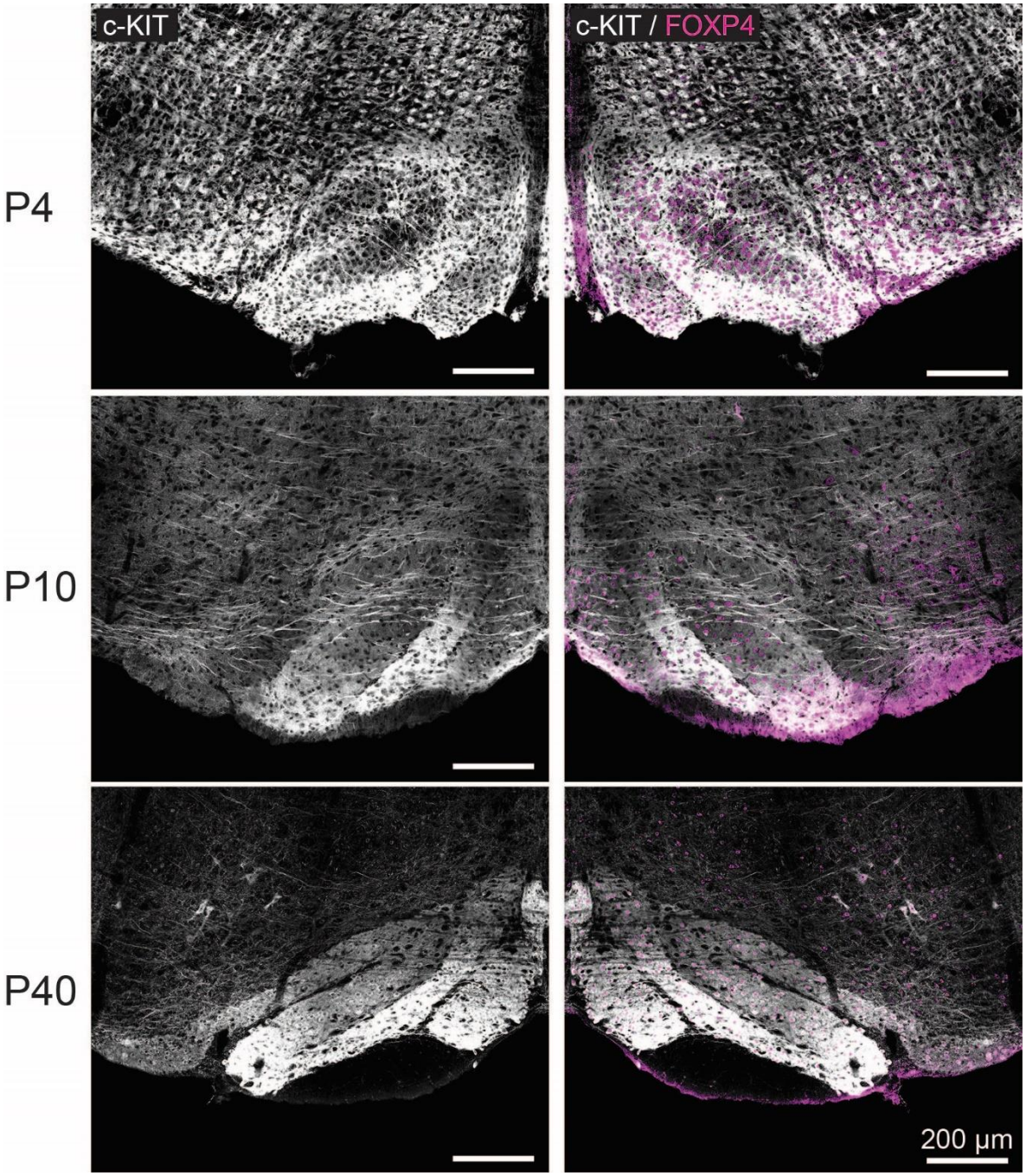

Figure S2. The c-KIT protein is heterogeneously expressed by IONs during postnatal development. Co-immunolabeling for c-KIT (grayscale, *left and right column*) and FOXP4 (magenta, *right column, mirror image of left column*) on coronal sections of the brainstem at P4, P10, and P40 shows the heterogeneous expression of c-KIT by IONs during different ages. Scale bars = 200 µm. The c-KIT intensity at P4 is much higher than the other ages in the inferior olive, so the settings for c-KIT channel at P4 is different than P10 and P40 which have the same parameters. The settings for FOXP4 channel are adjusted separately for each age.

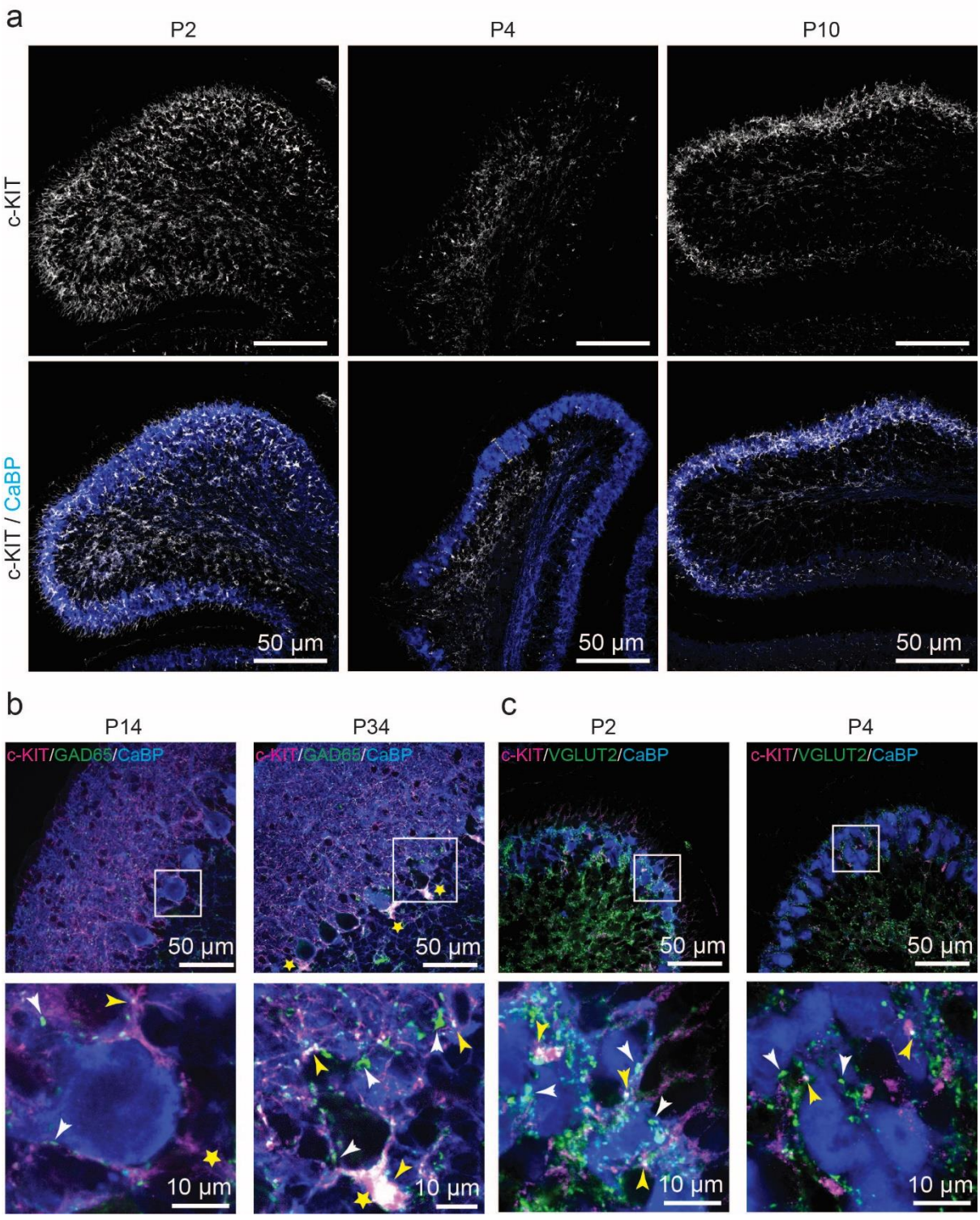

Figure 2. The c-KIT receptor is present on both MLI and CF synaptic contact sites on Purkinje cells. a) Co-immunolabeling for c-KIT and CaBP in parasagittal sections of the vermis of the mouse cerebellum at P2, P4 and P10 shows the localization of c-KIT in different layers of cerebellar cortex, especially in the Purkinje layer (yellow dashed line). Scale bar = 50 µm. b) Co-immunolabeling for c-KIT, MLI-PC presynaptic marker GAD65 and CaBP was performed on parasagittal sections of P14 and P34 cerebellar cortices. At P14, c-KIT is

observed all over the Purkinje and molecular layers, labeled with CaBP (*left panel*). Scale bar = 50 µm. Higher magnification of the region in the Purkinje layer delineated by the white square shows co-localization of c-KIT with some GAD65 boutons (yellow arrowhead), but not all of them (white arrowhead). c-KIT is observed around the axon initial segments of PCs (yellow star). Scale bar = 10 µm. At P34, c-KIT is observed in the molecular layer, but highly localized around the axon initial segments of PCs, in a structure called pinceau (yellow star). Scale bar = 50 µm. Higher magnification of the region in the Purkinje layer delineated by the white square shows co-localization of c-KIT with some GAD65 boutons (yellow arrowhead), but not all of them (white arrowhead) at P34. Scale bar = 10 µm. c) Co-immunolabeling for c-KIT, the CF-PC presynaptic bouton marker VGLUT2 and the soluble CaBP labeling PCs was performed in parasagittal sections of P2 and P4 cerebellar cortex of wild-type animals. Scale bar = 50 µm. Higher magnification of indicated white square shows co-localization of c-KIT with some VGLUT2 boutons (yellow arrowhead), but not all of them (white arrowhead) (*left panel*). The c-KIT^{+} VGLUT2 boutons are observed on the soma of Purkinje cells at P2 and P4 (yellow arrowhead). Scale bars = 10 µm.

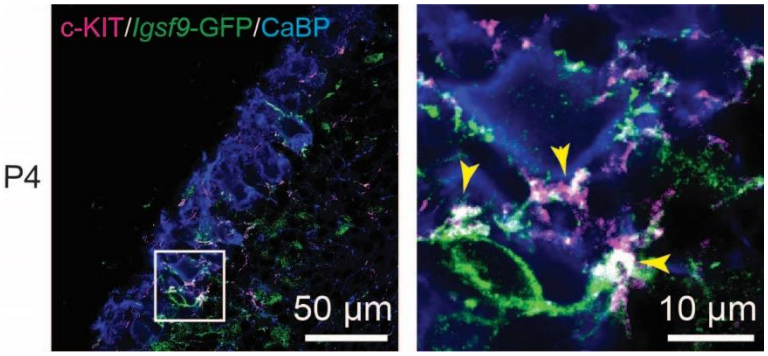

Figure S3. c-KIT is localized at the climbing fibers in the cerebellar cortex. Co-immunolabeling for GFP, c-KIT, and the PC marker CaBP was performed in parasagittal sections of the cerebellar cortex from *Igsf9*-GFP animals at P4. c-KIT localization is observed in the Purkinje cell layer where GFP^+ CFs are located around PCs. Scale bar = 50 µm. Higher magnification of the region delineated by the white square shows partial colocalization of c-KIT and GFP in some CFs in the proximity of PCs (yellow arrowhead).

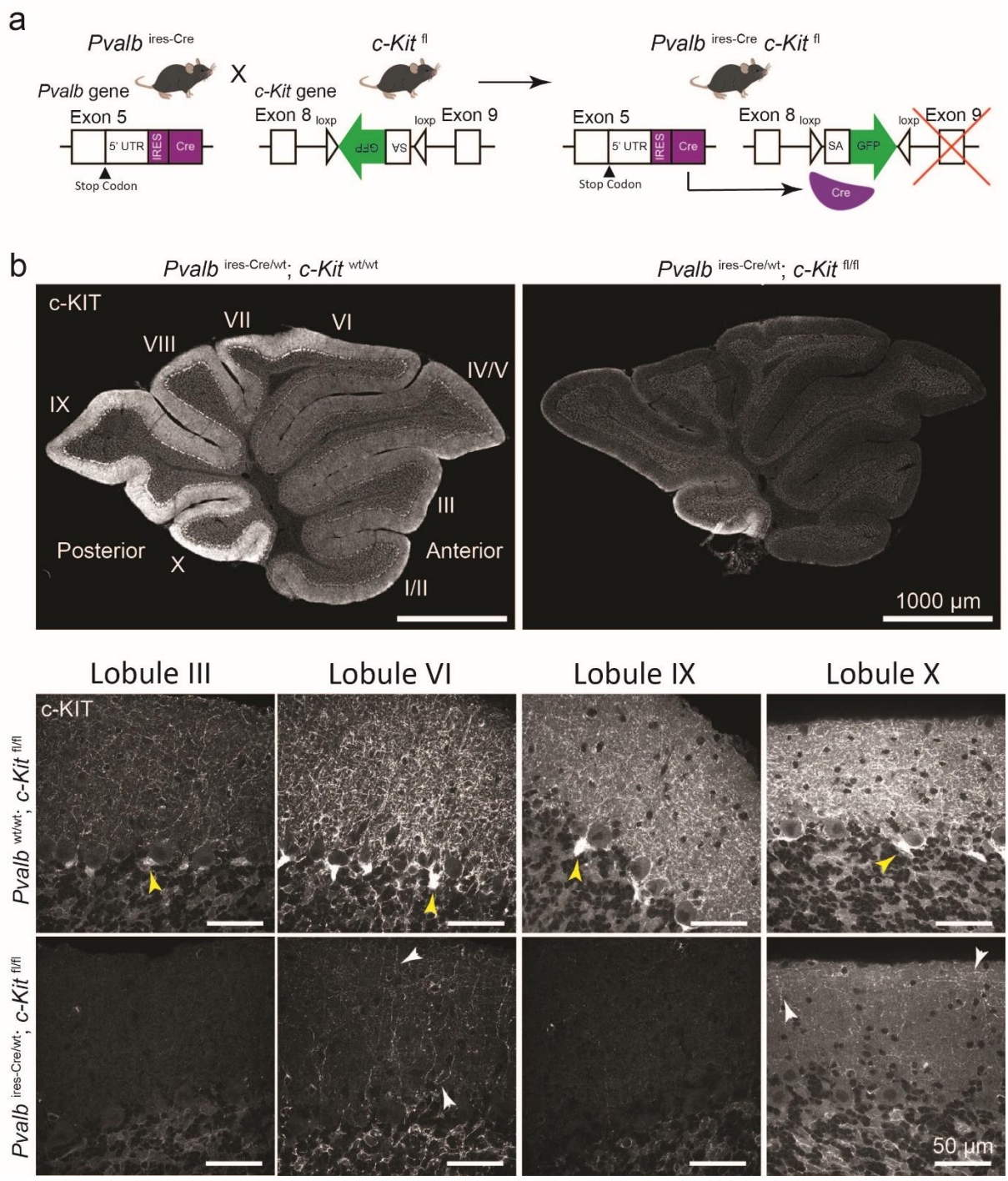

Figure 3. c-KIT is heterogeneously expressed by various inhibitory interneurons in the cerebellar cortex. a) Diagram of the breeding scheme used to conditionally knockout *c-Kit* in parvalbumin-expressing cells. The expression of CRE in *Pvalb*$^{+}$ cells flips the cassette coding a splice acceptor site (SA) and GFP with two polyadenylation/stop signals, leading to termination of the c-Kit transcript before its transmembrane (Exon 10) and kinase domain. b) Immunolabeling for c-KIT in parasagittal sections of the vermis of the cerebellum from >P28 control mouse show gradient in c-KIT from anterior to posterior lobules (*left panel*). c-KIT staining is almost gone in the cerebellar cortex of *c-Kit* conditional knockout mice (*Pvalb*$^{ires-}$

$^{Cre/wt}$; *c-Kit*$^{fl/fl}$) (*right panel*). Scale bar = 1000 µm. c) Higher magnification of the molecular layer of four different lobules shows complete lack of c-KIT in lobules III and IX in the *Pvalb*$^{ires\text{-}Cre/wt}$; *c-Kit*$^{fl/fl}$ animals, while some fibers in lobules VI and X still express c-KIT (white arrowhead). The high localization of c-KIT in the basket cell pinceau (yellow arrowhead) is completely absent in *Pvalb*$^{ires\text{-}Cre/wt}$; *c-Kit*$^{fl/fl}$ mice. Scale bar = 50 µm.

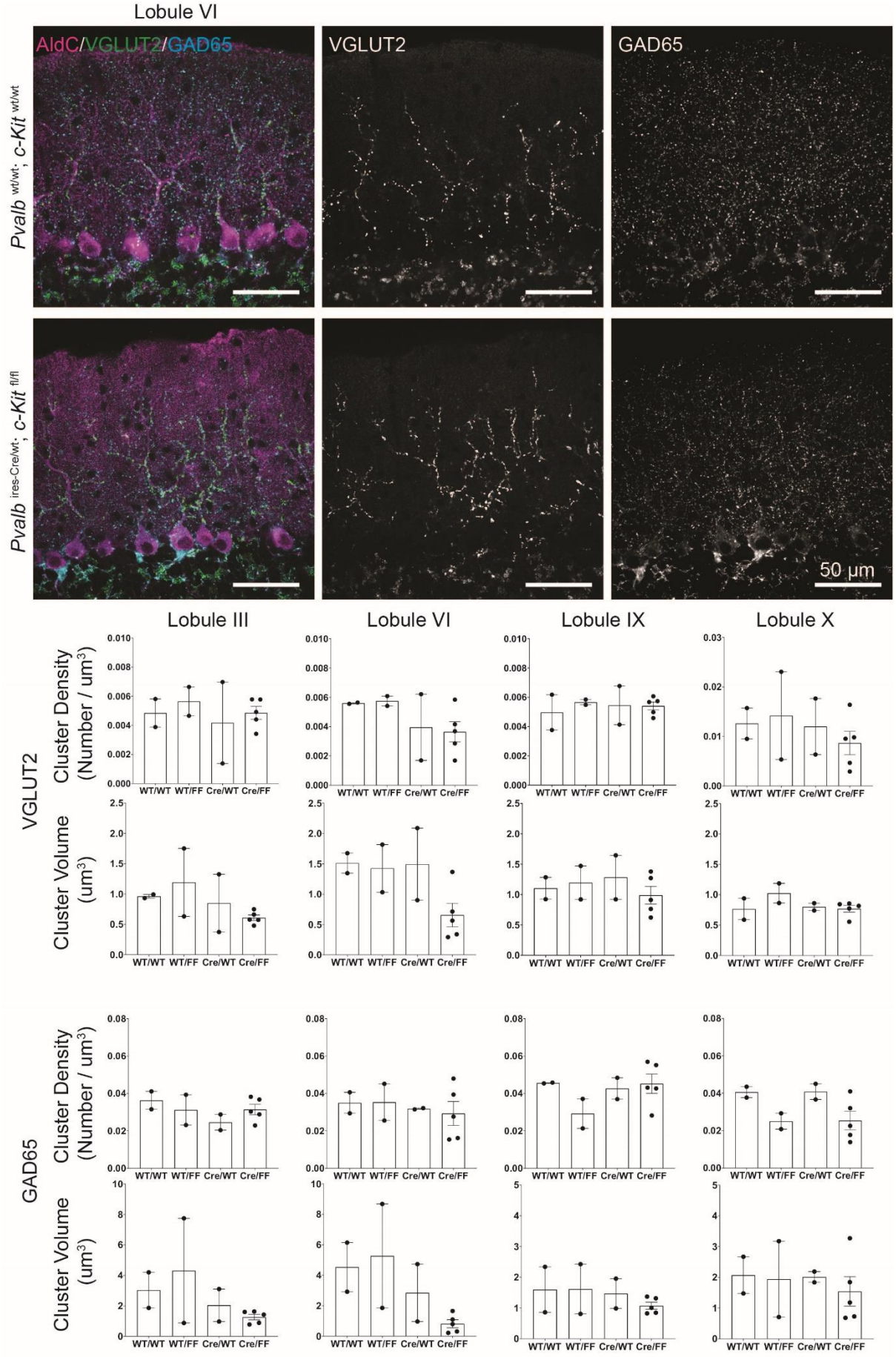
Lobule VI
AldC/VGLUT2/GAD65
VGLUT2
GAD65
Pvalb wt/wt; c-Kit wt/wt
Pvalb ires-Cre/wt; c-Kit fl/fl
50 μm
Lobule III
Lobule VI
Lobule IX
Lobule X
VGLUT2
GAD65
Cluster Density (Number / um3)
Cluster Volume (um3)
WT/WT WT/FF Cre/WT Cre/FF

Figure 4. Loss of function of *c-Kit* in cerebellar inhibitory interneurons might have lobule-specific effect on the connectivity of PCs with both MLI and CF afferents. Co-immunolabeling for Aldolase C (AldC), VGLUT2 and GAD65 was performed on parasagittal sections of P28-P34 cerebellar cortex (lobule VI) of control and *Pvalb*$^{ires\text{-}Cre/wt}$*; c-Kit*$^{fl/fl}$ mice (*top panel*). Scale bars = 50 µm. Quantification of the density and volume of VGLUT2 (*middle panel*) and GAD65 (*bottom panel*) clusters in the *Pvalb*$^{ires\text{-}Cre/wt}$*; c-Kit*$^{fl/fl}$ (Cre/FF) and the three controls (*Pvalb*$^{wt/wt}$*; c-Kit*$^{wt/wt}$: WT/WT, *Pvalb*$^{wt/wt}$*; c-Kit*$^{fl/fl}$: WT/FF, *Pvalb*$^{ires\text{-}Cre/wt}$*; c-Kit*$^{wt/wt}$: Cre/WT) in lobules III, VI, IX, and X shows a tendency in the decrease of the volume of VGLUT2 & GAD65 clusters in lobule VI, but not in other analyzed lobules. Data are represented as mean ± SEM. WT/WT, WT/FF, Cre/WT: n = 2 animals. Cre/FF: n = 5 animals.

Part 2: Mapping and targeting of *C1ql1*-expressing cells in the mouse.

Article in preparation.

Title:

Mapping and targeting of *C1ql1*-expressing cells in the mouse

Authors:

Shayan Moghimyfiroozabad[1], Maëla A. Paul[1], Séverine M. Sigoillot[1†*], Fekrije Selimi[1†*].

Affiliations:

[1]Center for Interdisciplinary Research in Biology (CIRB), College de France, CNRS, INSERM, Université PSL, Paris, France

[†] These authors contributed equally to this work

*corresponding authors: Fekrije Selimi and Séverine M. Sigoillot.

Abstract:

The C1Q complement protein C1QL1 is highly conserved in mammals where it is expressed in various tissues including the brain. It interacts with Brain-specific Angiogenesis Inhibitor 3, BAI3/ADGRB3, and controls synapse formation and maintenance. *C1ql1* is expressed in the inferior olivary neurons that send projections to cerebellar Purkinje cells, but its expression in the rest of the brain is less documented. To map *C1ql1* expression in the brain and enable the specific targeting of *C1ql1*-expressing cells, we characterized a knockin mouse model expressing the Cre recombinase under the *C1ql1* promoter. We characterized the capacity of the Cre to recombine in the brain and mapped its expression pattern in various neuron types using Cre-dependent reporter mouse lines. Using an intersectional strategy with viral particle injections, we show that this line can be used to target specific afferents of Purkinje cells. As *C1ql1* is also expressed in other regions of the brain, as well as in other tissues such as adrenal glands, placenta, colon and testis, our mouse model could be used to target *C1ql1*-expressing cells in a broad variety of tissues.

Introduction:

C1QL1 belongs to the subfamily of Complement component 1 Q subcomponent-Like proteins (C1QL). This subfamily is part of the C1Q complement family characterized by a C-terminal globular gC1Q signature domain involved in the formation of hetero- or homo-trimers (1,2). The N-terminal region of C1QL proteins contains two conserved cysteines allowing trimers to form higher-order oligomers (3). C1QLs are absent in plants, yeasts and several invertebrates (e.g. nematodes or insects), while they are found in fish, frog and mammals (3). Among mammals, the C1QL proteins are highly conserved with more than 90% amino acid identity between human and mouse orthologs (3).

In rodents, *C1ql1* is expressed in the brain (3,4), as well as the adrenal glands, placenta, colon and testis (Mouse ENCODE transcription data: https://www.ncbi.nlm.nih.gov/gene/23829). In the central nervous system, its expression is mostly associated with motor-related areas. Some nuclei in the medulla, pons, midbrain, olfactory bulb, hippocampus and cortex express *C1ql1* during postnatal development and adulthood (3,4). In the olivo-cerebellar network, transient expression of *C1ql1* is observed in the external granular layer (EGL) of the cerebellum at P7, where the precursors of the granule cells reside (3). *C1ql1* is also expressed in inferior olivary neurons (IONs) starting from birth and throughout the life of the mouse (3,4). C1QL1 is a secreted synaptic protein known to be released by the IONs and to bind to its postsynaptic receptor, the Adhesion-G Protein Coupled Receptor (GPCR) Brain-specific Angiogenesis Inhibitor 3 (BAI3, ADGRB3), on cerebellar Purkinje cells (PCs) (4,5). The interaction between C1QL1 and BAI3 is essential for the formation and maintenance of excitatory synapses between climbing fibers (CFs), axons from IONs, and their PC targets, as the removal of each of these two components results in loss of a significant amount of these synapses (4,5).

In order to fully understand the role of C1QL1 in different brain circuits, it is imperative to be able to specifically target *C1ql1*-expressing cells. To genetically manipulate the *C1ql1*-expressing cells *in vivo*, we developed the *C1ql1*^{Cre} knockin mouse model. We characterized the specificity and capacity of this mouse line as a driver using several reporter mouse lines. Finally, we show its usefulness for specific targeting of IONs *in vivo* using an intersectional strategy with viral vectors.

Results:

Characterization of the driver capacity of the *C1ql1*^{Cre} mouse line

To develop a mouse line expressing the Cre recombinase under the control of the *C1ql1* regulatory elements without modifying the coding sequence (CDS) of the *C1ql1* gene, we targeted its last exon (in collaboration with genOway company). A transgene was designed to contain two flippase recognition target (FRT) flanking a neomycin (neo) coding sequence, followed by the Exon 2 of the *C1ql1* gene where an IRES-Cre CDS cassette is inserted after the *C1ql1* stop codon. This transgene was knocked in the corresponding region on chromosome 11 by homologous recombination (Fig 1A). The neomycin sequence was removed later by breeding the transgenic mice with a flippase (Flp)-expressing mouse (Fig 1A). Identification of the *C1ql1*^{Cre} F0 transgenic mice containing the IRES-Cre CDS sequence was subsequently performed by PCR (Fig 1B).

To visualize and characterize the driver capacity of the *C1ql1*^{Cre} mouse line in the brain, homozygous *C1ql1*$^{Cre/Cre}$ mice were crossed with the Cre-dependent reporter mouse line *R26*$^{Cas9,-GFP/Cas9,-GFP}$ (6) (Fig 1C). In this reporter mouse, the presence of the CRE cleaves the STOP codon before the Cas9-P2A-GFP cassette. Due to the ubiquitous activity of the *Rosa26* locus (*R26*) and the use of the CAG promoter, Cas9 and soluble GFP are expressed permanently in all the cells that have expressed Cre and their potential progeny. This expression history was mapped in *C1ql1*$^{Cre/WT}$/*R26*$^{Cas9,-GFP/WT}$ heterozygotes at P30 using immunofluorescence on brain sagittal sections with an anti-GFP antibody to increase the signal to noise ratio (Fig 1D). The GFP-positive cells were observed in different regions of the forebrain, midbrain, brainstem and cerebellum (Fig 1D). At low magnification, two GFP-expressing regions were identified distinctly: the brainstem and the cerebellum (Fig 1D, a). In the brainstem, all the inferior olivary neurons (IONs) expressed GFP strongly (Fig 1D, a), in concordance with previous results showing homogenous expression of *C1ql1* among these neurons from early development until adult age (3). In the cerebellum, many granule cells (GCs) expressed GFP in a heterogeneous manner and in an antero-posterior gradient, with highest GFP signal in the anterior lobules. Based on *in situ* hybridization data (3), it is not the mature granule cells, but cells in the external granular layer that express *C1ql1* during the first two postnatal weeks. This suggests that the Cre-dependent recombination happens at the progenitor level in the granule cell lineage. Altogether, these results show that *C1ql1*^{Cre} mouse line is a powerful tool to genetically target two components of the olivo-cerebellar circuit, the IONs and the GCs.

At higher magnification, other GFP-expressing regions were identified in the brain of *C1ql1*$^{Cre/WT}$/*R26*$^{Cas9,-GFP/WT}$ mice (Fig 1D, a'-d'). According to the Allen Reference Brain atlas

(https://mouse.brain-map.org/static/atlas), we found GFP-expressing cells in several motor-related areas in the midbrain: ventral tegmental area, periaqueductal gray (Fig 1D, a and a'), substantia nigra pars reticulata and red nucleus (Fig 1D, b and b'). Adjacent to these regions, several GFP-positive cells were detected in two medial nuclei of the hypothalamus: supramammillary nucleus and Medial mammillary nucleus (Fig 1D, a and a'). In the pons, two nuclei were labelled with GFP: pontine reticular nucleus (motor related-area) (Fig 1D, b and b') and nucleus of the lateral lemniscus (sensory-related area) (Fig 1D, d and d'). In addition to the IONs (Fig 1D, a and a''), two other motor-related nuclei were expressing GFP in the medulla: paragigantocellular reticular nucleus (Fig 1D, b and b'') and vestibular nuclei (Fig 1D, c and c''). Expression of GFP is not restricted to the midbrain or hindbrain. In the forebrain, the accessory olfactory bulb and anterior olfactory nucleus are labelled with anti-GFP antibody (Fig 1D, c and c'). Altogether, different nuclei and regions, especially motor-related areas in the midbrain, pons and brainstem, can be targeted genetically with the *C1ql1*^{Cre} mouse model, in addition to the olivo-cerebellar network.

Effects of Cre transgene knockin on climbing fiber/Purkinje cell synapses in *C1ql1*$^{Cre/WT}$ heterozygotes

To detect the expression of the Cre recombinase in different brain regions, RT-qPCR was performed on RNA extracts from the cerebellum, the brainstem, the hippocampus and the cortex at P14. No expression of Cre was observed in extracts from control (wild-type, WT) mice, while Cre was detected in all tested regions of the brain in heterozygous *C1ql1*$^{Cre/WT}$ animals (Fig 2A). As expected, the highest expression of Cre was seen in the brainstem extracts where IONs are located (mean expression normalized to *Rpl13a* ± SEM = 6.40 ± 0.54 in the brainstem, *versus* 2.54 ± 0.54, 2.60 ± 0.57, and 1.53 ± 0.18 in the cerebellum, hippocampus, and cortex, respectively). We also assessed by RT-qPCR whether the insertion of the transgene had any impact on the expression of the endogenous *C1ql1* gene. At P14 in the heterozygous animals, the expression of *C1ql1* is decreased by 50-60% in all regions tested, compared to WT animals (Fig 2A), showing that the insertion of the transgene prevents the proper expression of *C1ql1* from the locus where it is inserted.

To test whether decreased *C1ql1* expression has a functional effect in heterozygous *C1ql1*$^{Cre/WT}$ mice, we performed morphological and functional analysis of climbing fiber/Purkinje cell (CF/PC) synapses. Indeed, C1QL1 loss of function leads to detectable phenotypes in CF/PC synapse formation and function in the olivo-cerebellar network with knockout levels of more than 90% (4,5). Morphological analyses were performed in two lobules of the cerebellum: lobules VI and IX, at P30 when the olivo-cerebellar circuit is well

established (7), using immunofluorescence against vesicular glutamate transporter 2 (VGLUT2), to label the presynaptic boutons of CFs, and Calbindin (CaBP) to label PCs. Quantification of the extension of CFs on the dendritic tree of PCs and of the size of the molecular layer of the cerebellar cortex showed no major difference in the CF territory and the thickness of molecular layer between *C1ql1*$^{WT/WT}$ and *C1ql1*$^{Cre/WT}$ heterozygotes, besides a 10.7% reduction in CF territory in lobule VI (Fig 2C; mean ± SEM = 120.7 ± 3.93 *vs* 107 ± 1.10; Statistics: unpaired student t test with Welsh's correction). Loss of function of *C1ql1* at a level >90% leads to decreased density of VGLUT2 clusters (4,5). Quantification did not detect any differences in the volume and density of VGLUT2 labelled presynaptic boutons between *C1ql1*$^{WT/WT}$ and *C1ql1*$^{Cre/WT}$ heterozygotes (Fig 2C). Loss of function of C1ql1 at a level >90% also leads to impaired transmission at CF/PC synapses (4,5). Using patch clamp to analyse the electrophysiological properties of these synapses during the fourth postnatal week, no difference was observed between the *C1ql1*$^{WT/WT}$ and *C1ql1*$^{Cre/WT}$ heterozygote mice (Fig 2B). Altogether, the expression of Cre and concomitant decrease of *C1ql1* expression in *C1ql1*$^{Cre/WT}$ heterozygous animals do not impact morphological or electrophysiological properties of CF/PC synapses. The *C1ql1*^{Cre} mouse line can thus be used to manipulate the olivo-cerebellar circuit when used as heterozygote without detrimental effect on normal development and function of the circuit.

Targeting different cell types in the olivo-cerebellar network using the *C1ql1*^{Cre} mouse line

The *C1ql1*^{Cre} mouse line allows the expression of the Cre recombinase in the olivo-cerebellar network, and in particular in IONs and GCs, the two excitatory inputs of the PCs. Different strategies can be used with this mouse line to, either target both excitatory inputs or only one of them. First, we crossed *C1ql1*$^{Cre/Cre}$ homozygous mice with *R26*$^{hM4Di,-mCitrine/WT}$ heterozygous mice (8) to produce *C1ql1*$^{Cre/WT}$/WT and *C1ql1*$^{Cre/WT}$/*R26*$^{hM4Di,-mCitrine/WT}$ heterozygous mice (Fig 3A). In this mice the DREADD hM4Di and soluble mCitrine are co-expressed in cells following the excision by the Cre of the Stop cassette preceding the hM4Di-P2A-mCitrine sequence (8). Immunofluorescence on brain sagittal sections at P30 using an anti-GFP antibody revealed that, contrary to the *C1ql1*$^{Cre/WT}$/WT controls, the *C1ql1*$^{Cre/WT}$/R26$^{hM4Di,-mCitrine/WT}$ heterozygous animals expressed mCitrine in the inferior olive in the brainstem, CFs being clearly seen in this region (Fig 3A) as well as in the molecular layer (Fig 3B). mCitrine-positive cells were also observed in the granule cell layer (GCL) from the cerebellum, more precisely in the GCs whose axons, the parallel fibers (PFs), are also mCitrine-labelled in the molecular layer. Of note, these results were obtained when a *C1ql1*$^{Cre/Cre}$ male was bred with *R26*$^{hM4Di,-mCitrine/WT}$ females,

whereas breeding a *R26*$^{hM4Di,-mCitrine/WT}$ male with *C1ql1*$^{Cre/Cre}$ females, led to mCitrine expression in the Bergmann glia cells in the cerebellum (Fig 3B), suggesting paternal imprinting of the locus.

To specifically target the IONs using *C1ql1*$^{Cre/WT}$ heterozygous mice, we developed an intersectional strategy. A retrograde AAV driving the expression of the Cre-dependent VAMP2-GFP construct under the CamKII promoter was injected in the cerebellum of postnatal day 0 (P0) mouse pups or P27 juvenile mice. As CamKII is expressed in IONs but not in GCs, the conditional expression of VAMP2-GFP was specific to the inferior olive, both at P27 and P44 after P0 and P27 injections, respectively (Fig. 4A). Contrary to what is observed with the breeding of *C1ql1*$^{Cre/Cre}$ with, for example, the reporter mouse line *R26*$^{Cas9,-GFP/\ Cas9,-GFP}$ (Fig 1D, a and a"), only subpopulations of IONs are targeted using this AAV strategy. Using immunofluorescent labeling of brain sagittal sections at P27 or P44 (data not shown), with an anti-GFP antibody (Fig 4B), GFP-positive climbing fibers were observed in different lobules in the cerebellum, in particular in lobules V to X in the vermis or paravermis (Fig 4B, *top panel*). At higher magnification, GFP-positive climbing fibers were visualized along the proximal dendrites of PCs (Fig. 4B, *bottom panel*). No GFP-positive GCs were observed, showing the high specificity of expression only in one of the two excitatory afferents of the PCs.

Discussion:

C1QL1 is a secreted protein involved in synapse formation and maintenance between inferior olivary neurons and Purkinje cells in the olivo-cerebellar circuit (4,5). Since the expression of *C1ql1* was identified in inferior olivary neurons and in the external granular layer during development, we developed a *C1ql1*^{Cre} mouse model by inserting an IRES-Cre cassette after the stop codon of *C1ql1*, to enable the genetic manipulation of the two sources of excitatory inputs to PCs, IONs and GCs, *in vivo*. Using RT-qPCR, the expression of Cre is detected in the cerebellum, brainstem, hippocampus and cortex. The specificity and capacity of the *C1ql1* driver was characterized by crossing the *C1ql1*^{Cre} mouse line with two CRE-dependent reporter mouse models: *R26*$^{Cas9,-GFP}$ and *R26*$^{hM4Di,-mCitrine}$. The expression of the reporter proteins is observed not only in IONs and GCs, but also in some other nuclei in the brainstem, midbrain and olfactory bulb. To specifically target IONs during postnatal development and adulthood, a viral strategy has been developed *via* stereotaxic injection of a retrograde rAAV2 with a CRE-dependent reporter gene in the cortex of the cerebellum at P0 or P27, resulting in the transduction of numerous IONs and CFs 2-4 weeks after the injection. In general, the *C1ql1*^{Cre} mouse model is a powerful genetic tool to target and manipulate *C1ql1*-expressing cells in the brain, in particular inferior olivary neurons in the brainstem.

The ectopic expression of Cre and loxP recombination is one of the disadvantages of using the Cre/lox system. Several examples of maternal or paternal biased Cre/loxP recombination have been reported (9). Thus, it is highly recommended to report the breeding strategy (10). In the crossings of *C1ql1*$^{Cre/Cre}$ with Cre-dependent *R26*$^{hM4Di,-mCitrine/WT}$ reporter mice we observed that the direction of the cross, whether *C1ql1*$^{Cre/Cre}$ is male or female, changes the pattern of expression of the reporter mCitrine in the cerebellar cortex. When *C1ql1*$^{Cre/Cre}$ is male, the *C1ql1*$^{Cre/WT}$/*R26*$^{hM4Di,-mCitrine/WT}$ offspring express mCitrine only in GCs in the cerebellar cortex, while when *C1ql1*$^{Cre/Cre}$ is female, not only GCs, but also BGs express mCitrine. These unexpected results are not observed in the crosses with the other reporter mouse line, *R26*$^{Cas9,-GFP}$. The expression of *C1ql1* in BGs is not reported in single-cell RNA sequencing performed on adult mouse cerebellum (11), but no data is available during postnatal development. The ectopic expression of mCitrine in BGs could be probably due to a spontaneous recombination dependent on the parental genotypes (9,12). Given our results, attention should be paid to the direction of the breeding when using *C1ql1*^{Cre} mouse model.

Using the Cre-dependent reporter mouse models to map the location of *C1ql1*-expressing cells, we show the localization of the reporter gene in several nuclei in different regions of the brain. These nuclei are involved in different functions (e.g. olfaction, arousal and consciousness), but some of them found in the brainstem, cerebellum, pons and midbrain, such as inferior olive, red nucleus, substantia nigra pars reticulata and GCs, are motor-related structures. We have not checked the expression of *C1ql1* and Cre in other organs than the brain in *C1ql1*^{Cre} mouse model, but several studies show the expression of *C1ql1* in testis, liver (3), adipose tissue (13), the adrenal glands, colon (https://www.ncbi.nlm.nih.gov/gene/23829), and ovaries (14). The function of C1QL1 in ovarian folliculogenesis has been investigated in mice using a full knockout model, showing its anti-apoptotic effect on granulosa cell apoptosis (14). Loss of function of *C1ql1* using a *C1ql1* constitutive knockout mouse model results in abnormal hair cell innervation in the cochlea and loss of audition (15). The *C1ql1*^{Cre} mouse model will thus be useful to study the role of C1QL1 in non-neuronal tissues.

In addition to physiological conditions, several studies suggest that C1QL1 might be involved in some malignancies. C1QL1 is upregulated in colorectal cancer, one of the most common malignant cancers (16), differentiated thyroid carcinoma (17), as well as lung adenocarcinoma (18). RNA-seq analyses have shown that *C1ql1* expression is higher in glioblastoma compared to the normal brain (16). All these studies show the diversity in the function of C1QL1 in health and disease in different systems of the body. Thus, *C1ql1*^{Cre} mouse could potentially be a useful model to study the role of *C1ql1*-expressing cells in different physiological and pathological conditions.

Methods and Materials:

Animals:

All mice were kept in the authorized animal facilities of CIRB, College de France, under a 12 hours light: 12 hours dark cycle with water and food supplied ad libitum. All animal protocols and animal facilities were approved by the Comité Régional d'Ethique en Expérimentation Animale (#2001) and the veterinary services (D-75-05-12). *C1ql1*^{Cre} mouse model was generated by genOway. The Cre-dependent reporter mouse lines, *R26*$^{Cas9\text{-}GFP}$ (B6J.129(B6N)-Gt (ROSA)26Sortm1(CAG-cas9*,-EGFP)Fezh/J, strain #026175) (6) and *R26*$^{hM4Di,\text{-}mCitrine}$ (B6.129-Gt(ROSA)26Sortm1(CAG-CHRM4*,-mCitrine)Ute/J, strain #026219) (8) were received from The Jackson Laboratory. All the lines are maintained on the C57BL/6J background. In all experiments, littermate mice from both sexes were used as controls for the analysis.

Viral particles and Stereotaxic injections

Injections of AAV particles were performed in the cerebellar vermis of ice-anesthetized P0 *C1ql1*$^{Cre/WT}$ heterozygous mice or isoflurane-anesthetized P27 *C1ql1*$^{Cre/WT}$ heterozygous mice, at 1 mm depth from the skull and 3.2 mm relative to Bregma or at 1.5 mm depth from drilled skull and 2.7 mm from Lambda respectively, to target Purkinje cell layer. AAV2/retrograde serotype was used to target IONs. 0.25µl of AAV was injected per animal using pulled calibrated pipets. AAVrg-CamKII-DIO-mVAMP2/eGFP-WPRE expressing the floxed mVAMP2-GFP, under the CaMKII promoter were obtained from Vector Biolabs: # AAV-275950 (RefSeq # BC055105), with a titer of 3.2x10^13 GC/mL.

Generation of C1ql1-IRES-Cre (C1ql1^{Cre}*) knockin mouse:*

C1ql1^{Cre} mice were generated using homologous recombination (genOway). A targeting vector containing Neomycin positive-selection cassette flanked with two FRT sites, and exon2 of *C1ql1* gene where an IRES-Cre cassette was inserted downstream of the stop codon in this exon, was electroporated into ES cells. The homologous recombination in the targeted ES cell clones was validated by PCR and DNA sequencing. The recombined ES cells with the correct sequence were injected into blastocysts. These blastocysts were then implanted in pseudo-pregnant females. Chimerism rate was then assessed in the progeny by coat color markers comparison. Highly chimeric males (chimerism rate above 50%) were generated and crossed with C57BL/6J Flp deleter female mice were used to excise the Neomycin selection cassette

and to generate heterozygous mice carrying the Neo-excised Neo-devoid Knockin. 16 heterozygous mice were screened by PCR followed by sequencing to make sure of the germline transmission.

PCR genotyping is carried out by multiplex PCR using two primers (forward primer: 5'-GCCCAGATGTATTCTGCCCTAGAATCC-3'; reverse primer: 5'-ATTGCACTGGCCCGCACCTAAG-3') to detect the WT (269 bp) and the targeted knock-in alleles (342 bp) (Fig. 1B). Transgenic founders were backcrossed and maintained on the C57Bl/6J background.

Characterization of C1ql1^{Cre} knockin mouse:

Gene expression analysis

RNA extraction and cDNA synthesis:

The cerebellum, brainstem, hippocampus and a piece of cortex were extracted from *C1ql1$^{WT/WT}$* or *C1ql1$^{Cre/WT}$* P14 mice and frozen immediately in liquid nitrogen, and stored at -80C°. Using the Qiagen RNeasy mini kit (Qiagen, Venlo, Netherlands, #74104), the total RNA was purified according to manufacturer's instruction. cDNA was synthetized using 100 ng of total RNA and SuperScript™ VILO™ cDNA Synthesis Kit (Life Technologies, California, USA, #11754050) according to manufacturer's instruction.

qPCR:

Quantitative PCR on cDNA samples was performed using FAM-labeled *C1ql1* (Taqman Gene Expression Assay, ThermoFisher, Assay ID: Mm00657289_m1) or *Cre* (Taqman Gene Expression Assay, ThermoFisher, Assay ID: Mr00635245_cn) probes and VIC-labeled *Rpl13a* probe as a reference (Taqman Gene Expression Assay, ThermoFisher, Assay ID: Mm01612986-gH) and the TaqMan Universal Master Mix II, with UNG (Applied Biosystems, #4440038) according to manufacturer's instructions. Bio-Rad CFX Manager was used for data analysis. The relative expression of *C1ql1* to *Rpl13a* or *Cre* to *Rpl13a* was calculated based on the following formula: Relative expression = ($2^{(\text{Cq of } C1ql1 \text{ or } Cre - \text{Cq of } Rpl13a)}$) x 100

Immunofluorescence:

Mice tissues were fixed using intracardiac perfusion of 4% PFA in PBS solution. Brains were extracted, post-fixed with the same solution at 4°C for 2 - 4 hours, and transferred to 30%

sucrose/PBS for 48 hours at 4°C for cryoprotection. 30 µm-thick sections were obtained using a freezing microcome, and kept in 0.02% NaN_3 in PBS solution at 4°C until use.

To perform immunolabeling, sections were incubated in blocking buffer (4% donkey serum and 1% Triton X-100 in PBS solution) for 30 min to 1 hour at room temperature, followed by incubation with primary antibodies in 1% donkey serum and 1% Triton X-100 in PBS for overnight at 4°C with agitation. Primary antibodies were: GFP (1:1000, chicken, ab13970, Sigma or 1:2000, rabbit, ab6556, Sigma), CaBP (1:2000, rabbit, CB38, Swant or 1:2000, mouse, #300), and VGLUT2 (1:7000, guinea pig, AB2251, Millipore). The slices were washed 3 times in 1% Triton X-100 in PBS for 5 to 10 minutes, followed by incubation with secondary antibodies (Alexa Fluor 488-, and 568- and 647-labeled donkey/goat anti-mouse, rat, rabbit, or chicken IgGs (H+L); 1:1000, Invitrogen or Life Technologies) in 1% Triton X-100 in PBS for 1 to 2 hours at room temperature. Then, sections were washed 3 times in 1% Triton X-100 in PBS for 5 to 10 minutes, and incubated for another 10 min at room temperature with Hoechst 33342 (0,2 mg/mL, Sigma, Gothenburg, Sweden, cat#H6024) and 0.4% Triton X-100 in PBS. Sections were mounted using ProLong Gold Antifade Reagent (Invitrogen, cat#P36930).

Image acquisition and analysis:

The mosaic images for global brain morphology (Fig. 1D) were obtained using a Zeiss Axiozoom V16 macroscope, equipped with a digital camera (AxioCam HRm) using a 160x (pixel size: 0.4037 µm), reconstructed using the Zeiss Zen software. Images for VGLUT2 quantifications (Fig. 2C) were acquired using a Zeiss spinning-disk confocal CSU-W1 microscope with 63x oil objective (Z-plane step size: 0.19 µm). Images for GFP analyses were acquired using the same spinning-disk confocal microscope with 63x (Fig. 3B) or 25x (Fig. 3A and Fig. 4) oil objectives (single plane). The mosaic images for GFP visualization were reconstructed using the stitching program from metamorph software (Fig. 3B *top panel*).

VGLUT2 quantification (cluster density and volume) were performed as described previously (19). All the images were normalized using the quantile-based normalization plugin in Fiji. The intensity distribution of the images has been normalized using 256 quantiles for each staining. The synaptic boutons were extracted from the background using the 3D Weka Segmentation plugin (https://imagej.net/Trainable_Weka_Segmentation) after manual selection of signal and background samples. The Fiji built-in plugin 3D object counter was then used in order to count and measure every object (cluster of VGLUT2 positive signal). CF territory and ML thickness were measured manually using Fiji. All the steps were performed in blind condition.

Electrophysiology:

Acute parasagittal cerebellar slices were obtained from *C1ql1*^{Cre} mice from P25 to P30. 200 µm-thick slices were cut at room temperature with a Campden Ci 7000 smz microtome in (in mM): Sucrose 120, NaCl 60, KCl 2.5, D(+)Glucose 25, NaHCO3 25, NaH2PO4 1.25, CaCl2 0.1, MgCl2 3, ascorbic acid 0.4, myo-inositol 3, NaPyruvate 2, pH=7.3-7.4. Slices were then transferred and allowed to recover for one hour at room temperature in the following solution (in mM): NaCl 125, KCl 2.5, D(+)Glucose 25, NaHCO3 25, NaH2PO4 1.25, CaCl2 2, MgCl2 1, ascorbic acid 0.4, myo-inositol 3, NaPyruvate 2, pH=7.3-7.4, oxygenated. This solution was used to fill the stimulation pipette and, complemented with picrotoxin (100 µM) was used as external solution for 5 recordings. Borosilicate glass pipettes with 2-5 MΩ resistance were used for recordings and filled with the following internal solution (in mM): CsCl2 155, Hepes 10, EDTA 5, QX314 5, pH=7.35 adjusted with CsOH. Responses to CF stimulation were recorded at a holding membrane potential of −10 mV in Purkinje cells of lobule VI using a MultiClamp 700B amplifier (Molecular Devices, CA) and acquired using the freeware WinWCP written by John Dempster (https://pureportal.strath.ac.uk/en/datasets/strathclyde-electrophysiology-software-winwcp-winedr). Series resistance was compensated by 80–90% and cells were discarded if significant changes were detected. CF-mediated responses were identified by the typical all-or-none response and strong depression displayed by the second response elicited during paired pulse stimulations (20 Hz). Electrophysiological data were analyzed using the software Clampfit 10.7 (Molecular Devices).

References:

1. Kishore U, Gaboriaud C, Waters P, Shrive AK, Greenhough TJ, Reid KBM, et al. C1q and tumor necrosis factor superfamily: modularity and versatility. Trends Immunol. 2004 Oct 1;25(10):551–61.
2. Ghai R, Waters P, Roumenina LT, Gadjeva M, Kojouharova MS, Reid KBM, et al. C1q and its growing family. Immunobiology. 2007 Jun 26;212(4):253–66.
3. Iijima T, Miura E, Watanabe M, Yuzaki M. Distinct expression of C1q-like family mRNAs in mouse brain and biochemical characterization of their encoded proteins. Eur J Neurosci. 2010;31(9):1606–15.
4. Sigoillot SM, Iyer K, Binda F, González-Calvo I, Talleur M, Vodjdani G, et al. The Secreted Protein C1QL1 and Its Receptor BAI3 Control the Synaptic Connectivity of Excitatory Inputs Converging on Cerebellar Purkinje Cells. Cell Rep. 2015 Feb 10;10(5):820–32.

5. Kakegawa W, Mitakidis N, Miura E, Abe M, Matsuda K, Takeo YH, et al. Anterograde C1ql1 Signaling Is Required in Order to Determine and Maintain a Single-Winner Climbing Fiber in the Mouse Cerebellum. Neuron. 2015 Jan 21;85(2):316–29.
6. Platt RJ, Chen S, Zhou Y, Yim MJ, Swiech L, Kempton HR, et al. CRISPR-Cas9 Knockin Mice for Genome Editing and Cancer Modeling. Cell. 2014 Oct 9;159(2):440–55.
7. Watanabe M, Kano M. Climbing fiber synapse elimination in cerebellar Purkinje cells. Eur J Neurosci. 2011;34(10):1697–710.
8. Zhu H, Aryal DK, Olsen RHJ, Urban DJ, Swearingen A, Forbes S, et al. Cre dependent DREADD (Designer Receptors Exclusively Activated by Designer Drugs) mice. Genes N Y N 2000. 2016 Aug;54(8):439–46.
9. Luo L, Ambrozkiewicz MC, Benseler F, Chen C, Dumontier E, Falkner S, et al. Optimizing Nervous System-Specific Gene Targeting with Cre Driver Lines: Prevalence of Germline Recombination and Influencing Factors. Neuron. 2020 Apr 8;106(1):37-65.e5.
10. Song AJ, Palmiter RD. Detecting and Avoiding Problems When Using the Cre/lox System. Trends Genet TIG. 2018 May;34(5):333–40.
11. Kozareva V, Martin C, Osorno T, Rudolph S, Guo C, Vanderburg C, et al. A transcriptomic atlas of mouse cerebellar cortex comprehensively defines cell types. Nature. 2021 Oct;598(7879):214–9.
12. Andrusaite A, Milling S. Should we be more cre-tical? A cautionary tale of recombination. Immunology. 2020 Feb;159(2):131–2.
13. Guan H, Shi T, Liu M, Wang X, Guo F. C1QL1/CTRP14 Is Largely Dispensable for Atherosclerosis Formation in Apolipoprotein-E-Deficient Mice. J Cardiovasc Dev Dis. 2022 Oct 6;9(10):341.
14. Lu X, Ding F, Chen Y, Ke S, Yuan S, Qiu H, et al. Deficiency of C1QL1 Reduced Murine Ovarian Follicle Reserve Through Intraovarian and Endocrine Control. Endocrinology. 2022 Jun 1;163(6):bqac048.
15. Qi Y, Xiong W, Yu S, Du Z, Qu T, He L, et al. Deletion of C1ql1 Causes Hearing Loss and Abnormal Auditory Nerve Fibers in the Mouse Cochlea. Front Cell Neurosci [Internet]. 2021 [cited 2023 May 2];15. Available from: https://www.frontiersin.org/articles/10.3389/fncel.2021.713651
16. Qiu X, Feng JR, Wang F, Chen PF, Chen XX, Zhou R, et al. Profiles of differentially expressed genes and overexpression of NEBL indicates a positive prognosis in patients with colorectal cancer. Mol Med Rep. 2018 Feb;17(2):3028–34.

17. Celestino R, Nome T, Pestana A, Hoff AM, Gonçalves AP, Pereira L, et al. CRABP1, C1QL1 and LCN2 are biomarkers of differentiated thyroid carcinoma, and predict extrathyroidal extension. BMC Cancer. 2018 Jan 10;18:68.
18. Gao YJ, Chen F, Zhang LJ. C1q-like 1 is frequently up-regulated in lung adenocarcinoma and contributes to the proliferation and invasion of tumor cells. J Chemother. 2021 Oct 3;33(7):476–85.
19. Veleanu M, Urrieta-Chávez B, Sigoillot SM, Paul MA, Usardi A, Iyer K, et al. Modified climbing fiber/Purkinje cell synaptic connectivity in the cerebellum of the neonatal phencyclidine model of schizophrenia. Proc Natl Acad Sci U S A. 2022 May 24;119(21):e2122544119.

Acknowledgments: We would like to thank Yves Dupraz for the development of tools for stereotaxic injections in neonates, and the personnel from the CIRB animal and imaging facilities.

Funding:

This work was supported by funding from:

European Research Council ERC consolidator grant SynID 724601 (FS)

Q-life ANR-17-CONV-0005 (FS)

ANR-10-LABX-54 MEMO LIFE (FS)

INCA PEDIAHR21-014 (FS)

Sorbonne Université ED158 (MAP)

Collège de France (MAP)

Ecole des neurosciences de Paris Ile-de-France (SM)

La Ligue Nationale Contre le Cancer (SM)

Author Contributions:

Conceptualization: FS

Methodology: FS, SM, SMS, MAP

Investigation: SM, SMS, FS, MAP

Visualization: SM, SMS, FS

Funding acquisition: FS

Project administration: FS

Supervision: FS and SMS

Writing – original draft: SM and SMS

Writing – review & editing: SMS, SM, FS

Competing Interest Statement: The authors declare no competing interest.

Data and materials availability: All data are available in the main text.

Figures

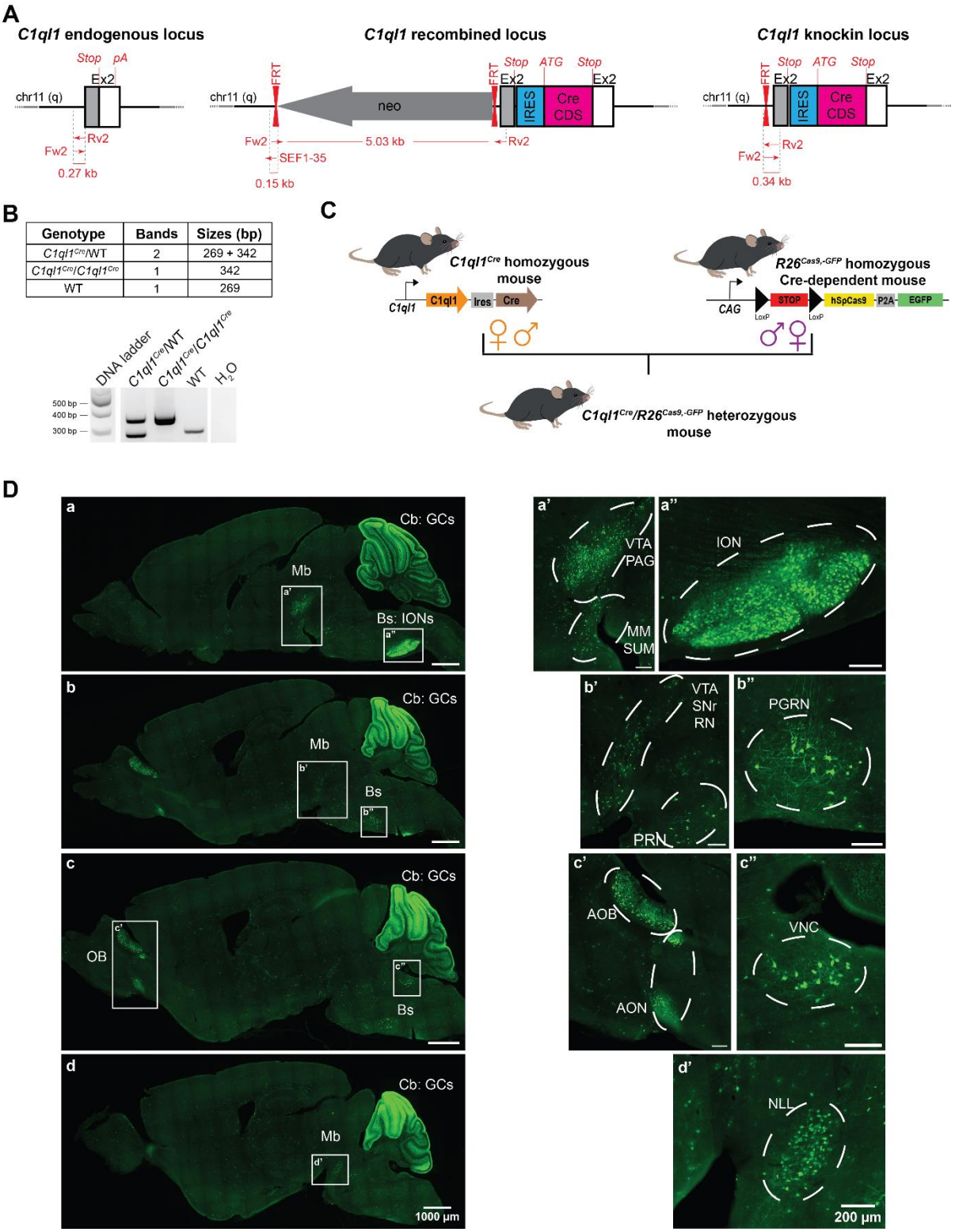

Fig 1. Characterization of the driver capacity of the *C1ql1*^{Cre} mouse line.

(A) Illustration of the mouse *C1ql1* locus at the 2nd exon and flanking regions. Homologous recombination was used to insert a neomycin cassette upstream of the *C1ql1* exon2 and an IRES-Cre cassette downstream of the stop codon in the *C1ql1* exon2. After neomycin selection and mice generation, the neomycin cassette was removed using flippase to obtain C1ql1-IRES-Cre knockin mice (*C1ql1*^{Cre}). **(B)** *Top panel:* Table of the genotyping PCR amplicon bands and their respective sizes depending on the genotype. *Bottom panel:* Representative image of a genotyping PCR run. **(C)** Schematic illustration of the breeding strategy used to generate *C1ql1*^{Cre}/*R26*$^{Cas9,-GFP}$ double heterozygous mice. Crossings in the two directions were tested. **(D)** Medial to lateral sagittal sections from P30 *C1ql1*^{Cre}/*R26*$^{Cas9,-GFP}$ mouse brain were immunostained for GFP at P30. Mosaic images were acquired using a spinning disk confocal microscope (a – d). EGFP was highly expressed in the cerebellum (Cb), in particular in Granule Cells (GCs), and in the brainstem (Bs), and present in other nuclei from the midbrain (Mb) and olfactory bulb (OB). Scale bars = 1000 µm. (a' – d') High magnification of different nuclei or neurons expressing eGFP in P30 *C1ql1*^{Cre}/*R26*$^{Cas9,-GFP}$ mice. Scale bars = 200 µm. AOB: Accessory Olfactory Bulb, AON: Anterior Olfactory Nucleus, ION: Inferior Olivary Nuclei, MM: Medial Mammillary nucleus, NLL: Nucleus of the Lateral Lemniscus, PAG: Periaqueductal Gray, PGRN: Paragigantocellular Reticular Nucleus, PRN: Pontine Reticular Nucleus, RN: Red Nucleus, SNr: Substantia Nigra pars reticulata, SUM: Supramammillary nucleus, VNC: Vestibular Nuclei, VTA: Ventral Tegmental Area.

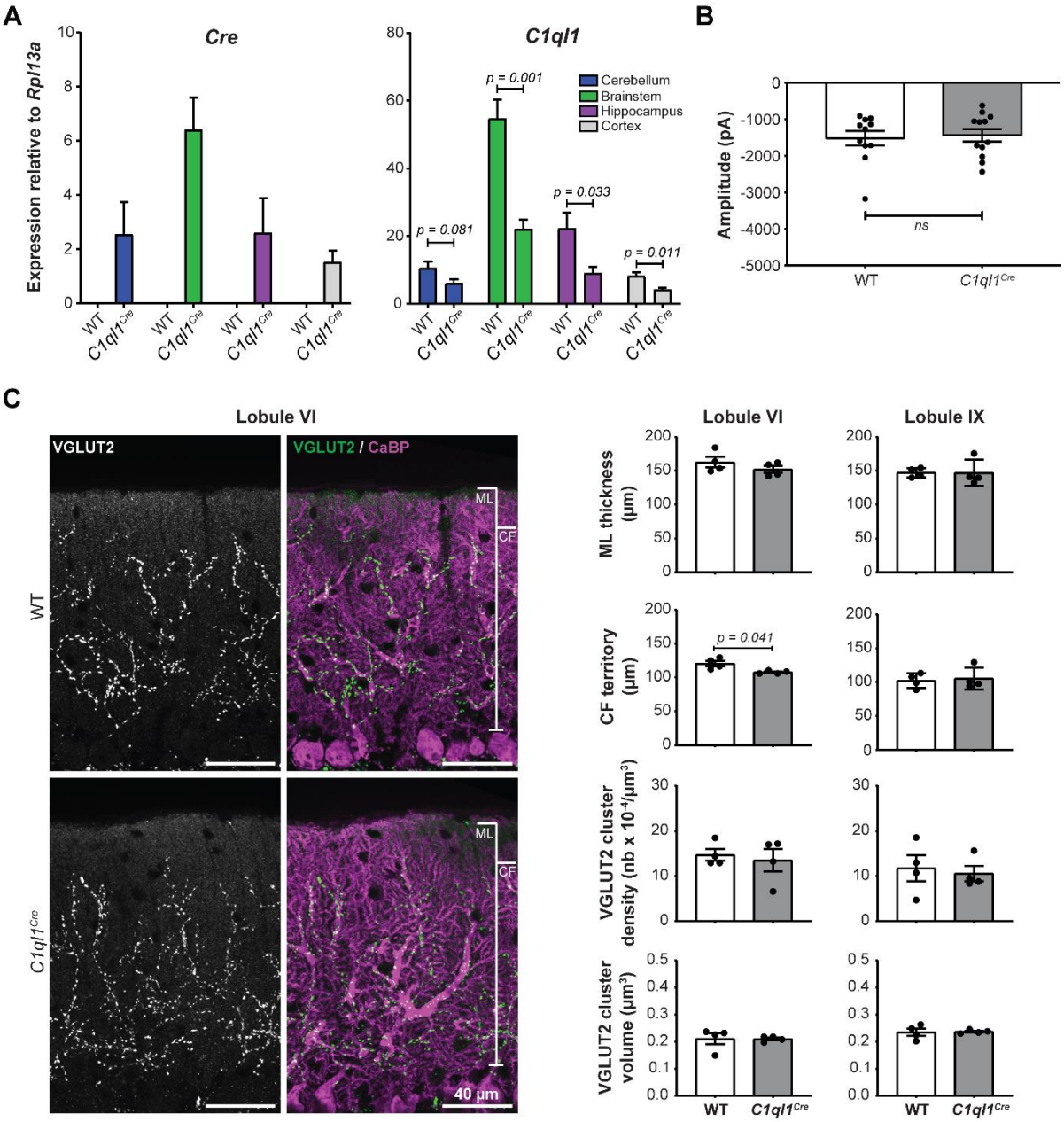

Fig 2. Effects of Cre transgene knockin on climbing fiber/Purkinje cell synapses in *C1ql1*^{Cre} heterozygotes

(A) The expression of *Cre* and *C1ql1* mRNAs was assessed using quantitative RT-PCR on RNA extracts from four different regions of WT or *C1ql1*^{Cre}/WT mouse brains, fourteen days after birth (P14). The *Cre* recombinase expression was detected only in *C1ql1*^{Cre} mice, in the cerebellum, the brainstem, the hippocampus and the cortex. The expression of *C1ql1* was decreased in these regions of the brain at the same age compared to WT mice. Data are represented as mean ± SEM, unpaired student t test with Welsh's correction, n = 5 – 6 animals per genotype. **(B)** Properties of CF/PC transmission was assessed in WT and heterozygous *C1ql1*^{Cre} mice recording the mean amplitude of the currents of CF on PCs. This analysis

revealed no difference between the two genotypes. Data are represented as mean ± SEM, Mann Whitney test, n = 11 – 12 cells per genotype. **(C)** *Left panel:* CF presynaptic boutons and PCs and their dendritic tree were revealed by immunostaining for VGLUT2 (green), and calbindin (magenta) respectively, in parasagittal cerebellar sections from P30 WT and *C1ql1*^{Cre}/WT mice. Images were acquired using a spinning disk confocal microscope. *Right panel:* analyses of the morphology of the cerebellar cortex and connectivity of CFs were performed on cerebellar lobules VI and IX. The thickness of molecular layer, territory of the CFs in the molecular layer, volume and density of the boutons of CFs on PCs were not modified in lobules VI and IX of *C1ql1*^{Cre} heterozygous animals compared to WT, except for the small reduction observed in the CF territory in lobule VI. Molecular layer (ML) and CF extension are indicated on the merge images. Data are represented as mean ± SEM, unpaired student t test with Welsh's correction, n = 4 animals per genotype. Scale bars: 40 µm.

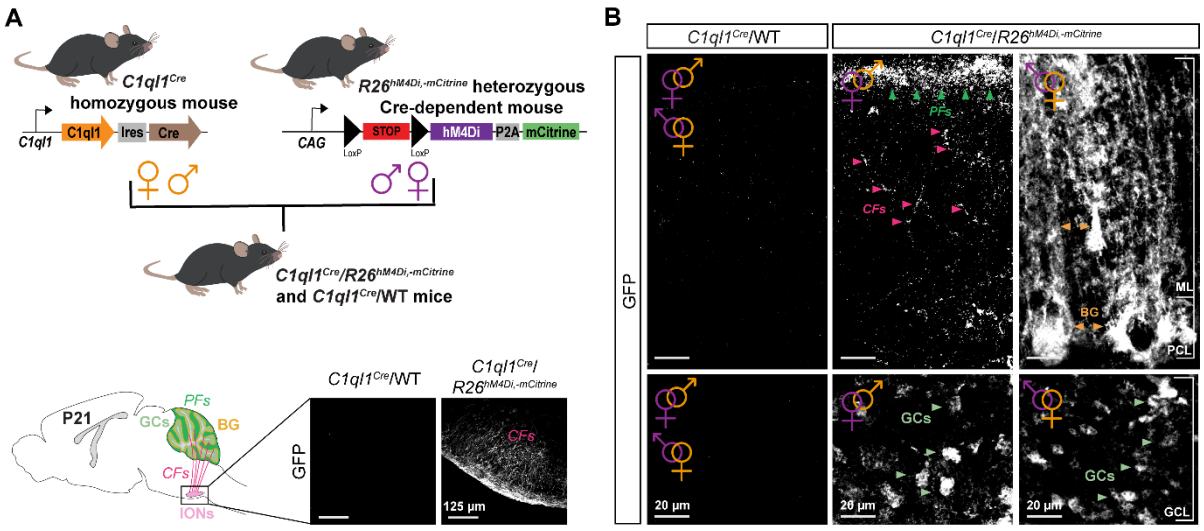

Fig 3. Targeting different cell types in the olivo-cerebellar network using the *C1ql1*^{Cre} mouse line.

(A) *Top panel:* Schematic illustration of the crossings used to generate *C1ql1*^{Cre}/WT and *C1ql1*^{Cre}/*R26*$^{hM4Di,-mCitrine}$ heterozygous mice. *Bottom panel:* parasagittal cerebellar sections from P21 C1ql1^{Cre}/WT and *C1ql1*^{Cre}/*R26*$^{hM4Di,-mCitrine}$ mice were immunostained for GFP. Axons from IONs, the Climbing Fibers (CFs), were mCitrine labelled in the brainstem region. Scale bars = 125 µm. **(B)** Parasagittal cerebellar sections immunostained for GFP in P21 *C1ql1*^{Cre}/WT and *C1ql1*^{Cre}/*R26*$^{hM4Di,-mCitrine}$ mice born from different crosses and acquired using a spinning disk confocal microscope. *C1ql1*^{Cre}/*R26*$^{hM4Di,-mCitrine}$ born from a *C1ql1*^{Cre} male revealed mCitrine signal in Granule Cells (GCs) and in their axons, the parallel fibers (PFs), as well as in the CFs, as expected. *C1ql1*^{Cre}/*R26*$^{hM4Di,-mCitrine}$ born from a *C1ql1*^{Cre} female also revealed mCitrine signal in Bergmann Glia (BG). ML: Molecular Layer, PCL: Purkinje cell layer, GCL: Granule Cell Layer. Scale bars = 20 µm.

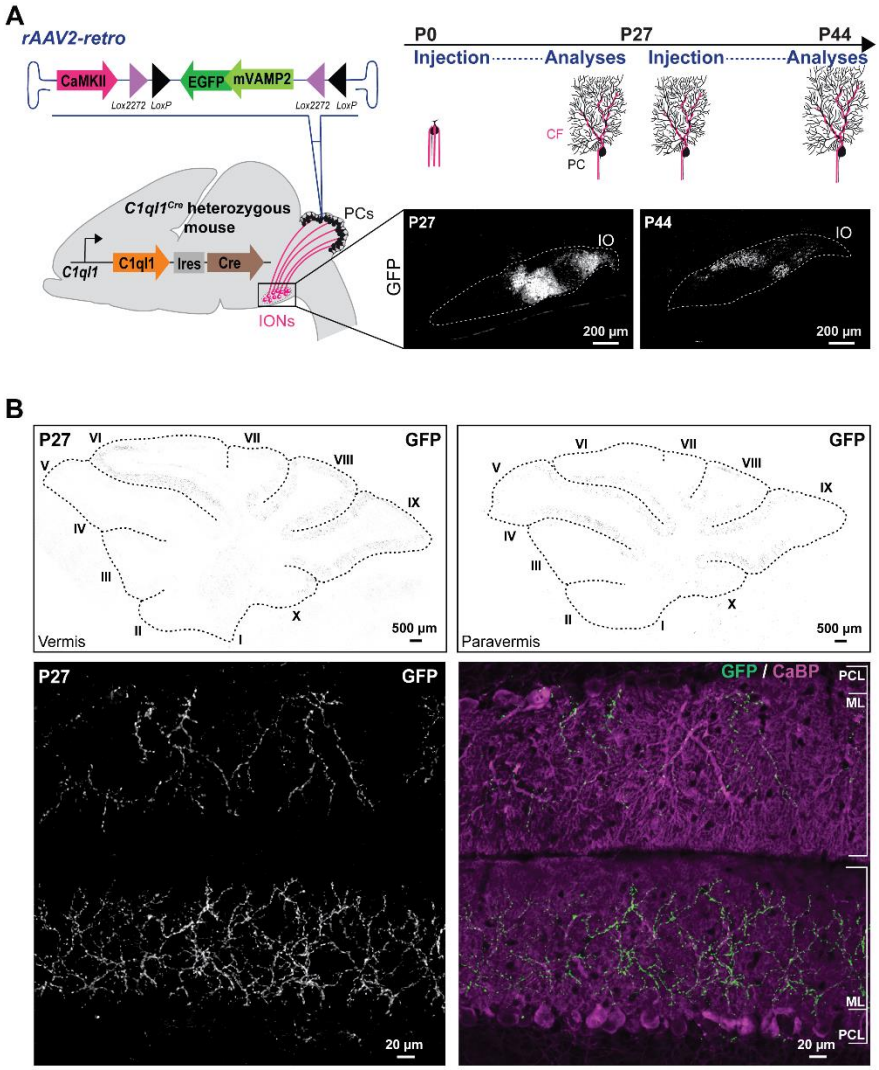

Fig 4. Specific targeting of inferior olivary neurons using an intersectional strategy.

(A) Schematic illustration of the strategy to specifically express the mouse GFP-tagged vesicle-associated membrane protein 2 (mVAMP2) in IONs. P0 or P27 stereotaxic injections of retrograde rAAVs expressing the floxed mVAMP2-GFP, under the CaMKII promoter, were performed in the cerebellum of *C1ql1*^{Cre} mice. Analyses were done at P27 for P0 injections or P44 for P27 injections, in parasagittal cerebellar sections. Subpopulations of IONs were labelled for GFP after anti-GFP immunostaining. IO is indicated by dotted lines. Scale bars, 200 µm. **(B)** *Top panel:* Vermal (left) and paravermal (right) sagittal cerebellar sections from *C1ql1*^{Cre}/WT P27 mouse injected at P0 and immunostained for GFP revealed large region of GFP labelled CFs in different lobules of the cerebellum. Images were acquired using a spinning disk confocal microscope. Lobules are indicated as roman numerals. Scale bars, 500 µm. *Bottom panel:* CFs of transduced IONs and Purkinje cells from P27 *C1ql1*^{Cre}/WT mouse injected at P0 were immunostained for GFP (green) and calbindin (magenta), respectively.

ML: Molecular Layer, PCL: Purkinje cell layer are indicated on the merge image. Scale bars = 20 μm.

Part 3: A molecularly-defined non-redundant subpopulation of OPCs controls the generation of myelinating oligodendrocytes during postnatal development.

Article in preparation.

Title:

A molecularly-defined non-redundant subpopulation of OPCs controls the generation of myelinating oligodendrocytes during postnatal development.

Shayan Moghimyfiroozabad[1], Maela A. Paul[1], Lea Bellenger[2], Fekrije Selimi[1]

[1]Center for Interdisciplinary Research in Biology (CIRB), College de France, CNRS, INSERM, Université PSL, Paris, France

[2]Sorbonne Université, Paris, France

Abstract:

Oligodendrocyte precursor cells (OPCs) are a class of glial cells that uniformly tiles the whole central nervous system. They play several key functions across the brain including the generation of oligodendrocytes and the control of myelination. Whether the functional diversity of OPCs is the result of genetically defined subpopulations or of their regulation by external factors has not been definitely established. We discovered that a subpopulation of OPCs found across the brain is defined by the expression of *C1ql1*, a gene previously described for its synaptic function in neurons. This subpopulation starts to appear during the first postnatal week in the mouse brain. Ablation of *C1ql1*-expressing OPCs in the mouse is not compensated by the remaining OPCs, and results in a massive lack of oligodendrocytes and myelination in many brain regions. Therefore, *C1ql1* is a molecular marker of a functionally non-redundant subpopulation of OPCs, which controls the generation of myelinating oligodendrocytes.

Introduction:

Oligodendrocyte precursor cells (OPCs) are a type of glial cells that homogeneously populate the central nervous system (CNS) starting during postnatal development and throughout adulthood[1]. Several functions have been attributed to OPCs[2]. OPCs have been documented to control vascularization and angiogenesis[3], engulfment of axons and refinement of neural circuits[4,5], and antigen presenting[6]. However, a major, and their initially described, role is to differentiate into oligodendrocytes (OLs)[7–9]. In rodents, the generation of OLs from OPCs starts at birth and continues during adulthood[10,11]. OPC differentiation peaks

during the second postnatal week and then decreases gradually[10]. A portion of OPCs continues to proliferate to keep the density of their population constant throughout the mature brain[1]. OPCs are thus essential for proper development and function of brain circuits. OPCs are characterized by the expression of neural/glial antigen 2 (NG2) and platelet-derived growth factor receptor A (PDGFRa), which immediately disappear upon differentiation into OLs[1,9].

OPCs are generated in the CNS through sequential waves and in a ventro-dorsal manner[7]. In the forebrain, three waves with different spatial origins and genetic lineages generate OPCs[12]. The first two waves are originally ventral and embryonic. The third wave is generated dorsally after birth[12]. The elimination of each wave of OPCs is rapidly compensated by the other waves without any significant consequences on OPC dynamics or myelination of the developing brain[12]. Even the ablation of all three waves in the forebrain is compensated by OPCs coming from the diencephalon within two weeks[7,13]. These data suggest that, despite their different origins, various waves of OPCs are functionally redundant. However, functional data also suggest heterogeneity in OPCs [14]. For example, OPCs coming from the first wave in the forebrain migrate towards the optic nerve via a Nrg1-ErbB4-mediated chemo-affinity mechanism, while OPCs from the 2nd wave and occupying the optic nerve postnatally are Nrg1-insensitive[15]. Another example is the modulation of the generation of first wave OPCs via Shh signaling, while the other waves are Shh-independent[16]. Independent of their origin, OPCs have slightly different morphologies based on their location[1,17]. For example, OPCs in the white matter have an elongated soma packed tightly between the myelinated axons, with extended processes in parallel to the direction of the fibers, while OPCs in the gray matter have a star-shape structure with several long and thin branches extending in all directions[1]. OPCs can also have different dynamics in terms of proliferation, migration and differentiation rate[8]. For example, OPCs in the corpus callosum differentiate into oligodendrocytes faster than OPCs in the cortex[8]. OPCs are also heterogeneous based on their transcriptomes, cell surface proteins (e.g. receptors and ion channels) or electrophysiological properties[17–19]. Single-cell RNA-seq experiment performed on OPCs coming from mouse forebrain in different stages during development (E13.5, P7 and P21) shows that OPCs originating from several regions of the forebrain become transcriptionally equivalent at P7[20]. Despite this transcriptional equivalence, OPCs in ventral and dorsal forebrain respond differently to DNA damage by promoting senescence or apoptosis, respectively. These two different responses are linked to different molecular mechanisms and developmental origin of OPCs, showing molecular and functional heterogeneity in OPCs[21]. In addition to heterogeneity associated with the origin, OPC heterogeneity can change with age too[19]. Spitzer *et al.* showed that OPCs lack any ion channels at E13.5 in different regions of the brain, while they start to express voltage-gated ion channels and glutamate receptors differentially throughout development in concordance

with their functional states[19]. All these studies demonstrate that OPCs are a diverse population and their diversity changes based on the brain region and age.

A fundamental question is whether the functional diversity in OPCs arises from molecularly defined subpopulations with distinct functions or whether it is a result of their interaction with the environment[1,17]. In this study, we show that *C1ql1*, a gene known for its role in synapse formation[22,23], is a molecular marker of a subpopulation of OPCs all over the mouse brain. The expression of *C1ql1* in this subpopulation starts from the first postnatal week. Using genetic ablation, we show that the elimination of this subpopulation is not compensated by the remaining OPCs and leads to lack of OLs in the dorsal forebrain. Consequently, the myelination of the brain is massively decreased. Thus, for the first time, we identify a molecular signature for a non-redundant subpopulation of OPCs that generates myelinating OLs during the postnatal development of mouse forebrain.

Results:

A subpopulation of OPCs is characterized by *C1ql1* expression.

The *C1ql1*^{Cre} knockin mouse model (*manuscript in preparation*) can be used to determine the history of expression of *C1ql1* during brain development. In particular, we used the Cre-dependent *R26*$^{Cas9\text{-}GFP}$ (known as Rosa26-Cas9 knockin)[24] reporter mouse line allowing simultaneous expression of the CAS9 protein and the green fluorescent protein (GFP) upon CRE-mediated recombination (Figure 1A). In addition to the expected expression in certain neuronal populations (*manuscript in preparation*), we noticed the presence of GFP-expressing cells throughout the brain at postnatal day 30 (P30) (Figure 1B). These cells did not appear to be neurons, an observation that was confirmed using immunolabeling for NeuN (Figure S1). Indeed, while cerebellar granule cells and inferior olivary neurons were both GFP and NeuN positive as expected (Figure S1), the other GFP cells were NeuN negative. Because the morphology of the GFP-expressing cells was suggestive of glia, we tested markers for the various glial populations. The GFP-positive cells were not labeled using an anti-GFAP antibody showing that they were not astrocytes (Figure S1). Finally, using NG2, a well-characterized marker of oligodendrocyte precursor cells (OPCs), we determined that the non-neuronal cells labeled using the *C1ql1*^{Cre} knockin mouse line were a subpopulation of OPCs as some, but not all, NG2 labeled cells were also GFP-positive (Figure 1B).

This genetic experiment indicates that a subpopulation of OPCs, or their progenitors, express *C1ql1*. To determine whether OPCs themselves express *C1ql1*, we performed duplex single molecule fluorescence in situ hybridization (smFISH) for *C1ql1* together with *Cspg4*

(coding the marker NG2) on brain sections from P30 mice (Figure 1C). *C1ql1* puncta were observed together with *Cspg4* puncta in a subset of cells throughout the brain. Quantification showed that about 57%, 50% and 61% of *Cspg4* expressing cells in the cortex, cerebellum, and brainstem respectively, express *C1ql1* (Figure 1C). Single-cell transcriptomics of the oligodendrocyte lineage at embryonic (E13.5) and postnatal stages (P7, juvenile and adult) has previously shown that, besides a subpopulation of cycling OPCs, OPCs form a rather homogenous cell population at the transcriptome level at P7[20]. Our reanalysis of these data using uniform manifold approximation and projection (UMAP) reduction and K-nearest neighbor (KNN) clustering identified 10 clusters including three OPC subpopulations (Figure 1D). Two of these subpopulations were the same as the ones found by Marques *et al.*[20] (including the cycling OPC subpopulation), while a small third one was defined by the enriched expression of genes associated with the GO terms “mRNA processing” and “mRNA splicing”, suggesting a specific metabolism of RNA. *C1ql1*-expressing cells were found in all three OPC clusters as well as in committed OPCs (COP) cells that are differentiating into oligodendrocytes (Figure 1D). *C1ql1* expression was almost undetected in newly formed oligodendrocytes.

Thus, genetic and transcriptomic data altogether demonstrate that a subpopulation of OPCs expresses *C1ql1* in the juvenile brain. They also raise the question as to whether *C1ql1* expression defines a subpopulation of OPCs with a specific function or a transient state during differentiation.

Ablation of *C1ql1*-expressing OPCs is not compensated during postnatal development.

In the adult mouse brain, OPCs maintain their homeostasis by local proliferation[25]. Ablation, differentiation or apoptosis of OPCs leads to proliferation and migration of the adjacent cells to replace the missing ones[25]. OPCs that are generated in different waves show functional redundancy, as ablation of one wave using *Sox10*-driven expression of diphtheria toxin (DTA) is compensated by the other two waves in the cortex during the first two postnatal weeks[12]. Even ablation of all three waves induces repopulation by the OPCs from other regions of the brain (e.g. diencephalon) within a few weeks, showing the strong capacity of OPCs for compensation of each other’s elimination[12,13,25]. We used the previously established DTA-based ablation method to test whether *C1ql1*-expressing OPCs have a specific function or are functionally redundant with other OPCs. For this, the $C1ql1^{Cre}$ mouse line was crossed with the $Sox10^{DTA}$ mouse line expressing DTA in a Cre-dependent manner[12] (Figure 2A). In the absence of Cre, all the oligolineage cells, OPC, COPs and OLs, express GFP in the $Sox10^{DTA}$ mouse line. *C1ql1* is not expressed in progenitors of OPCs (Figure 1D). Thus, the

expression of the Cre recombinase using the *C1ql1*^{cre} locus induces DTA expression and death of the Cre-expressing cells in the oligolineage without affecting *C1ql1*-expressing neurons. The *C1ql1*^{Cre}*; Sox10*^{DTA} mice did not survive beyond three to four postnatal weeks. All the animals survived until P16, the age chosen for analysis, without any major visually detectable behavior or motor deficit. Morphological analysis of coronal and parasagittal brain sections showed a massive reduction in the number of GFP-expressing cells all over the brain, and in particular in the forebrain, in *C1ql1*$^{+}$ OPC-ablated (*C1ql1*^{Cre}*; Sox10*^{DTA}) animals compared to *C1ql1*^{wt}*; Sox10*^{DTA} controls (Figure 2B, 2C and 2D). Since the development of oligolineage cells is well-known in the forebrain, particularly in the corpus callosum and the cortex[12], we selected the central and lateral parts of the corpus callosum (CC-center & CC-lateral), as well as the retrosplenial area of the cortex for detailed analysis (Figure 2C and 2D). Quantification of the number of GFP^{+} (oligolineage) cells showed a 66% decrease in the center (mean ± SEM = 41.2 ± 2.1 vs 13.9 ± 1.2 x 10^{-5} cells/µm^3 in the control and ablation conditions, respectively) and a 85% decrease in the lateral (39.1 ± 3.0 vs 5.7 ± 0.6 x 10^{-5} cells/µm^3) parts of the corpus callosum, while a 46% decrease is observed in the cortex (10.0 ± 1.5 vs 5.4 ± 0.5 x 10^{-5} cells/µm^3) (Figure 2C). Since GFP labels the entire oligolineage cells in the *Sox10*^{DTA} mouse model, the OPC marker NG2[1,9] was used to quantify the magnitude of ablation in the OPC subpopulation. A 57% and 80% reduction in the density of NG2^{+} GFP^{+} cells was found in the center and lateral parts of the corpus callosum, respectively (25.0 ± 4.1 vs 10.7 ± 1.0 and 24.3 ± 3.2 vs 4.8 ± 0.6 x 10^{-5} cells/µm^3, respectively). A 32% decrease was also observed in the cortex (mean ± SEM = 7.4 ± 1.6 vs 5.0 ± 0.5 x 10^{-5} cells/µm^3). PDGFRa is another marker of OPCs[1,9]. In comparison with NG2 staining, PDGFRa immunolabeling is more concentrated on the somata of OPCs and allows easier quantification of individual OPCs (Figure 2C and 2D). Our quantifications found a 74% (mean ± SEM = 20.1 ± 1.2 vs 5.3 ± 0.7 x 10^{-5} cells/µm^3) and 79 % (26.5 ± 3.3 vs 5.7 ± 0.4 x 10^{-5} cells/µm^3) decrease in the density of PDGFRa^{+} GFP^{+} cells in the central and lateral parts of the corpus callosum, respectively, and a 29% reduction in the cortex (mean ± SEM = 7.9 ± 0.8 vs 5.6 ± 0.4 x 10^{-5} cells/µm^3). Altogether, using the two most common markers of OPCs, NG2 and PDGFRa, we confirm that DTA expression using the *C1ql1*^{Cre} knockin as a driver leads to the significant ablation of OPCs in several regions of the forebrain. This result was completely unexpected as it shows that remaining OPCs cannot compensate for the loss of *C1ql1*$^{+}$ OPCs during postnatal development, contrary to what is seen when ablating OPCs from different waves[12,13].

C1ql1 expression in OPCs starts from the first postnatal week and leads to different dynamics in the dorsal forebrain.

The magnitude of OPC loss at P16 in the *C1ql1*^{cre}; *Sox10*^{DTA} mice is bigger in the corpus callosum than in the cortex. In the cortex, 30% of OPCs are missing, a percentage inferior to the one of OPCs expressing *C1ql1* by P30 (about 60% as found by smFISH). We wondered whether these regional differences and in particular the smaller loss in the cortex were due to differences in the timing of expression of *C1ql1* in OPCs during postnatal development. Analysis of previously published data from single-cell transcriptomics of oligolineage cells[20] shows a negligible expression of *C1ql1* at E13.5, while a considerable number of OPCs express *C1ql1* already by P7 and juvenile stage (Figure 3A) suggesting that *C1ql1* expression is induced during the first postnatal week in a subpopulation of OPCs in the forebrain. To quantify *C1ql1* expression during the first two postnatal weeks, we performed duplex smFISH for *C1ql1* and *Cspg4* on brain sections from wildtype mouse at P7 and P15 (Figure 3A). Similar to our observations at P30 (Figure 1C), *C1ql1* labeling was detected in a subgroup of *Cspg4*$^{+}$ cells (Figure 3A). Quantification demonstrated that 72% and 68% of *Cspg4*$^{+}$ cells in the cortex express *C1ql1* at P7 and P15, respectively, a percentage higher by about 10% than the percentage quantified at P30 (Figure 1C). *C1ql1* expression is thus acquired in a subpopulation of OPCs as early as the first week of postnatal development.

In the corpus callosum, the percentage of OPCs expressing *C1ql1* is in the range of the OPC loss observed in *C1ql1*^{Cre}*; Sox10*^{DTA} mice at P16. However, in the cortex the OPC loss (30%) is smaller than the percentage of *C1ql1*-expressing OPCs even at P7 (60-70%). Quantification showed that ablation of *C1ql1*$^{+}$ OPCs has already an effect on the number of oligolineage cells by P7 (Figure 3B and 3C): The number of GFP cells is already decreased by 40-50% in the corpus callosum (Center: mean ± SEM = 32.7 ± 1.9 in the control vs 16.3 ± 1.5 x 10^{-5} cells/µm^3; Lateral: mean ± SEM = 45.9 ± 2.5 vs 26.6 ± 2.5 x 10^{-5} cells/µm^3). No change was observed in the cortex at this stage (mean ± SEM = 13.3 ± 1.0 vs 15.9 ± 3.2 x 10^{-5} cells/µm^3) (Figure 3B). Using NG2 to distinguish OPCs from other oligolineage cells, we observed that the number of NG2^{+} *Sox10*-GFP^{+} cells is decreased by 38% (mean ± SEM = 20.1 ± 1.3 vs 12.4 ± 1.7 x 10^{-5} cells/µm^3) in the center of the corpus callosum, while in the lateral part of corpus callosum a 28% decrease is measured, albeit not statistically significant (mean ± SEM = 12.1 ± 0.8 vs 8.7 ± 1.3 x 10^{-5} cells/µm^3, p = 0.0828). No significant changes are detected in the cortex (mean ± SEM = 6.6 ± 0.5 vs 7.0 ± 1.1 x 10^{-5} cells/µm^3). Similarly, analysis of PDGFRa staining shows the density of PDGFRa^{+} *Sox10*-GFP^{+} cells is decreased by 56% (mean ± SEM = 17.1 ± 1.2 vs 7.6 ± 2.5 x 10^{-5} cells/µm^3) and 54% (mean ± SEM = 14.9 ± 1.3 vs 6.9 ± 2.1 x 10^{-5} cells/µm^3) in the center and lateral corpus callosum respectively, while there is no change in the cortex (mean ± SEM = 7.1 ± 0.4 vs 6.9 ± 2.5 x 10^{-5} cells/µm^3).

These results show that the genetic ablation of *C1ql1*-expressing OPCs has already started during the first postnatal week and is not compensated in the center and lateral part of corpus callosum, while in the cortex, OPC loss is not observed despite the fact that *C1ql1* is already detected in OPCs. This suggests that in the cortex the loss of OPCs due to ablation is compensated during the first postnatal week by the migration of newly formed OPCs. Indeed this migration process is not finished at this stage[12]. It might also indicate a lower efficiency for recombination and DTA expression in OPCs from this region of the brain. All the OPCs from the 3 different waves are settled in the dorsal forebrain by P10 and their proportions do not change afterwards[12]. Thus, starting at that age, the progressive loss of OPCs in $C1ql1^{Cre}$; $Sox10^{DTA}$ mice is not compensated by the remaining OPCs during postnatal development.

Ablation of *C1ql1*-expressing OPCs leads to lack of oligodendrocytes and myelination.

C1ql1-expressing cells are present in all OPC clusters defined by single-cell transcriptomics (Figure 1D). This suggests that rather than defining a genetically defined subpopulation, *C1ql1* is a marker of a specific transitional state and/or of a specific function. Gene Ontology (GO) analysis of the single-cell transcriptomics data[20] was performed to determine whether $C1ql1^+$ OPCs were enriched in specific GO terms compared to other OPCs. “Gliogenesis” and “glial cell differentiation” were the two most significantly overrepresented terms (gene ratio = 0.19 and 0.15 respectively) in $C1ql1^+$ OPCs (Figure 4A and Figures S2). Moreover, *C1ql1* expression is also detected in some committed oligodendrocyte precursors (COPs) and disappears in newly formed oligodendrocytes (Figure 1D). Altogether, these results suggest that *C1ql1* expression in OPCs might control their ability to generate differentiated oligodendrocytes. Indeed, quantification of the number of GFP cells after ablation of *C1ql1*-positive OPCs showed a massive decrease not only in $NG2^+$ GFP^+ cells, but also in $NG2^-$ GFP^+ cells (Figure 2 and 3). Because GFP expression is driven by the *Sox10* promoter, this suggested that DTA ablation using the *C1ql1* driver results in the reduction not only in OPC numbers but also in COPs and oligodendrocytes. Indeed, by P16 these cells are completely absent as shown by the almost complete lack of $NG2^-$ GFP^+ cells. Using immunolabeling of P16 forebrain coronal slices for CC1, a marker of oligodendrocytes, we confirmed the massive reduction in OL numbers after ablation of *C1ql1*-expressing OPCs, with almost complete absence of $CC1^+$ cells in the cortex (Figure 4B). Quantification demonstrates a 77%, 98%, and 83% reduction in the number of $CC1^+$ GFP^+ cells in the center (mean ± SEM = 18.9 ± 2.3 vs 4.2 ± 1.9 x 10^{-5} cells/μm^3), lateral corpus callosum (mean ± SEM = 15.2 ± 1.7 vs 0.2 ± 0.0 x 10^{-5} cells/μm^3), and in the cortex (mean ± SEM = 1.2 ± 0.3 vs 0.2 ±

0.1 x 10^{-5} cells/μm^3), respectively. Thus *C1ql1*-expressing OPCs are essential for the generation and/or survival of OLs.

OL generation starts around birth (P0) in mice and continues throughout life[10]. Myelination starts from the end of the first postnatal week and increases rapidly to reach its maximum level by the end of the second week[10]. This intense period of myelination coincides with the timing of the defects in generation of OLs observed after ablation of *C1ql1*-expressing OPCs. Immunolabeling for myelin binding protein (MBP) revealed a dramatic decrease in MBP protein in different regions of the forebrain at P16 (Figure 5A), suggesting a lack of myelination. Quantification was performed to assess the thickness and intensity of MBP labeling in the corpus callosum and the cortex (Figure 5B). In the center of the corpus callosum, a slight but statistically not significant decrease was observed in the thickness of the myelinated region (mean ± SEM = 320.9 ± 16.8 vs 293.6 ± 12.8 µm), while a huge decrease was observed in the lateral part (mean ± SEM = 144.6 ± 16.8 vs 23.6 ± 4.9 µm) and the cortex (mean ± SEM = 305.5 ± 52.2 vs 89.6 ± 7.6) (Figure 5B). To rule out an indirect consequence of elimination of *C1ql1*-expressing OPCs via disturbance of axonogenesis, we assessed the integrity of axons and neuronal fibers using immunolabeling for the neurofilament protein (NF[9,26]) (Figure 5C). No difference was observed in the thickness of fiber tracts in the center of the corpus callosum (mean ± SEM = 326.5 ± 12.3 vs 292.7 ± 17.1 µm) and the intensity of NF labeling in the cortex (mean ± SEM = 742.4 ± 193.1 vs 957.7 ± 208.5). A 19% reduction in the thickness of fiber tracts in the lateral part of the corpus callosum was detected (mean ± SEM = 129.1 ± 7.8 vs 104.9 ± 2.8 µm). Given the nearly full absence of MBP in this area, this reduction was probably more the reflection of lack of myelination rather than of deficits in axonogenesis. In the center of the corpus callosum the effect of ablation of *C1ql1*-expressing OPCs was not obvious as the thickness of MBP and NF labelling remained the same. Of note, however, the maximum intensity of MBP labelling was significantly increased in this region (mean ± SEM = 427.0 ± 60.6 vs 909.1 ± 132.0), while gaps in the MBP staining were observed between the myelinated fibers (Figure S3). This suggests that the remaining OLs couldnot expand their territories but rather try to compensate by increased MBP expression. Additionally, some OLs that did not express *Sox10* were observed in the center of corpus callosum (Figure 3B). It has been reported that 4% of oligodendroglia in the brain are *Sox10*-negative[27]. Since these were not eliminated using the *Sox10*-DTA line, they probably compensated the myelination of the center of corpus callosum. Overall, our results show a major lack of myelination at P16 in various parts of the forebrain as a consequence of ablation of *C1ql1*-expressing OPCs and lack of oligodendrocytes.

C1ql1 expression per se is not necessary for generation of myelinating oligodendrocytes.

C1QL1 is a secreted synaptic protein involved in synapse formation in the olivocerebellar circuit[22,23], as well as in proliferation and migration of lung cancer cells[28]. Its role in OPCs, in particular for regulating proliferation and differentiation into myelinating oligodendrocytes, has never been assessed. We developed a constitutive knockout mouse of *C1ql1* using the CRISPR/Cas9 technology in which the entire Exon 1 has been removed (Figure 6A). Quantitative RT-PCR on whole brain extracts and smFISH on sections of the inferior olive (the site of highest expression of *C1ql1*) both confirmed complete lack of *C1ql1* expression in the brain of these mice (Figure 6A). To investigate the effect of loss of function of C1QL1 on OPCs, immunolabeling for the OPC markers NG2 (Figure S4) and PDGFRa (Figure 6B) was performed on sections from P16–18 mouse forebrains. No change was observed in the density of OPCs between control (WT) and *C1ql1* knockout brain sections whether measured by PDGFRa immunostaining (CC-center : mean ± SEM = 7.2 ± 1.5 vs 10.0 ± 1.3 x 10^{-5} cells/μm^3; CC-lateral : mean ± SEM = 5.5 ± 1.3 vs 5.6 ± 0.6 x 10^{-5} cells/μm^3; cortex :mean ± SEM = 3.6 ± 1.1 vs 3.8 ± 0.5 x 10^{-5} cells/μm^3) (Figure 6B) or NG2 (Figure S4; CC-center: mean ± SEM = 17.1 ± 4.8 vs 23.4 ± 3.7 x 10^{-5} cells/μm^3; CC-lateral: mean ± SEM = 17.3 ± 5.7 vs 22.8 ± 4.1 x 10^{-5} cells/μm^3; cortex : mean ± SEM = 10.1 ± 2.3 vs 13.5 ± 3.4 x 10^{-5} cells/μm^3). Thus, C1QL1 loss of function has no major effect on the generation and survival of OPCs during development. C1QL1 signaling could play a role in controlling the generation of OLs and myelination. Immunostaining of coronal sections of the forebrain of P16–18 mice for MBP revealed similar myelination in WT and *C1ql1* KO conditions (Figure 6C). Quantification confirmed that there is no difference in the thickness of MBP labeling in the center (mean ± SEM = 312.2 ± 6.7 vs 301.8 ± 14.5 µm), lateral corpus callosum (mean ± SEM = 126.0 ± 7.2 vs 124.9 ± 4.0 µm), and in the intensity of MBP staining in the cortex (mean ± SEM = 707.3 ± 119 vs 587.6 ± 63.2) (Figure 6C). Thus, loss of function of C1QL1 per se does not have a major impact on OPCs and myelination in the forebrain during postnatal development.

Discussion:

OPCs have various functions[2,14]. Whether this is related to their molecular heterogeneity or is simply the result of interaction with their local environment is unresolved. In this study, we identified a subpopulation of OPCs in the mouse brain defined by the expression of the synaptic molecule *C1ql1* which appears starting from the first postnatal week. Ablation of *C1ql1*-expressing OPCs is not compensated by remaining OPCs in the dorsal forebrain during postnatal development and leads to OL and myelination deficiency.

C1QL1 is a synaptic molecule involved in excitatory synapse formation and maintenance between neurons[22,23,29]. A proliferative and tumor-promoting function in two different cancers, one inside the brain and the other one outside, was attributed to C1QL1 recently[28,30]. Additionally, an inhibitory effect on apoptosis of granulosa cells in the mouse ovarian follicle is observed for C1QL1[31]. Given the lack of OL after ablation of *C1ql1*$^{+}$ OPCs, these data suggested a role for C1QL1 in the control of proliferation and/or differentiation of OPCs especially when an equilibrium between apoptosis and proliferation of oligolineage cells is essential[1,32]. We did not observe any phenotype in the constitutive KO of *C1ql1* in the density of OPCs and myelination of the forebrain. Due to the use of constitutive KO in our experiments, it is possible that compensatory mechanisms are in place, or that the role of C1QL1 would be uncovered only in a situation where the system is challenged[33]. Furthermore, loss of function of C1QL1 specifically in some or all OPCs would maybe uncover its function in oligolineage cell development. Finally, C1QL1 in OPCs might have roles in their interaction with their local environment. C1QL1 has been known to be secreted from pre-synaptic partners and interact with its postsynaptic receptor brain angiogenesis inhibitor 3 (BAI3)[22,23,29]. Since OPCs receive synaptic inputs from excitatory neurons[34,35], it is possible that C1QL1 participates in the formation of neuron-OPC connectivity as well. Additionally, C1QL1 could have a stimulatory effect on vascularization via binding to its receptor BAI3[36]. Considering all these results, the role of C1QL1 in OPCs could be independent of OPC differentiation and control of myelination.

Single-cell RNA sequencing of oligodendroglia during embryonic and postnatal development has demonstrated that OPCs with different origins and transcriptomes converge transcriptionally at P7 to form a homogeneous and equivalent population[20]. The idea of the equivalency and homogeneity of OPCs has been challenged recently[18,21]. In one study, performing single-cell transcriptomics on adult mouse OPCs shows two separate subpopulations of OPCs with distinct molecular markers and biological processes[18]. In another study, removal of Citron-kinase results in accumulation of DNA damage in OPCs, which affects differentially the two subpopulations of OPCs located dorsally and ventrally in the forebrain, showing that the dorsal OPCs are more vulnerable than the ventral ones to oxidative stress and DNA damage[21]. Here, we present new evidence for molecular and functional diversity of OPCs. The expression of *C1ql1* appears postnatally. *C1ql1*-expressing OPCs arrive to their maximum number at P7 and decrease gradually until P30 in the cortex. Several transcriptomic data show the expression of *C1ql1* is maintained in the adult[18,37], which suggests the importance of *C1ql1*-expressing OPCs in myelination/re-myelination even after the first postnatal month. We found *C1ql1*-expressing OPCs in various regions of the brain and in both white (such as brainstem) and gray matters (e.g. cerebral cortex). In the zebrafish spinal cord, OPCs have been classified into two subpopulations based on several characteristics,

including their location, function, calcium activity and dynamics[17]. Since *C1ql1*-expressing OPCs are not restricted to a specific region (white vs gray matter), germinal zone or OPC specific cluster, C1QL1 could be a marker of a transitory state that happens before the differentiation of OPCs into OLs, or could be induced by interaction of OPCs with the microenvironment or other cells in the tissue. The interaction of OPCs with different types of cells in the brain, such as microglia[2,38] or endothelial cells[39], have already been described. These interactions are not only necessary for the function of those cells, but also for proper development of OPCs[2,38,39]. Is it possible that the expression of *C1ql1* is the direct result of these mutual interactions? BAI3, the postsynaptic receptor of C1QL1, is not only found in some neurons[22,23], but also expressed by some glial cells[40], bringing the possibility for OPCs to interact with both neurons and other glia via C1QL1-BAI3 signaling.

Demyelination is a pathological condition where the myelin around the axons is lost, due to the damage to the myelin sheath or loss of myelinating OLs. Dysmyelination is another condition where the myelin is not formed properly[41]. Oligolineage cells are at the center of understanding the etiology and treatment of both conditions. For example, in multiple sclerosis (MS), a type of demyelination condition, OPCs have been traditionally studied for the development of remyelination strategies. However, a recent study showed that OPCs might be directly involved in the etiology of the disease: a switch occurs leading to immune like OPCs that are not found in normal brains[42], and this switch might be directly involved in the etiology of the disease. This switch impairs the ability of OPCs for remyelination[6]. Since no significant change is reported at the level of expression of *C1ql1* in oligolineage cells and the number of *C1ql1*-expressing OPCs upon demyelination in a mouse model of MS using single cell transcriptomics[42], it seems that this subpopulation is not strongly affected in MS. Due to its importance in myelination during postnatal development, *C1ql1*-expressing OPCs could be a potential target for therapeutic approaches for demyelination/dysmyelination conditions.

Methods and Materials:

Animals:

All mice were kept in the authorized animal facilities of CIRB, College de France, under a 12 hour light: 12 hour dark cycle with water and food supplied ad libitum. All animal protocols and animal facilities were approved by the Comité Régional d'Ethique en Expérimentation Animale (#2001) and the veterinary services (D-75-05-12). *C1ql1*^{Cre} mouse model was generated and characterized previously in the lab. The Cre-dependent reporter mouse line *R26*$^{Cas9\text{-}GFP}$ (B6J.129(B6N)-Gt (ROSA)26Sortm1(CAG-cas9*,-EGFP)Fezh/J, strain #026175)[24] was received from The Jackson Laboratory. *C1ql1* KO mice were generated using

the CRISPR/Cas9 system (in collaboration with F. El Marjou, Transgenesis facility, Curie Institute, see below). All the lines are maintained on the C57BL/6J background. C57Bl6/J and OF1 mice (Charles River Laboratories, Wilmington, USA) were used for the smFISH. *Sox10*^{DTA} mice (Sox10-lox-GFP-STOP-lox-DTA, MGI:4999728)[12] were a kind gift from Pr. William D. Richardson (University College London, UK). They were maintained on a mixed CBA/CaCrl and C57BL/6J background in the original animal facility and were crossed with *C1ql1*^{Cre} line upon arrival to CIRB, College de France. In all experiments, littermate mice from both sexes were used as controls for the analysis.

Generation of *C1ql1* constitutive knockout mice:

C1ql1 KO mice were generated using the CRISPR/Cas9 system and oocyte injection in collaboration with the transgenesis facility at Curie Institute (Paris). Two RNA guides were designed to remove the first exon of *C1ql1* by targeting the genomic sequence: 5'-GCG TAT TGG ATC AGA GTC GAC -3' and 5'-GCG CTC AAG GGC GGT CCG GCG-3'. 33 founder mice were obtained and the one with the biggest deletion was selected. The totality of the exon1 was removed as well as a small part of the 5'-UTR and the intron between exon1 and 2. The subsequent F1 generation was screened by PCR followed by sequencing. Genotyping was designed to detect the WT allele (forward primer: 5'-TCA CCT ACC ACG TCC TCA TG-3'; reverse primer: 5'- GGT GCC CGC TAA TTA CAA CC -3') and the targeted KO segment (forward primer: 5'-CAA CGG AGG AGG CAG TGG-3'; reverse primer: 5'-GGT GCC CGC TAA TTA CAA CC-3'). Transgenic founders were backcrossed and maintained on the C57Bl/6J background.

Gene expression analysis

RNA extraction and RT-qPCR:

Whole brains were dissected from *C1ql1* WT or *C1ql1* KO adult mice and frozen immediately in liquid nitrogen and stored at -80C°. Using the Qiagen RNeasy mini kit (Qiagen, Venlo, Netherlands, #74104), the total RNA was purified according to manufacturer's instruction. cDNA was synthetized using 50 ng of total RNA and SuperScript™ VILO™ cDNA Synthesis Kit (Life Technologies, California, USA, #11754050) according to manufacturer's instruction.

Quantitative PCR on cDNA samples was performed using FAM-labeled *C1ql1* probe (Taqman Gene Expression Assay, ThermoFisher, Assay ID: Mm00657289_m1) and VIC-

labeled *Rpl13a* probe as a reference (Taqman Gene Expression Assay, ThermoFisher, Assay ID: Mm01612986-gH) and the TaqMan Universal Master Mix II, with UNG (Applied Biosystems, #4440038) according to manufacturer's instructions. Bio-Rad CFX Manager was used for data analysis. The threshold for both FAM and VIC channels was set at 500. The relative expression of *C1ql1* to *Rpl13a* was calculated based on the following formula: Relative expression = $(2^{(\text{Cq of } C1ql1 - \text{Cq of } Rpl13a)} \times 100$

Single molecule Fluorescent *In situ* Hybridization (smFISH):

Mice at P7, P15 and P30 were perfused intracardially with 4% paraformaldehyde (PFA) phosphate-buffered saline (PBS) solution. Brains were post-fixed with the same solution at 4°C for 24 hours, transferred to 20% and 30% sucrose/PBS at 4°C sequentially for 24 hours. 30 µm-thick sections (P7 and P15: coronally, P30: parasagittally) were obtained using a freezing microtome and stored at -20°C in cryo-preservative solution until use. The smFISH labelling was performed using RNAscope Multiplex Fluorescent Assay kit (Advanced Cell Diagnostics, Newark, USA, cat#323100) according to manufacturer's instructions. Duplex in situ hybridization was performed with the *Cspg4* (ACD, cat#404131) and *C1ql1* RNAscope probes (ACD, cat#465081). The nuclei were labelled with DAPI. Sections were mounted with Prolong Gold Antifade reagent (Invitrogen, cat#P36930). Images were taken using a Zeiss spinning-disk confocal CSU-W1 microscope with 40x oil objective. A home-made plugin in ImageJ/Fiji was used to detect and quantify the number of individual RNA puncta and their total surface inside each segmented nucleus. The nuclei with a total surface of the RNA puncta of > 1.5 μm^2 were selected positive for that probe.

Immunofluorescence:

Mice at P7, P16-18, and P30 were fixed using intracardiac perfusion of 4% PFA in PBS solution. Brains were extracted, post-fixed with the same solution at 4°C for 2 - 4 hours, and transferred to 30% sucrose/PBS at 4°C for cryoprotection. 60 µm-thick sections were obtained using a freezing microtome, and kept in 0.02% NaN_3 in PBS solution at 4°C until use. For CC1 staining (Figure 3B and 3C), 2% PFA in PBS was used for perfusion and post-fixation.

To perform immunolabeling, slices were incubated in blocking buffer (4% donkey serum and 1% Triton X-100 in PBS solution) for 1 hour at room temperature, followed by incubation with primary antibodies in 1% donkey serum and 1% Triton X-100 in PBS, overnight at 4°C with agitation. Primary antibodies were: Anti-GFP chicken (1:1000, Abcam, ab13970); Anti-NG2 rabbit (1:1000, Sigma, AB5320); Anti- APC/CC1 mouse (1:200, Calbiochem, OP80);

Anti- PDGFRa rat (1:500, eBioscience, 14-1401-81); Anti-MBP rat (1:2000, Abcam, ab7349); Anti-NF chicken (1:1000, Abcam, ab4680); Anti-GFAP mouse (1:500, Sigma, G3893); Anti-NeuN rabbit (1:500, Abcam, ab177487). The slices were washed 3 times in 1% Triton X-100 in PBS for 10 minutes, followed by incubation with secondary antibodies (Alexa Fluor 488-, and 568- and 647-labeled donkey/goat anti-mouse, rat, rabbit, or chicken IgGs (H+L); 1:1000, Invitrogen or Life Technologies) in 1% Triton X-100 in PBS for 2 hours at room temperature. Then, sections were washed 3 times in 1% Triton X-100 in PBS for 10 minutes, and incubated for another 10 min at room temperature with Hoechst 33342 (0,2 mg/mL, Sigma, cat#H6024) in 0.4% Triton X-100 in PBS. Sections were mounted using ProLong Gold Antifade Reagent (Invitrogen, cat#P36930).

Image acquisition and analysis:

Images for global brain morphology (Figure 2B, Figure 4B, Figure 5A, and Figure 6C) were obtained using a Zeiss Axiozoom V16 macroscope, equipped with a digital camera (AxioCam HRm) using a 16x (pixel size: 4.037 µm), 63x (pixel size: 1.032 µm) or 80x objectives (pixel size: 0.813 µm). Images for NG2, PDGFRa or CC1 quantifications were acquired using a Zeiss spinning-disk confocal CSU-W1 microscope with 25x oil objective (Z-plane step size: 0.68 µm). The first 15 z-planes were projected and shown in the figures.

Thickness of the corpus callosum (labelled with MBP or NF) was measured manually using “Measure” function in ImageJ/Fiji[43]. For MBP or NF labelling in the cortex, the first 15 z-planes of each image were projected using “Z Project” function. An ROI was drawn around the region of interest. Background was subtracted using “Subtract Background”. The raw integrated density of the signal was measured using “Measure” function. The value was divided by the area of the ROI in µm² and reported. All the steps were performed in Fiji.

The maximum intensity of MBP labeling was measured manually. The first 15 z-planes of each image were projected using “Z Project” function. A line crossing the center of corpus callosum vertically was drawn. Background was subtracted using “Subtract Background”. The maximum intensity of the signal was measured using “Measure” function in ImageJ/Fiji.

A home-made plugin was used to quantify the number of *Sox10*-GFP, NG2, PDGFRa, and CC1 cells. Since NG2 is a chondroitin sulfate proteoglycan which is expressed on the cell surface of OPCs[44], it is difficult to segment the NG2 labeling and count them automatically. Therefore, in this plugin, Hoechst and GFP signals are segmented using the StarDist plugin in Fiji. The volume of the signal is filtered by the minimum and maximum values selected by the user. For GFP signal, there is a threshold for minimum intensity. This minimum intensity is

measured manually by the user based on the comparison of the signal of the real GFP versus the background. The detected nuclei colocalized with segmented GFP signals are considered as the OL lineage cells (*Sox10*-GFP cells). Then, the plugin dilates the area of each segmented nucleus by 1 µm and measures “meanIntCor” for NG2, PDGFRa or CC1, based on the following formula:

$$meanIntCor = meanInt - bg$$

“meanInt” is the mean intensity of the signal of interest (NG2, PDGFRa, CC1) for dilated nucleus. “bg” is the mean intensity of the minimum signal in the projection.

Then, a threshold is selected for “meanIntCor” value to count the number of OPCs (NG2 or PDGFRa) or OLs (CC1).

Single-cell transcriptomics data analysis:

Metadata and expression matrix from sequencing of single cells of the oligolineage at E13.5, P7 and juvenile/adult mouse (NCBI GEO Series: GSE95194; Marques et al. (2018)) were downloaded as .RDS from https://cells.ucsc.edu/?ds=oligo-lineage-dev . R version 4.1.0 (2021-05-18) and Seurat_4.1.0 packages were used for analysis. Data were normalized and scaled before running the principal component analysis (PCA). Cell cycle scoring did not show any bias that could impact the PCA analysis. The Jackstraw and Elbowplot methods were used for determining the number of dimensions to be used for reduction using Uniform Manifold Approximation and Projection (UMAP). Because further analysis showed a batch effect between the developmental and juvenile/adult data, we used Harmony (v 0.1.1) to integrate the data and rerun the UMAP. k.param nearest neighbors (KNN) were computed to construct the shared nearest neighbor (SNN) graph and identify the cell clusters. Cell clusters were visualized using clustree (v_0.5.0) to determine the useful resolution. Assignment of clusters to cell types was performed using msigdbr (v_7.5.1) and the data from the original Marques et al. (2018) analysis. Gene Ontology (GO) term overrepresentation and Gene Set Enrichement analysis were performed to compare C1ql1 positive versus negative cells.

Acknowledgements:

We would like to thank Fatima El Marjou from the Curie Institute for CRISPR mice generation, Lamia Bouslama-Oueghlani and Noemie Ades from ICM, Paris for their scientific suggestions, Philippe Mailly and Heloise Monet from CIRB Imaging facility (ORION) for their contribution in developing the home-made plugins to quantify the smFISH and

immunofluorescence data, William D. Richardson from UCL, London for *Sox10^{DTA}* mice and scientific suggestion, and CIRB administration and animal facility personnels. This work was supported by funding from: European Research Council ERC consolidator grant SynID 724601 (to FS), INCA PEDIAHR21-014 (to FS). SM received a PhD thesis funding from la Ligue Nationale Contre le Cancer and Ecole des neurosciences de Paris ile-de-France (ENP). Since 2019, ENP has changed to la Fondation des Neurosciences Paris (FNP).

References:

1. Dawson, M. R. L., Polito, A., Levine, J. M. & Reynolds, R. NG2-expressing glial progenitor cells: an abundant and widespread population of cycling cells in the adult rat CNS. *Mol. Cell. Neurosci.* **24**, 476–488 (2003).
2. Akay, L. A., Effenberger, A. H. & Tsai, L.-H. Cell of all trades: oligodendrocyte precursor cells in synaptic, vascular, and immune function. *Genes Dev.* **35**, 180–198 (2021).
3. Minocha, S. *et al.* NG2 glia are required for vessel network formation during embryonic development. *eLife* **4**, e09102 (2015).
4. Xiao, Y., Petrucco, L., Hoodless, L. J., Portugues, R. & Czopka, T. Oligodendrocyte precursor cells sculpt the visual system by regulating axonal remodeling. *Nat. Neurosci.* **25**, 280–284 (2022).
5. Buchanan, J. *et al.* Oligodendrocyte precursor cells prune axons in the mouse neocortex. 2021.05.29.446047 Preprint at https://doi.org/10.1101/2021.05.29.446047 (2021).
6. Kirby, L. *et al.* Oligodendrocyte precursor cells present antigen and are cytotoxic targets in inflammatory demyelination. *Nat. Commun.* **10**, 3887 (2019).
7. Bergles, D. E. & Richardson, W. D. Oligodendrocyte Development and Plasticity. *Cold Spring Harb. Perspect. Biol.* **8**, a020453 (2016).
8. Baxi, E. G. *et al.* Lineage tracing reveals dynamic changes in oligodendrocyte precursor cells following cuprizone-induced demyelination. *Glia* **65**, 2087–2098 (2017).
9. Rivers, L. E. *et al.* PDGFRA/NG2 glia generate myelinating oligodendrocytes and piriform projection neurons in adult mice. *Nat. Neurosci.* **11**, 10.1038/nn.2220 (2008).
10. Nishiyama, A., Shimizu, T., Sherafat, A. & Richardson, W. D. Life-long oligodendrocyte development and plasticity. *Semin. Cell Dev. Biol.* **116**, 25–37 (2021).
11. Kang, S. H., Fukaya, M., Yang, J. K., Rothstein, J. D. & Bergles, D. E. NG2+ CNS Glial Progenitors Remain Committed to the Oligodendrocyte Lineage in Postnatal Life and following Neurodegeneration. *Neuron* **68**, 668–681 (2010).

12. Kessaris, N. *et al.* Competing waves of oligodendrocytes in the forebrain and postnatal elimination of an embryonic lineage. *Nat. Neurosci.* **9**, 173–179 (2006).
13. Iannarelli, P. Oligodendrocyte Population Dynamics and Plasticity Probed by Genetic Manipulation in Mice. *Doctoral thesis, UCL (University College London).* ?-? (UCL (University College London), 2017).
14. van Tilborg, E. *et al.* Origin and dynamics of oligodendrocytes in the developing brain: Implications for perinatal white matter injury. *Glia* **66**, 221–238 (2018).
15. Ortega, M. C. *et al.* Neuregulin-1/ErbB4 signaling controls the migration of oligodendrocyte precursor cells during development. *Exp. Neurol.* **235**, 610–620 (2012).
16. Nery, S., Wichterle, H. & Fishell, G. Sonic hedgehog contributes to oligodendrocyte specification in the mammalian forebrain. *Development* **128**, 527–540 (2001).
17. Marisca, R. *et al.* Functionally distinct subgroups of oligodendrocyte precursor cells integrate neural activity and execute myelin formation. *Nat. Neurosci.* **23**, 363–374 (2020).
18. Beiter, R. M. *et al.* Evidence for oligodendrocyte progenitor cell heterogeneity in the adult mouse brain. *Sci. Rep.* **12**, 12921 (2022).
19. Spitzer, S. O. *et al.* Oligodendrocyte Progenitor Cells Become Regionally Diverse and Heterogeneous with Age. *Neuron* **101**, 459-471.e5 (2019).
20. Marques, S. *et al.* Transcriptional Convergence of Oligodendrocyte Lineage Progenitors during Development. *Dev. Cell* **46**, 504-517.e7 (2018).
21. Boda, E. *et al.* Molecular and functional heterogeneity in dorsal and ventral oligodendrocyte progenitor cells of the mouse forebrain in response to DNA damage. *Nat. Commun.* **13**, 2331 (2022).
22. Sigoillot, S. M. *et al.* The Secreted Protein C1QL1 and Its Receptor BAI3 Control the Synaptic Connectivity of Excitatory Inputs Converging on Cerebellar Purkinje Cells. *Cell Rep.* **10**, 820–832 (2015).
23. Kakegawa, W. *et al.* Anterograde C1ql1 Signaling Is Required in Order to Determine and Maintain a Single-Winner Climbing Fiber in the Mouse Cerebellum. *Neuron* **85**, 316–329 (2015).
24. Platt, R. J. *et al.* CRISPR-Cas9 Knockin Mice for Genome Editing and Cancer Modeling. *Cell* **159**, 440–455 (2014).
25. Hughes, E. G., Kang, S. H., Fukaya, M. & Bergles, D. E. Oligodendrocyte progenitors balance growth with self-repulsion to achieve homeostasis in the adult brain. *Nat. Neurosci.* **16**, 668–676 (2013).

26. Georgiadis, M. *et al.* Nanostructure-specific X-ray tomography reveals myelin levels, integrity and axon orientations in mouse and human nervous tissue. *Nat. Commun.* **12**, 2941 (2021).
27. Tripathi, R. B. *et al.* Dorsally and Ventrally Derived Oligodendrocytes Have Similar Electrical Properties but Myelinate Preferred Tracts. *J. Neurosci.* **31**, 6809–6819 (2011).
28. Gao, Y.-J., Chen, F. & Zhang, L.-J. C1q-like 1 is frequently up-regulated in lung adenocarcinoma and contributes to the proliferation and invasion of tumor cells. *J. Chemother.* **33**, 476–485 (2021).
29. Bolliger, M. F., Martinelli, D. C. & Südhof, T. C. The cell-adhesion G protein-coupled receptor BAI3 is a high-affinity receptor for C1q-like proteins. *Proc. Natl. Acad. Sci. U. S. A.* **108**, 2534–2539 (2011).
30. Wang, X. *et al.* Sequential fate-switches in stem-like cells drive the tumorigenic trajectory from human neural stem cells to malignant glioma. *Cell Res.* **31**, 684–702 (2021).
31. Lu, X. *et al.* Deficiency of C1QL1 Reduced Murine Ovarian Follicle Reserve Through Intraovarian and Endocrine Control. *Endocrinology* **163**, bqac048 (2022).
32. Barres, B. A. & Raff, M. C. Control of oligodendrocyte number in the developing rat optic nerve. *Neuron* **12**, 935–942 (1994).
33. Torkildsen, O., Brunborg, L. A., Myhr, K.-M. & Bø, L. The cuprizone model for demyelination. *Acta Neurol. Scand. Suppl.* **188**, 72–76 (2008).
34. Bergles, D. E., Roberts, J. D. B., Somogyi, P. & Jahr, C. E. Glutamatergic synapses on oligodendrocyte precursor cells in the hippocampus. *Nature* **405**, 187–191 (2000).
35. Káradóttir, R., Hamilton, N. B., Bakiri, Y. & Attwell, D. Spiking and nonspiking classes of oligodendrocyte precursor glia in CNS white matter. *Nat. Neurosci.* **11**, 450–456 (2008).
36. Liu, F. *et al.* C1ql1/Ctrp14 and C1ql4/Ctrp11 promote angiogenesis of endothelial cells through activation of ERK1/2 signal pathway. *Mol. Cell. Biochem.* **424**, 57–67 (2017).
37. Floriddia, E. M. *et al.* Distinct oligodendrocyte populations have spatial preference and different responses to spinal cord injury. *Nat. Commun.* **11**, 5860 (2020).
38. Pepper, R. E., Pitman, K. A., Cullen, C. L. & Young, K. M. How Do Cells of the Oligodendrocyte Lineage Affect Neuronal Circuits to Influence Motor Function, Memory and Mood? *Front. Cell. Neurosci.* **12**, (2018).
39. Tsai, H.-H. *et al.* Oligodendrocyte precursors migrate along vasculature in the developing nervous system. *Science* **351**, 379–384 (2016).
40. Wang, J. *et al.* RTN4/NoGo-Receptor Binding to BAI Adhesion-GPCRs Regulates Neuronal Development. *Cell* **184**, 5869-5885.e25 (2021).

41. Love, S. Demyelinating diseases. *J. Clin. Pathol.* **59**, 1151–1159 (2006).
42. Falcão, A. M. *et al.* Disease-specific oligodendrocyte lineage cells arise in multiple sclerosis. *Nat. Med.* **24**, 1837–1844 (2019).
43. Schindelin, J. *et al.* Fiji - an Open Source platform for biological image analysis. *Nat. Methods* **9**, 10.1038/nmeth.2019 (2012).
44. Nishiyama, A., Dahlin, K. J., Prince, J. T., Johnstone, S. R. & Stallcup, W. B. The primary structure of NG2, a novel membrane-spanning proteoglycan. *J. Cell Biol.* **114**, 359–371 (1991).

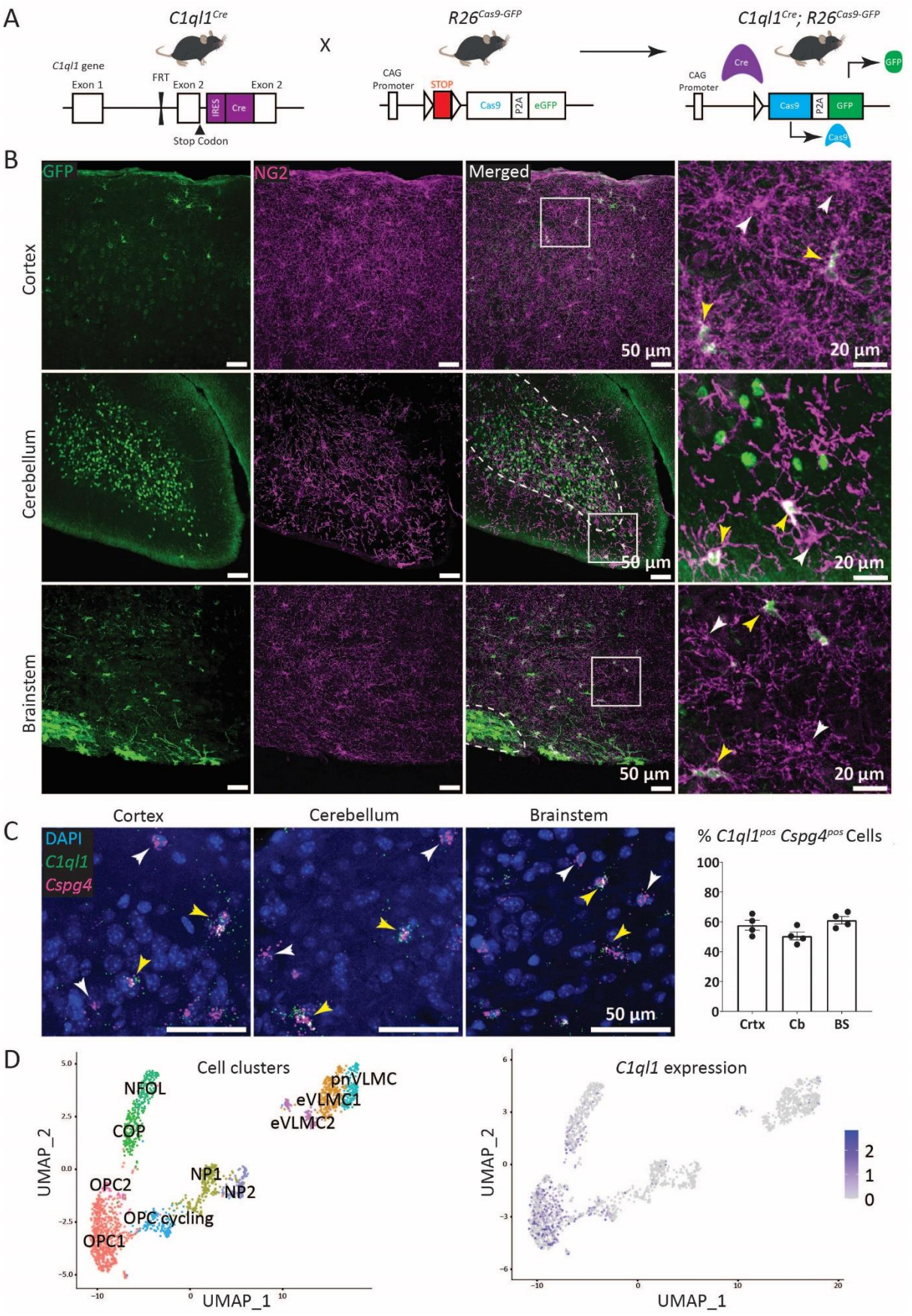
A
C1ql1Cre
X
R26Cas9-GFP
C1ql1Cre; R26Cas9-GFP
C1ql1 gene
Exon 1
FRT
Exon 2
IRES
Cre
Exon 2
Stop Codon
CAG Promoter
STOP
Cas9
P2A
eGFP
Cre
GFP
B
GFP
NG2
Merged
Cortex
Cerebellum
Brainstem
50 µm
20 µm
C
Cortex
Cerebellum
Brainstem
DAPI
C1ql1
Cspg4
50 µm
% C1ql1pos Cspg4pos Cells
100
80
60
40
20
0
Crtx
Cb
BS
D
Cell clusters
NFOL
COP
OPC2
OPC cycling
OPC1
NP1
NP2
pnVLMC
eVLMC1
eVLMC2
UMAP_2
UMAP_1
C1ql1 expression
2
1
0

Figure 1. A subpopulation of Oligodendrocyte Precursor Cells expresses *C1ql1*. A) Diagram of the breeding scheme used to determine the cell types expressing *C1ql1* in the mouse brain. The *C1ql1*^{Cre} mouse line was crossed with the Cre-dependent *R26*$^{Cas9\text{-}GFP}$ reporter mice. B) GFP expressing cells and Oligodendrocyte Precursor Cells (OPCs) were visualized using co-immunolabeling for GFP (green) and NG2 (magenta) respectively, in sagittal brain sections from *C1ql1*^{Cre}*; R26*$^{Cas9\text{-}GFP}$ animals at postnatal day 30 (P30). In the cerebellum and the brainstem, GFP is strongly expressed by granule cells (GCs) and inferior olivary neurons (IONs), respectively (internal granular layer and inferior olive delineated by the white dashed line). Scale bars = 50 µm. Higher magnification of the regions delineated by the white squares show the presence of GFP$^-$ (white arrowhead) and GFP$^+$ (yellow arrowhead) NG2 cells in all analyzed regions of the brain. Scale bars = 20 µm. C) Duplex smFISH labeling of *C1ql1* and *Cspg4* (coding for NG2) mRNAs was performed in parasagittal sections of the somatosensory cortex, cerebellum and brainstem from P30 wild-type animals. Both *C1ql1*$^-$ (white arrowhead) and *C1ql1*$^+$ (yellow arrowhead) *Cspg4*$^+$ cells are detected. Scale bars = 50 µm. Quantification of the percentage of *C1ql1*-expressing *Cspg4*$^+$ cells was performed in the somatosensory cortex (Crtx), cerebellum (Cb) and brainstem (BS). Data are represented as mean ± SEM. n = 4 animals. D) UMAP analysis of single-cell transcriptomic data from Marques *et al.*[20], confirms the expression of *C1ql1* (*right panel*) in a subset of OPCs and COP cells (*left panel*). COP: committed oligodendrocyte precursors, eVLMC: embryonic vascular and leptomeningeal cells, NFOL: newly formed oligodendrocyte, NP: neural progenitor, OPC: oligodendrocyte precursor cell, PLC: pericyte lineage cells.

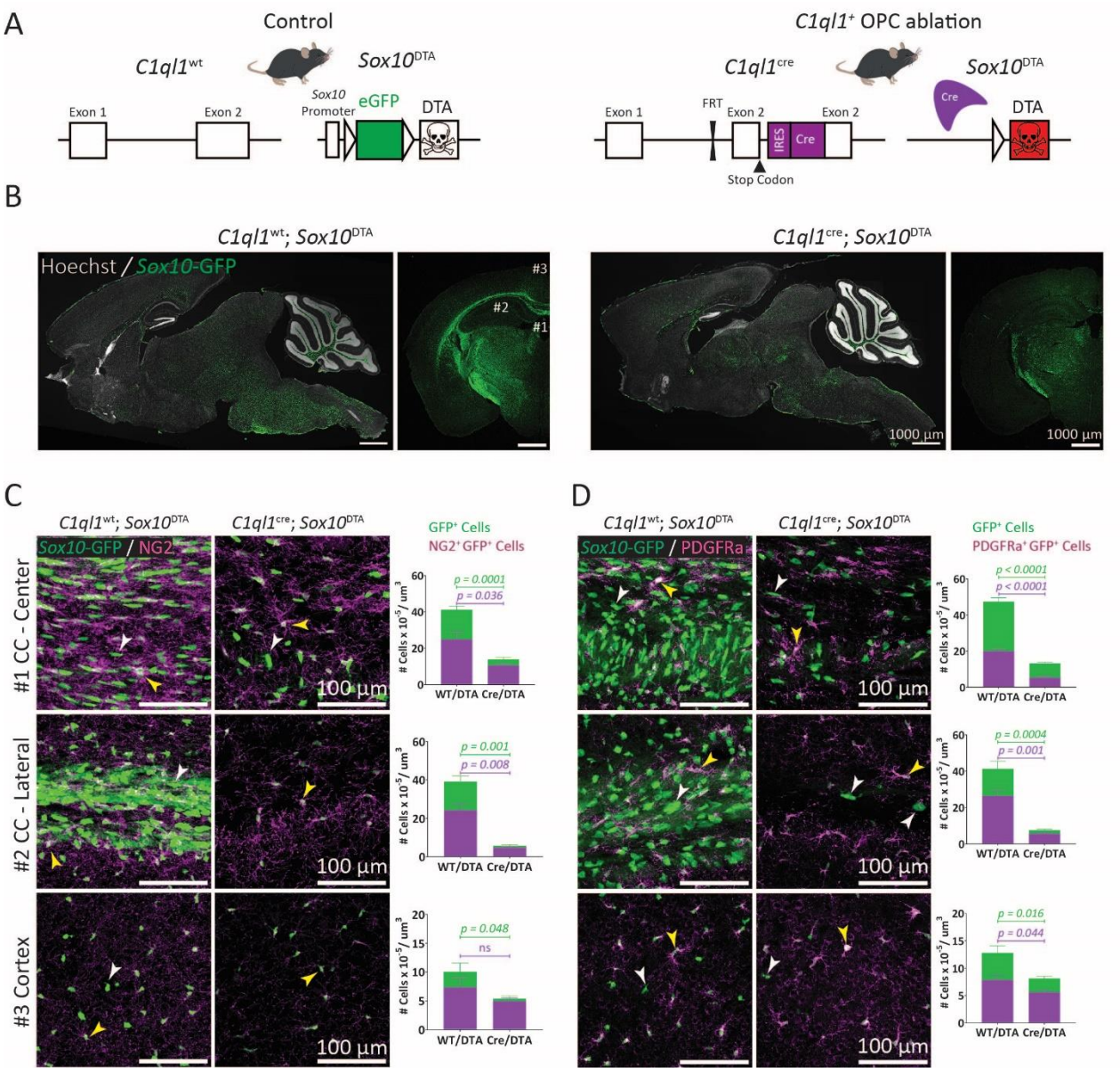

Figure 2. Ablation of *C1ql1*-expressing OPCs is not compensated by remaining OPCs during postnatal development. A) Diagram of the breeding scheme used to ablate *C1ql1*-expressing oligolineage cells in the mouse brain via *Sox10*-driven expression of diphtheria toxin (DTA). The *C1ql1*^{Cre} mouse line was crossed with the Cre-dependent *Sox10*^{DTA} mice. B) Parasagittal and coronal sections from P16 brains of control (*C1ql1*^{wt}*; Sox10*^{DTA}) and *C1ql1*$^{+}$ OPC-ablated (*C1ql1*^{Cre}*; Sox10*^{DTA}) mice. Direct GFP fluorescence and Hoechst staining are shown. Scale bars = 1000 µm. C) OPCs were immunolabeled for NG2 (magenta) in coronal sections from P16 brains of the control and *C1ql1*-ablated conditions. Both NG2^{+} (yellow arrowhead) and NG2^{-} (white arrowhead) *Sox10*-GFP cells are detected in the two conditions in the center and lateral part of corpus callosum (CC) as well as the cortex, but less in the ablated condition. Scale bars = 100 µm. Quantification of the density of *Sox10*-GFP^{+} (green) and NG2^{+} *Sox10*-GFP^{+} (magenta) was performed in CC-center (#1), CC-lateral (#2) and

cortex (#3) from the two genotypes. Data are represented as mean ± SEM. *C1ql1*^{wt}*; Sox10*^{DTA}: n = 4 animals. *C1ql1*^{Cre}*; Sox10*^{DTA}: n = 7 animals. p values are from Unpaired t test with Welch's corrections. D) OPCs were immunolabeled for PDGFRa (magenta) in coronal sections from P16 brains of the control and *C1ql1*^{Cre}*; Sox10*^{DTA} mice. Like NG2 staining, both PDGFRa^{+} (yellow arrowhead) and PDGFRa^{-} (white arrowhead) *Sox10*-GFP cells are observed in the two groups in the center and lateral part of corpus callosum (CC) as well as the cortex, but with different ratios. Scale bars = 100 µm. Quantification of the density of *Sox10*-GFP^{+} (green) and PDGFRa^{+} *Sox10*-GFP^{+} (magenta) in the two genotypes confirms the decrease in the number and ratio of the oligolineage cells and OPCs upon ablation of *C1ql1*-expressing *Sox10*$^{+}$ cells. Data are represented as mean ± SEM. *C1ql1*^{wt}*; Sox10*^{DTA}: n = 6 animals. *C1ql1*^{Cre}*; Sox10*^{DTA}: n = 10 animals. p values are from Unpaired t test with Welch's corrections. ns = not significant.

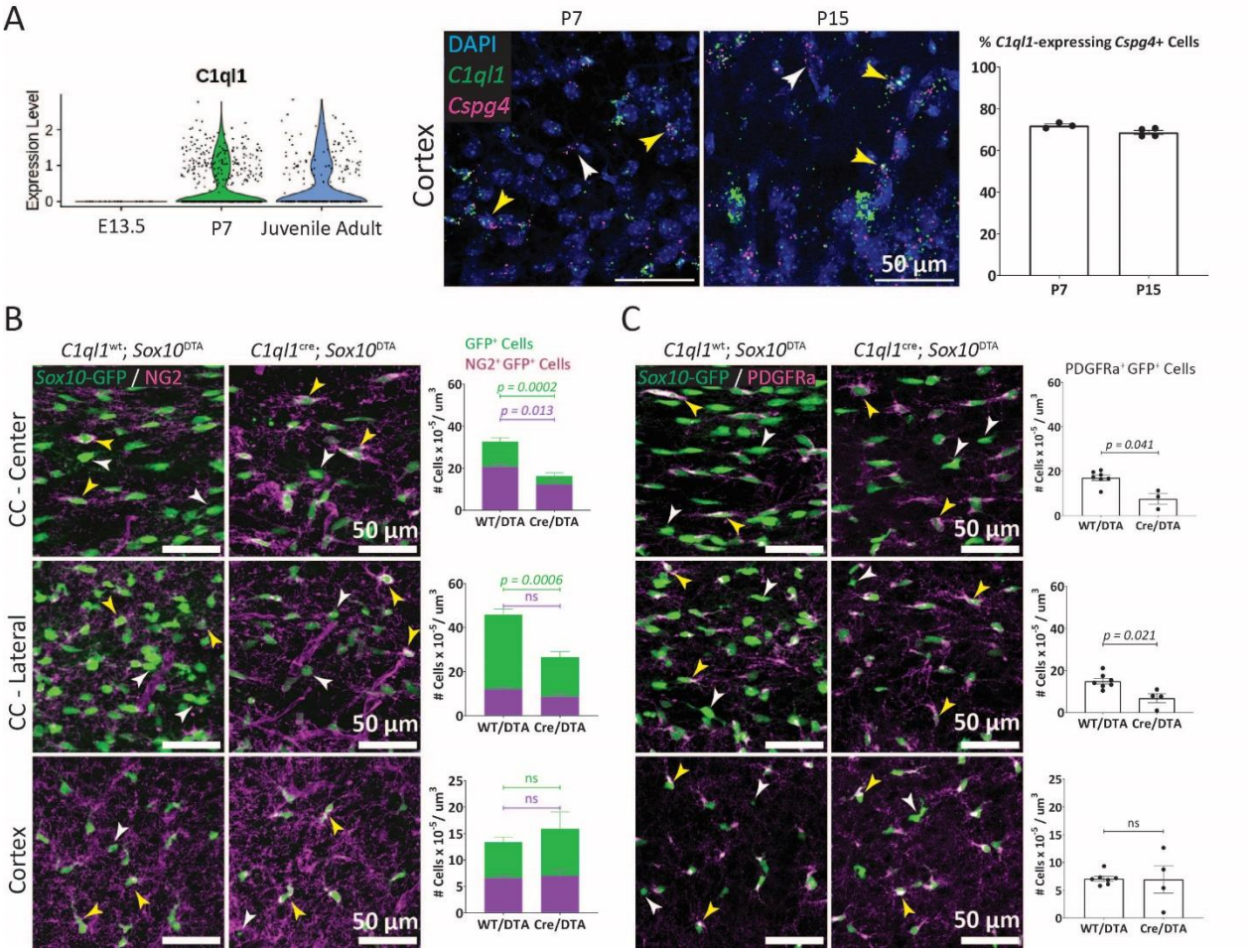

Figure 3. Loss of OPCs starts as early as the first postnatal week in some brain regions after genetic ablation of *C1QL1*-expressing OPCs. A) Violin plot of single-cell RNA seq data (from Marques *et al.*[20]) during embryonic and postnatal development shows expression of *C1ql1* as early as P7, but not at E13.5. Duplex smFISH labeling of *C1ql1* and *Cspg4* mRNAs was performed in coronal cortical slices from P7 and P15 wild-type mice. Both *C1ql1*$^{-}$ (white arrowhead) and *C1ql1*$^{+}$ (yellow arrowhead) *Cspg4*$^{+}$ cells are observed. Scale bars = 50 µm. Quantification of the percentage of *C1ql1*-expressing *Cspg4*$^{+}$ cells was performed in cortical sections from P7 and P15 animals. Data are represented as mean ± SEM. P7: n = 3 animals. P15: n = 4 animals. Scale bars = 50 µm. B) OPCs were immunostained for NG2 (magenta) in coronal sections from P7 control or *C1ql1*^{Cre}*; Sox10*^{DTA} animals. NG2^{+} (yellow arrowhead) or NG2^{-} (white arrowhead) *Sox10*-GFP cells are identified in the CC-center, CC-lateral and the cortex. Scale bars = 50 µm. Quantification of *Sox10*-GFP^{+} (green) or NG2^{+} *Sox10*-GFP^{+} (magenta) cells in both genotypes shows a decrease in the density of oligolineage cells in CC-center and lateral, but not in the cortex. Data are represented as mean ± SEM. *C1ql1*^{wt}*; Sox10*^{DTA}: n = 7 animals. *C1ql1*^{Cre}*; Sox10*^{DTA}: n = 3 - 4 animals. Unpaired t test with Welch's corrections. C) PDGFRa immunolabeling of OPCs (magenta) in the same regions used for NG2 staining confirms the decrease in OPC density in both regions of the corpus callosum at

P7 after *C1ql1*-expressing OPC ablation. PDGFRa^{+} (yellow arrowhead) or PDGFRa^{-} (white arrowhead) *Sox10*-GFP^{+} cells are observed in both groups. Scale bars = 50 µm. Data are represented as mean ± SEM. *C1ql1*^{wt}*; Sox10*^{DTA}: n = 7 animals. *C1ql1*^{Cre}*; Sox10*^{DTA}: n = 3 - 4 animals. Unpaired t test with Welch's corrections. ns = not significant.

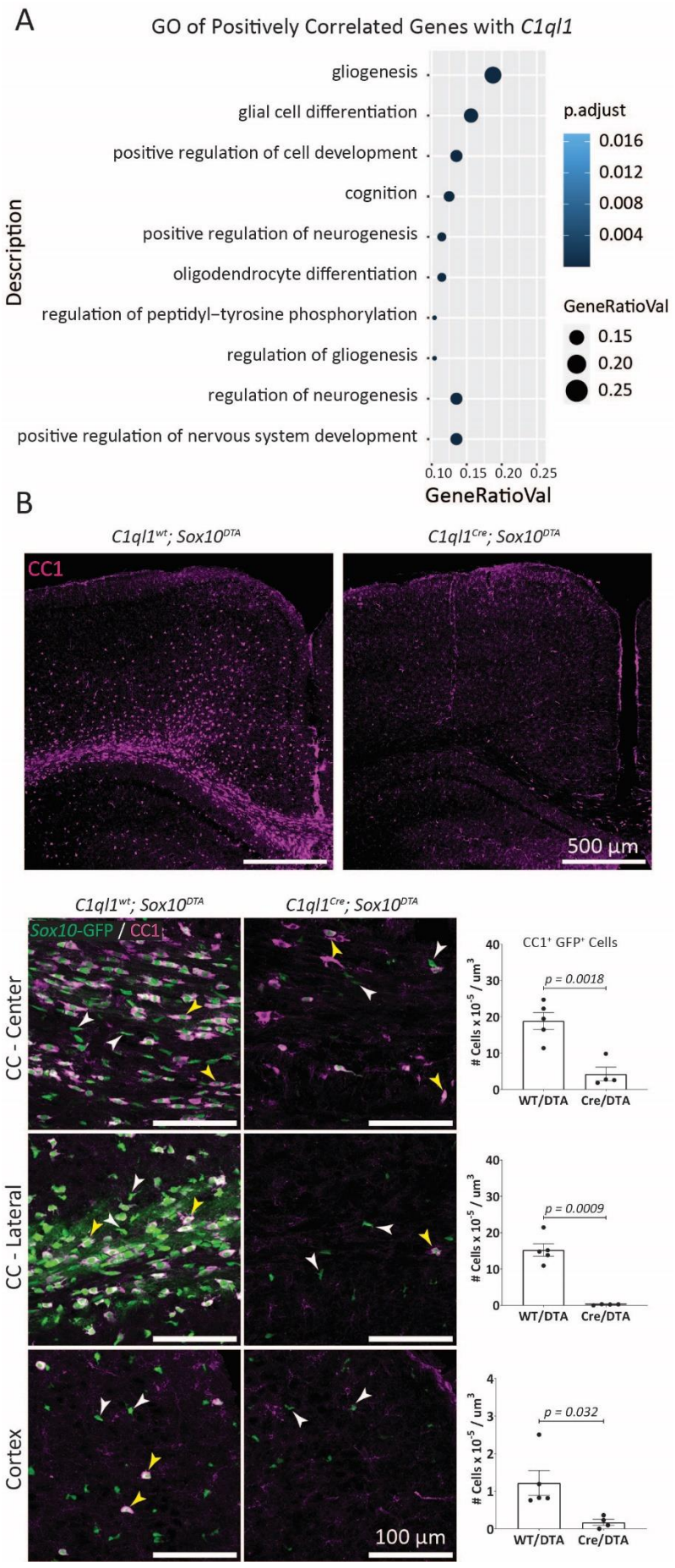
A
GO of Positively Correlated Genes with C1ql1
gliogenesis
glial cell differentiation
positive regulation of cell development
cognition
positive regulation of neurogenesis
oligodendrocyte differentiation
regulation of peptidyl−tyrosine phosphorylation
regulation of gliogenesis
regulation of neurogenesis
positive regulation of nervous system development
Description
p.adjust
0.016
0.012
0.008
0.004
GeneRatioVal
0.15
0.20
0.25
0.10 0.15 0.20 0.25
GeneRatioVal
B
C1ql1wt; Sox10DTA
C1ql1Cre; Sox10DTA
CC1
500 µm
C1ql1wt; Sox10DTA
C1ql1Cre; Sox10DTA
Sox10-GFP / CC1
CC - Center
CC - Lateral
Cortex
100 µm
CC1+ GFP+ Cells
p = 0.0018
# Cells x 10-5 / um3
WT/DTA
Cre/DTA
p = 0.0009
p = 0.032

Figure 4. Lack of oligodendrocyte after DTA-mediated ablation of *C1ql1*-expressing OPCs. A) Gene ontology analysis shows the biological functions of the genes enriched in *C1ql1*-expressing OPCs compared to negative OPCs. Data from Marques *et al.*[20]. B) Low magnification of coronal cortical sections from *C1ql1*^{wt}*; Sox10*^{DTA} and *C1ql1*^{Cre}*; Sox10*^{DTA} P16 mice immunolabeled with CC1, a marker of oligodendrocytes. Scale bars = 500 µm. High magnification of the coronal sections in the center and lateral parts of CC and cortex with CC1 immunolabeling (magenta) shows the dramatic decrease or absence of OLs in *C1ql1*^{Cre}*; Sox10*^{DTA} at P16. CC1^{+} (yellow arrowhead) or CC1^{-} (white arrowhead) *Sox10*-GFP^{+} cells are shown. Scale bars = 100 µm. Quantification of the density of *Sox10*-GFP^{+} (green) or CC1^{+}-*Sox10*-GFP^{+} (magenta) in the three analyzed regions (CC-center, CC-lateral and cortex) shows a heterogeneous decrease in OL generation in the *C1ql1*$^{+}$ OPC-ablated condition. Data are represented as mean ± SEM. *C1ql1*^{wt}*; Sox10*^{DTA}: n = 5 animals. *C1ql1*^{Cre}*; Sox10*^{DTA}: n = 4 animals. Unpaired t test with Welch's corrections. ns = not significant.

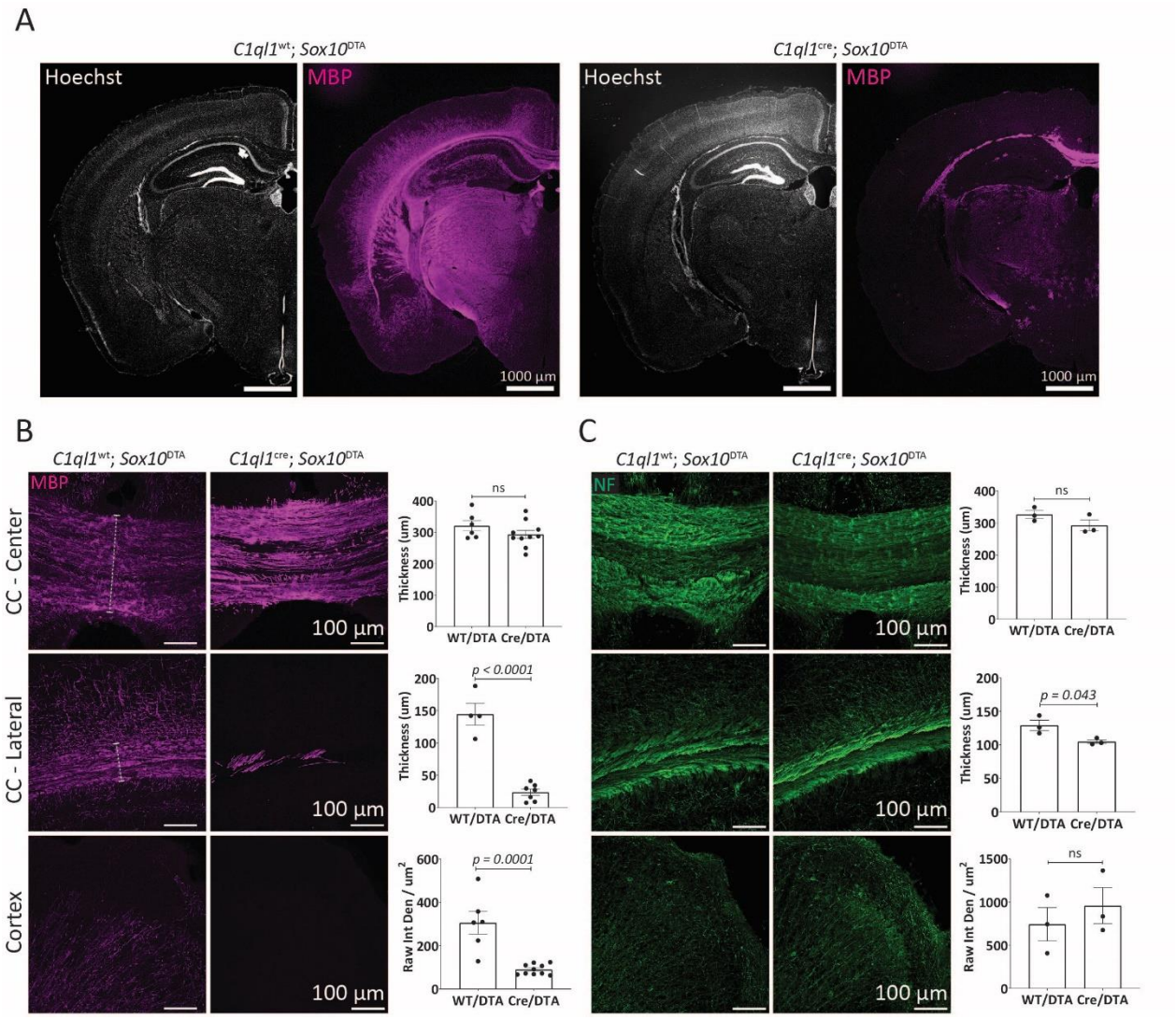

Figure 5. Lack of myelination in the forebrain after genetic ablation of *C1ql1*-expressing OPCs. A) Immunolabeling of coronal brain sections at P16 for myelin binding protein (MBP, magenta) illustrates the almost total absence of myelination in the forebrain upon genetic ablation of *C1ql1*-expressing OPCs, without gross morphological changes. Scale bars = 1000 µm. B) Myelinated fibers (immunolabeled for MBP, magenta) were visualized in coronal sections of the CC-center, CC-lateral and cortex of the two conditions at P16. The thickness of the myelinated regions in CC, delineated by the white dashed lines, was measured. Scale bars = 100 µm. Quantification of the thickness of myelinated regions in the corpus callosum and the intensity of MBP in the cortex shows an almost complete absence of MBP in CC-lateral and cortex. Data are represented as mean ± SEM. *C1ql1*^{wt}; *Sox10*^{DTA}: n = 4 animals. *C1ql1*^{cre}; *Sox10*^{DTA}: n = 7 - 10 animals. Unpaired t test with Welch's corrections. Raw Int Den: Raw integrated density. C) Neuronal fibers were immunolabeled for neurofilament (NF, green) in coronal P16 sections of the three regions of interest (CC-center, CC-lateral and cortex), to compare the effect of *C1ql1*-expressing OPC ablation on axogenesis. No deficit is observed

when comparing both conditions. Scale bars = 100 µm. Quantification of the thickness of the fiber bundles in the corpus callosum and the intensity of NF in the cortex shows a small decrease in the thickness of the CC-lateral, probably explained by the lack of myelination. Data are represented as mean ± SEM. *C1ql1*^{wt}; *Sox10*^{DTA}: n = 3 animals. *C1ql1*^{cre}; *Sox10*^{DTA}: n = 3 animals. Unpaired t test. ns = not significant.

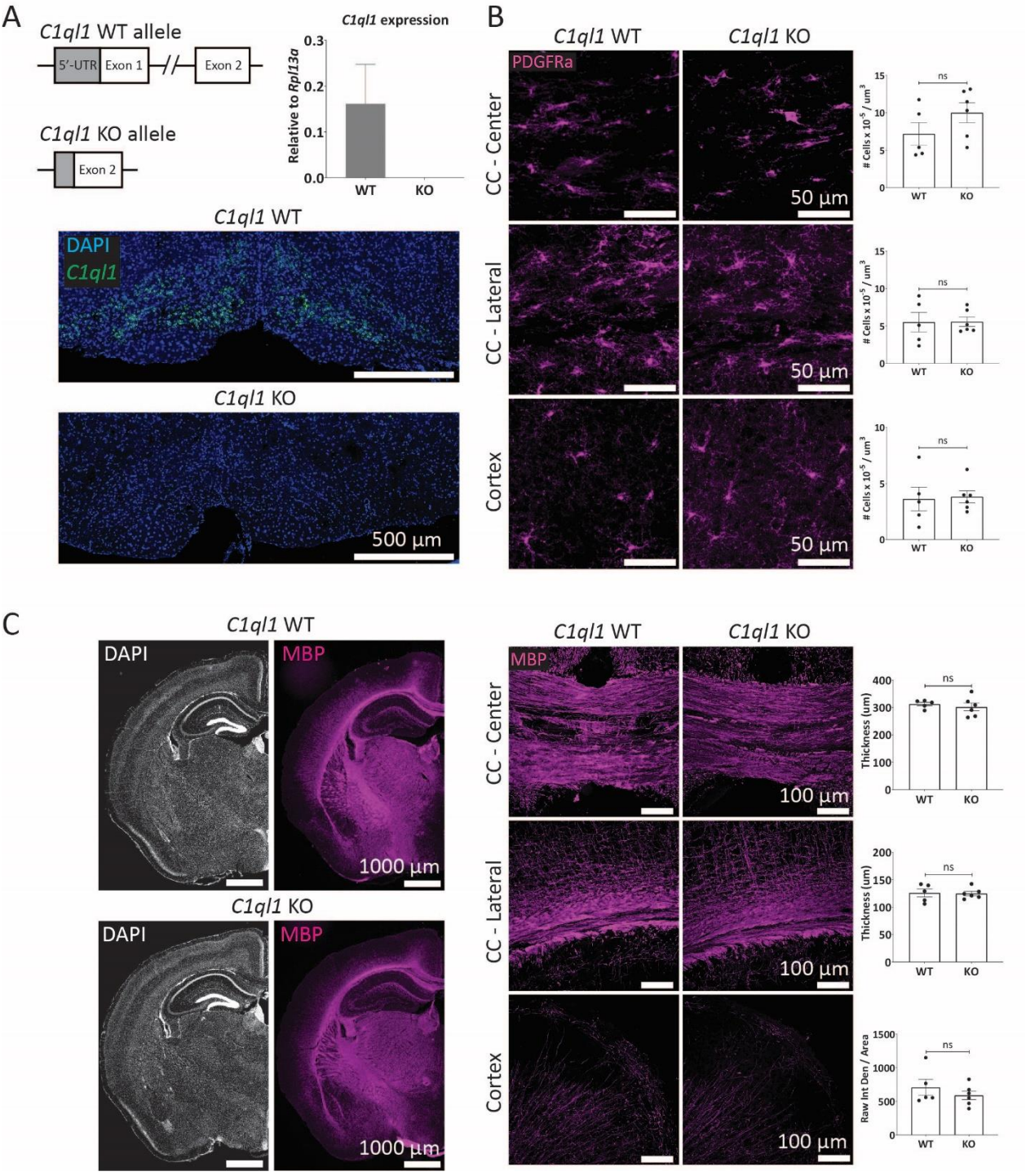

Figure 6. Loss of function of *C1ql1* does not affect OPC numbers and myelination in the mouse forebrain. A) Diagram of the genomic locus of *C1ql1* in WT and constitutive knockout (KO) mice. Exon 1, intron between exons 1 and 2, and a part of the 5'-UTR are removed from the *C1ql1* gene using CRISPR/Cas9 gene editing approach. RT-qPCR detects the expression of *C1ql1* in the whole adult brain of the control, but no trace of its expression in *C1ql1* KO animals. Data are represented as mean ± SEM. n = 3 animals per genotype. smFISH labeling of *C1ql1* mRNA was performed in coronal sections of the brainstem at the level of inferior

olivary nuclei from adult *C1ql1* WT and *C1ql1* KO animals. No *C1ql1* is detected in the *C1ql1* KO, while its strong expression is observed in WT mice. Scale bars = 500 µm. B) OPCs were immunolabeled for PDGFRa (magenta) in coronal sections of CC-center, CC-lateral and cortex from P16–18 *C1ql1* WT and *C1ql1* KO animals. Scale bars = 50 µm. Quantification of the density of PDGFRa cells does not show any difference between the control and *C1ql1* KO mice. Data are represented as mean ± SEM. WT: n = 5 animals. KO: n = 6. Unpaired t test with Welch's corrections. C) MBP immunolabeling of coronal sections of the forebrain from P16-18 mice show no gross change in myelination between *C1ql1* WT and *C1ql1* KO mice. Scale bars = 1000 µm. D) Higher magnification of CC-center, CC-lateral and cortex shows no difference in the immunolabeling for MBP (magenta) between the two genotypes at P16–18. Scale bars = 100 µm. Quantification of the thickness of myelinated fibers in the corpus callosum and the intensity of MBP in the cortex. Data are represented as mean ± SEM. WT: n = 5 animals. KO: n = 6. Unpaired t test with Welch's corrections. ns = not significant.

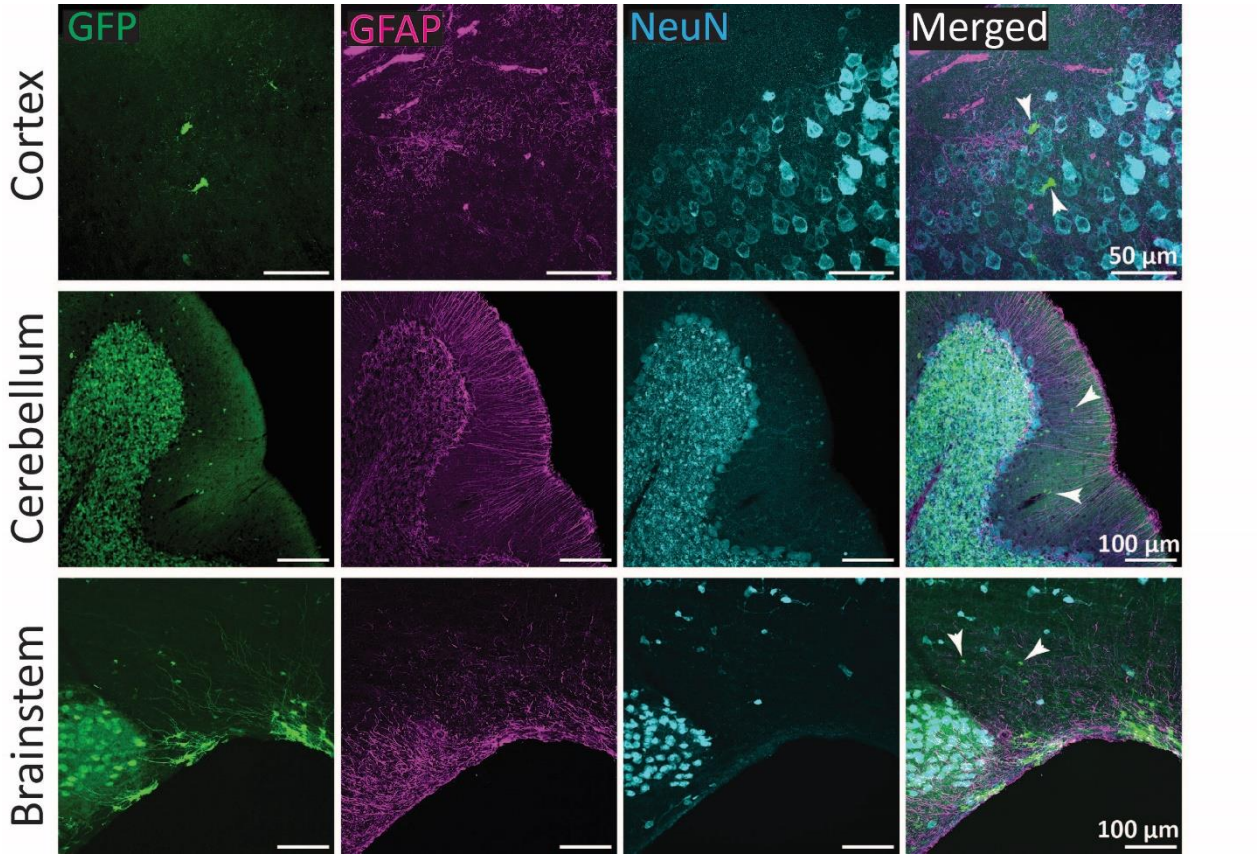

Figure S1. GFP-expressing cells in *C1ql1*^{Cre}; *R26*$^{Cas9\text{-}GFP}$ brains are not astrocytes or neurons (except granule cells and inferior olivary neurons). GFP expressing cells, astrocytes and neurons were visualized using co-immunolabeling for GFP (green), Glial fibrillary acidic protein (GFAP), and NeuN respectively, in sagittal brain sections from *C1ql1*^{Cre}; *R26*$^{Cas9\text{-}GFP}$ animals at P30. The granule cells (GCs) in the cerebellum and inferior olivary neurons (IONs) in the brainstem are co-labeled with GFP and NeuN. GFP^{+} GFAP^{-} NeuN^{-} cells (white arrowhead) are observed in all analyzed regions of the brain. Scale bars = 50 µm for cortex and 100 µm for cerebellum and brainstem.

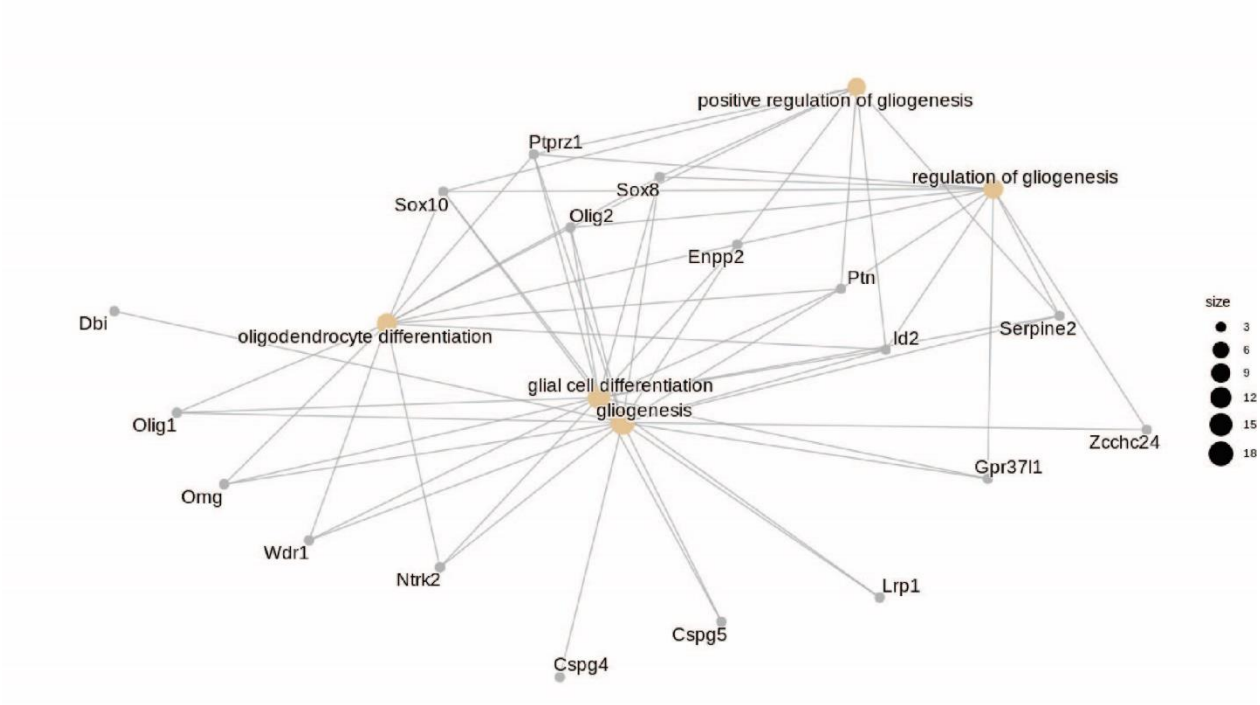

Figure S2. Genes involved in gliogenesis and their differentiation are enriched in *C1ql1*-expressing OPCs. Network analysis shows the genes co-enriched with *C1ql1* in E13.5, P7 and juvenile adult *Pdgfra*-GFP^{+} cells. Data from Marques *et al.*[20].

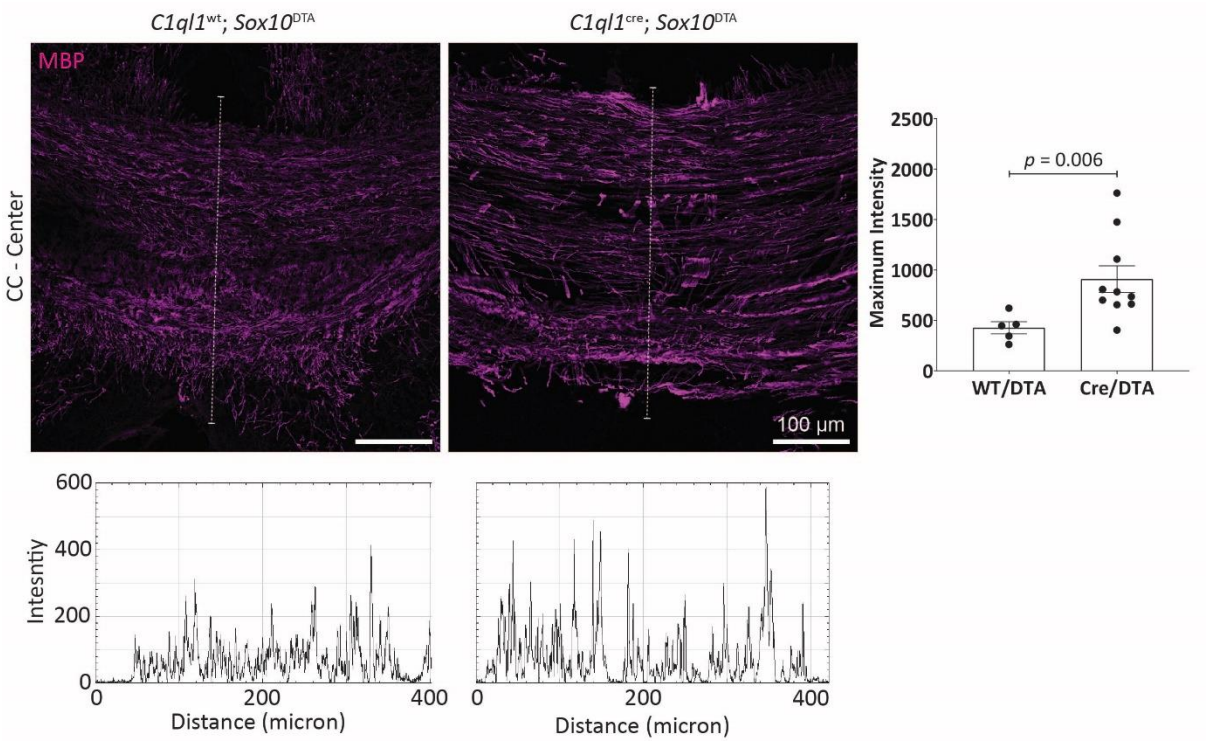

Figure S3. Maximum intensity of MBP staining is increased in the center of corpus callosum after genetic ablation of *C1ql1*-expressing OPCs. Myelinated fibers were immunolabeled for MBP (magenta) in coronal sections of the CC-center at P16. Background was subtracted from the images for analysis. The maximum intensity of the myelinated regions delineated by the white dashed lines, was measured. Scale bars = 100 µm. The plots show the intensity of the dashed white lines from top to down as an example. Quantification of the maximum intensity of MBP in the center of corpus callosum shows an increase in MBP, due to overcompensation by the remaining OLs. Data are represented as mean ± SEM. *C1ql1^{wt}; Sox10^{DTA}*: n = 5 animals. *C1ql1^{Cre}; Sox10^{DTA}*: n = 10 animals. Unpaired t test with Welch's corrections.

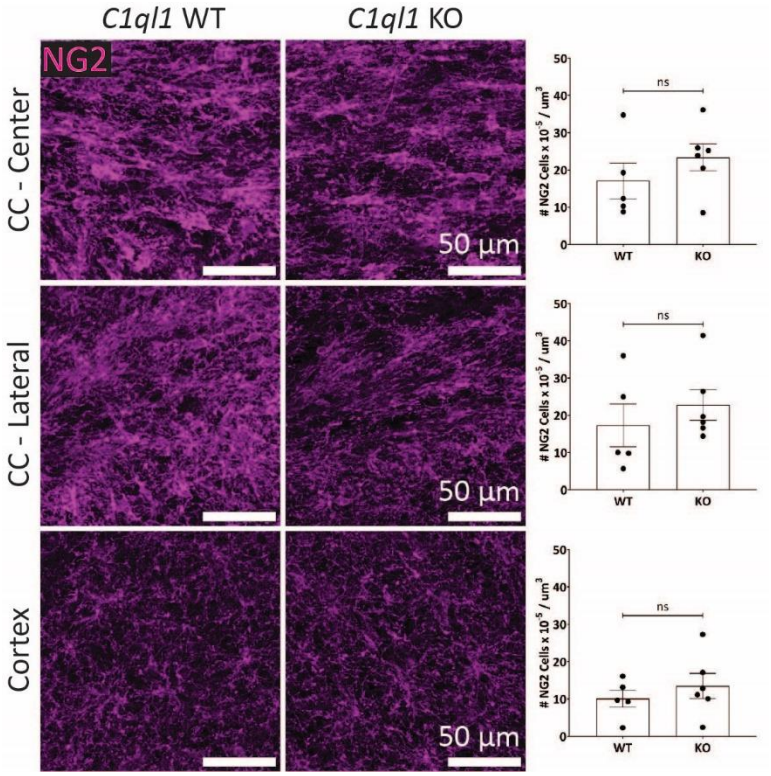

Figure S4. NG2 cells number is not affected in the forebrain of *C1ql1* constitutive knockout mouse. OPCs were immunolabeled for NG2 (magenta) in the coronal sections of CC-center, CC-lateral and cortex from the P16–18 *C1ql1* WT and *C1ql1* KO animals. Scale bars = 50 µm. Quantification of the density of NG2 cells does not show any difference between the control and *C1ql1* KO mice. Data are represented as mean ± SEM. WT: n = 5 animals. KO: n = 6. Unpaired t test with Welch's corrections. ns = not significant.

General Discussion

The main objective of my PhD was to identify and study new signaling pathways that might be regulated by activity and control the recognition between IONs and PCs in the olivocerebellar circuit. In this context, I have studied two molecular synaptic pathways that are also relevant for our understanding of other aspects of postnatal brain development. One of these two pathways had been known as a proto-oncogene involved in cellular proliferation in different tissues and cancers. Our data also suggest a role in the connectivity between IONs, MLIs and their target PCs. The other pathway had been known for its synaptic role in the olivocerebellar circuit, and we discovered it might have non-synaptic functions in non-neuronal cells in the brain.

1. **Summary of the main results:**

Cell surface proteins (CSPs) contribute to different aspects of brain development such as cell division, differentiation and connectivity between various types of cells. In this manuscript, two CSP pathways and their role during postnatal mouse brain development have been studied: c-KIT and C1QL1.

c-KIT is a receptor tyrosine kinase that plays critical role in cell division, survival and integrity of several tissues such as the hematopoietic system. Using bacTRAP transcriptomics we performed comparative analysis of two populations of IONs. Gene ontology analysis and data curation of the Allen brain atlas suggested *c-Kit*, *Cdh9*, and *Pcdh20* as candidates involved in the topographically organized connectivity between IONs and PCs, due to their differential expression in IONs during postnatal development. Among these three candidate genes, only the expression of *c-Kit* was modulated by chronic sensory deprivation using whisker trimming, so c-KIT was selected for further analysis. Data from the Allen brain atlas show that the gene coding the *c-Kit* ligand, *Scf*, is expressed in the target neuron (PC), suggesting a potential role for the c-KIT/SCF complex in the formation and maintenance of cell-cell contacts in the olivocerebellar circuit. Using immunostaining, the presence of c-KIT was identified at different types of synapses targeting PCs during postnatal development: inhibitory synapses made by MLIs in the cerebellar cortex, and excitatory synapses made by the CFs coming from IONs in the brainstem. Conditional knockout of *c-Kit* in MLIs, after the formation of their inhibitory synapses on PCs, shows that removal of c-KIT during the fourth postnatal week might decrease the volume of the presynaptic boutons of both MLIs and CFs on PCs, only in lobule VI, while their density remains unchanged. Since this loss of c-KIT happens after the formation of both excitatory and inhibitory synapses in this model, these results suggest a role for the c-KIT/SCF pathway in maintaining proper connectivity and

function of the olivocerebellar circuit, and identify a potential new role for this member of receptor tyrosine kinases (RTKs) in brain function.

In parallel, I characterized a new Cre-driver mouse line that was generated to enable inferior olivary neuron- specific knockout of *c-Kit* during postnatal development. In this line, Cre is knocked in the gene coding for C1QL1, a secreted molecule involved in CF-PC synapse formation and highly expressed in inferior olivary neurons. During this characterization, I discovered that C1QL1 is expressed in a subtype of glial cells, oligodendrocyte precursor cells (OPCs). OPCs tile the whole central nervous system during development and adulthood. They play several key functions across the brain including the generation of oligodendrocytes. Whether the functional diversity of OPCs is the result of genetically defined subpopulations or of their regulation by external factors has not been established. We discovered that a subpopulation of OPCs found across the brain starts to express *C1ql1* during the first postnatal week in the mouse brain. Ablation of *C1ql1*-expressing OPCs, which constitute about 30-50% of total OPCs, in the mouse is not compensated by the remaining OPCs, and results in a large decrease in oligodendrocyte numbers and lack of myelination in many brain regions. Therefore, *C1ql1* is a molecular marker of a functionally non-redundant subpopulation of OPCs, which controls the generation of myelinating oligodendrocytes.

Overall, my thesis work shows that a given CSP can control various aspects of synapse formation and function between neurons while playing roles in other aspects of brain development, such as defining the functional diversity of non-neuronal cells. Whether these CSPs trigger their canonical pathways, or they function through other non-canonical mechanisms in different contexts of development should be further investigated.

2. **What are the underlying mechanisms of c-KIT/SCF interaction in cell-cell connectivity?**

Investigating the role of RTKs in the function and formation of synapses has been a research topic for more than 20 years (Kotecha et al., 2002). Some RTKs have been discovered to indeed play roles at synapses. For example, vascular endothelial growth factor (VEGF) receptors (VEGFR) are members of the Class IV of RTKs (Lemmon and Schlessinger, 2010). Their two homologs in *C. elegans* are VER-1 and -4. Loss of function experiments show the role of these two RTKs in modulation of glutamate signaling in these worms, by regulating the surface level of glutamate receptors on the postsynaptic cell. This regulatory role of VER-1 and -4 depends on their interaction with their ligand, PVF-1, released from muscles (Luth et al., 2021). PDGFRβ is another RTK belonging to the same Class as c-KIT (Class III) (Lemmon and Schlessinger, 2010). PDGFRβ in CA1 neurons in the hippocampus are transactivated by dopaminergic receptors (D2/D4) on the same neurons upon application of dopamine,

triggering calmodulin- and Ca^{2+}-dependent cascades that inactivate NMDAR and inhibit LTP (Kotecha et al., 2002). These studies show the role of RTKs in synaptic transmission, but their function in synaptic formation remains unanswered.

SCF has three isoforms, two membrane-bound and one soluble (Figure 9). The two membrane-bound isoforms of SCF are the results of alternative splicing. One of these two isoforms can be cleaved to generate soluble SCF, while the other one stays as membrane SCF (Lennartsson and Rönnstrand, 2012). Both membrane and soluble SCF can bind and activate their receptor, c-KIT, by interacting with its extracellular domain, but they trigger distinct downstream signaling pathways inside the cell (Cardoso et al., 2014). For example, membrane SCF/c-KIT interaction triggers cell proliferation via extracellular signal-regulated kinase (ERK) in erythroid progenitors, while soluble SCF/c-KIT works through p38 (Kapur et al., 2002). In addition to the signaling pathway, the time of binding and activity of c-KIT is different based on attachment to soluble or membrane SCF. Soluble SCF/c-KIT has shorter activation and faster degradation, while membrane SCF activates c-KIT for its whole life-time (Cardoso et al., 2014). Our results show the localization of c-KIT in both excitatory synapses and axons coming from IONs and inhibitory ones coming from MLIs. Since we did not have access to a SCF antibody to localize the c-KIT ligand and identify its isoform via immunolabeling and western blot, respectively, we do not know the nature of the interaction of SCF/c-KIT: whether it is membrane or soluble SCF, the duration of receptor activation and degradation, and the downstream signaling mechanisms. More experiments are required to answer these questions. There are several potential scenarios for c-KIT/SCF interaction in this system: 1) If only membrane SCF is synthetized by PCs, not only the longer activation of c-KIT (its tyrosine kinase activity), but also the physical attachment of membrane SCF/c-KIT is involved in the connectivity of MLIs / CFs to PCs. For example, in the xenopus embryonic epidermis, c-KIT expressed by multiciliated cells interacts with membrane SCF expressed by outer-layer cells to act as an adhesive between these two types of cells, while its interaction with soluble SCF leads to the next scenario (#2) (Chuyen et al., 2021). 2) If soluble SCF is released from PCs with repulsive effect on c-KIT-expressing cells. In this scenario, c-KIT^+ afferents should avoid contacting SCF^+ PCs, and removal of c-KIT would probably increase their contacts on PCs. For example, in the case of xenopus embryonic epidermis, soluble SCF released from outer-layer cells triggers a signaling cascade via c-KIT on the surface of multiciliated cells which results in their repulsion (Chuyen et al., 2021). 3) If soluble SCF is released from PCs to attract or stabilize c-KIT expressing afferents. In this scenario, SCF triggers downstream signaling mechanisms of c-KIT that ends in attraction and guidance of the afferents toward the PCs. Similar to the previous scenario, since there is no physical attachment of SCF to the membrane, this scenario is fully tyrosine kinase-dependent. For

example, the role of c-KIT/SCF interaction has been shown recently in the maintenance of sensory innervation of the skin of zebrafish larvae. In the zebrafish larvae, *kitb*, one of the two paralogues of c-KIT in this species, is expressed specifically in Rohon–Beard (RBs) neurons innervating the trunk skin during larval stage. During the same stage at the trunk, *kitlb*, one of the two paralogues of SCF, is expressed by the epithelial cells of the two layers of the skin. Knockout of *kitb* in RBs or inhibiting its kinase activity using specific multikinase inhibitors (e.g. Sorafenib, Ponatinib, or Dasatinib) causes retraction of axon terminal and loss of axonal density in the skin of zebrafish larvae, but not axonal growth and arborization, showing the role of *kitb* in stabilization of axonal innervation. Injecting *kitb* mRNA into *kitb* mutant larvae rescues the phenotype of loss of axonal cutaneous innervation. Overexpression of *kitlb* in some of skin cells increases the axonal innervation highly localized around the overexpressing cells. The effect of *kitb* is executed via one of its downstream targets, Src family kinases (SFKs). Inhibiting the activity of SFKs or preventing their interaction with *kitb* reproduces the loss of axonal cutaneous innervation phenotype (Tuttle et al., 2022). Even though, the nature of *kitlb* (soluble or membrane) in the skin of zebra fish larvae is not identified, its effect is mainly via the tyrosine kinase activity of *kitb*, as expression of mutant *kitb* unable to interact and phosphorylate SFKs results in retraction of axonal terminals from the skin (Tuttle et al., 2022). This is an example where the tyrosine kinase activity of c-KIT function as stabilizer of cell-cell contacts. 4) If SCF or c-KIT can bind to other cell surface proteins (non-canonical interaction). Recently, a new ligand with high affinity was identified for c-KIT in the endothelial cells of the adult mammalian heart, called monocyte- and macrophage-derived cytokine meteorin-like (METRNL) (Reboll et al., 2022). Both in vitro and in vivo studies show that secreted METRNL binds to c-KIT expressed by endothelial cells to induce their proliferation after ischemia. Loss of function of METRNL in mouse stops c-KIT-dependent angiogenesis after myocardial infarction, and causes severe heart failure (Reboll et al., 2022). METRNL is expressed at low levels in a subpopulation of several types of cells in the cerebellum, including PCs, MLIs, and astrocytes, based on single-cell transcriptomics data obtained from adult mice (Kozareva et al., 2021). During development, its expression is exclusively restricted to the floor plate, and from E13.5 to the inner ear and dorsal root ganglions (Zheng et al., 2016). In the nervous system, METRNL has neurotrophic activity inducing neuronal survival in vivo and neuroblast migration and neurite outgrowth in vitro. It is homologous to the neurotrophin METRN protein which is highly expressed in BGs in the adult cerebellum (Zheng et al., 2016). There is no data showing if METRN, similar to METRNL, could bind to c-KIT. In addition to this question, we do not know if METRNL can interact with SCF as well, or if its release in the cortex of the cerebellum can interfere with the interaction between c-KIT and SCF. Nevertheless, the expression of METRN or METRNL is not restricted to PCs, suggesting a more general role than only controlling neuronal connectivity or axon growth of both MLIs and CFs.

There are still some questions left regarding the c-KIT/SCF interaction during the development of the cerebellar cortex circuitry. What happens if SCF is conditionally removed from PCs in the olivocerebellar circuit? Do we reproduce the same phenotype as the conditional knockout of *c-Kit* in MLIs by *Pvalb*$^{ires\text{-}Cre}$ mouse? To answer this question, and generally investigate the role of SCF in connectivity between MLIs/CFs to PCs, we are crossing a *L7(Pcp2)*$^{ires\text{-}Cre}$ (a PC-specific CRE mouse model) with *Scf* $^{fl/fl}$ mice (Ding et al., 2012) to specifically remove SCF from PCs. The primary characterization of the offspring of this breeding shows loss of *Scf* mRNA from cerebellar extracts at P28. We need to investigate when the loss of *Scf* starts in the cerebellar extracts to be able to compare the results with the loss of function of c-KIT in MLIs. Since we do not have access to a SCF antibody to characterize the conditional knockout at the protein level, and no data is available about the half-life of SCF in neurons, specifically in PCs, we do not know when the loss of *Scf* mRNA will result in loss of SCF at the protein level. The other strategy is to inject Cre-expressing AAVs with a serotype/promoter compatible with PCs into the cerebellar cortex as early as possible during postnatal development (e.g. P0) to remove SCF during this period.

3. **Is c-KIT/SCF interaction involved in topographical organization of the olivocerebellar circuit?**

The topographical organization of the olivocerebellar circuit develops postnatally in the mouse. At birth, a crude map is established between CFs and PCs which is refined in the following three weeks into a very precise topographical pattern defined by distinct AldC^{+}/PLCβ4^{-} zones/stripes or vice versa with sharp boundaries (Reeber et al., 2013). Some of the underlying mechanisms involved in this complex process have been identified. For example, expression of Eph-A receptors in some IONs that project to PCs which express ephrinA ligands, defines the distinct zones that match with olivocerebellar modules in chicken (Nishida et al., 2002). Misexpression of Eph-A receptors in IONs prevents the growth of CFs in a region-specific manner and disrupts the olivocerebellar topography (Nishida et al., 2002). Even though the underlying mechanism of Eph-A receptors/ephrinA ligands interaction in the establishment of topographical organization in olivocerebellar circuit is unknown, several hypothetical models have been suggested (Nishida et al., 2002). PC neurotransmission has been shown to modulate the molecular pattern of cerebellar modules as well (White et al., 2014b). Loss of function of the vesicular GABA transporter (VGAT) specifically in PCs during development of the olivocerebellar circuit, which stops the GABA transmission by PCs, changes the boundaries of expression of AldC, PLCβ4, and some other markers of cerebellar zones, inferring an alteration in the topographical organization (White et al., 2014a). In accord with these changes in modular patterning, silencing PC neurotransmission also alters the

topographical organization of basket cells based on the size of their pinceaux (Zhou et al., 2020a). In control conditions, the size of the pinceaux of basket cells innervating AldC^{-}/PLCβ4^{+} PCs is bigger than the ones innervating AldC^{+}/PLCβ4^{-} PCs (Zhou et al., 2020b). These two examples show that both genetically defined mechanisms as well as activity-related ones are involved in the establishment of olivocerebellar map.

Our results show that c-KIT and SCF are differentially expressed in IONs and PCs, respectively, during postnatal development and adulthood. The question raised here is the role of c-KIT expressed by IONs and localized on CFs in topographical formation of olivocerebellar circuit during postnatal development? To answer this question, the *C1ql1*^{cre} knockin mouse model used to target *C1ql1*-expressing OPCs was crossed with the floxed *c-Kit* (*c-Kit* ^{fl}) mice used to knockout *c-Kit* in MLIs. Single cell transcriptomic data from adult mouse cerebellum shows none of the cerebellar neuronal or glial cell types express both of *C1ql1* and *c-Kit* together (Kozareva et al., 2021), thus *C1ql1*^{cre}*; c-Kit* $^{fl/fl}$ enable the study of *c-Kit* loss of function specifically in IONs. The characterization of this cross shows that the loss of function of c-KIT does not happen before P40, much after the refinement of the olivocerebellar map. Due to this reason, the development of a viral strategy similar to the one developed in the lab to target IONs using retrograde AAVs (Figure 3 of Results Part 2: Specific targeting of inferior olivary neurons combining *C1ql1*^{Cre} mouse and recombinant AAV strategy) is ongoing to knockout *c-Kit* specifically in IONs during the first postnatal week, and evaluate its effect on the expression pattern of AldC and PLCβ4 in PCs.

The map of ION projections to AldC-defined zones in the cerebellar cortex of adult rats has been identified at the IO subnuclear level using labeling of CFs with biotinylated dextran injected into various small regions in all the IO nuclei (Sugihara and Shinoda, 2004). Based on this map, IO nuclei are divided into five groups whose projection targets are represented in all the stripes/zones and lobules of the cerebellar cortex (Sugihara and Shinoda, 2004). Our results show that some IO nuclei express c-KIT stronger than the others. Combining Sugihara's olivocerebellar map (Sugihara and Shinoda, 2004) and mapping c-KIT expression by IONs or MLIs, we can see whether there is a correlation between the IO subnuclei and the cerebellar cortical zones whose MLIs express c-KIT differentially. These results will help us to better understand the role of c-KIT in olivocerebellar topography.

4. **What is the potential role of C1QL1 in OPCs development?**

C1QL1 is a secreted protein which plays role in the formation and maintenance of the excitatory synapses between neurons (Bolliger et al., 2011; Kakegawa et al., 2015; Sigoillot et al., 2015). Recently, other functions in health and malignancies inside and outside of the brain have been discovered for C1QL1. For example, C1QL1 is involved in proliferation of some tumor cells (Gao et al., 2021; X. Wang et al., 2021) as well as inhibition of granulosa cells apoptosis in the mouse ovaries (Lu et al., 2022). Our results show that ablation of *C1ql1*$^{+}$ OPCs leads to the lack of oligodendrocytes and subsequently hypomyelination. No phenotype was observed in the constitutive KO of *C1ql1* in the myelination and number of OPCs in the forebrain. To identify the role of *C1ql1* in OPCs, I plan to overexpress *C1ql1* in rat cultured OPCs (in collaboration with the lab of Lamia Bouslama, Institut du cerveau, Paris). We will measure the proliferation and differentiation of OPCs 3 days after transduction with lentiviral particles expressing *C1ql1* and GFP under the PGK promoter (Sigoillot et al., 2015) by performing immunolabeling for GFP, OLIG2 (a marker of oligodendrocyte lineage cells) and BM28 (a marker for proliferation) or MBP (a marker for oligodendrocytes). In parallel and in collaboration with the same team, we plan to study the cellular and molecular mechanisms of *C1ql1*$^{+}$ vs *C1ql1*$^{-}$ OPCs in an ex vivo model of myelination developed by our collaborators (Baudouin et al., 2021). In this model, GFP^{+} NG2^{+} and GFP^{-} NG2^{+} cells from young C1ql1^{Cre}; R26$^{Cas9\text{-}GFP}$ mice are sorted by FACS and seeded separately on the organotypic cerebellar slices deprived of endogenous OLs. Proliferation, differentiation and myelination rate of these two subpopulations of OPCs are measured in this model (Baudouin et al., 2021).

5. C1QL1 and c-KIT signaling pathways: cell surface molecules at the crossroads between neuronal synaptogenesis and brain tumorigenesis?

A vast variety of neuronal populations need to be precisely connected through synapses that are formed via trans-synaptic adhesion and molecular signaling. Neurons are also in close contact and interact with glial cells such as astrocytes, OPCs and oligodendrocytes that are often at the origin of gliomas. Brain tumors can either be primary, such as gliomas or medulloblastomas, or secondary via invasion of metastasis and growth of a tumor in a favorable environment of the brain. Misregulation of molecular pathways that regulate normal brain development and connectivity contributes to tumorigenesis, such as the SHH/NOTCH pathway in medulloblastoma (Cordeiro et al., 2014), or cadherins and protocadherins (Cao et al., 2019). Recently, the role of neuronal activity in promoting tumor growth, in particular gliomas, through the shedding of the extracellular domain of a synaptic molecule, neuroligin-3, has been demonstrated (Venkatesh et al., 2017, 2015). Furthermore, increased neuronal activity results in the synthesis of numerous synaptic proteins in gliomas

(Venkatesh et al., 2017). Thus, understanding the molecular pathways that are at the crossroads between neuronal synaptogenesis and brain tumorigenesis is important both for our fundamental understanding of how brain tumors arise and invade the brain, but also in terms of treatment design, since perturbations of these signaling pathways could have secondary effects on brain development and function.

In this context, the c-KIT/SCF signaling pathway is particularly interesting. *c-Kit* mutations are found in different types of cancers and tumors, and components of the *c-KIT* signaling pathway have been popular targets for cancer research (Stankov et al., 2014). For example, sorafenib, ponatinib, imatinib and axitinib are tyrosine kinase inhibitors used for the treatment of KIT positive cancers (Liu et al., 2019; Tuttle et al., 2022). One of the side effects of chemotherapy with kinase inhibitors is axon degeneration (Tuttle et al., 2022). It is thus extremely important to understand the potential role of c-KIT in normal brain development, in particular in circuit formation, and study the role of tyrosine kinase inhibitor treatment on brain development and function. Our results regarding the effect of c-KIT loss of function in the olivocerebellar circuit formation and function warrants the study of the potential side effects of cancer treatment with tyrosine kinase inhibitors. In this perspective, we plan to chronically inject the imatinib (100 mg/kg/day; (Kovács-öller et al., 2020)) in the cerebellum at different stages of circuit development and in the mature mouse. We will assess the connectivity between IONs and inhibitory neurons with their target PCs both using morphological analyses and functional assessment of synaptic transmission using patch-clamp recordings of PC responses. Another strategy is to apply the inhibitor on cultured mouse olivocerebellar (hindbrain) explants whose development has been well characterized (Letellier et al., 2009).

The second cell surface pathway involves the interaction between the secreted protein C1QL1 and the adhesion-GPCR BAI3 (Lanoue et al., 2013; Sigoillot et al., 2015). Several lines of evidence suggest that C1QL1 might contribute to various types of cancers and might be a therapeutic target. C1QL1 is upregulated in colorectal cancer, one of the most common malignant cancers (Qiu et al., 2018), differentiated thyroid carcinoma (Celestino et al., 2018), as well as lung adenocarcinoma (Gao et al., 2021). RNA-seq analyses have shown that C1QL1 has higher expression in glioblastoma compared to the normal brain (X. Wang et al., 2021). In the case of lung adenocarcinoma cells, C1QL1 promotes colony formation and migration (Gao et al., 2021). Overexpression of C1QL1 in a model of glioblastoma promotes the formation of colony by neural stem cells in vitro, and accelerates the formation of malignant tumors in vivo (X. Wang et al., 2021). C1QL1 is a ligand for the BAI3 receptor, a member of the adhesion-GPCR BAI family mostly expressed in the central nervous system (Bolliger et al., 2011). All three BAI members are overexpressed in gliomas in comparison with other cancers (TGCA data set). Misregulation of their expression is also observed in different types

of tumors outside of the nervous system (e.g. ovarian, breast, and lung cancers). For example, misregulation of BAI1 and BAI3 expression and methylation is observed in one of the most invasive subtypes of lung adenocarcinoma (Jin et al., 2016; Zhang et al., 2021; Zohrabian et al., 2007). BAI2 & 3 expression is also decreased in malignant gliomas and are suggested as the prognostic markers of high-grade glioma (Kee et al., 2004). Expression of BAI1 reduces tumor vascularization and tumor growth in several cancer models (reviewed by (Nair et al., 2021)). The C1QL1/BAI3 signaling pathway might also be particularly relevant for pediatric brain cancers. Based on single-cell RNA-seq data, the percentage of expressing cells and mean scaled expression of C1QL1 & C1QL4 are increased in pediatric glioblastoma in comparison with adult ones (Neftel et al., 2019). Our results (in Part 3) show that *C1ql1* expression defines a subpopulation of OPCs that contributes to differentiation of myelinating OLs. OPCs (as well as neural stem cells) are considered at the origin of glioblastoma (GBM) (Lei et al., 2011; Loras et al., 2023). The proliferation and migration of OPCs is regulated by neuronal activity (Hide and Komohara, 2020; Mangin et al., 2012). Similar to OPCs, GBM cells express glutamatergic receptors whose activation leads to the proliferation and migration of GBM cells (Hide and Komohara, 2020). Interaction between OPCs and GBM cells at the border of GBM tumors can support proliferation and migration of the tumor cells (Hide and Komohara, 2020). It is thus important to identify the potential role of *C1ql1* expression in OPCs in the development of different primary brain tumors, including glioblastoma. In this regard, we have started a collaboration with the team of Giorgio Seano (Institut Curie, Orsay), to determine the effect of C1QL1 released from OPCs on the development of glioblastoma. Our preliminary analysis using RT-qPCR on four glioblastoma cell lines, GL261, CT2A, mGB1 and mGB2, shows the expression of both *C1ql1* and *Bai3* in mGB1 and mGB2, while GL261 expresses only *C1ql1*, and CT2A does not express these genes. mGB2 is more aggressive and has lower survival rate than mGB1 (Costa et al., 2021). To test whether interaction with C1QL1 from the host brain might modulate tumor growth and invasion, we injected mGB2 cells in one of the hemispheres of *C1ql1* constitutive knockout or control mice. We are measuring the survival rate, as well as the growth of the tumor as the indicators for the effect of absence or presence of C1QL1 in the microenvironment on aggressivity of glioblastoma.

Bibliography

Aflalo, T.N., Graziano, M.S.A., 2006. Possible Origins of the Complex Topographic Organization of Motor Cortex: Reduction of a Multidimensional Space onto a Two-Dimensional Array. J. Neurosci. 26, 6288–6297. https://doi.org/10.1523/JNEUROSCI.0768-06.2006

Akay, L.A., Effenberger, A.H., Tsai, L.-H., 2021. Cell of all trades: oligodendrocyte precursor cells in synaptic, vascular, and immune function. Genes Dev. 35, 180–198. https://doi.org/10.1101/gad.344218.120

Amat, S.B., Rowan, M.J.M., Gaffield, M.A., Bonnan, A., Kikuchi, C., Taniguchi, H., Christie, J.M., 2017. Using c-kit to genetically target cerebellar molecular layer interneurons in adult mice. PLoS ONE 12, e0179347. https://doi.org/10.1371/journal.pone.0179347

Andrusaite, A., Milling, S., 2020. Should we be more cre-tical? A cautionary tale of recombination. Immunology 159, 131–132. https://doi.org/10.1111/imm.13170

Ango, F., Gallo, N.B., Van Aelst, L., 2021. Molecular mechanisms of axo-axonic innervation. Curr. Opin. Neurobiol. 69, 105–112. https://doi.org/10.1016/j.conb.2021.03.002

Arakawa, H., Erzurumlu, R.S., 2015. Role of whiskers in sensorimotor development of C57BL/6 mice. Behav. Brain Res. 287, 146–155. https://doi.org/10.1016/j.bbr.2015.03.040

Auguste, Y.S.S., Ferro, A., Kahng, J.A., Xavier, A.M., Dixon, J.R., Vrudhula, U., Nichitiu, A.-S., Rosado, D., Wee, T.-L., Pedmale, U.V., Cheadle, L., 2022. Oligodendrocyte precursor cells engulf synapses during circuit remodeling in mice. Nat. Neurosci. 25, 1273–1278. https://doi.org/10.1038/s41593-022-01170-x

Barres, B.A., Raff, M.C., 1994. Control of oligodendrocyte number in the developing rat optic nerve. Neuron 12, 935–942. https://doi.org/10.1016/0896-6273(94)90305-0

Baudouin, L., Adès, N., Kanté, K., Czarnecki, A., Bachelin, C., Baskaran, A., Langui, D., Millécamps, A., Gurchenkov, B., Velut, Y., Duarte, K., Barnier, J.-V., Nait Oumesmar, B., Bouslama-Oueghlani, L., 2021. Co-culture of exogenous oligodendrocytes with unmyelinated cerebella: Revisiting ex vivo models and new tools to study myelination. Glia 69, 1916–1931. https://doi.org/10.1002/glia.24001

Bausch-Fluck, D., Milani, E.S., Wollscheid, B., 2019. Surfaceome nanoscale organization and extracellular interaction networks. Curr. Opin. Chem. Biol., Omics 48, 26–33. https://doi.org/10.1016/j.cbpa.2018.09.020

Baxi, E.G., DeBruin, J., Jin, J., Strasburger, H.J., Smith, M.D., Orthmann-Murphy, J.L., Schott, J.T., Fairchild, A.N., Bergles, D.E., Calabresi, P.A., 2017. Lineage tracing reveals dynamic changes in oligodendrocyte precursor cells following cuprizone-induced demyelination. Glia 65, 2087–2098. https://doi.org/10.1002/glia.23229

Beiter, R.M., Rivet-Noor, C., Merchak, A.R., Bai, R., Johanson, D.M., Slogar, E., Sol-Church, K., Overall, C.C., Gaultier, A., 2022. Evidence for oligodendrocyte progenitor cell

heterogeneity in the adult mouse brain. Sci. Rep. 12, 12921. https://doi.org/10.1038/s41598-022-17081-7

Bergles, D.E., Richardson, W.D., 2016. Oligodendrocyte Development and Plasticity. Cold Spring Harb. Perspect. Biol. 8, a020453. https://doi.org/10.1101/cshperspect.a020453

Bergles, D.E., Roberts, J.D.B., Somogyi, P., Jahr, C.E., 2000. Glutamatergic synapses on oligodendrocyte precursor cells in the hippocampus. Nature 405, 187–191. https://doi.org/10.1038/35012083

Birey, F., Kloc, M., Chavali, M., Hussein, I., Wilson, M., Christoffel, D.J., Chen, T., Frohman, M.A., Robinson, J.K., Russo, S.J., Maffei, A., Aguirre, A., 2015. Genetic and Stress-Induced Loss of NG2 Glia Triggers Emergence of Depressive-like Behaviors through Reduced Secretion of FGF2. Neuron 88, 941–956. https://doi.org/10.1016/j.neuron.2015.10.046

Boda, E., Lorenzati, M., Parolisi, R., Harding, B., Pallavicini, G., Bonfanti, L., Moccia, A., Bielas, S., Di Cunto, F., Buffo, A., 2022. Molecular and functional heterogeneity in dorsal and ventral oligodendrocyte progenitor cells of the mouse forebrain in response to DNA damage. Nat. Commun. 13, 2331. https://doi.org/10.1038/s41467-022-30010-6

Bolliger, M.F., Martinelli, D.C., Südhof, T.C., 2011. The cell-adhesion G protein-coupled receptor BAI3 is a high-affinity receptor for C1q-like proteins. Proc. Natl. Acad. Sci. U. S. A. 108, 2534–2539. https://doi.org/10.1073/pnas.1019577108

Boucard, A.A., Maxeiner, S., Südhof, T.C., 2014. Latrophilins Function as Heterophilic Cell-adhesion Molecules by Binding to Teneurins. J. Biol. Chem. 289, 387–402. https://doi.org/10.1074/jbc.M113.504779

Buchanan, J., Elabbady, L., Collman, F., Jorstad, N.L., Bakken, T.E., Ott, C., Glatzer, J., Bleckert, A.A., Bodor, A.L., Brittan, D., Bumbarger, D.J., Mahalingam, G., Seshamani, S., Schneider-Mizell, C., Takeno, M.M., Torres, R., Yin, W., Hodge, R.D., Castro, M., Dorkenwald, S., Ih, D., Jordan, C.S., Kemnitz, N., Lee, K., Lu, R., Macrina, T., Mu, S., Popovych, S., Silversmith, W.M., Tartavull, I., Turner, N.L., Wilson, A.M., Wong, W., Wu, J., Zlateski, A., Zung, J., Lippincott-Schwartz, J., Lein, E.S., Seung, H.S., Bergles, D.E., Reid, R.C., Costa, N.M. da, 2021. Oligodendrocyte precursor cells prune axons in the mouse neocortex. https://doi.org/10.1101/2021.05.29.446047

Cadilhac, C., Bachy, I., Forget, A., Hodson, D.J., Jahannault-Talignani, C., Furley, A.J., Ayrault, O., Mollard, P., Sotelo, C., Ango, F., 2021. Excitatory granule neuron precursors orchestrate laminar localization and differentiation of cerebellar inhibitory interneuron subtypes. Cell Rep. 34. https://doi.org/10.1016/j.celrep.2021.108904

Calver, A.R., Hall, A.C., Yu, W.-P., Walsh, F.S., Heath, J.K., Betsholtz, C., Richardson, W.D., 1998. Oligodendrocyte Population Dynamics and the Role of PDGF In Vivo. Neuron 20, 869–882. https://doi.org/10.1016/S0896-6273(00)80469-9

Cao, Z.-Q., Wang, Z., Leng, P., 2019. Aberrant N-cadherin expression in cancer. Biomed. Pharmacother. 118, 109320. https://doi.org/10.1016/j.biopha.2019.109320

Cardoso, H.J., Figueira, M.I., Correia, S., Vaz, C.V., Socorro, S., 2014. The SCF/c-KIT system in the male: Survival strategies in fertility and cancer. Mol. Reprod. Dev. 81, 1064–1079. https://doi.org/10.1002/mrd.22430

Celestino, R., Nome, T., Pestana, A., Hoff, A.M., Gonçalves, A.P., Pereira, L., Cavadas, B., Eloy, C., Bjøro, T., Sobrinho-Simões, M., Skotheim, R.I., Soares, P., 2018. CRABP1, C1QL1 and LCN2 are biomarkers of differentiated thyroid carcinoma, and predict extrathyroidal extension. BMC Cancer 18, 68. https://doi.org/10.1186/s12885-017-3948-3

Cerminara, N.L., Lang, E.J., Sillitoe, R.V., Apps, R., 2015. Redefining the cerebellar cortex as an assembly of non-uniform Purkinje cell microcircuits. Nat. Rev. Neurosci. 16, 79–93. https://doi.org/10.1038/nrn3886

Chaumont, J., Guyon, N., Valera, A.M., Dugué, G.P., Popa, D., Marcaggi, P., Gautheron, V., Reibel-Foisset, S., Dieudonné, S., Stephan, A., Barrot, M., Cassel, J.-C., Dupont, J.-L., Doussau, F., Poulain, B., Selimi, F., Léna, C., Isope, P., 2013. Clusters of cerebellar Purkinje cells control their afferent climbing fiber discharge. Proc. Natl. Acad. Sci. 110, 16223–16228. https://doi.org/10.1073/pnas.1302310110

Chédotal, A., Bloch-Gallego, E., Sotelo, C., 1997. The embryonic cerebellum contains topographic cues that guide developing inferior olivary axons. Development 124, 861–870. https://doi.org/10.1242/dev.124.4.861

Chuyen, A., Rulquin, C., Daian, F., Thomé, V., Clément, R., Kodjabachian, L., Pasini, A., 2021. The Scf/Kit pathway implements self-organized epithelial patterning. Dev. Cell 56, 795-810.e7. https://doi.org/10.1016/j.devcel.2021.02.026

Cioni, J.-M., Telley, L., Saywell, V., Cadilhac, C., Jourdan, C., Huber, A.B., Huang, J.Z., Jahannault-Talignani, C., Ango, F., 2013. SEMA3A Signaling Controls Layer-Specific Interneuron Branching in the Cerebellum. Curr. Biol. 23, 850–861. https://doi.org/10.1016/j.cub.2013.04.007

Cordeiro, B.M., Oliveira, I.D., Alves, M.T. de S., Saba-Silva, N., Capellano, A.M., Cavalheiro, S., Dastoli, P., Toledo, S.R.C., 2014. SHH, WNT, and NOTCH pathways in medulloblastoma: when cancer stem cells maintain self-renewal and differentiation properties. Childs Nerv. Syst. ChNS Off. J. Int. Soc. Pediatr. Neurosurg. 30, 1165–1172. https://doi.org/10.1007/s00381-014-2403-x

Costa, B., Fletcher, M.N.C., Boskovic, P., Ivanova, E.L., Eisemann, T., Lohr, S., Bunse, L., Löwer, M., Burchard, S., Korshunov, A., Coltella, N., Cusimano, M., Naldini, L., Liu, H.-K., Platten, M., Radlwimmer, B., Angel, P., Peterziel, H., 2021. A Set of Cell Lines Derived from a Genetic Murine Glioblastoma Model Recapitulates Molecular and Morphological Characteristics of Human Tumors. Cancers 13, 230. https://doi.org/10.3390/cancers13020230

Dawson, M.R.L., Polito, A., Levine, J.M., Reynolds, R., 2003. NG2-expressing glial progenitor cells: an abundant and widespread population of cycling cells in the adult rat CNS. Mol. Cell. Neurosci. 24, 476–488. https://doi.org/10.1016/S1044-7431(03)00210-0

Dieudonné, S., 2016. Golgi Neurons, in: Gruol, D.L., Koibuchi, N., Manto, M., Molinari, M., Schmahmann, J.D., Shen, Y. (Eds.), Essentials of Cerebellum and Cerebellar Disorders: A Primer For Graduate Students. Springer International Publishing, Cham, pp. 201–205. https://doi.org/10.1007/978-3-319-24551-5_24

Ding, L., Saunders, T.L., Enikolopov, G., Morrison, S.J., 2012. Endothelial and perivascular cells maintain haematopoietic stem cells. Nature 481, 457–462. https://doi.org/10.1038/nature10783

Duan, X., Krishnaswamy, A., De la Huerta, I., Sanes, J.R., 2014. Type II Cadherins Guide Assembly of a Direction-Selective Retinal Circuit. Cell 158, 793–807. https://doi.org/10.1016/j.cell.2014.06.047

Falcão, A.M., van Bruggen, D., Marques, S., Meijer, M., Jäkel, S., Agirre, E., Samudyata, Floriddia, E.M., Vanichkina, D.P., ffrench-Constant, C., Williams, A., Guerreiro-Cacais, A.O., Castelo-Branco, G., 2019. Disease-specific oligodendrocyte lineage cells arise in multiple sclerosis. Nat. Med. 24, 1837–1844. https://doi.org/10.1038/s41591-018-0236-y

Floriddia, E.M., Lourenço, T., Zhang, S., van Bruggen, D., Hilscher, M.M., Kukanja, P., Gonçalves dos Santos, J.P., Altınkök, M., Yokota, C., Llorens-Bobadilla, E., Mulinyawe, S.B., Grãos, M., Sun, L.O., Frisén, J., Nilsson, M., Castelo-Branco, G., 2020. Distinct oligodendrocyte populations have spatial preference and different responses to spinal cord injury. Nat. Commun. 11, 5860. https://doi.org/10.1038/s41467-020-19453-x

Gao, Y.-J., Chen, F., Zhang, L.-J., 2021. C1q-like 1 is frequently up-regulated in lung adenocarcinoma and contributes to the proliferation and invasion of tumor cells. J. Chemother. 33, 476–485. https://doi.org/10.1080/1120009X.2021.1906035

Georgiadis, M., Schroeter, A., Gao, Z., Guizar-Sicairos, M., Liebi, M., Leuze, C., McNab, J.A., Balolia, A., Veraart, J., Ades-Aron, B., Kim, S., Shepherd, T., Lee, C.H., Walczak, P., Chodankar, S., DiGiacomo, P., David, G., Augath, M., Zerbi, V., Sommer, S., Rajkovic, I., Weiss, T., Bunk, O., Yang, L., Zhang, J., Novikov, D.S., Zeineh, M., Fieremans, E., Rudin, M., 2021. Nanostructure-specific X-ray tomography reveals myelin levels,

integrity and axon orientations in mouse and human nervous tissue. Nat. Commun. 12, 2941. https://doi.org/10.1038/s41467-021-22719-7

Ghai, R., Waters, P., Roumenina, L.T., Gadjeva, M., Kojouharova, M.S., Reid, K.B.M., Sim, R.B., Kishore, U., 2007. C1q and its growing family. Immunobiology 212, 253–266. https://doi.org/10.1016/j.imbio.2006.11.001

Giera, S., Luo, R., Ying, Y., Ackerman, S.D., Jeong, S.-J., Stoveken, H.M., Folts, C.J., Welsh, C.A., Tall, G.G., Stevens, B., Monk, K.R., Piao, X., 2018. Microglial transglutaminase-2 drives myelination and myelin repair via GPR56/ADGRG1 in oligodendrocyte precursor cells. eLife 7, e33385. https://doi.org/10.7554/eLife.33385

Gordon, S., Hamann, J., Lin, H.-H., Stacey, M., 2011. F4/80 and the related adhesion-GPCRs. Eur. J. Immunol. 41, 2472–2476. https://doi.org/10.1002/eji.201141715

Grangeray, A., Dorgans, K., Roux, S., Bossu, J.-L., 2016. The Purkinje Cell: As an Integrative Machine, in: Gruol, D.L., Koibuchi, N., Manto, M., Molinari, M., Schmahmann, J.D., Shen, Y. (Eds.), Essentials of Cerebellum and Cerebellar Disorders: A Primer For Graduate Students. Springer International Publishing, Cham, pp. 183–188. https://doi.org/10.1007/978-3-319-24551-5_21

Grimaldi, P., Parras, C., Guillemot, F., Rossi, F., Wassef, M., 2009. Origins and control of the differentiation of inhibitory interneurons and glia in the cerebellum. Dev. Biol. 328, 422–433. https://doi.org/10.1016/j.ydbio.2009.02.008

Guan, H., Shi, T., Liu, M., Wang, X., Guo, F., 2022. C1QL1/CTRP14 Is Largely Dispensable for Atherosclerosis Formation in Apolipoprotein-E-Deficient Mice. J. Cardiovasc. Dev. Dis. 9, 341. https://doi.org/10.3390/jcdd9100341

Guijarro, P., Wang, Y., Ying, Y., Yao, Y., Jieyi, X., Yuan, X., 2013. In vivo knockdown of ckit impairs neuronal migration and axonal extension in the cerebral cortex. Dev. Neurobiol. 73, 871–887. https://doi.org/10.1002/dneu.22107

Guo, F., Maeda, Y., Ma, J., Xu, J., Horiuchi, M., Miers, L., Vaccarino, F., Pleasure, D., 2010. Pyramidal Neurons Are Generated from Oligodendroglial Progenitor Cells in Adult Piriform Cortex. J. Neurosci. 30, 12036–12049. https://doi.org/10.1523/JNEUROSCI.1360-10.2010

Hagemeyer, N., Hanft, K.-M., Akriditou, M.-A., Unger, N., Park, E.S., Stanley, E.R., Staszewski, O., Dimou, L., Prinz, M., 2017. Microglia contribute to normal myelinogenesis and to oligodendrocyte progenitor maintenance during adulthood. Acta Neuropathol. (Berl.) 134, 441–458. https://doi.org/10.1007/s00401-017-1747-1

Hamann, J., Aust, G., Araç, D., Engel, F.B., Formstone, C., Fredriksson, R., Hall, R.A., Harty, B.L., Kirchhoff, C., Knapp, B., Krishnan, A., Liebscher, I., Lin, H.-H., Martinelli, D.C., Monk, K.R., Peeters, M.C., Piao, X., Prömel, S., Schöneberg, T., Schwartz, T.W., Singer, K., Stacey, M., Ushkaryov, Y.A., Vallon, M., Wolfrum, U., Wright, M.W., Xu, L.,

Langenhan, T., Schiöth, H.B., 2015. International Union of Basic and Clinical Pharmacology. XCIV. Adhesion G Protein–Coupled Receptors. Pharmacol. Rev. 67, 338–367. https://doi.org/10.1124/pr.114.009647

Hamann, J., Hsiao, C.-C., Lee, C.S., Ravichandran, K.S., Lin, H.-H., 2016. Adhesion GPCRs as Modulators of Immune Cell Function, in: Langenhan, T., Schöneberg, T. (Eds.), Adhesion G Protein-Coupled Receptors: Molecular, Physiological and Pharmacological Principles in Health and Disease, Handbook of Experimental Pharmacology. Springer International Publishing, Cham, pp. 329–350. https://doi.org/10.1007/978-3-319-41523-9_15

Hamann, J., Koning, N., Pouwels, W., Ulfman, L.H., van Eijk, M., Stacey, M., Lin, H.-H., Gordon, S., Kwakkenbos, M.J., 2007. EMR1, the human homolog of F4/80, is an eosinophil-specific receptor. Eur. J. Immunol. 37, 2797–2802. https://doi.org/10.1002/eji.200737553

Hamann, J., Vogel, B., van Schijndel, G.M., van Lier, R.A., 1996. The seven-span transmembrane receptor CD97 has a cellular ligand (CD55, DAF). J. Exp. Med. 184, 1185–1189. https://doi.org/10.1084/jem.184.3.1185

Hamoud, N., Tran, V., Aimi, T., Kakegawa, W., Lahaie, S., Thibault, M.-P., Pelletier, A., Wong, G.W., Kim, I.-S., Kania, A., Yuzaki, M., Bouvier, M., Côté, J.-F., 2018. Spatiotemporal regulation of the GPCR activity of BAI3 by C1qL4 and Stabilin-2 controls myoblast fusion. Nat. Commun. 9, 4470. https://doi.org/10.1038/s41467-018-06897-5

Hashimoto, K., Watanabe, M., Kano, M., 2016. Synaptogenesis and Synapse Elimination in Developing Cerebellum, in: Gruol, D.L., Koibuchi, N., Manto, M., Molinari, M., Schmahmann, J.D., Shen, Y. (Eds.), Essentials of Cerebellum and Cerebellar Disorders: A Primer For Graduate Students. Springer International Publishing, Cham, pp. 161–165. https://doi.org/10.1007/978-3-319-24551-5_18

Hashimoto, R., Hori, K., Owa, T., Miyashita, S., Dewa, K., Masuyama, N., Sakai, K., Hayase, Y., Seto, Y., Inoue, Y.U., Inoue, T., Ichinohe, N., Kawaguchi, Y., Akiyama, H., Koizumi, S., Hoshino, M., 2016. Origins of oligodendrocytes in the cerebellum, whose development is controlled by the transcription factor, Sox9. Mech. Dev. 140, 25–40. https://doi.org/10.1016/j.mod.2016.02.004

Heiman, M., Schaefer, A., Gong, S., Peterson, J.D., Day, M., Ramsey, K.E., Suárez-Fariñas, M., Schwarz, C., Stephan, D.A., Surmeier, D.J., Greengard, P., Heintz, N., 2008. A Translational Profiling Approach for the Molecular Characterization of CNS Cell Types. Cell 135, 738–748. https://doi.org/10.1016/j.cell.2008.10.028

Hide, T., Komohara, Y., 2020. Oligodendrocyte Progenitor Cells in the Tumor Microenvironment. Adv. Exp. Med. Biol. 1234, 107–122. https://doi.org/10.1007/978-3-030-37184-5_8

Hill, R.A., Nishiyama, A., 2014. NG2 cells (polydendrocytes): Listeners to the neural network with diverse properties. Glia 62, 1195–1210. https://doi.org/10.1002/glia.22664

Hippenmeyer, S., Vrieseling, E., Sigrist, M., Portmann, T., Laengle, C., Ladle, D.R., Arber, S., 2005. A Developmental Switch in the Response of DRG Neurons to ETS Transcription Factor Signaling. PLoS Biol. 3, e159. https://doi.org/10.1371/journal.pbio.0030159

Hirono, M., 2016. Lugaro Cells, in: Gruol, D.L., Koibuchi, N., Manto, M., Molinari, M., Schmahmann, J.D., Shen, Y. (Eds.), Essentials of Cerebellum and Cerebellar Disorders: A Primer For Graduate Students. Springer International Publishing, Cham, pp. 207–211. https://doi.org/10.1007/978-3-319-24551-5_25

Hirota, S., Ito, A., Morii, E., Wanaka, A., Tohyama, M., Kitamura, Y., Nomura, S., 1992. Localization of mRNA for c-kit receptor and its ligand in the brain of adult rats: an analysis using in situ hybridization histochemistry. Mol. Brain Res. 15, 47–54. https://doi.org/10.1016/0169-328X(92)90150-A

Hoshino, M., 2016. Specification of Cerebellar Neurons, in: Gruol, D.L., Koibuchi, N., Manto, M., Molinari, M., Schmahmann, J.D., Shen, Y. (Eds.), Essentials of Cerebellum and Cerebellar Disorders: A Primer For Graduate Students. Springer International Publishing, Cham, pp. 143–147. https://doi.org/10.1007/978-3-319-24551-5_15

Huang, E., Nocka, K., Beier, D.R., Chu, T.Y., Buck, J., Lahm, H.W., Wellner, D., Leder, P., Besmer, P., 1990. The hematopoietic growth factor KL is encoded by the Sl locus and is the ligand of the c-kit receptor, the gene product of the W locus. Cell 63, 225–233. https://doi.org/10.1016/0092-8674(90)90303-v

Hughes, E.G., Kang, S.H., Fukaya, M., Bergles, D.E., 2013. Oligodendrocyte progenitors balance growth with self-repulsion to achieve homeostasis in the adult brain. Nat. Neurosci. 16, 668–676. https://doi.org/10.1038/nn.3390

Iannarelli, P., 2017. Oligodendrocyte Population Dynamics and Plasticity Probed by Genetic Manipulation in Mice (Doctoral). Dr. Thesis UCL Univ. Coll. Lond. UCL (University College London).

Iijima, T., Miura, E., Watanabe, M., Yuzaki, M., 2010. Distinct expression of C1q-like family mRNAs in mouse brain and biochemical characterization of their encoded proteins. Eur. J. Neurosci. 31, 1606–1615. https://doi.org/10.1111/j.1460-9568.2010.07202.x

Jin, K., Mao, X.O., Sun, Y., Xie, L., Greenberg, D.A., 2002. Stem cell factor stimulates neurogenesis in vitro and in vivo. J. Clin. Invest. 110, 311–319. https://doi.org/10.1172/JCI15251

Jin, X., Liu, X., Li, X., Guan, Y., 2016. Integrated Analysis of DNA Methylation and mRNA Expression Profiles Data to Identify Key Genes in Lung Adenocarcinoma. BioMed Res. Int. 2016, 4369431. https://doi.org/10.1155/2016/4369431

Kakegawa, W., Mitakidis, N., Miura, E., Abe, M., Matsuda, K., Takeo, Y.H., Kohda, K., Motohashi, J., Takahashi, A., Nagao, S., Muramatsu, S., Watanabe, M., Sakimura, K., Aricescu, A.R., Yuzaki, M., 2015. Anterograde C1ql1 Signaling Is Required in Order to Determine and Maintain a Single-Winner Climbing Fiber in the Mouse Cerebellum. Neuron 85, 316–329. https://doi.org/10.1016/j.neuron.2014.12.020

Kang, S.H., Fukaya, M., Yang, J.K., Rothstein, J.D., Bergles, D.E., 2010. NG2+ CNS Glial Progenitors Remain Committed to the Oligodendrocyte Lineage in Postnatal Life and following Neurodegeneration. Neuron 68, 668–681. https://doi.org/10.1016/j.neuron.2010.09.009

Kapur, R., Chandra, S., Cooper, R., McCarthy, J., Williams, D.A., 2002. Role of p38 and ERK MAP kinase in proliferation of erythroid progenitors in response to stimulation by soluble and membrane isoforms of stem cell factor. Blood 100, 1287–1293. https://doi.org/10.1182/blood.V100.4.1287.h81602001287_1287_1293

Káradóttir, R., Hamilton, N.B., Bakiri, Y., Attwell, D., 2008. Spiking and nonspiking classes of oligodendrocyte precursor glia in CNS white matter. Nat. Neurosci. 11, 450–456. https://doi.org/10.1038/nn2060

Karpus, O.N., Veninga, H., Hoek, R.M., Flierman, D., van Buul, J.D., Vandenakker, C.C., vanBavel, E., Medof, M.E., van Lier, R.A.W., Reedquist, K.A., Hamann, J., 2013. Shear stress-dependent downregulation of the adhesion-G protein-coupled receptor CD97 on circulating leukocytes upon contact with its ligand CD55. J. Immunol. Baltim. Md 1950 190, 3740–3748. https://doi.org/10.4049/jimmunol.1202192

Katafuchi, T., Li, A.-J., Hirota, S., Kitamura, Y., Hori, T., 2000. Impairment of Spatial Learning and Hippocampal Synaptic Potentiation in c-kit Mutant Rats. Learn. Mem. 7, 383–392.

Kee, H.J., Ahn, K.Y., Choi, K.C., Won Song, J., Heo, T., Jung, S., Kim, J.-K., Bae, C.S., Kim, K.K., 2004. Expression of brain-specific angiogenesis inhibitor 3 (BAI3) in normal brain and implications for BAI3 in ischemia-induced brain angiogenesis and malignant glioma. FEBS Lett. 569, 307–316. https://doi.org/10.1016/j.febslet.2004.06.011

Kessaris, N., Fogarty, M., Iannarelli, P., Grist, M., Wegner, M., Richardson, W.D., 2006. Competing waves of oligodendrocytes in the forebrain and postnatal elimination of an embryonic lineage. Nat. Neurosci. 9, 173–179. https://doi.org/10.1038/nn1620

Kim, D., Im, J. o., Won, Y. j., Yoon, S. y., Lee, E. j., Lee, J. h., Hong, H. n., 2003. Upregulation of c-Kit receptor and stem cell factor in cerebellar inhibitory synapses in response to kainic acid. J. Neurosci. Res. 71, 72–78. https://doi.org/10.1002/jnr.10466

Kim, S.Y., Mo, J.W., Han, S., Choi, S.Y., Han, S.B., Moon, B.H., Rhyu, I.J., Sun, W., Kim, H., 2010. The expression of non-clustered protocadherins in adult rat hippocampal formation and the connecting brain regions. Neuroscience 170, 189–199. https://doi.org/10.1016/j.neuroscience.2010.05.027

Kimura, Y., Ding, B., Imai, N., Nolan, D.J., Butler, J.M., Rafii, S., 2011. c-Kit-Mediated Functional Positioning of Stem Cells to Their Niches Is Essential for Maintenance and Regeneration of Adult Hematopoiesis. PLOS ONE 6, e26918. https://doi.org/10.1371/journal.pone.0026918

Kirby, L., Jin, J., Cardona, J.G., Smith, M.D., Martin, K.A., Wang, J., Strasburger, H., Herbst, L., Alexis, M., Karnell, J., Davidson, T., Dutta, R., Goverman, J., Bergles, D., Calabresi, P.A., 2019. Oligodendrocyte precursor cells present antigen and are cytotoxic targets in inflammatory demyelination. Nat. Commun. 10, 3887. https://doi.org/10.1038/s41467-019-11638-3

Kishore, U., Gaboriaud, C., Waters, P., Shrive, A.K., Greenhough, T.J., Reid, K.B.M., Sim, R.B., Arlaud, G.J., 2004. C1q and tumor necrosis factor superfamily: modularity and versatility. Trends Immunol. 25, 551–561. https://doi.org/10.1016/j.it.2004.08.006

Koh, J.T., Lee, Z.H., Ahn, K.Y., Kim, J.K., Bae, C.S., Kim, H.H., Kee, H.J., Kim, K.K., 2001. Characterization of mouse brain-specific angiogenesis inhibitor 1 (BAI1) and phytanoyl-CoA alpha-hydroxylase-associated protein 1, a novel BAI1-binding protein. Brain Res. Mol. Brain Res. 87, 223–237. https://doi.org/10.1016/s0169-328x(01)00004-3

Kondo, T., Raff, M., 2000. Oligodendrocyte Precursor Cells Reprogrammed to Become Multipotential CNS Stem Cells. Science 289, 1754–1757. https://doi.org/10.1126/science.289.5485.1754

Kotecha, S.A., Oak, J.N., Jackson, M.F., Perez, Y., Orser, B.A., Tol, H.H.M.V., MacDonald, J.F., 2002. A D2 Class Dopamine Receptor Transactivates a Receptor Tyrosine Kinase to Inhibit NMDA Receptor Transmission. Neuron 35, 1111–1122. https://doi.org/10.1016/S0896-6273(02)00859-0

Kovács-öller, T., Ivanova, E., Szarka, G., Tengölics, Á.J., Völgyi, B., Sagdullaev, B.T., 2020. Imatinib sets pericyte mosaic in the retina. Int. J. Mol. Sci. 21, 1–15. https://doi.org/10.3390/ijms21072522

Kozareva, V., Martin, C., Osorno, T., Rudolph, S., Guo, C., Vanderburg, C., Nadaf, N., Regev, A., Regehr, W.G., Macosko, E., 2021. A transcriptomic atlas of mouse cerebellar cortex comprehensively defines cell types. Nature 598, 214–219. https://doi.org/10.1038/s41586-021-03220-z

Lanoue, V., Usardi, A., Sigoillot, S.M., Talleur, M., Iyer, K., Mariani, J., Isope, P., Vodjdani, G., Heintz, N., Selimi, F., 2013. The adhesion-GPCR BAI3, a gene linked to psychiatric disorders, regulates dendrite morphogenesis in neurons. Mol. Psychiatry 18, 943–950. https://doi.org/10.1038/mp.2013.46

LeDoux, M.S., Lorden, J.F., 2002. Abnormal spontaneous and harmaline-stimulated Purkinje cell activity in the awake genetically dystonic rat. Exp. Brain Res. 145, 457–467. https://doi.org/10.1007/s00221-002-1127-4

Lei, L., Sonabend, A.M., Guarnieri, P., Soderquist, C., Ludwig, T., Rosenfeld, S., Bruce, J.N., Canoll, P., 2011. Glioblastoma Models Reveal the Connection between Adult Glial Progenitors and the Proneural Phenotype. PLoS ONE 6, e20041. https://doi.org/10.1371/journal.pone.0020041

Lemmon, M.A., Schlessinger, J., 2010. Cell signaling by receptor-tyrosine kinases. Cell 141, 1117–1134. https://doi.org/10.1016/j.cell.2010.06.011

Lennartsson, J., Rönnstrand, L., 2012. Stem Cell Factor Receptor/c-Kit: From Basic Science to Clinical Implications. Physiol. Rev. 92, 1619–1649. https://doi.org/10.1152/physrev.00046.2011

Letellier, M., Wehrlé, R., Mariani, J., Lohof, A.M., 2009. Synapse elimination in olivo-cerebellar explants occurs during a critical period and leaves an indelible trace in Purkinje cells. Proc. Natl. Acad. Sci. 106, 14102–14107. https://doi.org/10.1073/pnas.0902820106

Leto, K., Hawkes, R., Consalez, G.G., 2016. Cerebellar Neurogenesis, in: Gruol, D.L., Koibuchi, N., Manto, M., Molinari, M., Schmahmann, J.D., Shen, Y. (Eds.), Essentials of Cerebellum and Cerebellar Disorders: A Primer For Graduate Students. Springer International Publishing, Cham, pp. 127–135. https://doi.org/10.1007/978-3-319-24551-5_13

Li, R., Zhang, P., Zhang, M., Yao, Z., 2020. The roles of neuron-NG2 glia synapses in promoting oligodendrocyte development and remyelination. Cell Tissue Res. 381, 43–53. https://doi.org/10.1007/s00441-020-03195-9

Lin, H.-H., Faunce, D.E., Stacey, M., Terajewicz, A., Nakamura, T., Zhang-Hoover, J., Kerley, M., Mucenski, M.L., Gordon, S., Stein-Streilein, J., 2005. The macrophage F4/80 receptor is required for the induction of antigen-specific efferent regulatory T cells in peripheral tolerance. J. Exp. Med. 201, 1615–1625. https://doi.org/10.1084/jem.20042307

Liu, F., Tan, A., Yang, R., Xue, Y., Zhang, M., Chen, L., Xiao, L., Yang, X., Yu, Y., 2017. C1ql1/Ctrp14 and C1ql4/Ctrp11 promote angiogenesis of endothelial cells through activation of ERK1/2 signal pathway. Mol. Cell. Biochem. 424, 57–67. https://doi.org/10.1007/s11010-016-2842-7

Liu, F., Zou, F., Chen, C., Yu, K., Liu, Xiaochuan, Qi, S., Wu, J., Hu, C., Hu, Z., Liu, Juan, Liu, Xuesong, Wang, L., Ge, J., Wang, W., Ren, T., Bai, M., Cai, Y., Xiao, X., Qian, F., Tang, J., Liu, Q., Liu, Jing, 2019. Axitinib overcomes multiple imatinib resistant cKIT mutations including the gatekeeper mutation T670I in gastrointestinal stromal tumors.

Ther. Adv. Med. Oncol. 11, 1758835919849757. https://doi.org/10.1177/1758835919849757

Liu, S.J., Dubois, C.J., 2016. Stellate Cells, in: Gruol, D.L., Koibuchi, N., Manto, M., Molinari, M., Schmahmann, J.D., Shen, Y. (Eds.), Essentials of Cerebellum and Cerebellar Disorders: A Primer For Graduate Students. Springer International Publishing, Cham, pp. 189–193. https://doi.org/10.1007/978-3-319-24551-5_22

Loras, A., Gonzalez-Bonet, L.G., Gutierrez-Arroyo, J.L., Martinez-Cadenas, C., Marques-Torrejon, M.A., 2023. Neural Stem Cells as Potential Glioblastoma Cells of Origin. Life 13, 905. https://doi.org/10.3390/life13040905

Love, S., 2006. Demyelinating diseases. J. Clin. Pathol. 59, 1151–1159. https://doi.org/10.1136/jcp.2005.031195

Lu, X., Ding, F., Chen, Y., Ke, S., Yuan, S., Qiu, H., Xiao, L., Yu, Y., 2022. Deficiency of C1QL1 Reduced Murine Ovarian Follicle Reserve Through Intraovarian and Endocrine Control. Endocrinology 163, bqac048. https://doi.org/10.1210/endocr/bqac048

Luo, Lin, Ambrozkiewicz, M.C., Benseler, F., Chen, C., Dumontier, E., Falkner, S., Furlanis, E., Gomez, A.M., Hoshina, N., Huang, W.-H., Hutchison, M.A., Itoh-Maruoka, Y., Lavery, L.A., Li, W., Maruo, T., Motohashi, J., Pai, E.L.-L., Pelkey, K.A., Pereira, A., Philips, T., Sinclair, J.L., Stogsdill, J.A., Traunmüller, L., Wang, J., Wortel, J., You, W., Abumaria, N., Beier, K.T., Brose, N., Burgess, H.A., Cepko, C.L., Cloutier, J.-F., Eroglu, C., Goebbels, S., Kaeser, P.S., Kay, J.N., Lu, W., Luo, Liqun, Mandai, K., McBain, C.J., Nave, K.-A., Prado, M.A.M., Prado, V.F., Rothstein, J., Rubenstein, J.L.R., Saher, G., Sakimura, K., Sanes, J.R., Scheiffele, P., Takai, Y., Umemori, H., Verhage, M., Yuzaki, M., Zoghbi, H.Y., Kawabe, H., Craig, A.M., 2020. Optimizing Nervous System-Specific Gene Targeting with Cre Driver Lines: Prevalence of Germline Recombination and Influencing Factors. Neuron 106, 37-65.e5. https://doi.org/10.1016/j.neuron.2020.01.008

Luth, E.S., Hodul, M., Rennich, B.J., Riccio, C., Hofer, J., Markoja, K., Juo, P., 2021. VER/VEGF receptors regulate AMPA receptor surface levels and glutamatergic behavior. PLoS Genet. 17, e1009375. https://doi.org/10.1371/journal.pgen.1009375

Mangin, J.-M., Li, P., Scafidi, J., Gallo, V., 2012. Experience-dependent regulation of NG2 progenitors in the developing barrel cortex. Nat. Neurosci. 15, 1192–1194. https://doi.org/10.1038/nn.3190

Marisca, R., Hoche, T., Agirre, E., Hoodless, L.J., Barkey, W., Auer, F., Castelo-Branco, G., Czopka, T., 2020. Functionally distinct subgroups of oligodendrocyte precursor cells integrate neural activity and execute myelin formation. Nat. Neurosci. 23, 363–374. https://doi.org/10.1038/s41593-019-0581-2

Marques, S., Bruggen, D. van, Vanichkina, D.P., Floriddia, E.M., Munguba, H., Väremo, L., Giacomello, S., Falcão, A.M., Meijer, M., Björklund, Å.K., Hjerling-Leffler, J., Taft, R.J., Castelo-Branco, G., 2018. Transcriptional Convergence of Oligodendrocyte Lineage Progenitors during Development. Dev. Cell 46, 504-517.e7. https://doi.org/10.1016/j.devcel.2018.07.005

Marques, S., Zeisel, A., Codeluppi, S., van Bruggen, D., Mendanha Falcão, A., Xiao, L., Li, H., Häring, M., Hochgerner, H., Romanov, R.A., Gyllborg, D., Muñoz Manchado, A., La Manno, G., Lönnerberg, P., Floriddia, E.M., Rezayee, F., Ernfors, P., Arenas, E., Hjerling-Leffler, J., Harkany, T., Richardson, W.D., Linnarsson, S., Castelo-Branco, G., 2016. Oligodendrocyte heterogeneity in the mouse juvenile and adult central nervous system. Science 352, 1326–1329. https://doi.org/10.1126/science.aaf6463

Martina, M., Sekerková, G., 2016. Unipolar Brush Cells, in: Gruol, D.L., Koibuchi, N., Manto, M., Molinari, M., Schmahmann, J.D., Shen, Y. (Eds.), Essentials of Cerebellum and Cerebellar Disorders: A Primer For Graduate Students. Springer International Publishing, Cham, pp. 213–218. https://doi.org/10.1007/978-3-319-24551-5_26

Martinelli, D.C., Chew, K.S., Rohlmann, A., Lum, M.Y., Ressl, S., Hattar, S., Brunger, A.T., Missler, M., Südhof, T.C., 2016. Expression of C1ql3 in Discrete Neuronal Populations Controls Efferent Synapse Numbers and Diverse Behaviors. Neuron 91, 1034–1051. https://doi.org/10.1016/j.neuron.2016.07.002

Mazaheri, F., Breus, O., Durdu, S., Haas, P., Wittbrodt, J., Gilmour, D., Peri, F., 2014. Distinct roles for BAI1 and TIM-4 in the engulfment of dying neurons by microglia. Nat. Commun. 5, 4046. https://doi.org/10.1038/ncomms5046

McLaughlin, T., O'Leary, D.D.M., 2005. Molecular gradients and development of retinotopic maps. Annu. Rev. Neurosci. 28, 327–355. https://doi.org/10.1146/annurev.neuro.28.061604.135714

Minocha, S., Valloton, D., Brunet, I., Eichmann, A., Hornung, J.-P., Lebrand, C., 2015. NG2 glia are required for vessel network formation during embryonic development. eLife 4, e09102. https://doi.org/10.7554/eLife.09102

Moon, S.Y., Shin, S.-A., Oh, Y.-S., Park, H.H., Lee, C.S., 2018. Understanding the Role of the BAI Subfamily of Adhesion G Protein-Coupled Receptors (GPCRs) in Pathological and Physiological Conditions. Genes 9, 597. https://doi.org/10.3390/genes9120597

Nair, M., Bolyard, C., Lee, T.J., Kaur, B., Yoo, J.Y., 2021. Therapeutic Application of Brain-Specific Angiogenesis Inhibitor 1 for Cancer Therapy. Cancers 13, 3562. https://doi.org/10.3390/cancers13143562

Nakano, M., Tamura, Y., Yamato, M., Kume, S., Eguchi, A., Takata, K., Watanabe, Y., Kataoka, Y., 2017. NG2 glial cells regulate neuroimmunological responses to maintain neuronal function and survival. Sci. Rep. 7, 42041. https://doi.org/10.1038/srep42041

Nakayama, H., Miyazaki, T., Kitamura, K., Hashimoto, K., Yanagawa, Y., Obata, K., Sakimura, K., Watanabe, M., Kano, M., 2012. GABAergic Inhibition Regulates Developmental Synapse Elimination in the Cerebellum. Neuron 74, 384–396. https://doi.org/10.1016/j.neuron.2012.02.032

Neftel, C., Laffy, J., Filbin, M.G., Hara, T., Shore, M.E., Rahme, G.J., Richman, A.R., Silverbush, D., Shaw, M.L., Hebert, C.M., Dewitt, J., Gritsch, S., Perez, E.M., Castro, L.N.G., Lan, X., Druck, N., Rodman, C., Dionne, D., Kaplan, A., Bertalan, M.S., Small, J., Pelton, K., Becker, S., Bonal, D., Nguyen, Q.-D., Servis, R.L., Fung, J.M., Mylvaganam, R., Mayr, L., Gojo, J., Haberler, C., Geyeregger, R., Czech, T., Slavc, I., Nahed, B.V., Curry, W.T., Carter, B.S., Wakimoto, H., Brastianos, P.K., Batchelor, Tracy.T., Stemmer-Rachamimov, A., Martinez-Lage, M., Frosch, M.P., Stamenkovic, I., Riggi, N., Rheinbay, E., Monje, M., Rozenblatt-Rosen, O., Cahill, D.P., Patel, A.P., Hunter, T., Verma, I.M., Ligon, K.L., Louis, D.N., Regev, A., Bernstein, B.E., Tirosh, I., Suvà, M.L., 2019. An integrative model of cellular states, plasticity and genetics for glioblastoma. Cell 178, 835-849.e21. https://doi.org/10.1016/j.cell.2019.06.024

Nery, S., Wichterle, H., Fishell, G., 2001. Sonic hedgehog contributes to oligodendrocyte specification in the mammalian forebrain. Development 128, 527–540. https://doi.org/10.1242/dev.128.4.527

Nishida, K., Flanagan, J.G., Nakamoto, M., 2002. Domain-specific olivocerebellar projection regulated by the EphA-ephrin-A interaction. Development 129, 5647–5658. https://doi.org/10.1242/dev.00162

Nishiyama, A., Dahlin, K.J., Prince, J.T., Johnstone, S.R., Stallcup, W.B., 1991. The primary structure of NG2, a novel membrane-spanning proteoglycan. J. Cell Biol. 114, 359–371. https://doi.org/10.1083/jcb.114.2.359

Nishiyama, A., Shimizu, T., Sherafat, A., Richardson, W.D., 2021. Life-long oligodendrocyte development and plasticity. Semin. Cell Dev. Biol., Special Issue: Myelin edited by Gonçalo Castelo-Branco and Roman Chrast / Special issue: Aging in the nervous system edited by Mara Mather 116, 25–37. https://doi.org/10.1016/j.semcdb.2021.02.004

Okajima, D., Kudo, G., Yokota, H., 2011. Antidepressant-like behavior in brain-specific angiogenesis inhibitor 2-deficient mice. J. Physiol. Sci. 61, 47–54. https://doi.org/10.1007/s12576-010-0120-0

O'Leary, D.D.M., Yates, P.A., McLaughlin, T., 1999. Molecular Development of Sensory Maps. Cell 96, 255–269. https://doi.org/10.1016/S0092-8674(00)80565-6

Orduz, D., Benamer, N., Ortolani, D., Coppola, E., Vigier, L., Pierani, A., Angulo, M.C., 2019. Developmental cell death regulates lineage-related interneuron-oligodendroglia

functional clusters and oligodendrocyte homeostasis. Nat. Commun. 10, 4249. https://doi.org/10.1038/s41467-019-11904-4

Ortega, M.C., Bribián, A., Peregrín, S., Gil, M.T., Marín, O., de Castro, F., 2012. Neuregulin-1/ErbB4 signaling controls the migration of oligodendrocyte precursor cells during development. Exp. Neurol., MicroRNAs—Human Neurobiology and Neuropathology 235, 610–620. https://doi.org/10.1016/j.expneurol.2012.03.015

Park, D., Tosello-Trampont, A.-C., Elliott, M.R., Lu, M., Haney, L.B., Ma, Z., Klibanov, A.L., Mandell, J.W., Ravichandran, K.S., 2007. BAI1 is an engulfment receptor for apoptotic cells upstream of the ELMO/Dock180/Rac module. Nature 450, 430–434. https://doi.org/10.1038/nature06329

Pasquale, E.B., 2008. Eph-Ephrin Bidirectional Signaling in Physiology and Disease. Cell 133, 38–52. https://doi.org/10.1016/j.cell.2008.03.011

Paul, M.A., Sigoillot, S.M., Marti, L., Delagrange, M., Mailly, P., Selimi, F., 2023. Stepwise molecular specification of excitatory synapse diversity on a target neuron. https://doi.org/10.1101/2023.01.03.521946

Pauwels, J., Fijałkowska, D., Eyckerman, S., Gevaert, K., 2022. Mass spectrometry and the cellular surfaceome. Mass Spectrom. Rev. 41, 804–841. https://doi.org/10.1002/mas.21690

Pepper, R.E., Pitman, K.A., Cullen, C.L., Young, K.M., 2018. How Do Cells of the Oligodendrocyte Lineage Affect Neuronal Circuits to Influence Motor Function, Memory and Mood? Front. Cell. Neurosci. 12.

Pierce, K.L., Premont, R.T., Lefkowitz, R.J., 2002. Seven-transmembrane receptors. Nat. Rev. Mol. Cell Biol. 3, 639–650. https://doi.org/10.1038/nrm908

Platt, R.J., Chen, S., Zhou, Y., Yim, M.J., Swiech, L., Kempton, H.R., Dahlman, J.E., Parnas, O., Eisenhaure, T.M., Jovanovic, M., Graham, D.B., Jhunjhunwala, S., Xavier, R.J., Langer, R., Anderson, D.G., Hacohen, N., Regev, A., Feng, G., Sharp, P.A., Zhang, F., 2014. CRISPR-Cas9 Knockin Mice for Genome Editing and Cancer Modeling. Cell 159, 440–455. https://doi.org/10.1016/j.cell.2014.09.014

Pozo, K., Goda, Y., 2010. Unraveling mechanisms of homeostatic synaptic plasticity. Neuron 66, 337–351. https://doi.org/10.1016/j.neuron.2010.04.028

Psachoulia, K., Jamen, F., Young, K.M., Richardson, W.D., 2009. Cell cycle dynamics of NG2 cells in the postnatal and ageing brain. Neuron Glia Biol. 5, 57–67. https://doi.org/10.1017/S1740925X09990354

Qi, Y., Xiong, W., Yu, S., Du, Z., Qu, T., He, L., Wei, W., Zhang, L., Liu, K., Li, Y., He, D.Z., Gong, S., 2021. Deletion of C1ql1 Causes Hearing Loss and Abnormal Auditory Nerve Fibers in the Mouse Cochlea. Front. Cell. Neurosci. 15.

Qiu, X., Feng, J.-R., Wang, F., Chen, P.-F., Chen, X.-X., Zhou, R., Chang, Y., Liu, J., Zhao, Q., 2018. Profiles of differentially expressed genes and overexpression of NEBL indicates a positive prognosis in patients with colorectal cancer. Mol. Med. Rep. 17, 3028–3034. https://doi.org/10.3892/mmr.2017.8210

Raff, M.C., Abney, E.R., Fok-Seang, J., 1985. Reconstitution of a developmental clock in vitro: a critical role for astrocytes in the timing of oligodendrocyte differentiation. Cell 42, 61–69. https://doi.org/10.1016/S0092-8674(85)80101-X

Raff, M.C., Miller, R.H., Noble, M., 1983. A glial progenitor cell that develops in vitro into an astrocyte or an oligodendrocyte depending on culture medium. Nature 303, 390–396. https://doi.org/10.1038/303390a0

Reboll, M.R., Klede, S., Taft, M.H., Cai, C.-L., Field, L.J., Lavine, K.J., Koenig, A.L., Fleischauer, J., Meyer, J., Schambach, A., Niessen, H.W., Kosanke, M., van den Heuvel, J., Pich, A., Bauersachs, J., Wu, X., Zheng, L., Wang, Y., Korf-Klingebiel, M., Polten, F., Wollert, K.C., 2022. Meteorin-like promotes heart repair through endothelial KIT receptor tyrosine kinase. Science 376, 1343–1347. https://doi.org/10.1126/science.abn3027

Reeber, S., White, J., George-Jones, N., Sillitoe, R., 2013. Architecture and development of olivocerebellar circuit topography. Front. Neural Circuits 6.

Ressl, S., Vu, B.K., Vivona, S., Martinelli, D.C., Südhof, T.C., Brunger, A.T., 2015. Structures of C1q-like Proteins Reveal Unique Features among the C1q/TNF Superfamily. Structure 23, 688–699. https://doi.org/10.1016/j.str.2015.01.019

Reynolds, R., Wilkin, G.P., 1988. Development of macroglial cells in rat cerebellum II. An in situ immunohistochemical study of oligodendroglial lineage from precursor to mature myelinating cell. Development 102, 409–425. https://doi.org/10.1242/dev.102.2.409

Rivers, L.E., Young, K.M., Rizzi, M., Jamen, F., Psachoulia, K., Wade, A., Kessaris, N., Richardson, W.D., 2008. PDGFRA/NG2 glia generate myelinating oligodendrocytes and piriform projection neurons in adult mice. Nat. Neurosci. 11, 10.1038/nn.2220. https://doi.org/10.1038/nn.2220

Robins, S.C., Trudel, E., Rotondi, O., Liu, X., Djogo, T., Kryzskaya, D., Bourque, C.W., Kokoeva, M.V., 2013. Evidence for NG2-glia Derived, Adult-Born Functional Neurons in the Hypothalamus. PLOS ONE 8, e78236. https://doi.org/10.1371/journal.pone.0078236

Sakry, D., Neitz, A., Singh, J., Frischknecht, R., Marongiu, D., Binamé, F., Perera, S.S., Endres, K., Lutz, B., Radyushkin, K., Trotter, J., Mittmann, T., 2014. Oligodendrocyte Precursor Cells Modulate the Neuronal Network by Activity-Dependent Ectodomain Cleavage of Glial NG2. PLoS Biol. 12, e1001993. https://doi.org/10.1371/journal.pbio.1001993

Sakry, D., Yigit, H., Dimou, L., Trotter, J., 2015. Oligodendrocyte Precursor Cells Synthesize Neuromodulatory Factors. PLoS ONE 10. https://doi.org/10.1371/journal.pone.0127222

Sanes, J.R., Yamagata, M., 2009. Many Paths to Synaptic Specificity. Annu. Rev. Cell Dev. Biol. 25, 161–195. https://doi.org/10.1146/annurev.cellbio.24.110707.175402

Sanes, J.R., Zipursky, S.L., 2020. Synaptic Specificity, Recognition Molecules, and Assembly of Neural Circuits. Cell 181, 536–556. https://doi.org/10.1016/j.cell.2020.04.008

Sarpong, G.A., Vibulyaseck, S., Luo, Y., Biswas, M.S., Fujita, H., Hirano, S., Sugihara, I., 2018. Cerebellar modules in the olivo-cortico-nuclear loop demarcated by pcdh10 expression in the adult mouse. J. Comp. Neurol. 526, 2406–2427. https://doi.org/10.1002/cne.24499

Sassoè-Pognetto, M., 2016. Development of Glutamatergic and GABAergic Synapses, in: Gruol, D.L., Koibuchi, N., Manto, M., Molinari, M., Schmahmann, J.D., Shen, Y. (Eds.), Essentials of Cerebellum and Cerebellar Disorders: A Primer For Graduate Students. Springer International Publishing, Cham, pp. 155–159. https://doi.org/10.1007/978-3-319-24551-5_17

Schindelin, J., Arganda-Carreras, I., Frise, E., Kaynig, V., Longair, M., Pietzsch, T., Preibisch, S., Rueden, C., Saalfeld, S., Schmid, B., Tinevez, J.-Y., White, D.J., Hartenstein, V., Eliceiri, K., Tomancak, P., Cardona, A., 2012. Fiji - an Open Source platform for biological image analysis. Nat. Methods 9, 10.1038/nmeth.2019. https://doi.org/10.1038/nmeth.2019

Schiöth, H.B., Nordström, K.J.V., Fredriksson, R., 2010. The Adhesion GPCRs; Gene Repertoire, Phylogeny and Evolution, in: Yona, S., Stacey, M. (Eds.), Adhesion-GPCRs: Structure to Function, Advances in Experimental Medicine and Biology. Springer US, Boston, MA, pp. 1–13. https://doi.org/10.1007/978-1-4419-7913-1_1

Sigoillot, S.M., Iyer, K., Binda, F., González-Calvo, I., Talleur, M., Vodjdani, G., Isope, P., Selimi, F., 2015. The Secreted Protein C1QL1 and Its Receptor BAI3 Control the Synaptic Connectivity of Excitatory Inputs Converging on Cerebellar Purkinje Cells. Cell Rep. 10, 820–832. https://doi.org/10.1016/j.celrep.2015.01.034

Sigoillot, S.M., Monk, K.R., Piao, X., Selimi, F., Harty, B.L., 2016. Adhesion GPCRs as Novel Actors in Neural and Glial Cell Functions: From Synaptogenesis to Myelination. Handb. Exp. Pharmacol. 234, 275–298. https://doi.org/10.1007/978-3-319-41523-9_12

Sillitoe, R.V., Hawkes, R., 2013. Zones and Stripes: Development of Cerebellar Topography, in: Manto, M., Schmahmann, J.D., Rossi, F., Gruol, D.L., Koibuchi, N. (Eds.), Handbook of the Cerebellum and Cerebellar Disorders. Springer Netherlands, Dordrecht, pp. 43–59. https://doi.org/10.1007/978-94-007-1333-8_3

Sillitoe, R.V., Joyner, A.L., 2007. Morphology, Molecular Codes, and Circuitry Produce the Three-Dimensional Complexity of the Cerebellum. Annu. Rev. Cell Dev. Biol. 23, 549–577. https://doi.org/10.1146/annurev.cellbio.23.090506.123237

Silva, J.-P., Lelianova, V.G., Ermolyuk, Y.S., Vysokov, N., Hitchen, P.G., Berninghausen, O., Rahman, M.A., Zangrandi, A., Fidalgo, S., Tonevitsky, A.G., Dell, A., Volynski, K.E., Ushkaryov, Y.A., 2011. Latrophilin 1 and its endogenous ligand Lasso/teneurin-2 form a high-affinity transsynaptic receptor pair with signaling capabilities. Proc. Natl. Acad. Sci. U. S. A. 108, 12113–12118. https://doi.org/10.1073/pnas.1019434108

Small, R.K., Riddle, P., Noble, M., 1987. Evidence for migration of oligodendrocyte–type-2 astrocyte progenitor cells into the developing rat optic nerve. Nature 328, 155–157. https://doi.org/10.1038/328155a0

Song, A.J., Palmiter, R.D., 2018. Detecting and Avoiding Problems When Using the Cre/lox System. Trends Genet. TIG 34, 333–340. https://doi.org/10.1016/j.tig.2017.12.008

Sotelo, C., 2011. Camillo Golgi and Santiago Ramon y Cajal: the anatomical organization of the cortex of the cerebellum. Can the neuron doctrine still support our actual knowledge on the cerebellar structural arrangement? https://doi.org/10.1016/j.brainresrev.2010.05.004

Sotelo, C., 2008. Development of “pinceaux” formations and dendritic translocation of climbing fibers during the acquisition of the balance between glutamatergic and γ-aminobutyric acidergic inputs in developing purkinje cells. https://doi.org/10.1002/cne.21501

Sotelo, C., Bourrat, F., Triller, A., 1984. Postnatal development of the inferior olivary complex in the rat. II. Topographic organization of the immature olivocerebellar projection. J. Comp. Neurol. 222, 177–199. https://doi.org/10.1002/cne.902220204

Spitzer, S.O., Sitnikov, S., Kamen, Y., Evans, K.A., Kronenberg-Versteeg, D., Dietmann, S., de Faria, O., Agathou, S., Káradóttir, R.T., 2019. Oligodendrocyte Progenitor Cells Become Regionally Diverse and Heterogeneous with Age. Neuron 101, 459-471.e5. https://doi.org/10.1016/j.neuron.2018.12.020

Stacey, M., Chang, G.-W., Davies, J.Q., Kwakkenbos, M.J., Sanderson, R.D., Hamann, J., Gordon, S., Lin, H.-H., 2003. The epidermal growth factor–like domains of the human EMR2 receptor mediate cell attachment through chondroitin sulfate glycosaminoglycans. Blood 102, 2916–2924. https://doi.org/10.1182/blood-2002-11-3540

Stankov, K., Popovic, S., Mikov, M., 2014. C-KIT signaling in cancer treatment. Curr. Pharm. Des. 20, 2849–2880. https://doi.org/10.2174/13816128113199990593

Stephenson, J.R., Paavola, K.J., Schaefer, S.A., Kaur, B., Van Meir, E.G., Hall, R.A., 2013. Brain-specific Angiogenesis Inhibitor-1 Signaling, Regulation, and Enrichment in the

Postsynaptic Density. J. Biol. Chem. 288, 22248–22256. https://doi.org/10.1074/jbc.M113.489757

Stichel, C.C., Kägi, U., Heizmann, C.W., 1986. Parvalbumin in cat brain: isolation, characterization, and localization. J. Neurochem. 47, 46–53. https://doi.org/10.1111/j.1471-4159.1986.tb02829.x

Strokes, N., Piao, X., 2010. Adhesion-GPCRs in the CNS, in: Yona, S., Stacey, M. (Eds.), Adhesion-GPCRs: Structure to Function, Advances in Experimental Medicine and Biology. Springer US, Boston, MA, pp. 87–97. https://doi.org/10.1007/978-1-4419-7913-1_7

Südhof, T.C., 2018. Towards an Understanding of Synapse Formation. Neuron 100, 276–293. https://doi.org/10.1016/j.neuron.2018.09.040

Sugihara, I., Shinoda, Y., 2007. Molecular, Topographic, and Functional Organization of the Cerebellar Nuclei: Analysis by Three-Dimensional Mapping of the Olivonuclear Projection and Aldolase C Labeling. J. Neurosci. 27, 9696–9710. https://doi.org/10.1523/JNEUROSCI.1579-07.2007

Sugihara, I., Shinoda, Y., 2004. Molecular, Topographic, and Functional Organization of the Cerebellar Cortex: A Study with Combined Aldolase C and Olivocerebellar Labeling. J. Neurosci. 24, 8771–8785. https://doi.org/10.1523/JNEUROSCI.1961-04.2004

Sun, L., Lee, J., Fine, H.A., 2004. Neuronally expressed stem cell factor induces neural stem cell migration to areas of brain injury. J. Clin. Invest. 113, 1364–1374. https://doi.org/10.1172/JCI200420001

Tabone-Eglinger, S., Calderin-Sollet, Z., Pinon, P., Aebischer, N., Wehrle-Haller, M., Jacquier, M.-C., Boettiger, D., Wehrle-Haller, B., 2014. Niche anchorage and signaling through membrane-bound Kit-ligand/c-kit receptor are kinase independent and imatinib insensitive. FASEB J. Off. Publ. Fed. Am. Soc. Exp. Biol. 28, 4441–4456. https://doi.org/10.1096/fj.14-249425

Tamamaki, N., Nojyo, Y., 1995. Preservation of topography in the connections between the subiculum, field CA1, and the entorhinal cortex in rats. J. Comp. Neurol. 353, 379–390. https://doi.org/10.1002/cne.903530306

Telley, L., Cadilhac, C., Cioni, J.-M., Saywell, V., Jahannault-Talignani, C., Huettl, R.E., Sarrailh-Faivre, C., Dayer, A., Huber, A.B., Ango, F., 2016. Dual Function of NRP1 in Axon Guidance and Subcellular Target Recognition in Cerebellum. Neuron 91, 1276–1291. https://doi.org/10.1016/j.neuron.2016.08.015

Thivierge, J.-P., Marcus, G.F., 2007. The topographic brain: from neural connectivity to cognition. Trends Neurosci. 30, 251–259. https://doi.org/10.1016/j.tins.2007.04.004

Torkildsen, O., Brunborg, L.A., Myhr, K.-M., Bø, L., 2008. The cuprizone model for demyelination. Acta Neurol. Scand. Suppl. 188, 72–76. https://doi.org/10.1111/j.1600-0404.2008.01036.x

Tripathi, R.B., Clarke, L.E., Burzomato, V., Kessaris, N., Anderson, P.N., Attwell, D., Richardson, W.D., 2011. Dorsally and Ventrally Derived Oligodendrocytes Have Similar Electrical Properties but Myelinate Preferred Tracts. J. Neurosci. 31, 6809–6819. https://doi.org/10.1523/JNEUROSCI.6474-10.2011

Triplett, J.W., Feldheim, D.A., 2012. Eph and ephrin signaling in the formation of topographic maps. Semin. Cell Dev. Biol. 23, 7–15. https://doi.org/10.1016/j.semcdb.2011.10.026

Trotter, J., Karram, K., Nishiyama, A., 2010. NG2 cells: Properties, progeny and origin. Brain Res. Rev., Synaptic Processes - the role of glial cells 63, 72–82. https://doi.org/10.1016/j.brainresrev.2009.12.006

Tsai, H.-H., Niu, J., Munji, R., Davalos, D., Chang, J., Zhang, H., Tien, A.-C., Kuo, C.J., Chan, J.R., Daneman, R., Fancy, S.P.J., 2016. Oligodendrocyte precursors migrate along vasculature in the developing nervous system. Science 351, 379–384. https://doi.org/10.1126/science.aad3839

Tuttle, A.M., Pomaville, M.B., Delgado, K.C., Wright, K.M., Nechiporuk, A.V., 2022. c-Kit Receptor Maintains Sensory Axon Innervation of the Skin through Src Family Kinases. J. Neurosci. 42, 6835–6847. https://doi.org/10.1523/JNEUROSCI.0618-22.2022

van Tilborg, E., de Theije, C.G.M., van Hal, M., Wagenaar, N., de Vries, L.S., Benders, M.J., Rowitch, D.H., Nijboer, C.H., 2018. Origin and dynamics of oligodendrocytes in the developing brain: Implications for perinatal white matter injury. Glia 66, 221–238. https://doi.org/10.1002/glia.23256

Veleanu, M., Urrieta-Chávez, B., Sigoillot, S.M., Paul, M.A., Usardi, A., Iyer, K., Delagrange, M., Doyle, J.P., Heintz, N., Bécamel, C., Selimi, F., 2022a. Modified climbing fiber/Purkinje cell synaptic connectivity in the cerebellum of the neonatal phencyclidine model of schizophrenia. Proc. Natl. Acad. Sci. 119, e2122544119–e2122544119. https://doi.org/10.1073/pnas.2122544119

Veleanu, M., Urrieta-Chávez, B., Sigoillot, S.M., Paul, M.A., Usardi, A., Iyer, K., Delagrange, M., Doyle, J.P., Heintz, N., Bécamel, C., Selimi, F., 2022b. Modified climbing fiber/Purkinje cell synaptic connectivity in the cerebellum of the neonatal phencyclidine model of schizophrenia. Proc. Natl. Acad. Sci. U. S. A. 119, e2122544119. https://doi.org/10.1073/pnas.2122544119

Venkatesh, H.S., Johung, T.B., Caretti, V., Noll, A., Tang, Y., Nagaraja, S., Gibson, E.M., Mount, C.W., Polepalli, J., Mitra, S.S., Woo, P.J., Malenka, R.C., Vogel, H., Bredel, M., Mallick, P., Monje, M., 2015. Neuronal Activity Promotes Glioma Growth through Neuroligin-3 Secretion. Cell 161, 803–816. https://doi.org/10.1016/j.cell.2015.04.012

Venkatesh, H.S., Tam, L.T., Woo, P.J., Lennon, J., Nagaraja, S., Gillespie, S.M., Ni, J., Duveau, D.Y., Morris, P.J., Zhao, J.J., Thomas, C.J., Monje, M., 2017. Targeting neuronal activity-regulated neuroligin-3 dependency in high-grade glioma. Nature 549, 533–537. https://doi.org/10.1038/nature24014

Vilen, Z., Reeves, A.E., O'Leary, T.R., Joeh, E., Kamasawa, N., Huang, M.L., 2022. Cell Surface Engineering Enables Surfaceome Profiling. ACS Chem. Biol. https://doi.org/10.1021/acschembio.1c00865

Voogd, J., Glickstein, M., 1998. The anatomy of the cerebellum. Trends Neurosci. 21, 370–375. https://doi.org/10.1016/S0166-2236(98)01318-6

Wandel, E., Saalbach, A., Sittig, D., Gebhardt, C., Aust, G., 2012. Thy-1 (CD90) Is an Interacting Partner for CD97 on Activated Endothelial Cells. J. Immunol. 188, 1442–1450. https://doi.org/10.4049/jimmunol.1003944

Wang, J., Miao, Y., Wicklein, R., Sun, Z., Wang, Jinzhao, Jude, K.M., Fernandes, R.A., Merrill, S.A., Wernig, M., Garcia, K.C., Südhof, T.C., 2021. RTN4/NoGo-Receptor Binding to BAI Adhesion-GPCRs Regulates Neuronal Development. Cell 184, 5869-5885.e25. https://doi.org/10.1016/j.cell.2021.10.016

Wang, T., Ward, Y., Tian, L., Lake, R., Guedez, L., Stetler-Stevenson, W.G., Kelly, K., 2005. CD97, an adhesion receptor on inflammatory cells, stimulates angiogenesis through binding integrin counterreceptors on endothelial cells. Blood 105, 2836–2844. https://doi.org/10.1182/blood-2004-07-2878

Wang, W.X., Qiao, J., Lefebvre, J.L., 2022. PV-IRES-Cre mouse line targets excitatory granule neurons in the cerebellum. Mol. Brain 15, 85. https://doi.org/10.1186/s13041-022-00972-1

Wang, X., Zhou, R., Xiong, Y., Zhou, L., Yan, X., Wang, M., Li, F., Xie, C., Zhang, Yiming, Huang, Z., Ding, C., Shi, K., Li, W., Liu, Y., Cao, Z., Zhang, Z.-N., Zhou, S., Chen, C., Zhang, Yan, Chen, L., Wang, Y., 2021. Sequential fate-switches in stem-like cells drive the tumorigenic trajectory from human neural stem cells to malignant glioma. Cell Res. 31, 684–702. https://doi.org/10.1038/s41422-020-00451-z

Watanabe, M., 2016. Basket Cells, in: Gruol, D.L., Koibuchi, N., Manto, M., Molinari, M., Schmahmann, J.D., Shen, Y. (Eds.), Essentials of Cerebellum and Cerebellar Disorders: A Primer For Graduate Students. Springer International Publishing, Cham, pp. 195–199. https://doi.org/10.1007/978-3-319-24551-5_23

Watanabe, M., Kano, M., 2011. Climbing fiber synapse elimination in cerebellar Purkinje cells. Eur. J. Neurosci. 34, 1697–1710. https://doi.org/10.1111/j.1460-9568.2011.07894.x

White, J.J., Arancillo, M., Stay, T.L., George-Jones, N.A., Levy, S.L., Heck, D.H., Sillitoe, R.V., 2014a. Cerebellar Zonal Patterning Relies on Purkinje Cell Neurotransmission. J. Neurosci. 34, 8231–8245. https://doi.org/10.1523/JNEUROSCI.0122-14.2014

White, J.J., Arancillo, M., Stay, T.L., George-Jones, N.A., Levy, S.L., Heck, D.H., Sillitoe, R.V., 2014b. Cerebellar Zonal Patterning Relies on Purkinje Cell Neurotransmission. J. Neurosci. 34, 8231–8245. https://doi.org/10.1523/JNEUROSCI.0122-14.2014

White, J.J., Sillitoe, R.V., 2013. Development of the cerebellum: from gene expression patterns to circuit maps. WIREs Dev. Biol. 2, 149–164. https://doi.org/10.1002/wdev.65

Williams, M.E., Wilke, S.A., Daggett, A., Davis, E., Otto, S., Ravi, D., Ripley, B., Bushong, E.A., Ellisman, M.H., Klein, G., Ghosh, A., 2011. Cadherin-9 Regulates Synapse-Specific Differentiation in the Developing Hippocampus. Neuron 71, 640–655. https://doi.org/10.1016/j.neuron.2011.06.019

Xiao, Y., Petrucco, L., Hoodless, L.J., Portugues, R., Czopka, T., 2022. Oligodendrocyte precursor cells sculpt the visual system by regulating axonal remodeling. Nat. Neurosci. 25, 280–284. https://doi.org/10.1038/s41593-022-01023-7

Yamada, M., Hoshino, M., 2016. Precerebellar Nuclei, in: Gruol, D.L., Koibuchi, N., Manto, M., Molinari, M., Schmahmann, J.D., Shen, Y. (Eds.), Essentials of Cerebellum and Cerebellar Disorders: A Primer For Graduate Students. Springer International Publishing, Cham, pp. 63–67. https://doi.org/10.1007/978-3-319-24551-5_7

Yamanaka, H., Yanagawa, Y., Obata, K., 2004. Development of stellate and basket cells and their apoptosis in mouse cerebellar cortex. Neurosci. Res. 50, 13–22. https://doi.org/10.1016/j.neures.2004.06.008

Young, K.M., Psachoulia, K., Tripathi, R.B., Dunn, S.-J., Cossell, L., Attwell, D., Tohyama, K., Richardson, W.D., 2013. Oligodendrocyte Dynamics in the Healthy Adult CNS: Evidence for Myelin Remodeling. Neuron 77, 873–885. https://doi.org/10.1016/j.neuron.2013.01.006

Yuen, T.J., Silbereis, J.C., Griveau, A., Chang, S.M., Daneman, R., Fancy, S.P.J., Zahed, H., Maltepe, E., Rowitch, D.H., 2014. Oligodendrocyte-encoded HIF function couples postnatal myelination and white matter angiogenesis. Cell 158, 383–396. https://doi.org/10.1016/j.cell.2014.04.052

Yuzaki, M., 2017. The C1q complement family of synaptic organizers: not just complementary. Curr. Opin. Neurobiol., Molecular Neuroscience 45, 9–15. https://doi.org/10.1016/j.conb.2017.02.002

Zeis, T., Enz, L., Schaeren-Wiemers, N., 2016. The immunomodulatory oligodendrocyte. Brain Res., Evolution of Myelin 1641, 139–148. https://doi.org/10.1016/j.brainres.2015.09.021

Zhang, S., Xu, Y., Zhao, P., Bao, H., Wang, X., Liu, R., Xu, R., Xiang, J., Jiang, H., Yan, J., Wu, X., Shao, Y., Liang, J., Wu, Q., Zhang, Z., Lu, S., Ma, S., 2021. Integrated Analysis of Genomic and Immunological Features in Lung Adenocarcinoma With Micropapillary Component. Front. Oncol. 11.

Zheng, S., Li, Z., Song, J., Liu, J., Miao, C., 2016. Metrnl: a secreted protein with new emerging functions. Acta Pharmacol. Sin. 37, 571–579. https://doi.org/10.1038/aps.2016.9

Zhou, H., Lin, Z., Voges, K., Ju, C., Gao, Z., Bosman, L.W., Ruigrok, T.J., Hoebeek, F.E., De Zeeuw, C.I., Schonewille, M., 2014. Cerebellar modules operate at different frequencies. eLife 3, e02536. https://doi.org/10.7554/eLife.02536

Zhou, J., Brown, A.M., Lackey, E.P., Arancillo, M., Lin, T., Sillitoe, R.V., 2020a. Purkinje cell neurotransmission patterns cerebellar basket cells into zonal modules defined by distinct pinceau sizes. eLife 9, e55569. https://doi.org/10.7554/eLife.55569

Zhou, J., Brown, A.M., Lackey, E.P., Arancillo, M., Lin, T., Sillitoe, R.V., 2020b. Purkinje cell neurotransmission patterns cerebellar basket cells into zonal modules defined by distinct pinceau sizes. eLife 9, e55569. https://doi.org/10.7554/eLife.55569

Zhu, H., Aryal, D.K., Olsen, R.H.J., Urban, D.J., Swearingen, A., Forbes, S., Roth, B.L., Hochgeschwender, U., 2016. Cre dependent DREADD (Designer Receptors Exclusively Activated by Designer Drugs) mice. Genes. N. Y. N 2000 54, 439–446. https://doi.org/10.1002/dvg.22949

Zhu, X., Bergles, D.E., Nishiyama, A., 2008a. NG2 cells generate both oligodendrocytes and gray matter astrocytes. Development 135, 145–157. https://doi.org/10.1242/dev.004895

Zhu, X., Hill, R.A., Nishiyama, A., 2008b. NG2 cells generate oligodendrocytes and gray matter astrocytes in the spinal cord. Neuron Glia Biol. 4, 19–26. https://doi.org/10.1017/S1740925X09000015

Zohrabian, V.M., Nandu, H., Gulati, N., Khitrov, G., Zhao, C., Mohan, A., Demattia, J., Braun, A., Das, K., Murali, R., Jhanwar-Uniyal, M., 2007. Gene expression profiling of metastatic brain cancer. Oncol. Rep. 18, 321–328.

Zuko, A., Oguro-Ando, A., Post, H., Taggenbrock, R.L.R.E., van Dijk, R.E., Altelaar, A.F.M., Heck, A.J.R., Petrenko, A.G., van der Zwaag, B., Shimoda, Y., Pasterkamp, R.J., Burbach, J.P.H., 2016. Association of Cell Adhesion Molecules Contactin-6 and Latrophilin-1 Regulates Neuronal Apoptosis. Front. Mol. Neurosci. 9, 143. https://doi.org/10.3389/fnmol.2016.00143

Summary:

Proper brain development relies on cellular proliferation, migration and differentiation of various cell populations, recognition and adhesion between different cell types. Cell surface molecular complexes are essential for many of these processes. A given receptor complex can be used at several stages and might play different roles in various cell populations. During my PhD, I worked on two cell surface molecular complexes and their role during postnatal development of the mouse brain. First, I studied the role of the c-KIT/SCF complex in neuronal connectivity. c-KIT is a well-known proto-oncogene and a transmembrane receptor tyrosine kinase that controls cell survival, proliferation and maintenance of various tissues (e.g. hematopoietic tissue) as well as cell-cell adhesion. I identified the presence of c-KIT at different types of synapses of cerebellar Purkinje cells (PC) during postnatal development: synapses made by the climbing fibers (CFs), the axons of inferior olivary neurons located in the brainstem, and synapses made by molecular layer interneurons (MLIs). Data from the Allen Brain Atlas show that the gene coding the c-KIT ligand, *Scf*, is expressed in the target neuron (PC), suggesting a potential role for the c-KIT/SCF complex in the formation and maintenance of cell-cell contacts in the olivocerebellar circuit. Using postnatal conditional knockout of *c-Kit* in MLIs, I showed that loss of function of c-KIT during the fourth postnatal week decreases the size of the presynaptic boutons of MLIs on PCs in a lobule-specific manner, while their density remains unchanged. The removal of c-KIT from MLIs also decreases the volume of presynaptic boutons from the CFs. Since this loss of c-KIT happens after synapse formation in this model, these data suggest a role for the c-KIT/SCF pathway in maintaining proper connectivity and function of the olivocerebellar circuit, and identify a potential new role for this class of receptor tyrosine kinases in brain function. In parallel, I characterized a new Cre-driver mouse line that was generated to enable inferior olivary neuron-specific knockout of *c-Kit* during postnatal development. In this line, Cre is knocked in the gene coding for C1QL1, a secreted molecule involved in CF-PC synapse formation and highly expressed in inferior olivary neurons. During this characterization, I discovered that *C1ql1* is expressed in a subtype of glial cells, oligodendrocyte precursor cells (OPCs). OPCs tile the whole central nervous system during development and adulthood. They play several key functions across the brain including the generation of oligodendrocytes. Whether the functional diversity of OPCs is the result of genetically defined subpopulations or of their regulation by external factors has not been established. We discovered that a subpopulation of OPCs found across the brain starts to express *C1ql1* during the first postnatal week in the mouse brain. Ablation of *C1ql1*-expressing OPCs, which constitute about 30-50% of total OPCs, in the mouse is not compensated by the remaining OPCs, and results in a large decrease in oligodendrocyte numbers and lack of myelination in many brain regions. Therefore, *C1ql1* is a molecular

marker of a functionally non-redundant subpopulation of OPCs, which controls the generation of myelinating oligodendrocytes. Overall my thesis work shows that a given cell surface molecular complex can control various aspects of synapse formation and function between neurons while playing roles in other aspects of brain development, such as defining the functional diversity of non-neuronal cells. Whether these complexes trigger their canonical pathways or they function through other non-canonical mechanisms in different contexts of development should be further investigated. It remains to be demonstrated whether this signaling redundancy underlies a common orchestration of various aspects of brain development and function.